UNIVERSIDADE DE SÃO PAULO
ESCOLA POLITÉCNICA

CARLOS ROBERTO ILÁRIO DA SILVA

Development of a novel RANS-based method for the computational aeroacoustics of high speed jets

São Paulo
2011

CARLOS ROBERTO ILÁRIO DA SILVA

Development of a novel RANS-based method for the computational aeroacoustics of high speed jets

Tese apresentada à Escola Politécnica da Universidade de São Paulo para a obtenção do título de Doutor em Ciências.

Área de Concentração: Engenharia Mecânica
de Energia e Fluidos
Orientador: Prof. Dr. Júlio Romano Meneghini

SÃO PAULO
2011

Este exemplar foi revisado e alterado em relação à versão original, sob responsabilidade única do autor e com a anuência de seu orientador.

São Paulo, de dezembro de 2011.

Assinatura do autor _____

Assinatura do orientador _____

FICHA CATALOGRÁFICA

Silva, Carlos Roberto Ilário da
Development of a novel RANS-based method for the computational aeroacoustics of high speed jets / C.R.I. da Silva. -- ed.rev. -- São Paulo, 2011.
208 p.

Tese (Doutorado) - Escola Politécnica da Universidade de São Paulo. Departamento de Engenharia Mecânica.

1. Acústica 2. Escoamento 3. Processamento de sinais acústicos 4. Estrutura de aeronaves 5. Dinâmica dos fluídos I. Universidade de São Paulo. Escola Politécnica. Departamento de Engenharia Mecânica II. t.

To my dear parents, Carlos and Luciane, with love, admiration and gratefulness for the endless endeavor in supporting me my entire life.

ACKNOWLEDMENTS

I would like to thank my advisor and my friend Prof. Dr. Julio R. Meneghini for his guidance, patience and also for believing in my work. I have very much appreciated the encouraging and needed talks we had during the duration of this research.

Many thanks also to Dr. Rod Self who gave me the opportunity to work as part of the Fluid Dynamics and Acoustics Group (FDAG) in the Institute of Sound and Vibration Research (ISVR) in UK. Dr. Rod Self also supervised this research and he was always available and happy to help and facilitate my work. It was an honor to work with you.

I would like to thank the many colleagues and officemates that I have had as a graduate student in USP (NDF – Fluid & Dynamics Research Group at Poli) and in Southampton (ISVR). I would specially thanks Dr. Mahdi Azarpeyvand for his help, support and advices on a countless number of technical aspects of this research. Mahdi was a constant source of new ideas and he always explained aeroacoustics in a way that even I understand. Thanks also to my friend Dr. Odenir de Almeida who introduced me to the engine noise problem years ago and convinced me to study aeroacoustics.

I would like to thank my parents, Carlos and Luciane, for providing me one of the most important and perineum asset: education. Thanks to my dear brothers, Rodolfo and Bárbara, for all the advices and support during the different phases of our lives.

To all my friends that are spread out around the world (Brazil, USA, UK, China, France, etc.) thanks very much. You are definitely part of this accomplishment.

I would like to gratefully acknowledge my funding for this research work, which has been provided by CAPES. Finally, thanks to EMBRAER S.A. for providing me the opportunity to conduct this work and FAPESP for the “Aeronave Silenciosa: Uma investigação em aeroacústica” research project.

ABSTRACT

A novel computational aeroacoustics tool based on RANS (Reynolds Averaged Navier-Stokes method) is developed for predicting the noise generated by complex three-dimensional jet flows. The new method is called LRT which arises from the combination of **L**ighthill's acoustic analogy with **R**ay-**T**racing acoustics. The powerful advantage of applying the LRT method for noise predictions is that it calculates not only the noise sources but it also models and takes into account sound-flow interaction effects without any geometric simplification, such as flow symmetries of the problem. This is now a strong requirement from aero-engines manufactures since investigations on asymmetric nozzles, as a means of noise reductions are in progress. The LRT method is a relatively fast jet noise prediction tool based on Lighthill's Acoustic Analogy and it uses a Reynolds-Average Navier-Stokes (RANS) computational fluid dynamics (CFD) simulation as input information. The sound-flow interaction is computed by solving the propagation using Ray-Tracing equations. The LRT method has been formulated as a general three-dimensional method and it has no restrictions on the type of the flow field or nozzle geometry for noise prediction. Successful numerical noise predictions have been carried out for a variety of jet flows (single, coaxial and asymmetric jets) using the LRT as an engineering tool. The outcome from this thesis is a numerical tool that allows noise predictions of complex exhaust systems and the variations in sound field due to modifications of the flow field generated by the interaction of the jet flow with high-lift surfaces. In addition, the LRT method can be applied to complement experimental analysis providing a better understanding about the flow and acoustics mechanisms for complex jets.

Keywords: aeroacoustics, noise prediction, jets, aeroacoustics analogy, sound-flow interaction.

RESUMO

Uma nova ferramenta de aeroacústica computacional baseada em simulações RANS (*Reynolds Averaged Navier-Stokes*) foi desenvolvida para a predição do ruído gerado pelo escoamento tri-dimensional de jatos complexos. O método é denominado de LRT o qual surgiu da combinação da analogia acústica de **L**ighthill com o método de acústica geométrica ***R**ay-**T**racing*. A grande vantagem da utilização do método LRT para predições de ruído é que este determina não apenas as fontes sonoras presentes no escoamento, mas também modela os efeitos da interação fluidoacústica e, sua influência no ruído em um campo distante. Esta característica tornou-se extremamente importante para a indústria de motores aeronáuticos já que investigações em bocais assimétricos estão atualmente em andamento devido à necessidade de redução de ruído. O método LRT é uma ferramenta relativamente rápida de predição de ruído de jatos baseado na Analogia Acústica de Lighthill e que usa como dados de entrada os resultados obtidos à partir de uma simulação RANS do escoamento. A interação fluidoacústica é calculada através da utilização da Teoria de Traçamento de Raios. O método LRT foi formulado como um método tri-dimensional e, portanto, não possui limitações de aplicabilidade para a predição sonora em relação ao tipo de escoamento ou à geometria do bocal. Diversas simulações numéricas foram conduzidas com sucesso para uma grande variedade de escoamento de jatos (jatos simples, coaxiais e assimétricos) utilizando o LRT como uma ferramenta de engenharia. O resultado deste trabalho é uma ferramenta numérica que permite a realização de predições de ruído para casos de escoamento de jatos complexos, assim como possibilita sua aplicação para a investigação de efeitos de interação do escoamento do jato com superfícies hiper-sustentadoras no campo acústico. Adicionalmente, o método LRT pode ser aplicado para complementar análises experimentais possibilitando,

portanto, um melhor entendimento sobre os mecanismos fluidodinâmicos e acústicos presentes em escoamentos de jatos complexos.

Palavras-chaves: aeroacústica, predição de ruído, jatos, analogia acústica, interação fluidoacústica.

CONTENTS

LIST OF FIGURES

LIST OF TABLES

LIST OF ABBREVIATIONS AND ACRONYMS

ANAC = Agência Nacional de Aviação Civil

AR = Area Ratio

B&K = Brüel & Kjaer

BLSS = Boundary Layer Suction System

CAA = Computational Aeroacoustics

CAPES = Coordenação de Aperfeiçoamento de Pessoal de Nível Superior

CARAD = Civil Aircraft Research and Development

CEAT = Centre d'Etudes Aero-dynamiques et Thermiques

CFD = Computational Fluid Dynamics

CGH = São Paulo Congonhas Airport

CoJEN = Computational of Coaxial Jet Noise (EU research program)

DNS = Direct Numerical Simulation

EPNdB = Effective Perceived Noise Level

FAA = Federal Aviation Administration

FAPESP = Fundação de Amparo à Pesquisa do Estado de São Paulo

FAR = Federal Aviation Regulation

FIFA = Fédération Internationale de Football Association

HP = High Pressure

IATA = International Air Transport Association

ICAO = International Civil Aviation Organization

IPCC = Intergovernmental Panel on Climate Change

ISVR = Institute of Sound and Vibration Research, University of Southampton - UK

JEAN = Jet Exhaust Aerodynamics & Noise (EU research program)

LCY = London City Airport

LES = Large-Eddy Simulation

LP = Low Pressure

LRT = Lighthill Ray Tracing method

MGBK = Mani Gliebe Balsa Khavaran

NAP = Noise Abatement Procedure

NASA = National Aeronautics and Space Agency

NTF = Noise Test Facility

OASPL = Overall Sound Pressure Level

OST = Offset Stream Technology

PAA = Propulsion Airframe Aeroacoustics

PDE = Partial Differential Equation

PNL = Perceived Noise Level

RANS = Reynolds Average Navier-Stokes

RT = Ray-Tracing

SPL = Sound Pressure Level

SYMPHONY = SYstem Manufacturing and Product design tHrough cOmponent Noise technologY (UK TSB research program)

TET = Turbulent Energy Transfer

TKE = Turbulent Kinetic Energy

TR = Temperature Ratio

TSB = Technology Strategy Board

USP = University of São Paulo

UCI = University of California Irvine

UK = United Kingdom

USA = United States of America

UTC = University Technology Centre

VR = Velocity Ratio

LIST OF SYMBOLS

A = ray-tube area, [m^2]

Ap = primary nozzle area, [m^2]

As = secondary nozzle area, [m^2]

c = speed of sound, [m/s]

c_l = turbulent length-scale coefficient

c_τ = turbulent time scale coefficient

D_j = jet diameter, [m]

D_p = primary jet diameter, [m]

D_s = secondary jet diameter, [m]

e = internal energy, [J]

f = frequency, [Hz]

$g(\tau)$ = temporal part of the correlation function

$g_s^2(r)$ = shielding function

k = turbulent kinetic energy [m^2/s^2]

L = length scale

M = Mach number

M_0 = local Mach number

M_c = convective Mach number

M_j = nozzle exit Mach number

$\vec{n}$ = unit vector normal to the wave-front

p = pressure, [Pa]

P_e = measured effective pressure amplitude of the sound wave, [Pa]

P_{ref} = reference effective pressure amplitude, [Pa]

q = heat flux, [W/m^2]

R = distance between the source and the observer, [m]

$R_{ij}(\vec{\xi})$ = spatial part of the correlation function

$\vec{s}$ = wave slowness vector (geometrical acoustics)

T = temperature, [K]

t = time, [s]

T_{ij} = Lighthill stress tensor

U = local flow velocity, [m/s]

u_1 = axial velocity component, [m/s]

u_2 = transverse velocity component, [m/s]

V = volume, [m^3]

$\vec{v}$ = fluid velocity, [m/s]

V_j = jet exit velocity, [m/s]

Vp = primary stream velocity, [m/s]

Vs = secondary stream velocity [m/s]

W = acoustic power, [W]

$\vec{x}$ = vector from origin to point with coordinates x, y, z

$\vec{x}_p$ = position of point P at a time t

Greek Symbols

α_c = empirical convection constant

α_T = calibrating coefficient

β = anisotropy level

Δ = length scale ratio

μ = fluid viscosity, [Pa·s]

ε = turbulent dissipation rate, [m^2/s^3]

θ = observer angle

θ_c = critical angle

ρ = density, mass per unit volume, [kg/m^3]

ω = observer radian frequency, [Hz]

τ = retarded time, [s]

τ_0 = turbulent time-scale

$\tau(\vec{x})$ = wavefront arrival time at $\vec{x}$, eikonel

τ_{ij} = viscous stress tensor, [Pa]

ψ = space factor

Γ = abbreviation for $1-\vec{v}\cdot\nabla\tau$ (waves in moving media)

Ω = source radian frequency, [Hz]

Ψ = size of the eddy

δ_{ij} = Kronecker delta function

Subscripts

j = jet exit condition

p = primary flow property

s = secondary flow property

0 = ambient condition

Chapter 1: Introduction

As aviation has grown along with every other part of industrialised society, the impact our life-style is having on our environment becomes a more pressing and important issue. Aircraft fuel consumption, NOx and other gaseous emissions, and most importantly noise, are some of the undesirable results from aircraft operation that strongly impacts society. As the objective of this thesis is related to aircraft noise, an overview of this problem is presented in this introductory chapter together with its effects and impacts on society. The chapter then moves on to give the motivation and the author's contribution to the research field as well as describing the thesis outline.

1.1 Understanding the role of aircraft noise in the society

To understand why aircraft noise is still the focus of intense research, even after more than 60 years since the first discussions on this subject began, and perhaps more importantly, to understand why aircraft noise became one of the biggest issues for air traffic growth, it is necessary to look at some statistical data. Figure 1.1 summarizes the world economic and air transport sector growth forecasts that were conducted by major aircraft manufacturers, government organizations, industry groups, and academia. According to Lee *et al.* [1], the annual growth rate for the air traffic is around 6%.

More recently, Boeing published its estimate for the world fleet development until 2029 in its Market Outlook 2010-2029 [2]. In their market study, which is summarized in Fig. 1.2, Boeing believes that the number of aircraft flying around the world will practically double in the next 18 years.

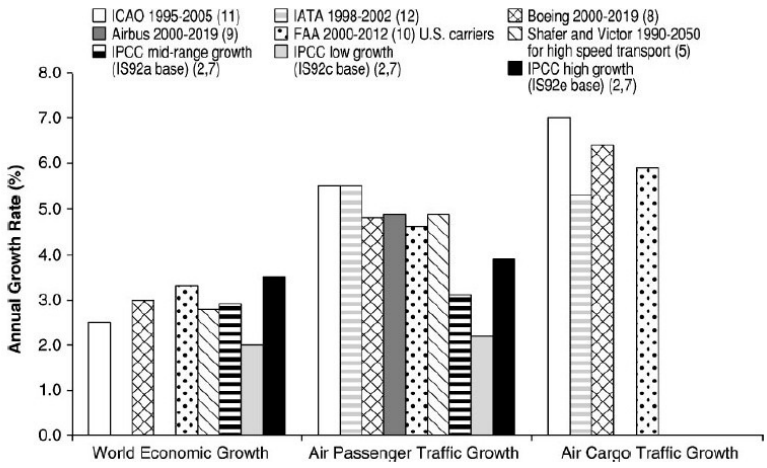

Figure 1.1 - World economic and air transport sector growth forecasts. (After Lee *et al*. [1]).

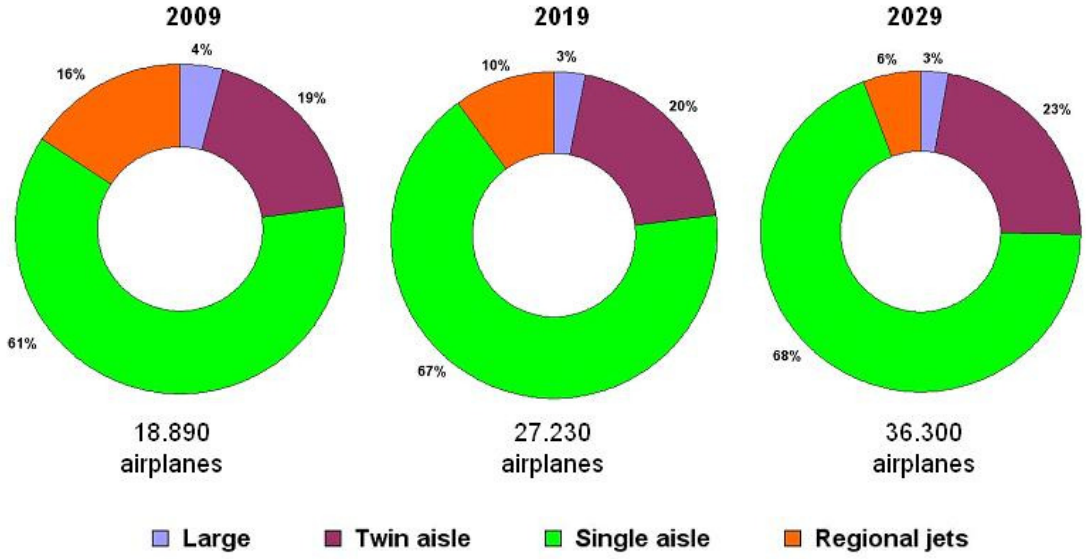

Figure 1.2 – Boeing's estimative for world fleet development in the next 20 years. [2].

This growth is not exclusive to the major countries, such as EUA or the ones in Europe. In fact, the air traffic increase is even more pronounced in a development country such as Brazil, where the economy is in a significant expansion. According to Fig. 1.3, which shows the number of jet powered airplanes register at ANAC ("Agência Nacional de Aviação Civil"), from 2006 to 2009 there was an increase of 45% on the number of aircraft landing and taking-off every single day from Brazilian airports. ANAC is the Brazilian agency

responsible for the regulation and the safety oversight of civil aviation. Moreover, it is reasonable to assume that this increase is far from becoming stable, especially with upcoming events like the FIFA World Cup and the Olympic Games to be held in Brazil in 2014 and 2016, respectively, which will require large investments in airport capacity and available fleet.

Undoubtedly, it is fair to say that the increase of the world fleet brings advantages to society such as low tickets prices, choice of flight availability, mail and freight services, and the possibility of connecting different places around the world. However, this also brings environment impacts through emissions of pollutant gases and noise. When noise is considered, the main people affected are the ones living in the neighbourhood of airports. This problem is enhanced in the principal economic cities (with high number of flights) where the airports are almost completed surrounded by houses and buildings. Figure 1.4 shows the locations of two important airports located in London (LCY) and in São Paulo (CGH) as an example of the high population density living in the vicinity of the runways

In order to enjoy the numerous benefits of air transportation, many people have to suffer high levels of noise intrusion, in most cases, not of their choice. This has been true since the introduction of jet engine powered aircraft into commercial airline service in the early 1960s. According to Smith [3], to overcome this problem in the late 1960s, after years of prevarication, governments introduced legal strictures on the manufacturing industry that demanded minimum noise standards before an aircraft could enter into service. For this goal, the Federal Aviation Agency (FAA) and the International Civil Aviation Organization (ICAO) created the first aircraft noise certification scheme that required that each aircraft manufactured (after the regulation came into face) must comply with the noise requirements. The next section will address in some detail the noise certification scheme as well as the effects this has had on the aeronautic industry.

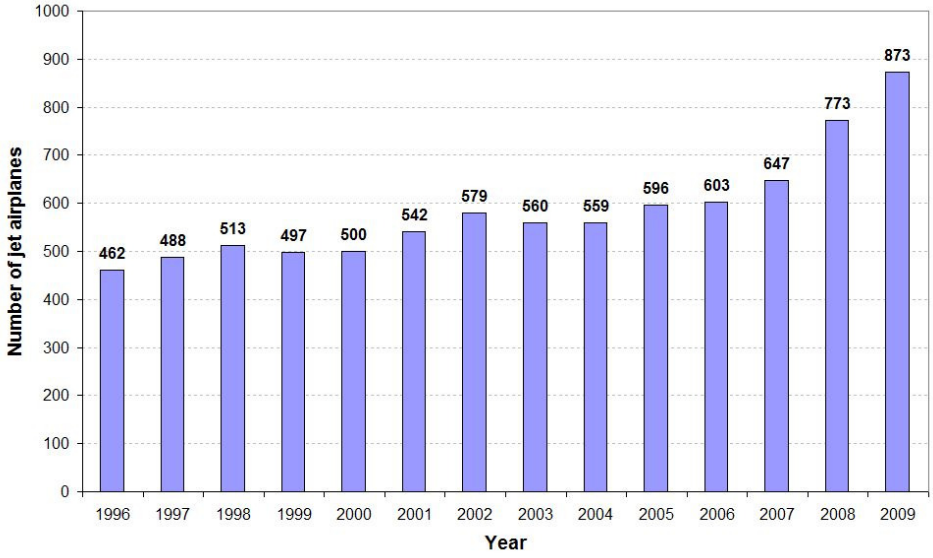

Figure 1.3 - History of the number of jet powered airplanes registered in ANAC[1].

(a) London City Airport – UK (b) Congonhas Airport – SP – Brazil

Figure 1.4 – Two important airports surrounded by edifications.

1.1.2 Regulations on aircraft noise and their impacts

Due to the high pressure from society, regulations for aircraft noise were first created in 1969 and they are in constant development, creating even more restrictive conditions for aircraft operation. As a consequence, all airplanes built today are required to meet the noise

[1] www.anac.gov.br

certification standards adopted by ICAO and FAA. More detailed information is contained in ICAO Annex 16 [4] and in FAA Federal Aviation Regulation (FAR) Part 36 [5].

In the certification process, the noise levels are measured in fly-over tests that are performed under controlled conditions with strict limits on weather conditions and flight path. Microphone measurements on the ground are taken during the flight test procedure for the three flight reference conditions: approach, sideline and take-off. For completeness, a sketch representation of the noise certification scheme is presented in Fig. 1.5, in which the reference points for noise measurements are shown. The approach reference noise measurement point is located on the extended runway centre line at a distance of 2000m from the landing threshold. On level ground this corresponds to a position of 120m vertically below the 3º glide path. The sideline reference point (sometimes referred to as full power or lateral), consists of two measurement points that are located on a line parallel to the runway at a distance of 450m from the runway centre line to the side. This point refers to where the take-off noise level is maximum. The reference point for the take-off procedure is located on the extended centre line of the runway at a distance of 6500m from the start of the roll.

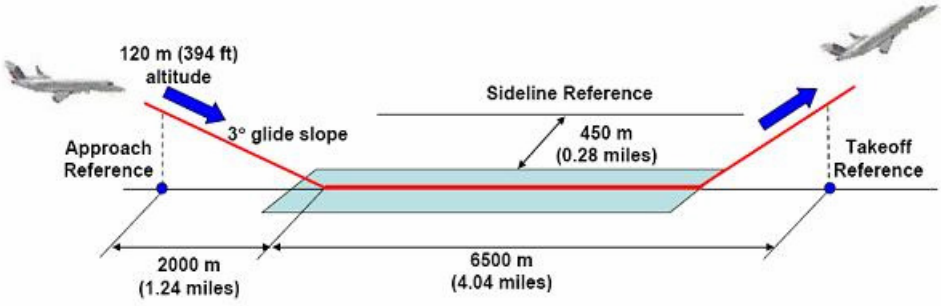

Figure 1.5 - Noise certification scheme showing the reference points for noise certification according to ICAO Annex 16 for approach, sideline and flyover.

The noise limits imposed by the regulations for the operation of aircraft are regularly reviewed and new stricter limits are defined with each such review. Since the first regulation in the late 1960s, the certification levels have evolved considerably as depicted in Fig. 1.6.

The initial noise standards for jet-powered aircraft designed before 1977 were included in Chapter 2 of ICAO Annex16, in which Boeing 727 and Douglas DC-9 are examples of aircraft covered by this standard. Subsequently, newer aircraft were required to meet the stricter standards contained in Chapter 3 of the Annex, in which Airbus A319, Boeing 767, Boeing 737-300/400, and Embraer EMB-170 are examples. Starting in 1 January 2006, a new Chapter 4 noise standard, which is more stringent than Chapter 3 became applicable to newly certified airplanes and to Chapter 3 airplanes for which re-certification to Chapter 4 was requested. For additional information, a noise database called *noisedB*[2] that lists the certification values for the entire world's certified aircraft is available on the Internet and is intended to be a general source of information for the public.

Beyond the noise regulations of ICAO and FAA, a huge number of airports have imposed local noise-control restrictions in order to diminish the impact on residents living near the runways. Figure 1.7 shows the number of airports that have some kind of operation restriction related to aircraft noise. As can be seen, the number of airports that require some kind of Noise Abatement Procedure (NAP) has dramatically increased since 1995. NAPs are very common nowadays and they are being employed to provide noise relief to communities around airports from both arriving and departing aircraft. The John Wayne Airport in Orange County (California), Kennedy Airport in New York, Heathrow Airport and London City Airport, both in London, are some examples of airports that have very strict operation restrictions for aircraft noise. In Brazil, the São Paulo Congonhas Airport (CGH) has its operational time restricted from 6:00 to 23:00 due to noise problems in the community.

[2] http://noisedb.stac.aviation-civile.gouv.fr

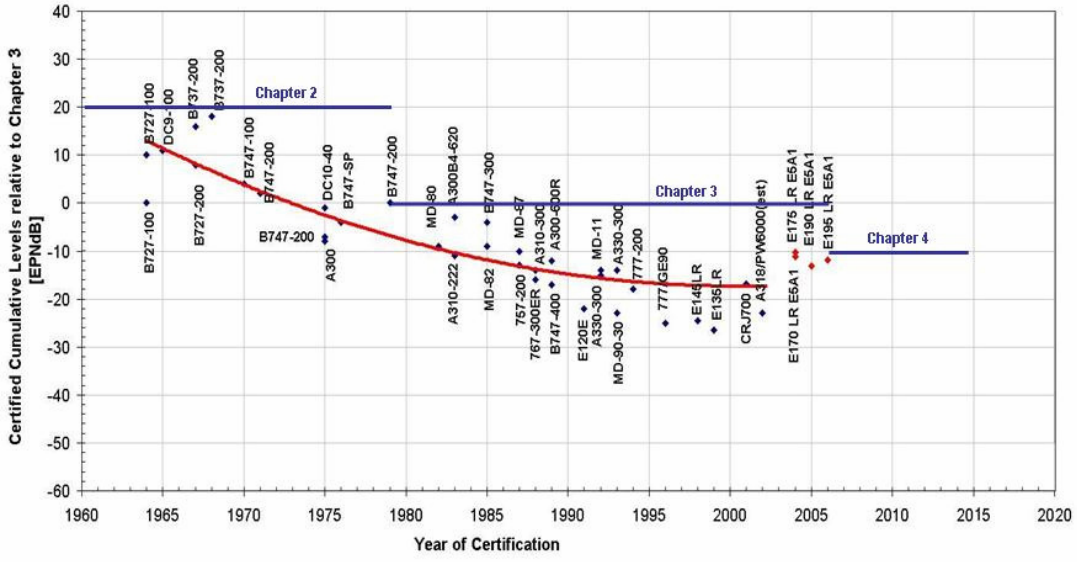

Figure 1.6 – Historical development of noise regulations for aircraft operation.

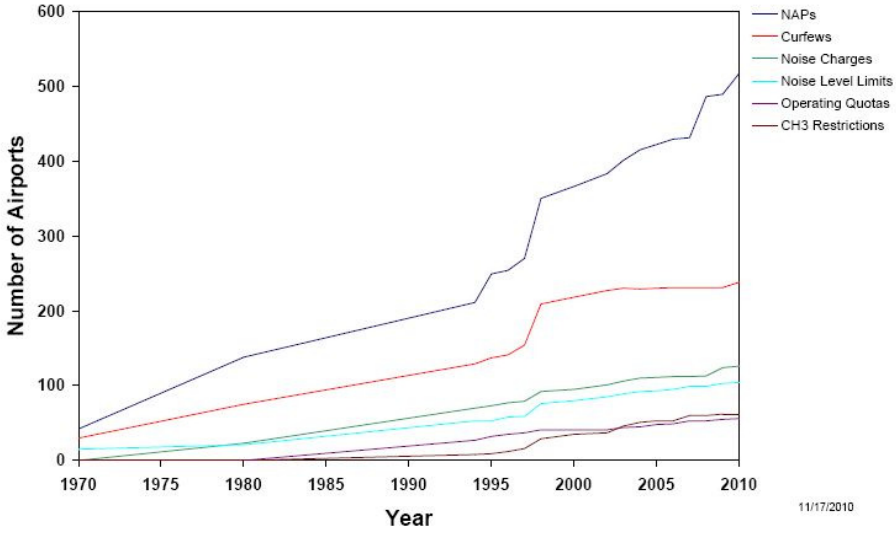

Figure 1.7 – Airports with specific restrictions for low-noise operation[3].

So far we have shown a general overview of the improvements to regulations and restrictions regarding the noise emitted by aircraft. These were, and still are, responsible for improving the quality of life of people, specially the airport community, although there is much more to be done. However, the regulations and restrictions forced the aircraft manufactures and related industries, such as engine producers, to expend considerable effort

[3]http://www.boeing.com/commercial/noise/restrictions.pdf

in developing solutions for low-noise that could be implemented in order to satisfy the conditions imposed by both the authorities (FAA, ICAO) and some specific airports. Moreover, aircraft industries have increasing competitive pressures to meet foreign noise restrictions while certification time and costs tend to be increasing. At the same time, the impact on airline companies is similar in many ways to that on the industry. According to Brentner [6], the increase of stringent local noise regulations, night time curfews and noise budgets limit the full utilization of the airline fleet. This loss of potential revenue is a cost that must be added to the increased acquisition cost of quieter new aircraft and the expense of retrofitting current aircraft to meet the newer standards. Airlines must also be concerned that flight safety can be compromised to some extent during noise abatement flight procedures. Governments also have additional expenses due to aircraft noise. For example, the most prevalent U.S. Department of Veterans Affairs disability claim is hearing loss, in which the U.S. military total costs associated with this problem have been estimated at $2-3billion per year [7]. This is mainly due to the high noise exposure that the soldiers suffer with the U.S. Navy, Marine Corps, and Air Force high-performance jet aircraft that can produce up to 130-150 dB noise on take-off.

Clearly then, there are several costs directly involved with aircraft noise. Nevertheless, as quieter aircraft and flight operations are developed each of the affected groups will realize a benefit. In fact, the feasibility and profitability of new aircraft will depend heavily on noise reductions and hence, many research projects, including the work done in this thesis, are underway to investigate means of achieving this goal.

1.2 Motivation and author's contributions

There have been significant advances in aircraft noise reduction efforts since the introduction of jet powered airplanes to the commercial airline service. Many noise reduction

strategies and devices have been developed and implemented, bringing current aircraft noise levels about 20dB below those of the first generation aircraft. However, more strict noise regulations and airport restrictions are constantly under discussion. Unfortunately, additional decibels of noise reduction are increasingly difficult and costly to obtain forcing therefore, the development of new strategies for noise reduction. As a large part of aircraft noise arises from the engine, manufacturers have taken steps to make them quieter. In the case of turbofan aircraft, this has been achieved largely by increasing the engine bypass ratio. However, today there is little room left for further reduction of noise in this way and more novel solutions must be found. One new strategy of aero-engine manufactures is to redesign exhaust nozzles in order to manipulate the flow in a way that gives an acoustic benefit, for example in non-circular nozzles a larger flow field may shield the noise sources more efficiently. In turn, this type of nozzle generates very complex flow dynamics. Therefore, an essential requirement for a jet noise prediction method for these novel nozzles is that it must be able to predict noise from complex three-dimensional flows, taking into account not only source identification but also the sound-flow interaction. Having the physics based capability is also desirable in order to develop a flexible and fast noise prediction method applicable to the investigation of advanced concepts and revolutionary configurations inside an industry timeframe context.

A new jet noise prediction method satisfying these objectives, which is called LRT, was developed in this thesis. The LRT method is a relatively fast jet noise prediction method based on Lighthill's Acoustic Analogy and it uses a Reynolds-Average Navier Stokes (RANS) computational fluid dynamics (CFD) simulation as input information. The sound-flow interaction is computed by solving the Ray-Tracing equations. The LRT method has been formulated as a general three-dimensional method and has no restriction on the type of flow field or nozzle geometry for noise prediction. Therefore, it can also be used to evaluate installation effects, such as jet-pylon interaction, which is another important area of

aeroacoustics. The LRT executable code is written in FORTRAN 90 and the pre- and post-processing tools are written in MATLAB.

Successful numerical noise predictions have been carried out for a variety of jet flows (single, coaxial and asymmetric jets) using the LRT as a novel computational aeroacoustics method. The contribution in the area of jet noise prediction, arising from this research, can be summarized as:

- Development of the LRT method, which is a novel fully three-dimensional RANS-based computational aeroacoustics method for industrial application in predicting the noise generated by complex jet flows.
- Development and implementation of a three-dimensional propagation method based on Ray-Tracing Theory to compute the refraction effects of the sound waves due to the jet flow. This overcomes a major limitation of the so-called MGBK method developed at NASA, which requires symmetry conditions for solving Lilley's Equation. In addition, it is reconfirmed in this thesis the real importance of the effects of sound-flow interaction when predicting the far-field noise from complex jet flows.
- Investigation of refraction effects as a function of Mach number, jet flow temperature, and flow dynamics. Identification of noise sources regions for symmetric and asymmetry jets.

As a result from this work, the outcome is a numerical tool that complies with the requirements of accuracy, reliability and relatively low computational effort allowing the noise predictions of complex exhaust systems and their interaction with high-lift surfaces. In

addition, the LRT method can be applied to complement experimental analysis providing a better understanding about the flow and acoustics mechanisms for complex jets.

1.3 Thesis outline

This thesis was developed as part of a Brazilian technological development project called "*Aeronave Silenciosa: Uma Investigação em Aeroacústica*" which was funded by the São Paulo Research Foundation (FAPESP) and EMBRAER S.A. This research was also supported by the Brazilian Federal Agency for Support and Evaluation of Graduate Education (CAPES) by granting a PhD scholarship to conduct part of the research in the United Kingdom. The research activities were conducted at the "Escola Politécnica" in the University of São Paulo (USP) with a one year period in the University of Southampton in the UK. The activities in the UK were conducted at the Institute of Sound and Vibration Research (ISVR) inside the Rolls-Royce University Technology Centre (UTC) in Gas Turbine Noise group. The work done in the UTC also contributed to part of a research programme called SYMPHONY, funded by the UK Technology Strategy Board (TSB), which involves collaborative work with Rolls-Royce, QinetiQ, Cambridge and Loughborough Universities, among others. SYMPHONY support activities on liner optimization for intake and bypass ducts, near-field open rotor noise, bleed valve noise, non-symmetric jet nozzles and installation effects.

The thesis is divided into eight chapters and two appendices as described below:

Chapter 1 gives an introduction to the problem represented by aircraft noise to society and it addresses the question of why noise became an important barrier for air traffic growth.

The motivation of this thesis and the main contributions of the author to the jet prediction area are also described.

In Chapter 2 an overview of some important concepts of acoustics and aeroacoustics is presented. The physics related to a jet flow and the noise generated by it is presented. The most relevant aspects of the noise generation and propagation to the far-field of single, coaxial and asymmetric nozzles together with engine-aircraft installation effects are identified. In addition, some design concepts for low jet noise currently under investigation are described.

Chapter 3 is devoted to presenting the sound propagation model used in the LRT method to simulate and calculate the effects of sound-flow interactions. The strategy used for solving the propagation problem is based on a geometrical acoustics theory called Ray-Tracing. Details of Ray-Tracing Theory are presented together with the methodology developed for generating the noise sources, procedure for launching the rays and the delta SPL concept.

Chapter 4 presents the mathematical model derived in this thesis for predicting noise generation and radiation from a jet flow. The basic concepts necessary to derive the LRT method are presented. First, Lighthill's Acoustic Analogy and its main limitations are described. Then, discussions about the improvements made by introducing Lilley's Equation (which is used in the MGBK code) in which Lilley separated the propagation effects from the source term together with its main limitation are presented. Finally, the LRT formulation showing all the equations and assumptions made throughout the method are provided. In addition, the necessary input information, the method applicability and a block diagram of the computational sequence for noise predictions are also presented in this chapter.

Chapter 5 presents the LRT noise predictions for a single stream jet operating at different flow conditions. Two experimental databases, acquired from different facilities,

were used to verify the LRT applicability. The results shown in this chapter validates the proposed method for predicting the noise from both isothermal and heated single jets. Moreover, Chapter 5 results show that the LRT method is able to produce better noise predictions than the well-known MGBK method, especially for shallow observer angles. This implies that the LRT method provides a better sound directivity prediction, for the angles outside the zone of silence, as it has the capability of accounting for the refraction effects generated by the sound-flow interaction. It is important to point out that the results shown for the sound refraction in this thesis are, as far as the author and the ISVR group know, unique.

Chapter 6 is devoted to investigate dual stream jet flows, which is the major application on modern engines for commercial aircraft. The LRT method was applied to predicting the noise from a large range of nozzle configurations and flow conditions. Nozzles with different area ratios, with long-duct and short-cowl configurations, different velocity ratios between the primary and secondary streams and different Mach numbers were investigated. Numerical predictions for noise in the far-field, sound directivity and refraction effects are presented.

Chapter 7 presents the results of the ultimate test for the LRT method. The LRT is used for predicting the noise from complex asymmetric nozzles and also to investigate the effects of the pylon interaction with a jet. In these cases, the noise propagation from each source throughout the jet flow region is significant to the far-field predictions and therefore the Ray-Tracing results make a significant contribution to the noise predictions. The main objective of Chapter 7 is to show the capability of the LRT method to capture these modifications on the noise generation and propagation mechanisms when asymmetries are present in the problem. The geometries, operation conditions and experimental data were obtained from the SYMPHONY project.

Finally, Chapter 8 presents the conclusions of this work. The advantages and disadvantages of using the LRT method for noise predictions are summarized as well as the suggestions for future work, aiming to continue with the development of the methodology described.

Appendix A gives a general overview of the use of Computational Fluid Dynamics (CFD) as a numerical tool to calculate the mean and turbulence quantities of a jet flow by using a Reynolds Average Navier-Stokes (RANS) methodology. These results are used only as input information to the LRT methodology. Some of the numerical aspects, such as mesh, turbulence model and boundary conditions used are described.

Appendix B provides the geometry details of the coaxial nozzles used in Chapter 6. These nozzles were used in a series of jet noise measurements made in 1989 and 1993 on coplanar nozzles in the NTF at QinetiQ and these data is used to corroborate the LRT predictions.

Chapter 2: Bibliography review

This chapter presents some basic concepts of aeroacoustics and computational aeroacoustics that will be required in the remaining chapters of this thesis. It also presents a general description of the theory related to jet flow and the noise associated with it. A review of the main characteristics of the noise generation process and propagation to the far-field for single, coaxial and asymmetric jets is presented and discussed.

2.1 Introduction and basic definitions

2.1.1 Noise levels

There are different forms for measuring noise and annoyance, such as sound pressure level, power spectra density, band level, A-weighted spectrum, perceived noise level (PNL), effective perceived noise level (EPNdB) and many others. We discuss the scales used in this thesis to present the noise results from the numerical predictions and the experimental data presented.

It is customary in acoustics to describe sound pressures and intensities using logarithmic scales known as sound levels. One of the reasons for this is the huge range of the human audible intensities which varies from 10^{-12} to $10\ \mathrm{W/m^2}$. The sound pressure level (*SPL*) is one of these scales and it is defined by

$$SPL = 20\log(P_e / P_{ref}) \tag{2.1}$$

where *SPL* is expressed in dB, P_e is the measured effective pressure amplitude of the sound wave and P_{ref} the reference effective pressure amplitude. The reference pressure in air is ostensibly the audible limit of the human ear, with a value defined as $P_{ref} = 20\mu\mathrm{Pa}$.

The decibel pressure levels in acoustic noise spectra are not always provided in terms of narrow-band data, i.e., pressure levels at each and every frequency. Instead, they can be presented over bands of width Δf (f being frequency). The one-third octave band filter is commonly used to analyze the noise from subsonic jet flows as it does not contain strong tones and also the noise levels are approximately independent of the filter bandwidth. Details of this filter will not be presented here but the convention for the one-third octave bands can be found in the European norm EN60651. When pressure levels are provided as octave bands, it is convenient to measure the overall acoustic noise intensity. The overall sound pressure level (OASPL) provides just such a measure and, for one-third octave band specifications, it can be calculated as the decibel equivalent of the root sum square pressure.

2.1.2 Radiation of Sound and noise sources

2.1.2.1 Monopole

A point source is called monopole if it is compact and the generating motion has no preferred direction producing a wave which spreads spherically outward as depicted in Fig. 2.1. If the medium is infinite in extent, the wave-front will depend only on the distance r from the centre of the source. The monopole source can physically be understood as a pulsating sphere (more specifically, if the diameter of the sphere is small compared with the wavelength of the sound radiated) which can alternately expand and contract.

2.1.2.2 Dipole

A dipole can be created by superposing two monopoles, close together, with opposite sign and equal in magnitude. The sound field of a harmonic dipole can be represented as an oscillating sphere being moved from the one source point to the other. The directivity of the sound pressure is shown in Fig. 2.1. The pressure reaches maxima for the angles 0 and 180 degrees, while it vanishes for 90 and 270 degrees.

2.1.2.3 Quadrupole

Quadrupoles can be created by superposing two opposite dipoles. There are two possibilities: Lateral Quadrupole or Linear Quadrupole. In a lateral quadrupole arrangement the two dipoles do not lie along the same line. The directivity pattern for a lateral quadrupole is depicted in Fig. 2.1. The regions where sound is cancelled shows up along the diagonals and there is also a 180 degrees phase difference between the horizontal and vertical wave-fronts.

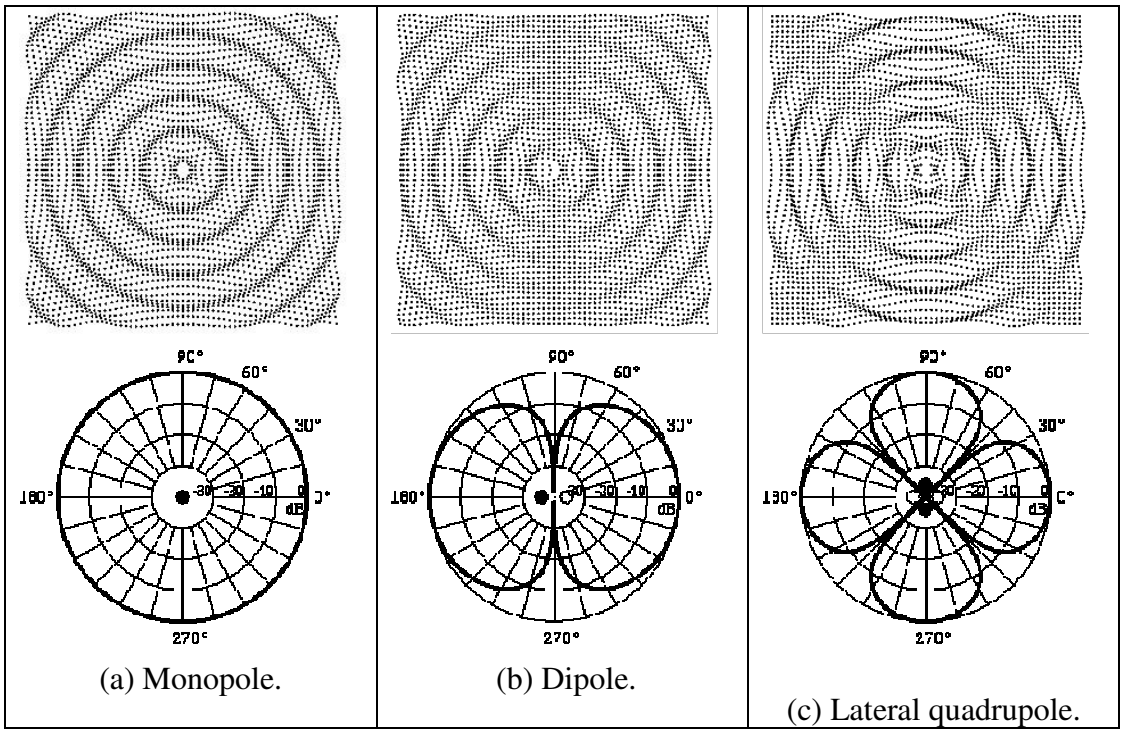

(a) Monopole. (b) Dipole. (c) Lateral quadrupole.

Figure 2.1 - Noise directivities patterns of a monopole, dipole and quadrupole point sources.[4]

2.2 Jet noise theory

The problem related to community noise due to aircraft powered with jet engines is not something new. According to Lilley [8] this issue was already being discussed in the late

[4] http://paws.kettering.edu/~drussell/Demos/rad2/mdq.html

1940s. At that time, aircraft engineers were aware that the future of the jet engine as a power plant for civil aircraft was dependant on methods that could be designed to limit its noise. It is possible to identify different types of noise sources on an aircraft. However, jet noise is still the major component of total aircraft noise at takeoff and climb conditions even for high bypass ratio turbofan engines.

After more than sixty years of dedicated research on jet noise it is fair to say that a lot of insights on the physics mechanisms of source generation and also sound propagation have been achieved. The aim of this section is to present a review of experimental and numerical research that contributed effectively to generate ways and technologies for understanding and reducing jet noise and therefore reducing engine noise.

2.2.1 Noise from single stream jets

Before starting the discussion on the noise generated by a jet, it is perhaps, convenient to first introduce an overview of the main concepts regarding the fluid-dynamics of a jet flow. According to List [9], a turbulent jet can be defined as fluid flow produced by a pressure drop through an orifice, in other words, a jet occurs when a relatively high speed flow of a fluid is injected into a larger ambient mass of the same or different fluid. The flow structure of a turbulent jet has been studied extensively by many experimentalists due to its vast application such as cleaning jets, valve flows, turbine exhaust and aero-engines.

Figure 2.2 shows two spark shadow photographs of a mixing layer at two different Reynolds number. The first picture shows nitrogen flowing at 1000 cm/s mixing with a helium-argon mixture at the same density flowing at 380 cm/s under a pressure of four atmospheres. The second picture shows the same flow but now at a Reynolds number twice that of the first regime. As can be seen, the jet flow structure is formed basically by a combination of small and large-scales turbulence structures. Doubling the Reynolds number

has produced more small-scale structure without significantly altering the large-scale structure.

A very straightforward description of a single jet flow structure is given by Goldstein [10]. Consider a high-Reynolds-number air jet issuing from a convergent nozzle into a stationary fluid, as shown in Fig. 2.3. As the jet leaves the nozzle, an annular mixing layer forms between the moving fluid and its surroundings. The flow in this region becomes turbulent within about one-half of a jet diameter downstream. It then spreads linearly in both directions until it fills the entire jet around five diameters downstream. Since the motion remains laminar within the conical domain enclosed by the turbulent flow this region is usually refered to as the potential core. Once the mixing layer fills the jet its uniform growth ceases and it evolves differently as it passes first through a transition region and finally, around eight diameters downstream, into a region of self-preserving flow called fully developed region.

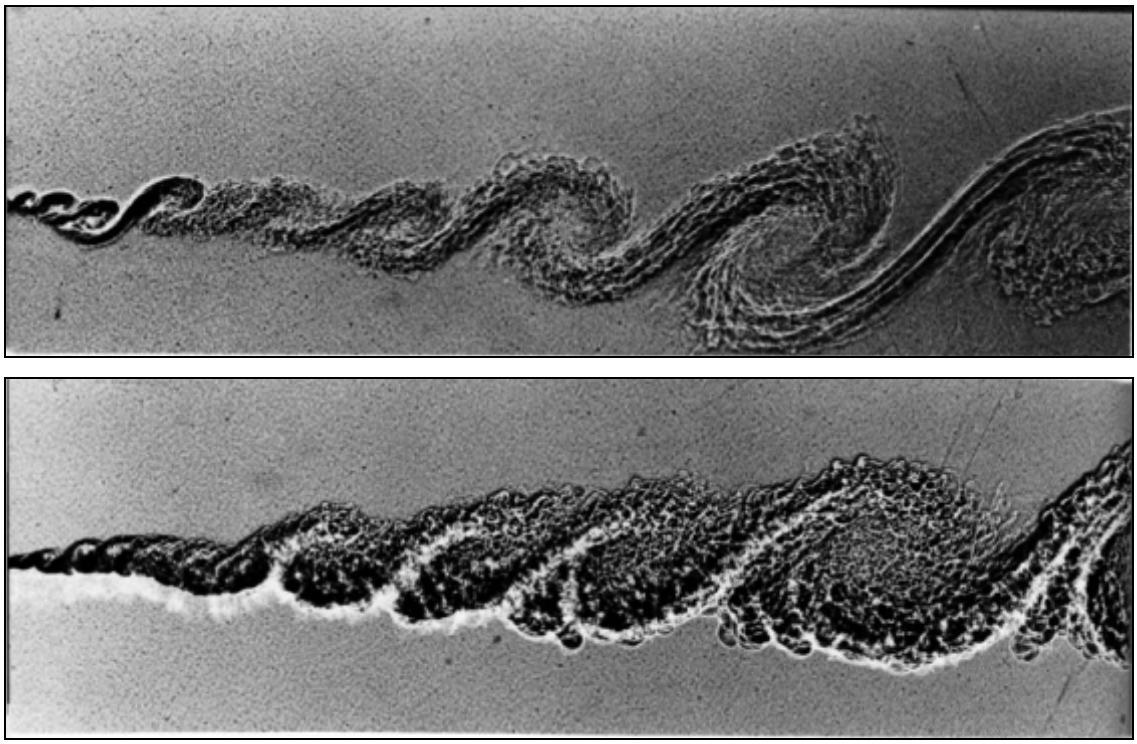

Figure 2.2 – Large and small-scales turbulence structures in a turbulent jet. (From Van Dyke [11]).

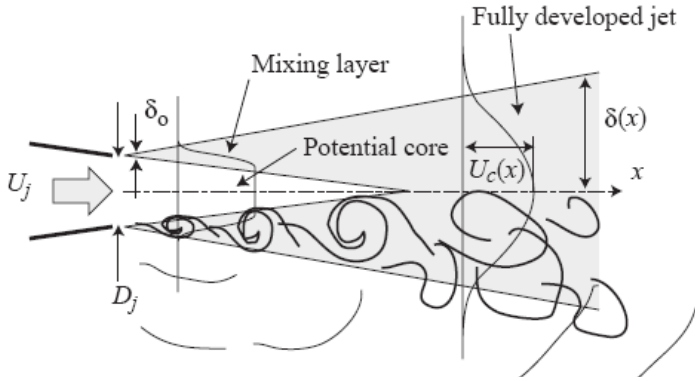

Figure 2.3 - Single stream jet structure. (Modified from Colonius and Lele [64]).

Despite identification of jet noise as an important by-product of the newly invented jet engine (Morley [12]), and as an impediment to the incipient commercial jet aircraft industry in the 1950s (Lighthill [13]; Lassiter & Hubbard [14]; Lighthill [15]; Lassiter & Hubbard [16]), a completely satisfactory description of jet noise has proven elusive. According to Bodony and Lele [17], two primary reasons for this difficulty are the lack of a universally agreed-upon theory of noise generation in turbulent flows and the challenge in taking experimental measurements in high-speed jets. Regardless, significant progress has been made on some of the theoretical descriptions of jet noise (Lighthill [13, 15]; Lilley [18]; Goldstein [19], for example) and in its experimental characterization (Davies *et al.* [20]; Bradshaw *et al.* [21]; Tanna [22, 23] and Viswanathan [24], for example).

As a consequence of these efforts, it is now largely accepted that jet noise is related to four basic components: 1) fine-scale fluctuations; 2) large-scale coherent structures; 3) screech tones; and 4) broadband shock-noise. The last two mechanisms are present only for supersonic jets, which is not within the scope of this thesis. For subsonic jets, the nature of the noise spectrum is broadband. Figure 2.4 presents typical subsonic jet noise spectra, measured experimentally, at 90º from the jet exhaust centreline for different jet velocities.

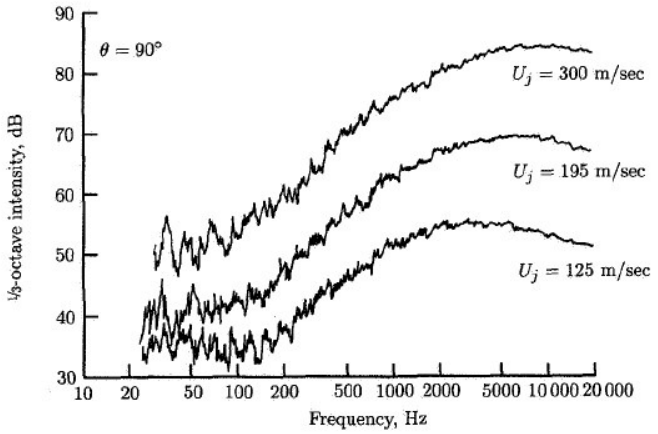

Figure 2.4 - Jet noise spectra at 90 degrees for various jet velocities. (From Hubbard [25]).

Undoubtedly, much of the advance in acoustic analysis has recently arisen due to the spectacular advance in both numerical techniques and the computing machines efficiency that were achieved in the last two decades. The jet noise problem have benefited immensely from the development of the field known as Computational Aeroacoustics. Nowadays, several groups of researchers are focused on developing numerical methods for the investigation of jet noise production and propagation. As an example, Fig. 2.5 presents the noise computations performed by Uzun *et al*. [26] for a Mach number 0.9, Reynolds number 400,000 jet using a LES (Large-Eddy Simulation) approach. This is a good example of a computational aeroacoustics investigation of a jet flow where it is possible to visualize both the flow dynamics and the sound that is being propagated to the far-field.

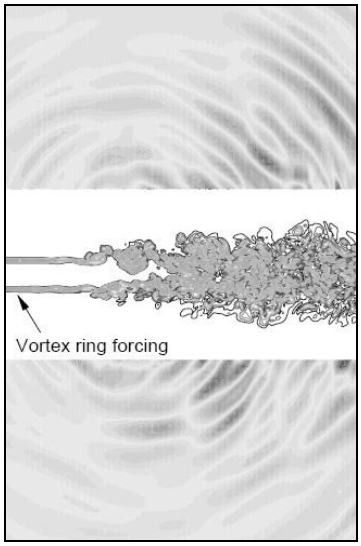

Figure 2.5 - Vorticity magnitude contours from a LES simulation of a jet flow. (Modified from Uzun *et al.* [26]).

2.2.2 Noise from coaxial dual stream jets

As a consequence of the continuous increasing restrictions on aircraft generated noise, many experimental tests in conjunction with analytical studies were carried out in order to gain and improve insights and knowledge of the noise generation mechanisms within a jet flow. One of the most important achievements on noise attenuation was the introduction of the coaxial bypass engine, also referred to turbofan engine. Figure 2.6 (a) depicts a schematic of the main parts of a turbofan engine, where *HP* and *LP* refer to high-pressure and low-pressure, respectively. Figure 2.6 (b) shows a modern turbofan engine installed on a Boeing 787 Dreamliner aircraft.

Historically, the turbofan engine was developed in order to achieve better propulsion efficiency at the high-subsonic cruise velocities, which is the velocity range important to civil aviation. At these flight-conditions (around Mach number 0.8 and high altitudes) the turboprop and turbojet engines alike operate at low efficiency, as the flight speed is too high for the turboprop but low to the turbojet [27].

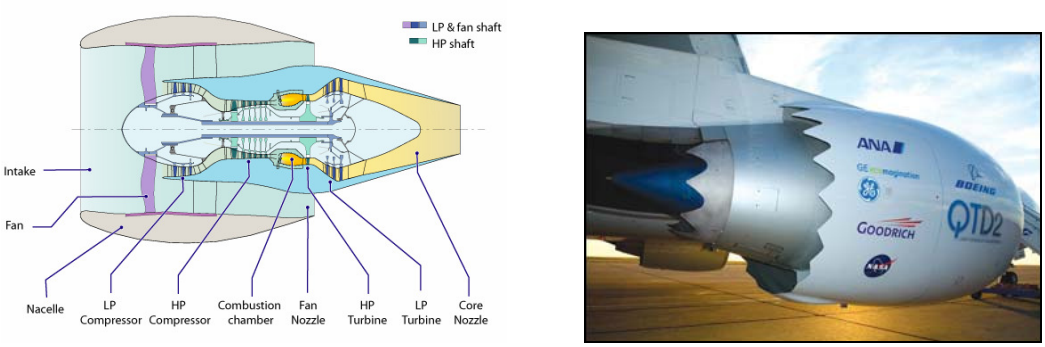

(a) Turbofan engine schematic. (b) Real turbofan installed on an aircraft.

Figure 2.6 - High bypass aircraft engines.

The turbine section of a turbofan is designed to absorb more energy from the hot gas than would be necessary to drive the compressor alone. The excess shaft power is used to drive a fan, a low-pressure compressor of a larger diameter arranged upstream of the main compressor. Part of the air entering the engine intake bypasses the inner or core engine and expands in a separate nozzle to provide “cold” thrust with low exhaust velocities. The amount of air that is bypassed in relation to the air that passes through the core engine is called the bypass-ratio. In very high-bypass engines the fan flow is responsible for more than 85% of total engine thrust. The turbofan has emerged as the most common type of gas turbine engine for aircraft propulsion, especially the high bypass-ratio engines, due to the increasing public awareness of atmospheric pollution, in particular aircraft noise [3].

The noise reduction achieved by the turbofan engine is a direct consequence of Lighthill’s eight power relation for jet velocity and noise, as will be shown in Eq. (4.12). The addition of a secondary stream of relatively low exhaust velocity (bypass flow) reduces the shear with the external flow compared to a single jet hence resulting in a direct noise reduction.

The following subsection presents the noise characteristics of a coaxial jet related to the turbulence structures that are present on the flow. The concepts that will be presented next are going to be investigated using the LRT method.

The aerodynamic development and noise generation in dual-stream nozzles are very complex and still require extensive research effort. Several parameters such as the stream temperatures, the nozzle geometry, the velocity ratio and the inflow conditions have significant effects on the physical mechanisms taking place within these jets. Important insights were provided by Ko & Kwan [28] in their experimental investigation of the initial region of a coaxial jet, identifying three mixing regions, which corresponds to three different noise source generation regions. These authors then proposed that coaxial jets can be considered as combinations of several single jets, an idea later used by Fisher *et al.* [29] to formulate basic noise models.

Figure 2.7 shows a sketch of the structure of a coaxial jet from the aero-engine noise point of view. According to Fisher *et al.* [29] three different regions can be identified. First, an Initial region, close to the nozzle, contains the potential cores of both the primary and secondary jets. In this region two shear layers are formed: a shear layer from the interaction between the primary and secondary flows, and a shear layer from the interaction between the secondary flow and external (ambient) air. In the far downstream region of the jet, beyond the end of the potential core of the primary jet, a mixed-flow region is generated where the flow will approach that which would pertain if the primary and secondary jets had been mixed at the nozzle exit plane. Between these extremities, there is an interaction region where the primary and secondary shear layers interact, forming a very complex set of flow dynamics. Within this zone there is one shear layer extending radially from the primary potential core to the ambient air. The size of each region is strongly dependant on the velocity ratio (VR) between the primary (Vp) and secondary (Vs) stream velocities as presented in Eq. (2.2). Another important parameter on the flow structure of coaxial nozzles is the area ratio (AR) between the primary (Ap) and secondary (As) nozzle areas as presented in Eq. (2.3).

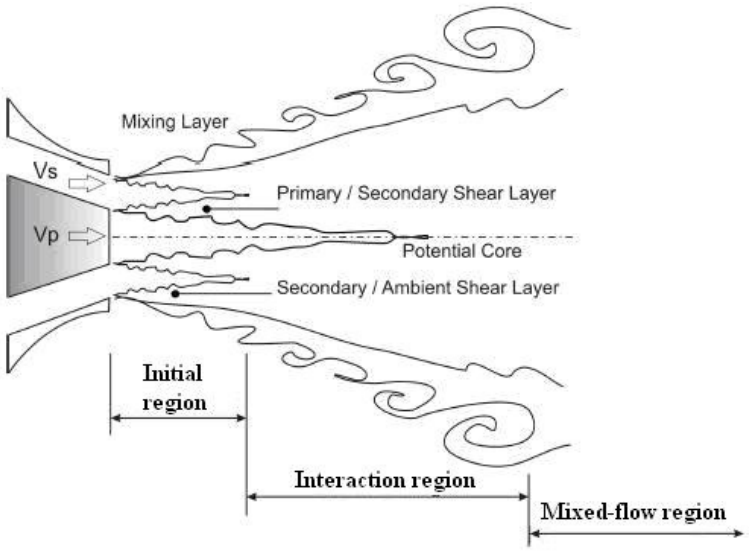

Figure 2.7 - Noise-producing regions for a coaxial jet. Modified from [30].

$$VR = \frac{Vs}{Vp} \tag{2.2}$$

$$AR = \frac{As}{Ap} \tag{2.3}$$

The character of the noise from these regions can be related to the fine-scale and large-scale turbulence structures in the flow, as follows [29]:

- The outer part of the initial region, where the secondary jet shear layer mixes with the ambient air, behaves as the initial part of a single-stream jet characterized by the secondary jet velocity, temperature and nozzle diameter. This region is of practical significance due to the presence of the small scale turbulence structures responsible for generating high frequency, and hence subjectively important, noise which will dominate the jet noise as the velocity ratio approaches unity. The shear layer between the primary and secondary flows in the inner part of this region is similar to the initial part of a single stream jet in flight condition and the noise source strength is a function of the relative jet velocity (*Vp*-*Vs*).

- The so-called interaction region in which the primary and secondary shear layers merge is still not completely understood. There are no known simple set of parameters to characterize the acoustic properties of this important noise-producing region.
- In the mixed-flow region, it is the mixed jet velocity, temperature and diameter that characterize the noise. This region is the principal source of the coaxial jet noise at low frequencies.

2.2.3 Complex jet flows

Focused program on jet noise research and development of nozzle designs for low noise have been underway in both Europe and the USA in the last decade. A large amount of research has been done on jet engine nozzles to improve the mixing of the shear layers, for instance the addition of chevrons has given noise reductions up to 2.5 EPNdB, [31-35].

Other concepts and ideas have also been pursued during the last few years. Papamoschou investigated experimentally a large number of different modifications on the nozzle by offsetting the flow either from the core or the by-pass stream with the aim of creating a virtual shield for the noise sources in both flyover or sideline conditions. Papamoschou reported very positive results and showed the potential of the offset concept for jet noise reduction, [36-39]. Zaman and Papamoschou [40] also investigated offset fan stream nozzles with an eccentric nozzle and found favourable noise reduction. Figure 2.8 shows an example of SPL reduction that can be achieved with an eccentric nozzle configuration with respect to a single and a coaxial jet. In an eccentric configuration, the axis of the primary (inner) nozzle is offset with respect to the axis of the secondary (outer) nozzle which produces an asymmetry in the flow. Significant noise reduction occurs in the direction of the thickened low-speed flow region on the underside of the core jet, and also in the sideline directions.

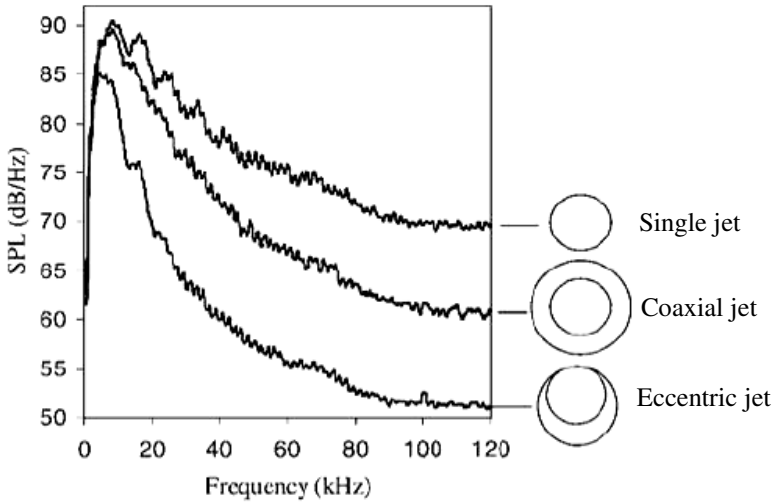

Figure 2.8 - SPL reduction of a coaxial jet and eccentric jet with respect to single jet. (From Shupe [41]).

There is no doubt that there are still room for jet noise reduction but the huge challenge imposed to engine manufacturers is to reduce jet noise without affecting the engine thrust and weight. Another important constraint regards to the engine installation on the aircraft, which means that any new design for jet noise reduction must be "clean" enough to avoid geometric interference with the aircraft devices, such as pylons, wing and landing gear. The next section will present some of the devices and concepts for reduced jet noise that have been studied. Most of them are already being applied to aircraft engines

2.2.4 Devices and concepts for jet noise reduction

According to Viswanathan [42], as a turbofan engine generally has separate nozzles for core and fan flows, it offers many possibilities for noise reduction since noise reduction strategies can be applied to either stream or both simultaneously. Numerous concepts such as the incorporation of vortex generators, tabs, serrations and other mixing devices, offset and non-concentric nozzles, thermal shielding, etc. have been investigated in the past years. In addition, there are some papers focusing on the aeroacoustics study of the noise from non-

conventional nozzles, such as rectangular, square and beveled nozzles, with the aim to investigate possible noise reductions. For completeness, some of the devices mentioned above will be briefly presented in this section.

2.2.4.1 Rectangular Nozzles

Research using both numerical and experimental techniques suggests that rectangular nozzles can reduce jet noise generation compared to their circular counterparts. For instance, Paliath and Morris [43] showed numerically (for an arbitrary aspect ratio) that at lower frequencies the noise spectra is slightly quieter than the circular nozzle, showing reductions up to 2dB on the peak frequency; while at higher frequencies the noise levels are similar. However, more detailed investigation regarding the physics mechanisms, such as, turbulence, vortex development, entrainment rate and noise distribution of rectangular jets are still needed. Rectangular nozzles are extensively used on high performance military applications. By enhancing mixing in the shear layer, the hot exhaust from the jet is able to mix more quickly with the cool ambient air that removes a significant amount of the heat signature of the jet, thus increasing stealth capabilities of these types of aircraft. Figure 2.9 depicts the use of rectangular exhausts for the military aircraft F22-A Raptor.

Figure 2.9 - The rectangular engine exhausts from a F22-A Raptor aircraft.[5]

[5] http://russiadefence.englishboard.net/t183p120-pak-fa-t-50-news

2.2.4.2 Chevrons

Chevron nozzles have drawn a lot of attention recently due to their noise reduction benefits and are currently one of the most popular jet noise reduction devices. Most of the commercial aircraft equipped with modern turbofan engines have chevrons on the end of their core nozzle and more recently also on their bypass duct. According to Bridges and Brown [34], chevrons typically reduce the low frequency noise at aft angles while they increase the high frequency noise at broadside angles relative to the jet. However, when it comes to aircraft noise, the high frequency noise is more efficiently absorbed by the atmosphere which therefore provides a net benefit from the noise point of view when chevrons are used.

The main effect of the chevrons is to modify the flow structure of the jet early upstream the flow, i.e., near the nozzle exit. The streamwise vorticity generated by this device enhances the mixing in the shear layers of the jet, which leads to a decrease or increase in noise over certain frequency ranges. Figure 2.10, shows an example of an engine with chevrons installed. As can be seeing in this figure, the geometry of the serration is not uniform around the nacelle which increase further the flow dynamics complexity and hence the physics of the noise sources and also the propagation path of the sound through the flow.

Figure 2.10 - Chevrons installed on the engine and nacelle from a Boeing 787 aircraft.[6]

[6] http://www.nasa.gov/topics/aeronautics/features/trl_demystified.html

Figure 2.11 presents a Lobe nozzle which is another type of passive device that also modifies the jet turbulence mixing noise and provides noise benefits. This kind of application is more common in small engines with low-bypass ratio and with long duct nacelles such as the ones used on the Embraer ERJ145 aircraft.

Figure 2.11 - The back end of a Williams FJ-33 turbofan showing the application of the mixer for jet noise reduction.[7]

Intuitively one would imagine the massive impact of adding these passive control devices for noise reduction on the flow dynamics of the jet. To support this, Fig. 2.12 presents the numerical results obtained by Birch *et al.* [44] where cross-sections of the flow from a chevron nozzle and a single round nozzle are shown at two axial stations. As can be seen, the differences between these two cases are notable. At an *x/D* of 1.0 the chevrons strongly distort the mixing layer to form a star shaped cross-section that greatly increases the contact area between the jet and the external flow. Further downstream at an *x/D* of 3, the continuing mixing of the shear layers causes the flow in the "arms" of the star to merge to again form a quasi-round mixing layer.

[7] http://picasaweb.google.com/lh/photo/jOg579bkPwWutdgWJEeTZA

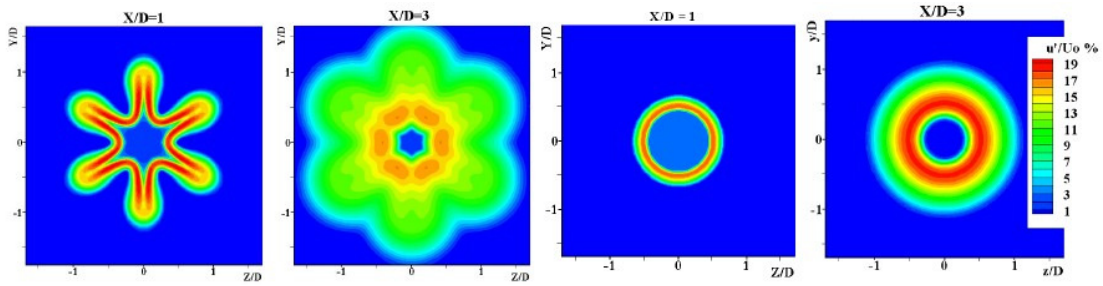

Figure 2.12 - Contours of turbulence levels for chevron and round nozzles at x/D = 1 and x/D = 3. (From Birch *et al.* [44]).

Due to the complexity on the flow involved with the use of chevrons and lobe nozzles, traditional predictions methods present deficiencies for correctly predicting the noise generated by the jet. The work of Engblom *et al.* [45] presents an example of applying the MGBK method, which will be presented in Chapter 3, to predicting the far-field acoustics from a jet with chevrons, resulting in discrepancies in the noise level predictions. Other prediction methods specifically designed for chevron nozzles are available in the literature, such as the one proposed by Stone *et al.* [46-48] where a semi-empirical model was developed. But still, the predictions are limited to certain jet operation conditions and also have geometric constraints (number of lobes) as the method was developed based entirely on experimental data.

The next two nozzle concepts, Beveled and Offset, that are presented in the sequence not only aim to modify the generation of sound, by changing the distribution and strength of the noise sources on the jets, but they also intend to modify the acoustic propagation path.

2.2.4.3 Beveled Nozzle

The beveled nozzle, illustrated in Fig. 2.13, has been focus of aeroacoustics investigations in the last years. This concept arose from the engine manufacturer desire to develop a novel type of nozzle that could be simple and “quieter” but also that could not led to penalties to the engine, such as thrust degradation, weight increase and issues with manufacturability.

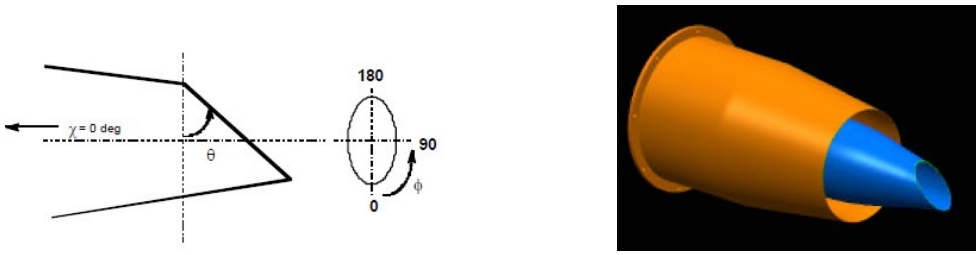

(a) Sketch of a beveled nozzle. (b) Beveled nozzle.

Figure 2.13 - Beveled concept for noise reduction from dual-stream jets. (From Viswanathan *et al.* [42]).

Figure 2.14 shows the LES numerical results from Viswanathan *et al.* [49] of magnitude of density gradient for a supersonic jet flow in a round and in a beveled nozzle. As can be seen, the beveled nozzle altered the flow pattern significantly. In their paper, Viswanathan *et al.* [49] report that a strong azimuthal variation of the noise field is introduced for the beveled nozzle with a jet noise reduction (compared to a round jet) being achieved in the azimuthal directions that are below the longer lip of the beveled nozzle. There is still a need for more experimental and numerical studies for the beveled nozzle in order to access the noise reduction for an installed configuration. This is especially true for wing-mounted engines as the interaction between the jet and the wing could be enhanced and therefore increasing the total aircraft noise.

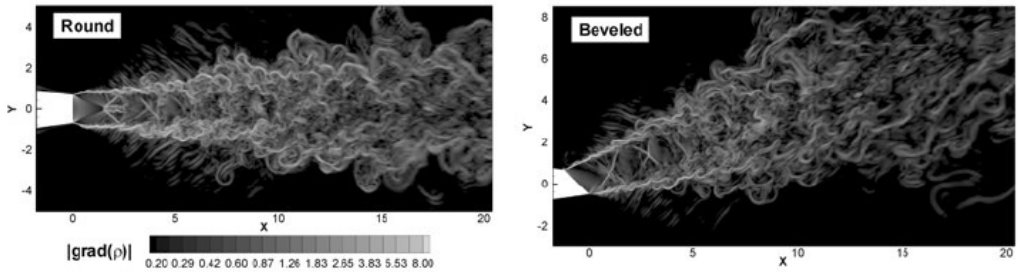

Figure 2.14 - Snapshot of magnitude of density gradient ("numerical schlierens") for a round and a beveled nozzle (bevel angle of 45º). (Adapted from Viswanathan *et al.* [49]).

2.2.4.4 Offset Nozzle

A series of investigative tests have been made of a number of noise reduction concepts during the 90s in the UK. The objective was to identify new techniques for reducing high-bypass ratio jet noise. The concern at that time was related to the aero-mechanical design limitation on the engines by increasing the bypass ratio even more. It is worth mentioning that this is still an issue nowadays. The results showed that one of the most promising concepts for noise reduction is offset nozzles. It was reported [50] that offsetting the core jet in the bypass flow implies changes in the refractive properties of the jet and, as a consequence, modifications in the noise field. In addition, due to the changes in the turbulent flow structure, the offset nozzle can also alter the mixing noise source strength and its spatial distribution providing significant reductions in the spectral levels relative to the zero offset build. This, however, is only true for an observer on the side of the jet having the largest clearance between the core and bypass nozzles.

Directional noise reductions were also reported by researchers at the University of California, Irvine (UCI) who investigated offsetting the core stream relative to the fan flow [51]. The work conducted at the UCI, led by Papamousch, on investigating the noise benefits using nozzles with an "offset stream" concept has inspired a research program at NASA in the USA called Offset Stream Technology (OST). The concept involves diverting the outer annular stream to one side with respect to the primary stream. When this is done, according to Zaman *et al.* [52], less noise is heard on the thicker annular side relative to the noise of the concentric case.

During the OST different nozzles concepts were tested in order to evaluate possible noise benefits. Flow-field and acoustic measurements were taken of the offset stream nozzles using vanes, S-ducts, and wedges to achieve the offset fan stream. The nozzles were all designed to reduce the impact of the jet noise generated by a separate flow engine by using

the engine geometry itself to alter the directionality of the sound produced. In all the concepts designed, the objective was to modify the fan stream to favorably modify the propagation of sound generated by the fan-core shear layer on one side of the jet. Brown *et al.* [53] reported that the offset jets tested during the OST generally had higher turbulent kinetic energy (TKE) near the nozzle exit and a more rapid decay of peak axial velocity when compared against the concentric baseline jet. They also found directional noise reduction depending on the jet operation condition and the ambient medium. The conclusion from the OST was that the offset stream technologies have a future for noise control in certain engine applications, especially for lower bypass ratio jets.

As has been seen, most of the investigations of offset nozzles in the past were done experimentally, probably due to the complex geometry and flow characteristics and also because of the lack of efficient numerical tools at that time. But recently, with the increasing desire to design low noise nozzles, numerical studies of offset nozzles are being conducted. Figure 2.15, for example, shows the numerical results of turbulent kinetic energy for a coaxial axisymmetric nozzle and an offset nozzle that was obtained by Dippold *et al.* [54]. From this result, it is clear that by offsetting the core stream relative to the jet centreline the flow becomes completely asymmetric.

One of the complex flow cases investigated in this thesis using the LRT method includes the effects of the interaction effects of the pylon with a jet flow. This type of problem is often refered to in the literature as the Propulsion Airframe Aeroacoustics (PAA). This is a practical and very difficult problem that must be tackled during the development phase of a new aircraft. Due to the flow-structure interaction, there are asymmetries properties of the flow which affects the noise generation and propagation. This type of problem also demonstrates the inadequacies of standard noise prediction methods and the need to develop new techniques. The next subsection is devoted to give a brief overview of PAA.

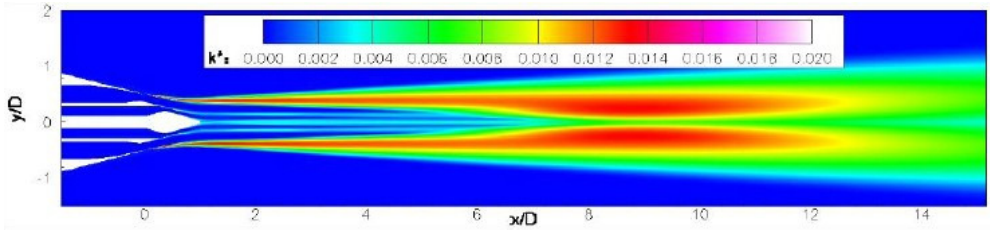

(a) LARC baseline nozzle – coaxial axisymmetric nozzle.

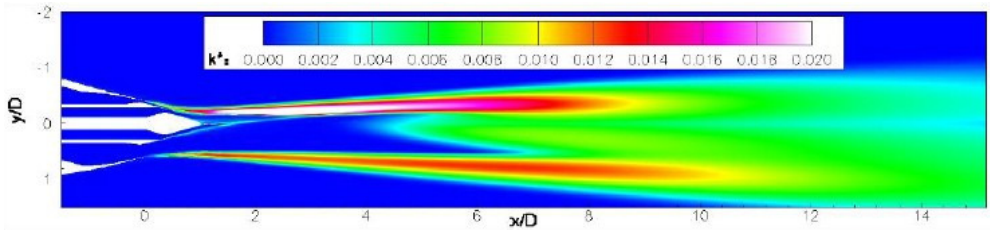

(b) Sduct-LaRC-93 nozzle – offset nozzle.

Figure 2.15 - Turbulence contours of a baseline coaxial nozzle and an offset nozzle. (From Dippold *et al.* [54]).

2.2.5 Propulsion Airframe Aeroacoustics

Engine airframe integration is defined as that process which is used whenever the performance of the integrated engine and airframe, when operated in a designed combination, is significantly different from the sum of the individual engine and airframe performances, that is, for given values of flight Mach number, angle of attack and power setting [55]. Nicholson [56] affirms that "the aircraft cannot be conceived first and the propulsive units considered afterwards". The focus in design of an aircraft must not rest too long on the individual components or the integration process will be entered too late and then the production can get very costly in time, manpower and in terms of lack of performance achievement. To a very large degree, it can be argued that the engine airframe integration process is at the heart of the overall aircraft design process.

As well as aircraft performance, it is now generally recognized that engine installation effects can significant change the noise of an isolated jet, affecting therefore the total external noise of the aircraft. Several different types of mechanism can be present in PAA, Fig. 2.16

illustrates two of them that can be observed statically for an under-wing installation. There are also effects that include jet interactions with both the pylon and the wing as depicted on Fig. 2.17.

According to Thomas and Kinzie [59], PAA has been underdeveloped and it represents an area of opportunity for noise reduction technology for conventional configurations. This opportunity includes both reducing the noise sources that arise specifically from integration of propulsion and airframe and also using the installation itself as a means to reduce noise of a particular airframe or propulsion source by shielding the noise. In this context, PAA became of major interest to aircraft and engine manufactures investigating design of low noise aircraft.

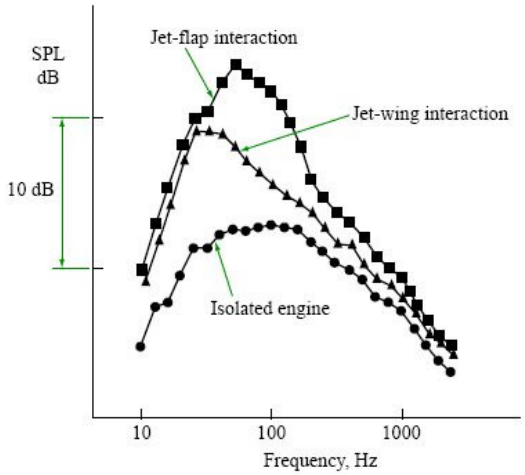

Figure 2.16 - Under-wing installation effects on noise for a static aircraft. (From [57]).

Similarly to the passive control devices presented before, the addition of the pylon on the jet flow strongly modify the fluid dynamics of the problem. Figure 2.18 shows the numerical result from Birch *et al* [60] of the flow-field of coaxial nozzles without and with a pylon. Although the changes presented in Fig. 2.18 between the two nozzles depends on the detailed geometries (nozzle and pylon) and on the jet operation condition, typically the

addition of the pylon turn the flow completely asymmetric. Due to this extremely complicated characteristic, which again influences source generation and propagation, according to Birch *et al* [60], there are significant differences in the results reported by different workers for the jet-pylon interaction effects and the reasons for these differences is not well understood.

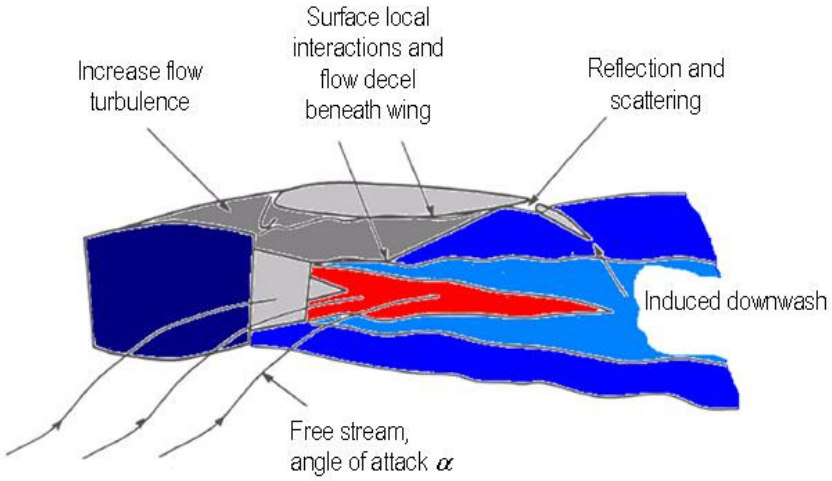

Figure 2.17 - Schematic of potential PAA effects. (From Elkoby [58]).

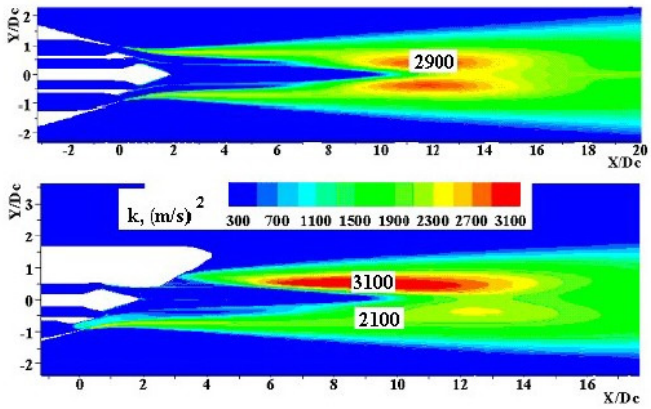

Figure 2.18 - Fields of turbulence energy along a coaxial nozzle jet without and with the pylon. (From Birch *et. al* [60]).

Finally, understanding PAA requires the development of noise predictions methods that can account not only for the complex flow structure modification but also sound propagation. The LRT method is applied to evaluate its applicability to a jet-pylon interaction

problem. The term jet-pylon interaction generally refers to the noise difference between the jet from an isolated nozzle and the jet from a nozzle pylon combination.

Further noise reduction is mandatory if the growth in the transportation system is to be accepted by people and their political representatives. To achieve this, the design process in industry needs support from computer-based noise predictions tools. Based on that, a relatively new approach called computational aeroacoustics (CAA) has come into sight. The next section will present a general overview of the main concepts of CAA.

2.3 Computational AeroAcoustics (CAA)

Since the pioneering work of Lighthill [13, 15], a large amount of research has been focused on understanding and evaluating the physics involved with flow-generated noise, known as aeroacoustics. The study of flow-induced noise is concerned with the sound generated by turbulent and/or unsteady vortical flows including the effects of any solid boundaries in the flow. Special attention has been given to numerical simulation approaches for solving aeroacoustics problems, encouraged mainly by the amazing success of CFD applied to aerodynamics.

An overall goal of computational aeroacoustics is to predict the sound radiated by a turbulent flow, and perhaps more importantly, to investigate strategies by which noise could be reduced. However, as discussed by Tam [61], aeroacoustics problems are substantially different from those of traditional fluid dynamics and hence they require independent re-evaluation and development of numerical schemes and methods. According to Colonius [62], some of the difficulties in CAA arise because (i) the flows of interest are usually turbulent and involve a range of length and time scales that are difficult to resolve in a numerical computation, (ii) the flows of interest stem from complex engineering systems, (iii) the physics is complicated when additional features such as shock waves, multiphase flow, chemical reactions, and so on are present, and (iv) the fact that all of these

complexities can occur in the same application. In this context, there have been a number of recent papers focused on the development of high-order numerical methods and new strategies suitable for CAA. Computational aeroacoustics has made significant advances over the last few years as reported in the recent reviews of Wang *et al.* [63] and Colonius and Lele [64].

Computational techniques for flow-generated sound can generally be classified into two broad categories: direct computational and indirect, or hybrid, computation. In the direct approach, the sound is computed together with its fluid dynamic source field by solving the compressible flow equations. In a hybrid approach, the computation of flow is decoupled from the computation of sound, which can be done in a post-processing step based on an aeroacoustics theory. Figure 2.19 shows a summary of the different computational approaches for noise predicting that are currently being developed by researchers in CAA and represent important unit problems in attacking noise prediction generally.

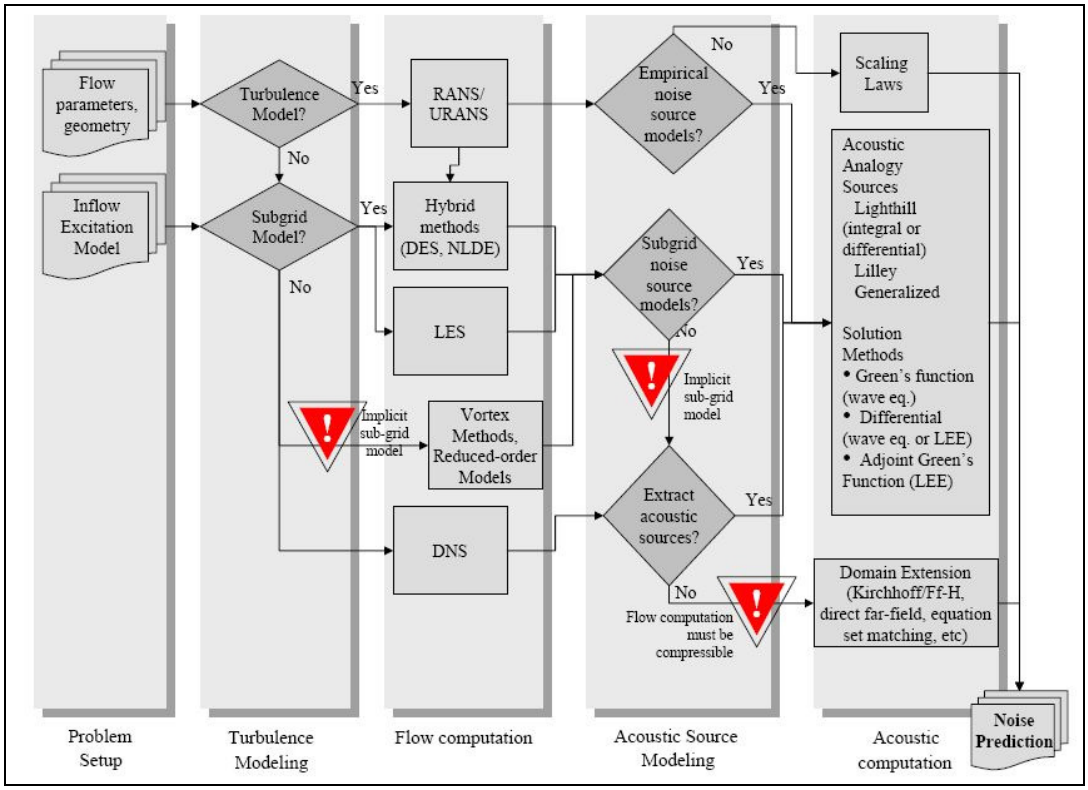

Figure 2.19 - A hierarchy of noise prediction methods. (After [64]).

2.3.1 Direct computation of sound

The direct computation of sound method aims to compute both the unsteady flow and the sound radiated by it by solving the compressible flow equations. These methods must use a domain that includes the noise-producing flow region and at least a part of the near-acoustic-field. Extension to the acoustic far field can then be achieved using a variety of analytical and numerical means, such as the analytical Kirchhoff integral (Farassat and Myers [65], Freund *et al.* [66], Lyrintzis [67]), the integral formulation of Ffowcs-Williams and Hawkings [68] and also the numerical linearized Euler equations (Freund *et al.* [69]). Furthermore, the computational mesh needs to be selected so that both the flow and its sound can be adequately represented.

Direct numerical simulation (DNS), which resolves all flow scales including the small dissipative scales, and large-eddy simulation (LES), which resolves only the dynamically important flow scales and models the effects of smaller scales, are examples of methods used for the direct computation of sound. It is also possible to use URANS methods to compute the noise of the largest flow features.

Because it avoids modelling approximations, the direct numerical simulation (DNS) is an ideal research tool for studying sound generation mechanisms and generating databases for developing and evaluation sound prediction models. The first DNS of flow-generated sound was a study of the noise generated by a pair of two-dimensional co-rotating vortices (Mitchell *et al.* [70, 71]), which permitted the first direct application of several acoustic analogies. Regarding the turbulent jet problem, the first DNS study was reported by Freund [69] and after that many other researches (Freund [72], Manning and Lele [73], Suzuki and Lele [74]) used this technique for investigating and producing valuable conclusions about jet noise. However, it is presently impossible to simulate a jet flow at high Reynolds number, which is the case in aeronautical applications, using DNS due to the massive computer requirements.

In this context, LES has emerged as an alternative and promising method for direct noise computation as it takes the approach of filtering out scales below a cut-off parameter which considerably reduces the computational cost of a simulation. Initial attempts at using LES to study compressible jets began in the late 1990s. Estivalezes and Gamet [75] and Gamet and Estivalezes [76] investigated the near-region of a Mach number 2.0 hot jet in two and three dimensions with a Kirchhoff surface to obtain the far-field sound. After that, the use of LES as a tool for jet noise research has increased and many exploratory investigations were, and still are, being conducted. To date, most of LES studies of far-field noise have been of moderate-to-high subsonic jets owing, in part, to the existence of quality experimental data and the desire to avoid cases with shocks present.

Even with improvements in the computational time provided by LES, direct noise computation methods are generally still too expensive to be used as an engineering prediction tool. In this context, there have been efforts to develop and use what is called hybrid methods. A hybrid method can be defined generally as a steady RANS calculation in conjunction with an acoustic analogy to generate acoustic source terms.

2.3.2 Hybrid approaches

In an engineering context it is advantageous to develop methods that do not directly capture the radiated sound but instead rely on a second calculation, or post-processing step, to predict the noise. These methods fall into the hybrid approach for noise calculation.

Hybrid approaches basically rely on a RANS calculation of the flow field which supplies mean quantities (eg. velocity, turbulence kinetic energy and dissipation) that will be used as inputs for different types of noise source models. The noise source models generally seek to represent the two-point correlation functions needed to statistically model Lighthill's

source term. Examples of available codes are the JeNO and MGBK software for jet noise predictions developed at NASA Glenn Research Center [77].

Another well-know modeling approach is called SNGR [78, 79] (Stochastic Noise Generation and Radiation) modeling. It is based on the idea that the linearized Euler equations are an exact wave operator for acoustic perturbations. Introducing suitable sources to the linearized Euler equations result in accurate predictions of the propagation of acoustic perturbations. In the case of jet noise predictions a RANS solution provides time averaged information about the flow field. The challenge in SNGR is to use the information given from the RANS solution to generate an unstationary turbulent field with the same local statistical properties as the RANS solution. This generated turbulent field is used to evaluate source terms in the linearized Euler equations. Solving the linearized Euler equations with the source terms provide the propagation of sound from the source region to the far-field. An example of SNGR application for jet noise prediction can be found in the work of Bilsson [80].

The LRT method developed in this thesis is a kind of a hybrid approach that also uses a RANS solution as an input for the source modeling and the refraction calculation. One of the main constraints of the LRT method is related to the computational time. The design brief was for a fast prediction tool that could be used as an engineering tool during a design phase. Chapter 3 and Chapter 4 will present details of the mathematical models used by the LRT method.

Chapter 3: Propagation Model: Ray-Tracing Theory

This chapter presents the Ray-Tracing Theory developed for the calculation of the flow-sound interaction that the sound waves experience during the propagation through a high-speed jet. The results from the Ray-Tracing and the noise source model, which will be presented in Chapter 4, forms the basic equations in the LRT method for predicting the noise on the far-field.

3.1 Introduction to sound propagation in aeroacoustics

As far as aeroacoustics is concerned, it is a common mistake to understand it as related solely with the noise source generation mechanism. The theory of aerodynamic sound not only takes into account the sound generation mechanisms but also the propagation of the sound waves through to the observer. In fact, the latter plays a very important role especially in aeroacoustics problems, i.e. in a presence of a moving media. Putnam [81], for example, affirms in his work that the ability to account for the propagation of noise through the atmosphere is fundamental for the control and reduction of aircraft community noise. At that time, Putnam was already aware that the effects of wind velocities and temperature gradients present in the atmosphere were responsible for the convergence or divergence of the sound at a particular receiving point. These effects of fluid flow and gradients of speed of sound on the acoustic propagation are enhanced when a high-speed jet flow is concerned. Moreover, if asymmetries are present in the problem that is being investigated, such as the flows from non-circular nozzles, the modification on the sound propagation paths that are caused by refractions, can significantly alter the sound characteristics at an observer point in the far-field.

Most of the classical theory of acoustics is devoted to the acoustics of a homogeneous fluid at rest. However, when motion relative to the medium is involved a re-examination of the problems of generation, propagation and detection of sound is necessary. According to Morse and Ingard [82], the motion of the medium makes it non-isotropic, since the speed of sound depends on the direction of propagation with respect to the direction of motion of the medium. If, in addition, the medium is inhomogeneous, so that the speed of sound and other medium characteristics vary from one point to another various refraction and scattering effects must be considered. This is usually what happens for noise from of a jet flow where sound must propagates through the jet flow until the waves reach the observer in the far-field.

The strategy adopted to model the refractions effects in the LRT method is based on geometric acoustics concepts where the Ray-Tracing Theory is applied to calculate the variation on the sound pressure level (ΔSPL) in the far-field due to the jet flow.

3.2. Ray-Tracing Theory applied to jet noise

Sound propagation through a jet represents an important part of the jet noise, especially for asymmetric jets and engine installation effects problems. A number of different approaches to this problem have been adopted in the past. For example, Powles and Tester [83, 84] adopted different approaches to the problem of modelling the scattering by a cylindrical jet of the sound radiated by a single-frequency monopole source. The first approach calculates a numerical Green's function for the Lilley equation. This method is based on previous work by Tester and Morfey [85], similar approaches have also been published by Wundrow and Khavaran [86], however the Powles and Tester work differs from these previous publications in that the solution is generalized to include sources both inside and outside the jet. The second approach is a high-frequency WKB analysis, which is an adaption of Wundrow and Khavarans WKB analysis on single stream jets [86]. Also a low

frequency model based on Gehold's [87] work on jet by jet shielding is given, and a ray model which is a generalization of Morfey and Joseph's [88] work on shear layer refraction effects. One assumption in all of the methods developed was that the jet fluid parameters didn't vary in the axial direction, i.e. that the jet was infinite parallel flow and not spreading. In the ray model developed by Powles and Tester [83], the shear layer of the jet is approximated by a vortex sheet, i.e. a plug jet flow assumption, and the rays are straight lines. For the LRT method there was a requirement for a ray-tracing code capable of propagating through a steady inhomogeneous moving medium, so it could calculate a real 3D jet flow, including shear layer and spreading jet effects.

Significant work on ray-tracing through jets in the past includes that of Suzuki and Lele [89], were a ray theory model is used to predict far acoustic pressure from source in transversely sheared mean flow. Other work includes a paper by Freund and Fleischman [90], were a ray theory including unsteady flow effects is developed, and used to quantify the significance of the effect of turbulence on propagation through jets. Spalart *et al.* [91] trace rays through the mean flow of a jet, based on LES simulations, and confirm that ray tracing through the mean flow can give good far-field prediction.

Ray tracing (RT) has been widely used in physics and inside the engineering context for a long time. Its applications can vary from petroleum exploration (seismic ray tracing), optical flow-visualization, to room acoustics. This is probably due not only because ray theory provides considerably good accuracy but also because it has a relatively simple implementation.

In this thesis, the aim is to develop a RT method that can be used to study the refraction effects of sound waves propagating through the mean field arising from an inhomogeneous, asymmetric turbulent jet. Moreover, the RT method is required to give useful information of the change on sound pressure level in the far-field so that these effects can be

taken into account by the LRT model to correctly predict the noise at a desired observer position. To illustrate the mechanism of sound refraction, Fig. 3.1 depicts a schematic of a discrete source positioned inside a jet flow together with the rays launched from it, which represents the propagation path of the wave-front, for two possible conditions: 1) if there was no flow and 2) with the jet flow showing the real refracted wave. As can be seen, when no flow is regarded, the ray propagates as a straight line which represents the spherical spreading of the wave-fronts. In contrast, when the source is inside the jet flow the presence of flow velocity and sound speed gradients causes sound refraction and therefore the rays bend away from the jet centre-line. The bending of rays is explicable in terms of wave-fronts. Since the portion of the wave-front on the low-sound-speed side of a ray is moving slower, the wave-front must tilt toward that side and as the ray remains normal to the wave-front, it bends in that direction.

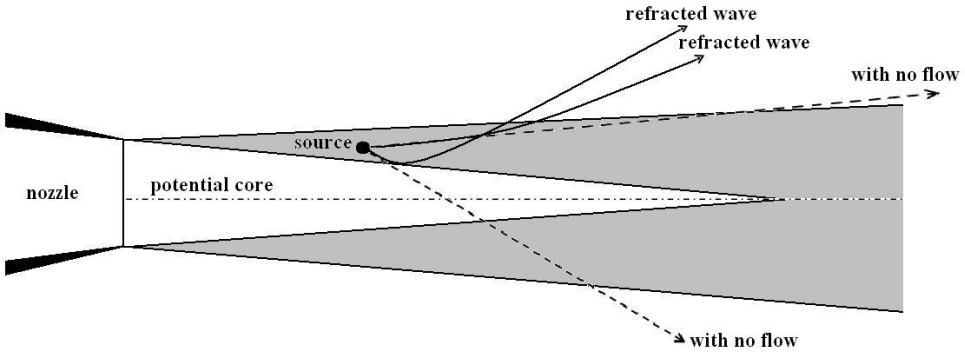

Figure 3.1 - Schematic representation of wave propagation through a high speed jet.

3.2 Mathematical Model

In this section, the mathematical descriptions of the Ray-Tracing equations are presented. Most of the concepts presented here were obtained from the classic acoustics book of Pierce [92].

3.2.1 Ray-Tracing Equations

The theory of plane-wave propagation predicts that wave-fronts move with speed c when viewed in a coordinate system in which the ambient medium appears at rest. If the ambient medium is moving with velocity $\vec{v}$, the wave velocity $\vec{n}\,c$ seen by someone moving with the fluid becomes $\vec{v}+\vec{n}c$ in a coordinate system at rest, where $\vec{n}$ is the unit vector normal to the wave-front.

Consider $\vec{x}_p$, the coordinated of a moving point that lies on the wave-front $t=\tau(\vec{x})$ at an initial time, this point will always lie on the moving wave-front if its velocity ($\vec{v}_{ray}$) obeys the following equation:

$$\frac{d\vec{x}_p}{dt}=\vec{v}\,(\vec{x}_p,t)+\vec{n}\,(\vec{x}_p,t)\;c(\vec{x}_p,t)=\vec{v}_{ray}\,. \tag{3.1}$$

Equation (3.1) represents the local point velocity as a superposition of convection, due to the moving media, and wave propagation relatively to the fluid. Furthermore, Eq. (3.1) allows for the possibility that $\vec{v}$ and c may vary with both position and time. The line described in space by $\vec{x}_p$ versus time is a ray path and the function $\vec{x}_p(t)$ is a ray trajectory.

Instead of dealing with the normal vector $\vec{n}$ in Eq. (3.1), which would require the construction of the wave-front surface in the vicinity of the ray at closely spaced time intervals, it is easier to define a vector parallel to $\vec{n}$, called the *wave-slowness vector* $\vec{s}$. The wave-slowness vector is derived in order to achieve an additional differential equation that allows the prediction of the time rate of change of $\vec{n}$ and, it is defined as follows:

$$\vec{s}(\vec{x})=\nabla(\vec{x})\,. \tag{3.2}$$

It can be shown that [92],

$$\vec{s}\cdot(c\vec{n}+\vec{v})=1, \tag{3.3}$$

or,

$$c\vec{s}\cdot\vec{n}=1-\vec{v}\cdot\vec{s} \tag{3.4}$$

and

$$\vec{n}=\frac{c\vec{s}}{\Gamma}, \tag{3.5}$$

where,

$$\Gamma=1-\vec{v}\cdot\vec{s}. \tag{3.6}$$

Finally, it is possible to find the following relation

$$s^2=\frac{\Gamma^2}{c^2}, \qquad (\nabla\tau)^2=\frac{\Gamma^2}{c^2}. \tag{3.7}$$

The partial-different equation showed in Eq. (3.7) is the so-called *eikonel equation*. A differential equation for the time rate of change of $\vec{s}$ along a ray trajectory can be derived from Eq. (3.7):

$$\frac{d\vec{s}(\vec{x}_p)}{dt}=(\dot{\vec{x}}_p\cdot\nabla)\vec{s}=c(\vec{n}\cdot\nabla)\vec{s}+(\vec{v}\cdot\nabla)\vec{s}, \tag{3.8}$$

where all the indicated quantities are evaluated at $\vec{x}_p(t)$. Because $\vec{n}$ is in the direction of $\vec{s}$, the first term on the right hand side of Eq. (3.8) has a factor $(\vec{s}\cdot\nabla)\vec{s}$, which can be expressed as

$$\begin{aligned}(\vec{s}\cdot\nabla)\vec{s} &= -\vec{s}\times(\nabla\times\vec{s}) + \frac{1}{2}\nabla s^2 \\ &= 0 + \frac{1}{2}\nabla\left(\frac{\Gamma^2}{c^2}\right) \\ &= -\frac{\Gamma}{c^2}\nabla(\vec{v}\cdot\vec{s}) - \frac{\Gamma^2}{c^3}\nabla c\end{aligned} \quad , \tag{3.9}$$

where $\nabla\times(\nabla\tau) = 0$ and a substitution for s^2 from Eq. (3.7) has been used. Subsequent insertion of Eq. (3.9) into Eq. (3.8) yields

$$\frac{d\vec{s}}{dt} = -\frac{\Gamma}{c}\nabla c - \nabla(\vec{v}\cdot\vec{s}) + (\vec{v}\cdot\nabla)\vec{s}\,. \tag{3.10}$$

The following vector identity can be used to give a further simplification of the equations:

$$\nabla(\vec{v}\cdot\vec{s}) = \vec{v}\times(\nabla\times\vec{s}) + \vec{s}\times(\nabla\times\vec{v}) + (\vec{v}\cdot\nabla)\vec{s} + (\vec{s}\cdot\nabla)\vec{v}\,, \tag{3.11}$$

where the first term is zero because $\vec{s}$ by definition is a gradient. Finally, the ray-tracing equations can be written as follows:

$$\frac{d\vec{x}}{dt} = \vec{v} + \frac{c^2\vec{s}}{\Gamma}\,, \tag{3.12}$$

$$\frac{d\vec{s}}{dt} = -\frac{\Gamma}{c}\nabla c - \vec{s}\times(\nabla\times\vec{v}) - (\vec{s}\cdot\nabla)\vec{v}\,, \tag{3.13}$$

or in Cartesian coordinates

$$\frac{dx_i}{dt} = v_i + \frac{c^2 s_i}{\Gamma}, \tag{3.14}$$

$$\frac{ds_i}{dt} = -\frac{\Gamma}{c}\frac{\partial c}{\partial x_i} - \sum_{j=1}^{3} s_j \frac{\partial}{\partial x_i} v_j \,. \tag{3.15}$$

Equation (3.14) and Eq. (3.15) form the basic equations of the Ray-Tracing Theory in Cartesian coordinates. These equations are numerically solved by the LRT method in order to calculate the ΔSPL for each region of the jet resulting from the propagation effects.

3.2.2 Amplitude determination

When tracing rays, changes in density of the medium are not considered, as a change in density will not alter the path of an individual ray. However change in density does have an effect on the pressure amplitude. If we know the density at the start and end of the ray tube we are considering, we can use the Blokhintzev invariant [93] to account for this change in pressure amplitude, it can be written as showed in Eq. (3.16):

$$\frac{p^2 \left|\vec{v}_{ray}\right| A}{(1 - v \cdot \nabla \tau)\rho c^2} = \text{const}, \tag{3.16}$$

where,

$$\left|\vec{v}_{ray}\right| = \vec{v} + c\vec{n} \,. \tag{3.17}$$

Figure 3.2 shows a simplified schematic representation of the concept of Ray-Tubes. From each source the ray is launched and its path is calculated until it reaches the far-field bins.

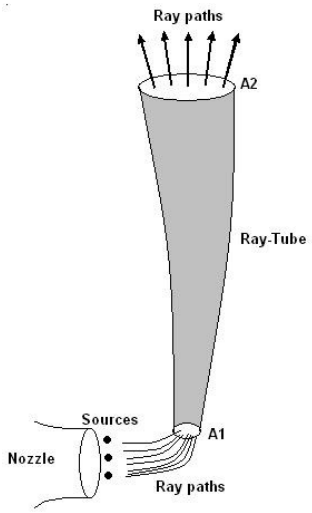

Figure 3.2 - Schematic description of the use of the ray-tube concept for noise amplitude determination on the far-field.

3.2.7 Change in Sound Pressure Level

The ultimate goal of the RT method presented here is to calculate the far-field change in sound pressure level due to the refractions caused by the sound propagation through the jet flow. This sound variation is called the ΔSPL and is calculated with the following equation:

$$\Delta SPL = 10\log\left(\frac{p_{jet}^2}{p_{ff}^2}\right), \tag{3.18}$$

where p_{jet} is the far-field pressure due to the source present inside the jet flow, and p_{ff} is the pressure that would be measured in the far-field from the same source but with no propagation effects. To calculate this, first consider the change in pressure along any ray-tube between two positions x_1 and x_2 which can be written as:

$$\frac{p(x_2)^2}{p(x_1)^2} \propto \frac{A(x_1)}{A(x_2)}. \tag{3.19}$$

Considering that the acoustic energy is conserved within a ray tube and then using the Blokhintzev invariant concept it is possible to write the following pressure relation:

$$\frac{p(x_2)^2}{p(x_1)^2} = \frac{\left|\vec{v}_{ray}(x_1)\right| A(x_1)}{(1-v(x_1)\cdot s(x_1))\rho(x_1)c(x_1)^2} \frac{(1-v(x_2)\cdot s(x_2))\rho(x_2)c(x_2)^2}{\left|\vec{v}_{ray}(x_2)\right| A(x_2)}. \tag{3.20}$$

Thus assuming at the source $A_{jet}x_s = A_{ff}x_s$ and $p_{jet}x_s = p_{ff}x_s$ it is possible to rewrite Eq. (3.18) as follows:

$$\Delta SPL = 10\log\left(\left(\frac{(1-v(x_s)\cdot s(x_s))\rho(x_s)c(x_s)^2}{\left|\vec{v}_{ray}(x_s)\right|} \frac{\left|\vec{v}_{ray}(x)\right|}{(1-v(x)\cdot s(x))\rho(x)c(x)^2}\right)\left(\frac{A_{jet}(x)}{A_{ff}(x)}\right)\right). \tag{3.21}$$

3.3 Numerical Implementation

The ray-tracing equations, Eq. (3.14) and Eq. (3.15) form a system of coupled non-linear first order ordinary differential equations, thus they are amenable to standard numerical integration techniques. It is possible to solve these equations as an initial value problem using a standard iterative numerical method. High order Runge-Kutta schemes are the most commonly used type of finite difference methods applied to CAA, mainly due to their stability and consistency. In this context, the full 3D ray-tracing code developed in this thesis uses a fourth order Runge-Kutta (RK4) method. The code was implemented by using the fast FORTRAN platform.

3.3.1 Source Generation

In a real jet, acoustic sources are distributed throughout the turbulent flow region. However, in order to be able to numerically calculate the refraction effects of such a flow field a coarser distribution of the sources is required. Therefore, one important step in the LRT method refers to the generation of the discrete point sources inside the jet flow field from where the rays will be launched. For this aim, an algorithm was developed for generating the coordinates of the sources that are necessary for the Ray-Tracing propagation code. The algorithm basically uses the information of the jet mean flow properties, such as flow velocity, to distribute spatially the point sources, generating then a data file containing the X, Y, Z coordinates values for each source. In addition, the algorithm is capable of distributing the sources in space following the spreading rate of the jet so that a higher concentration of sources is located near the high velocity gradients in the flow, i.e. shear layer.

Figure 3.3 shows an example of source distribution generated by the algorithm that was used in the LRT method. As can be seen, the sources are distributed in space following the spreading rate of the jet. The domain used to distribute the sources is shown in Fig. 3.3(a) which goes from the nozzle exhaust position down to $25D_j$ downstream covering the most important source regions. Figure 3.3(b) depicts the radial distribution of the sources near the nozzle exit. Here, D_j corresponds to the nozzle diameter. Each of the point sources depicted below are used on the LRT code to calculate the propagation properties of the jet flows.

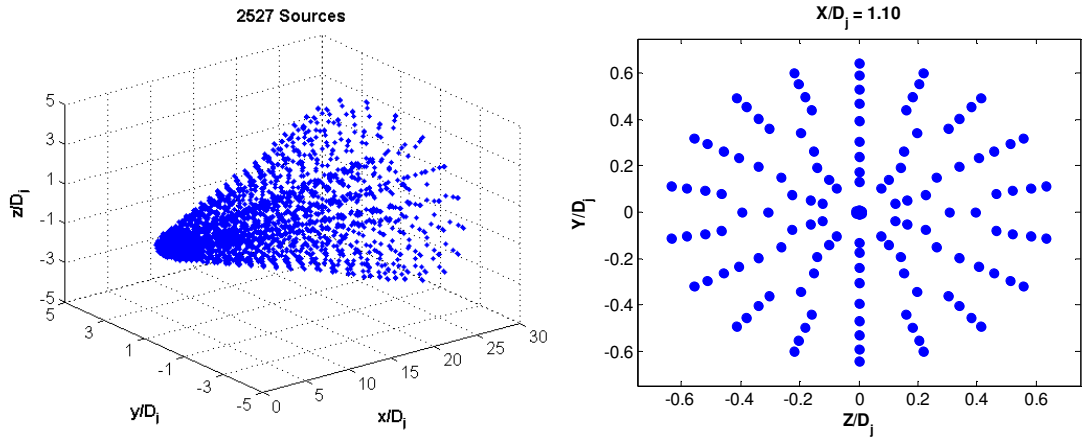

(a) (b)

Figure 3.3 - Point sources generated and used by the LRT method for the Ray-Tracing calculation. (a) 2527 sources distributed in the jet field. (b) Radial distribution of the sources near the nozzle exit, $X/D_j = 1.10$.

3.3.2 Launching rays in 3D

When launching rays to determine a full far-field solution in 3D, care needs to be taken as it not as straightforward as launching rays in 2D. Given that amplitude is calculated using ray density, rays launched from a monopole point source should be separated from neighbouring rays by a constant angle. This is to say launch points should be evenly distributed around the sphere, to deliver unbiased ray coverage in 3D. Ray shooting from the vertices of regular polyhedrons is the only way to exactly satisfy the two uniformity criteria [94]. Since no regular polyhedron has more than twenty vertices, we need to use other geometries to get a high ray resolution.

The geodesic sphere arises by tessellating the faces of regular polyhedron. Figure 3.4 shows how each face of the icosahedron can be recursively sub-divided to effectively tessellate a sphere. Caution should be taken when calculating new vertices like this, as each face shares edges with neighboring faces. However it should be noted that the geodesic sphere only approximates uniformity, there are discrepancies in angular separation of the launched

rays. Each ray emanating from the vertices of the icosahedron has only five neighboring rays rather than the usual six, however this type of aberration becomes insignificant for heavily tessellated spheres [95].

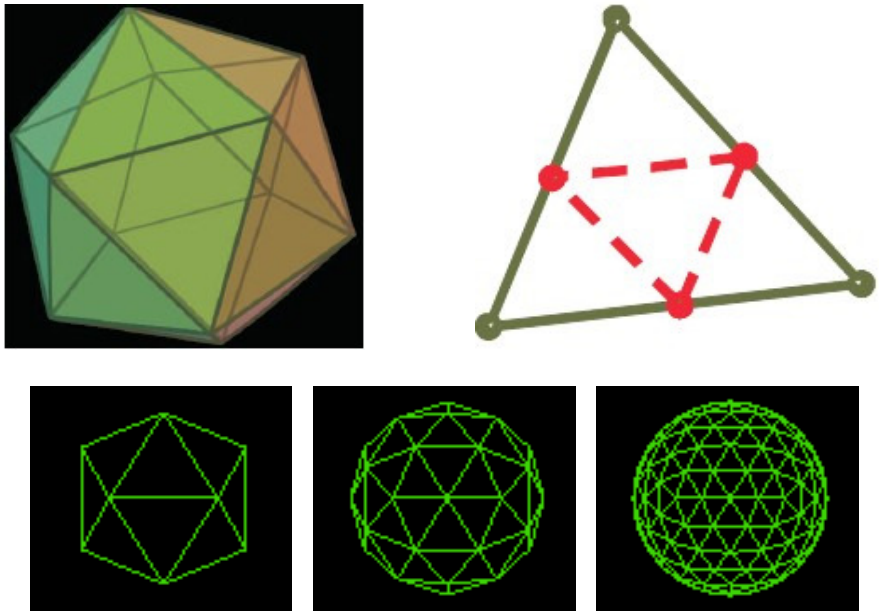

Figure 3.4 - An icosahedron can accurately tessellate a sphere, by recursively sub-dividing each of the faces.[8]

Figure 3.5 depicts an example of the ray paths from a single monopole source when 162 rays are launched in a three-dimensional form. This procedure is repeated for each source that is being modeled in the computational domain.

[8] http://student.ulb.ac.be/~claugero/sphere/index.html

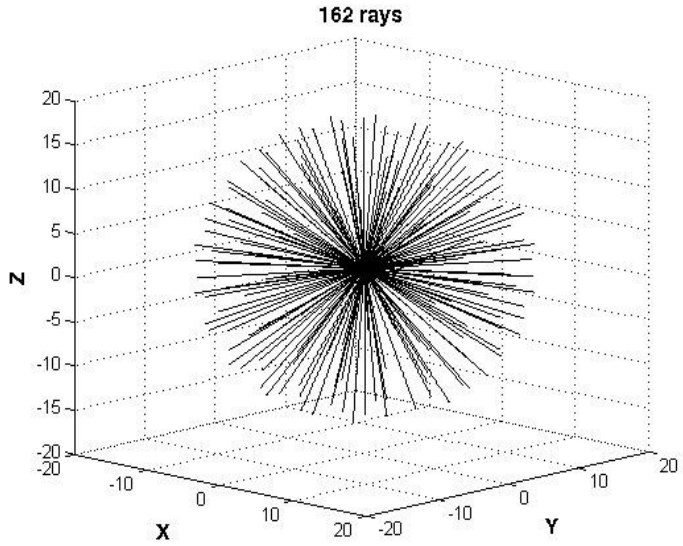

Figure 3.5 - 162 Ray paths in 3D launched from a single monopole source.

3.3.3 Sound Refraction Determination

When tracing rays through an inhomogeneous moving media, it is possible and often very likely, to have more than one ray arriving at the observer location. The pressure seen at this location is a combination (incoherent sum) of individual ray-tube pressures. A simple but effective way of dealing with this problem is to separate the far-field into an evenly distributed number of equally sized regions, here called “ray bins”. One can then launch a much larger number of rays from the source in all directions, and then do an incoherent sum of the pressure amplitudes in each ray bin. This is a similar approach as to that adopted by Freund and Fleischman [90] to investigate the effects of velocity fluctuations on the shear layer of a jet on the propagation path and it is also used by McLaughlin [96]. The number of rays needed for the far-field solution to converge can make this process computationally expensive.

3.4 Numerical Results for sound refraction due to a jet flow

In order to demonstrate the results that can be obtained from the 3D RT method developed in this thesis, six sources were distributed in specific positions inside an arbitrary

jet, as shown in Fig. 3.6. The first four sources are aligned within the lipline of the nozzle but varying in downstream position. The last two sources were positioned on the centreline of the jet, inside the potential core. (It is important to mention that there are no sources inside the potential core but the aim here is to show that only for the sources distributed on the centreline of an axisymmetric case the refraction effects are also symmetric). In this comparison, all the sources were positioned in the azimuthal angle of 90 degrees. Figure 3.7 shows the results of ΔSPL (dB) calculated using the Ray-Tracing code for a Mach number 0.75 isothermal jet.

Source 1: Figure 3.7(a), the zone of silence has a variable shape along the azimuthal angles. Region A, which is a straight line, shows that the critical angle is about 60 degrees and it goes from azimuthal angle 10 to 160 degrees. From this point beyond, Region B indicates the zone of silence, changing the critical angle in an elliptic form up to 20 degrees. Inside Region B, it is interesting to point out a high intensity amplification region just before the initial of the zone of silence which is due to the rays that enter the potential core of the jet, i.e. the rays that are not being totally reflected. The potential core in this situation acts like a lens for these rays, focusing them in a determined region hence explaining the amplification in this section. These results show how important is the effect of the potential core for sound blockage and also noise amplification for far-field noise predictions. Region C presents the area of peak noise amplification. The peak for this condition occurs at azimuthal angle 90 degrees and polar angle about 110 degrees.

Source 2: Figure 3.7(b) shows that region B changes considerably when the source is moved downstream, altering not only its shape but also the critical angle to approximately 40 degrees. Also, the noise amplification region before the zone of silence still plays an important role for this source. Regarding region C, the peak area is becoming sharper and it is

spreading along the polar angles. This can be understood by the fact that more rays are being convected by the flow due to the jet spreading.

Source 3: Figure 3.7(c), the same behaviour as Source 2 is presented as we move the source further downstream. The main differences are that the zone of silence is practically a straight line as showed by Region A and the critical angle has changed to a lower polar angle (~45 degrees). Region B is becoming less effective as an amplification section. Region C keeps moving to higher polar angles suffering more convective influences.

Source 4: Figure 3.7(d), it is shown that the blockage effect is minimized and it is no longer possible to identify Region B and C as the source is moved down to the end of the potential core. As shown before, the same characteristic for Region A is observed when going further downstream with the critical angle moving to 20 degrees.

Source 5: Figure 3.7(e), the source is now positioned on the jet's centreline, inside the potential core. Region A specifies the critical angle which is approximately constant and equal to 56 degrees. As can be seen from Region B, the high intensity amplification region is distributed evenly for all the azimuthal angles. As expected, Region C is now periodic which makes sense as the flow is axisymmetric.

Source 6: Fig. 3.7(f), moving the source to the end of the potential core but keeping it on the jet's centreline has not changed considerably the general trend of the refraction when compared to Source 5, apart from the critical angle and the magnitude of the peak amplification. The result keeps being periodic and the peak is concentrated at 110 degrees in the polar angle direction.

Further comparisons between Source 2 and Source 5 show that even though both sources are in the same axial position, their refraction effects are strongly dependant on the radial position of the source. The same conclusion can be made by comparing Source 4 and Source 6 where the critical angle varies considerably from 50º to 20º.

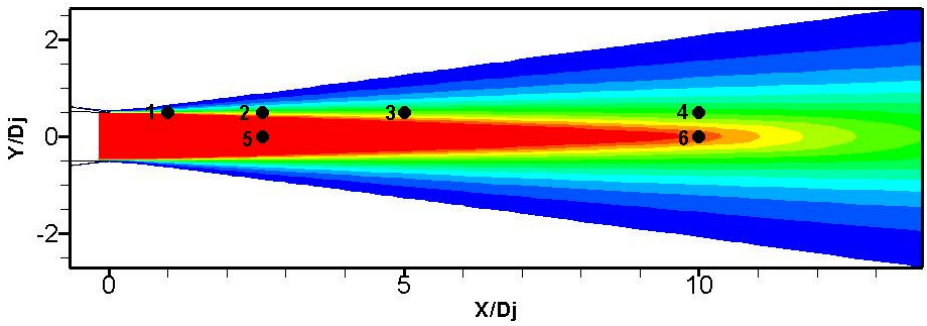

Figure 3.6 - Sources positions. Mach number contour.

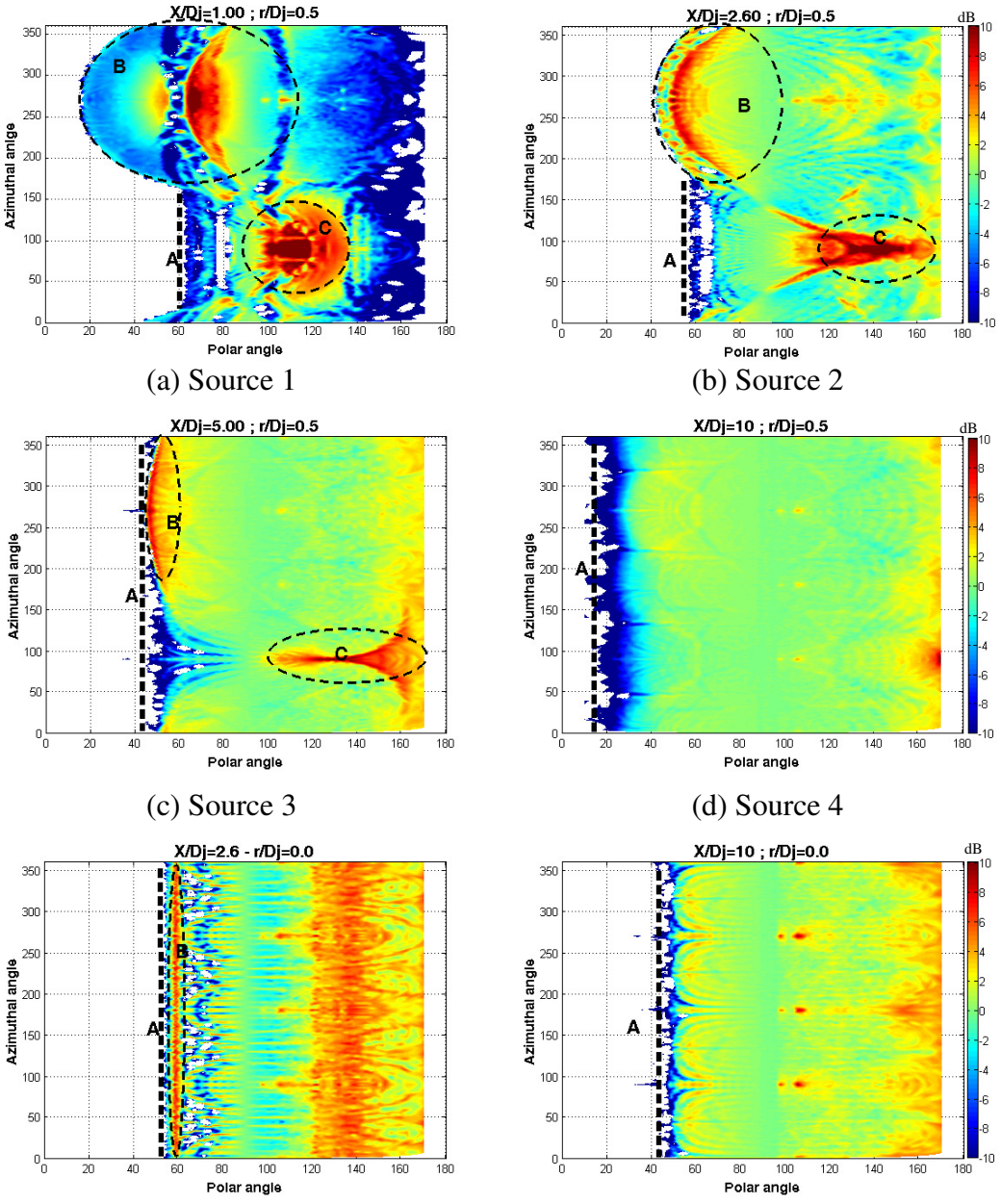

(a) Source 1 (b) Source 2

(c) Source 3 (d) Source 4

(e) Source 5 (f) Source 6

Figure 3.7 - Calculated sound-flow effects in ΔSPL (dB) for different sources inside the M=0.75 jet.

Chapter 4: Noise Prediction Method: Mathematical Model

This chapter presents the mathematical model of noise production and radiation from a jet flow that is used in the LRT Method. The basic concepts necessary to derive the LRT Method are presented in this chapter which is divided into three different parts. In the first part, Lighthill's Acoustic Analogy is presented and discussions on the main limitations are provided. The second part of the chapter is devoted to presenting Lilley's Equation in conjunction with the MGBK method that will be used in Chapter 5 to validate the noise predictions from the LRT method. Discussions about the improvements made by Lilley, by separating the propagation effects from the source term and also its main limitation are presented. Finally, the LRT formulation showing all the equations and assumptions made throughout the method are provided. In addition, the necessary input information, the method applicability and its block diagram of the computational sequence for noise predictions are also given in this section.

4.1 Background

Before presenting Lighthill's Acoustic Analogy it is important to introduce the Navier-Stokes equations which were used by Lighthill to derive his Acoustic Analogy in the early 1950s. The compressible continuity, momentum, and energy equations, also called Navier-Stokes equations, describe the motion of a fluid. Hence, according to Larsson [97], the solution to these equations, subject to boundary conditions, includes not only convection and diffusion, but also acoustic wave propagation. The acoustic part of the solution can not, in general, be separated from the rest of the solution. In many cases, though, it is possible to view the flow and the acoustics as two different fields.

Equation (4.1), Eq. (4.2) and Eq. (4.3) represent respectively the continuity, conservation of momentum and the energy equations in their conservative form. It should be noted that the following equations assume the absence of any external mass or force sources in the fluid.

$$\frac{\partial \rho}{\partial t} + \frac{\partial (\rho u_i)}{\partial x_i} = 0 , \tag{4.1}$$

$$\frac{\partial (\rho u_i)}{\partial t} + \frac{\partial (\rho u_i u_j)}{\partial x_j} + \frac{\partial p}{\partial x_i} - \frac{\partial \tau_{ij}}{\partial x_j} = 0 , \tag{4.2}$$

$$\frac{\partial e}{\partial t} + \frac{\partial}{\partial x_j}\left[(e + p)u_j - \tau_{ij}u_i + q_j\right] = 0 , \tag{4.3}$$

where,

$$e = \rho\left[e_i + \frac{1}{2}(u^2 + v^2 + w^2) \right]. \tag{4.4}$$

Due to the non-linearity of the governing equations and the importance of different scales it is a very difficult task to predict the sound production by fluid flows. As the sound field associated with subsonic flows represents only a very small fraction of the energy in the flow, the accuracy of numerical simulations must be very high to predict the sound generation. This is particularly complicated in free space and at low subsonic speeds. The fact that the sound field is in some sense a small perturbation of the flow, can however be used to obtain approximate solutions. Aeroacoustics analogies have been developed for this purpose.

The idea of an acoustic analogy is to restate the full Navier-Stokes equations as an equivalent wave equation, aimed at applying the standard Green's function technique to derive approximate solutions or numerical strategies. In a more extended view, this implies a wave operator and a field variable suited to a simplified solving technique. The first and

undoubtedly the most famous acoustic analogy was derived by Sir James Lighthill and it will be presented in the following section.

4.2 Lighthill's Acoustic Analogy

The work of Lighthill has been regarded as marking not only the beginning of jet noise research but also the birth of the research area named "Aeroacoustics", Tam [98].

Looking back in the context of the 1950s, Lighthill was interested in the following problem: "*given a fluctuation fluid flow, how do we estimate the sound radiated from it*". It is perhaps intuitive, that the first thing to do in order to develop a noise theory is to identify the sources of noise. Based on this, the idea of Lighthill [13, 15] was to reformulate the general equations of gas dynamics, in order to derive a wave equation. Lighthill introduced his theory of jet noise as follows.

Differentiating the continuity Eq. (4.1) with respect to time,

$$\frac{\partial^2 \rho}{\partial t^2} + \frac{\partial^2 \rho u_i}{\partial x_i \partial t} = 0\,, \tag{4.5}$$

taking the divergence of the momentum Eq. (4.2)

$$\frac{\partial^2 \rho u_i}{\partial x_i \partial t} + \frac{\partial^2 \rho u_i u_j}{\partial x_i \partial x_j} = -\frac{\partial^2 p}{\partial x_i^{\,2}} + \frac{\partial^2 \tau_{ij}}{\partial x_i \partial x_j}\,. \tag{4.6}$$

Substituting the first term of the left hand side of the equation above, yields,

$$\frac{\partial^2 \rho}{\partial t^2} - \frac{\partial^2 \rho u_i u_j}{\partial x_i \partial x_j} = \frac{\partial^2 p}{\partial x_i^{\,2}} - \frac{\partial^2 \tau_{ij}}{\partial x_i \partial x_j}. \tag{4.7}$$

In order to get a wave equation for the density, the convective term is moved to the right hand side, and a term $-c_0^2 \partial^2 \rho / \partial x_i^2$ is added to both sides of the equation. The result is an inhomogeneous wave equation, the famous so-called Lighthill's equation:

$$\frac{\partial^2 \rho}{\partial t^2} - c_0^{\,2} \frac{\partial^2 \rho}{\partial x_i^{\,2}} = \frac{\partial^2 T_{ij}}{\partial x_i \partial x_j}, \tag{4.8}$$

where T_{ij} is the Lighthill stress tensor, which is given by the following relation:

$$T_{ij} = \rho u_i u_j - \tau_{ij} + (p - c_0^{\,2} \rho)\delta_{ij}. \tag{4.9}$$

Here τ_{ij} denotes the strain rate in the fluid, and δ_{ij} the Kronecker delta function. Equation (4.8) and Eq. (4.9) are an exact restatement of the Navier–Stokes equation. The double divergence of the Lighthill stress tensor appears as a source term. But some care has to be taken to avoid misleading interpretation. Since no special assumption was made nor linearization introduced, this is an exact equation, therefore all aeroacoustics processes, including generation of sound by the flow non-homogeneities, sound propagation through the flow and sound dissipation by viscosity or heat conduction, are accounted for. In its most general form, the Eq. (4.8) is not tractable as a pure wave equation in linear acoustics as the right hand side contains the acoustic field to be determined and cannot be considered as a true source term. Hence the equation cannot be solved in an explicit way by means of the Green's function technique. This is only made possible by neglecting some of the mechanisms

included in Lighthill's equation. Indeed, only the aspects of sound generation justify the classification of all terms in the right hand side as source term. To remove this difficulty, Lighthill proposed some simplifications motivated by thinking that sound generation by the mixing of fluid is the dominant mechanism, especially at the high Reynolds numbers of interest in aeronautics.

For turbulent flows, at sufficient high Reynolds numbers, the contribution of the nonlinear term $\rho u_i u_j$ will be much larger than the contribution of the dissipation τ_{ij} and the entropy term $(p-c^2_0\rho)\delta_{ij}$. So for a turbulent flow it can be assumed that T_{ij} is approximately equal to $\rho u_i u_j$. The fluctuation density distribution ρ is then given by

$$\frac{\partial^2 \rho}{\partial t^2} - c_0^{\,2} \frac{\partial^2 \rho}{\partial x_i^{\,2}} = \frac{\partial^2 \rho u_i u_j}{\partial x_i \partial x_j} . \tag{4.10}$$

The right-hand side of this equation is only significant in regions where there is a spatial non-uniform fluid motion. Outside this region $\rho u_i u_j$ will be small and Eq. (4.10) reduces to an ordinary wave equation, which is valid for the propagation of sound in the linear approximation. If the right hand side is assumed known, and independent of the left hand side, the equation can be solved analytically to give

$$\rho(x,t) - \rho_0 = \frac{1}{4\pi c_0^2} \int_\infty \frac{1}{r} \frac{\partial^2 T_{ij}}{\partial y_i \partial y_j} dV(y) = \frac{1}{4\pi c_0^2} \frac{\partial^2}{\partial x_i \partial x_j} \int_\infty \frac{T_{ij}}{r} dV(y) , \tag{4.11}$$

where $T_{ij} = T_{ij}(y,\tau)$, $r = |x - y|$, and ρ_0 is a constant of integration. $\tau = t - r/c_0$ is the retarded time, i.e. the time at which the source radiates a fluctuation that reaches the observer at t.

Some of the limitations of the Lighthill's analogy are described below:

- The analogy does not take into account the presence of "back-reaction" i.e. when the sound produced in turn influences the flow. If there is a mutual dependence of the flow and the acoustics, i.e. that energy is being transferred both from the flow to the acoustics and vice versa, the problem is called a two-way coupled case. If the acoustic part is dependent on the flow, but the flow is independent of the acoustics, the problem is called a one-way coupled case;
- The theory is effectively confined in its application to completely subsonic flows. Supersonic flows are liable to give rise to shocks which are a source of noise not accounted for in Lighthill's theory.
- The theory neglects neighboring resonators and effects due to nearby solid surfaces, such as reflection, diffraction, absorption or scattering
- Estimates of radiated energy will only be valid in the far field. The far field is a region with negligible turbulence, and the mean flow field is typically homogeneous. No sound is being generated in this region, so the only phenomenon present is acoustic wave propagation.
- The theory suppresses all effects associated with the influence of the mean-flow velocity and temperature environment of the jet, i.e., convection, refraction and shielding of the radiation from the moving eddies.

Despite these limitations, an important result that can be derived from Lighthill's Acoustic Analogy is the noise scaling law. By using the Green's function for the wave equation, Lighthill obtained a formal solution of Eq. (4.10). On applying dimensional analysis to the formal solution, he established that the acoustic power (W) radiated by a jet should vary as the eighth power of the jet velocity V_j,

$$W = \frac{4\pi |x|^2 \overline{p'^2}}{\rho_0 c_0} \propto \rho_0 c_0^3 D^2 M^8 . \tag{4.12}$$

This became known as the Lighthill's V_j^8 Law, for more details the reader is referred to Lighthill's original papers [13, 15]. This Law leads to at least one notable idea for jet noise reduction. Since the thrust of a jet varies as $A_j V_j^2$ (where A_j is the jet exhaust area) and its acoustic power as $A_j V_j^8$, it is possible to demonstrate that jet noise could be reduced at constant thrust by raising exhaust area and lowering jet velocity. The high bypass ratio engines are an embodiment of this concept and remarkable reduced the engine noise component on aircraft noise in the last few decades.

In the years after the work of Lighthill, there have been many attempts to modify or improve Lighthill's Acoustic Analogy. Many of these efforts involved modifying the wave propagation operator on the left hand side of the equation and then producing slightly different set of noise source terms. For instance, Ffowcs-Williams [99] and Ribner [100] suggested considerable modifications to Lighthill's original work which explained most of the discrepancies from Lighthill theory to experimental measurements at the time. However it is not the aim of this thesis to describe and discuss all the existing aeroacoustics analogies and more detailed information can be found in Curle [101], Ffowcs-Williams and Hawkins [68], Howe [102], Möhring [103] and Powell [104].

In the next section, a more recent but more complex acoustic analogy derived by Lilley is presented. This overcomes many of the limitations of Lighthill's theory related to separation of source and propagation effects.

4.3 Lilley's Acoustic Analogy

4.3.1 Overview

It was shown that Lighthill, in his classic theory of jet noise, identified the most important source of jet noise as being the double divergence of the tensor $u_i u_j$. He also showed that the acoustic pressure fluctuations that are driven by this source obey the classical wave equation. Since the source of noise is embedded in the jet, the pressure fluctuations propagate through a region of non-uniform velocity (and sometimes temperature) before they reach the observer, i.e., the propagation path is affected by the flow field. As already discussed, Lighthill theory clearly fails to account for this physical effect. That is, it does not take acoustic mean flow interactions (also called refraction) into account explicitly.

This neglect of mean-flow effects in Lighthill development was pointed out by several researchers in the 1960s. Lighthill was, of course, aware of this but according to Freund and Fleischman [90], he concluded that refraction "may affect finer details, but it does not appear to be fundamental". Going back to the 1950s, Lighthill was not faced with the very stringent noise regulations that we are nowadays and therefore "finer details" are now much more important. The idea of systematically accounting for the effects of the jet flow interaction was pursued intensively first by Phillips [105] and subsequently somewhat more completely by Lilley *et al.* [106]. This section is devoted to presenting Lilley's Equation together with the so-called MGBK method for jet noise prediction.

4.3.2. The Lilley Equation

In order to obtain an equation in which all the propagation effects occurring in a transversely sheared mean flow are accounted for in the wave operator part of the analogy equation, Lilley derived a third-order Partial Differential Equation (PDE) by using the results from Phillips' equation [105]. It is in essence a modification of the Lighthill equation,

Eq. (4.8); from the full non-linear continuity and momentum equations, a single equation is derived for the field variable of interest, in which the left-hand side has a wave operator acting on the field variable, describing its propagation, and all other terms are collected on the right-hand side and treated as sources. The main difference between Lighthill's equation and Lilley's equation is that in the former, the wave operator used is that for a uniform stationary medium, whereas in the Lilley equation, the wave operator used is the Pridmore-Brown operator for propagation through a parallel sheared mean flow. For more detailed information of the ideas discussed here and their ramifications, see Chapter 6 of Goldstein's book [10].

Considering an inviscid flow, linearised about a uni-directional transversely sheared mean flow Lilley's equation can be written as,

$$\begin{aligned} L(p) &= c_s^{-2} D^3 p - D\Delta p - \frac{d}{dr}(\log c^2) D\frac{\partial p}{\partial r} + 2\frac{dU}{dr}\frac{\partial^2 p}{\partial x \partial r}, \\ &= \rho D \nabla\cdot\nabla\cdot(v_1 v_1 - \overline{v_1 v_1}) - 2\rho\frac{dU}{dr}\frac{\partial}{\partial x}\nabla\cdot(v_1 v_2 - \overline{v_1 v_2}), \end{aligned} \tag{4.13}$$

where t denotes time, p is acoustic pressure, v_1 and v_2 are the axial and radial turbulent velocity fluctuations, respectively. L is the Lilley wave operator term or also called Pridmore-Brown operator, and D is the material derivative:

$$D = \frac{\partial}{\partial t} + U\frac{\partial}{\partial x}, \tag{4.14}$$

and

$$\Delta = \frac{\partial^2}{\partial x^2} + \frac{\partial^2}{\partial r^2} + \frac{1}{r}\frac{\partial}{\partial r} + \frac{1}{r^2}\frac{\partial^2}{\partial \theta^2}. \tag{4.15}$$

The first term on the right-hand side of Eq. (4.13) denotes the typical quadrupole source term, which is due to the turbulence-turbulence interactions. The second term is attributed to the mean flow and turbulence interaction.

To derive the MGBK method, Mani *et al.* [107] worked on the high frequency Green's function solution for an axisymmetric case using Lilley's equation, Eq. (4.13). The details of the mathematical derivation of the Green's function solution to Lilley's equation are not within the aims of this thesis but more information can be found in [106] and [107]. The next section presents an overview of the MGBK method.

4.3.3 MGBK Method

The aim of this section is to provide a brief description of the famous MGBK Method which will be used to corroborate the noise predictions from the proposed jet noise prediction method (LRT) in Chapter 5 of this thesis. For a complete description of the MGBK method the reader is referred to Mani *et al.* [107] and Azarpeyvand [108].

The MGBK method is an updated version of a noise-prediction program called "MGB" developed during the 1970s by Mani, Gliebe and Balsa [107]. These authors provided a comprehensive analysis of the shielding effects of parallel jets when velocity and temperature profiles are functions of the radial variable only. The MGB method was then modified and improved by Khavaran, and is now referred to as MGBK method. Use of the MGBK method for subsonic jet flow [109, 110, 111] and predictions of radiated noise from supersonic jets [112, 113] has been numerously reported in the literature. One of its most important advantages is its fast compatibility for any required adjustment to the flow condition or the source term.

The starting point of the MGBK method is the farfield approximation of the Lighthill acoustic analogy, as given by Ribner [114] is

$$p^2(\vec{x},\tau) \propto \int_y I_{1111}(\vec{y},\tau)(a_{xx} + 4a_{xy} + 2a_{yy} + 2a_{yz})\,d\vec{y}\,, \tag{4.16}$$

where the directivity factors a_{xx}, a_{xy}, a_{yy} and a_{yz} are:

$$\begin{aligned} a_{xx} &= \frac{\cos^4\theta}{(1-M_c\cos\theta)^4}, \\ a_{xy} &= \frac{g_s^2\cos^2\theta}{2(1-M_c\cos\theta)^2}, \\ a_{yy} &= \frac{3}{8}g_s^4, \\ a_{yz} &= \frac{1}{8}g_s^4. \end{aligned} \tag{4.17}$$

where M_c is the convective Mach number and g_s is the value of the following function at the source point:

$$g_s{}^2(r) = \frac{(1-M_0\cos\theta)^2(c_0/c)^2 - \cos^2\theta}{(1-M_c\cos\theta)^2}, \tag{4.18}$$

where M_0 is the local jet Mach number and the proportionality factor, I_{1111} is given by,

$$I_{1111}(\vec{y},\tau) \propto \frac{1}{R^2}(1-M_c\cos\theta)^{-1}(1-M_0\cos\theta)^{-2}\int \frac{\partial^4}{\partial\tau^4}\overline{v_i v_j v_k v_l}\,d^3\vec{r}\,. \tag{4.19}$$

Although Ribner's directivity equation gave considerable improvement on noise prediction at that time, it is only correct when the shielding function, $g_s{}^2$, is positive. In the

case of any turning point (when $g_s^2 \leq 0$) one needs to modify the directivity terms using Lilley's equation.

The MGBK Method uses a generalized high frequency shielding theory derived from Lilley's Equation. The approach is to solve Lilley's equation for a convected point source of frequency ω using Balsa's work for the high frequency Green's function solution for an axisymmetric jet. Only the final equations as used in the MGBK method are presented here, all the mathematical derivation can be found in [107].

After taking the derivatives of the Green's function of each source with respect to the coordinates to make a quadrupole like sources, the directivity factors can be obtained as,

$$\begin{aligned} D_{11}^{(M)} &= \frac{\cos^4\theta}{(1-M_c\cos\theta)^4}\beta_{xx}, \\ D_{12}^{(M)} &= \frac{g_s^2\cos^2\theta}{2(1-M_c\cos\theta)^2}\beta_{xy}, \\ D_{22}^{(M)} &= \frac{3}{8}g_s^4\beta_{yy}, \\ D_{23}^{(M)} &= \frac{1}{8}g_s^4\beta_{yz}. \end{aligned} \tag{4.20}$$

The shielding coefficients, β_{xx}, β_{xy}, β_{yy} and β_{yz} depend upon the case encountered in Fig. 4.1 and their values are described in Table (4.1).

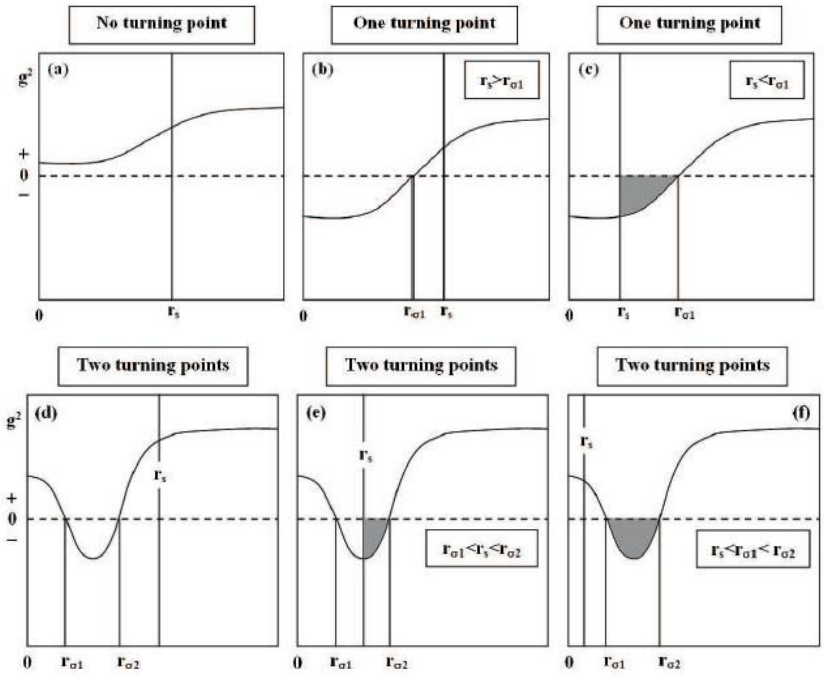

Figure 4.1 - Position of the turning points where shaded areas denote shielding of source. (From Azarpeyvand [108]).

Table 4.1: Shielding coefficients β_{ij}.

Case	β_{xx}	β_{xy}	β_{yy}	β_{yz}
a	1	1	1	1
b	1	1	1	1
c	β_{01}	0	0	0
d	1	1	1	1
e	β_{02}	0	0	0
f	β_{12}	β_{12}	β_{12}	β_{12}

The parameters $\beta_{01}, \beta_{02}, \beta_{12}$ are defined as:

$$\beta_{01} = \exp\left\{-2\frac{\Omega}{c}\int_{r_s}^{r_{\sigma 1}}\left|g^2(r)\right|^{0.5}dr\right\},$$
$$\beta_{02} = \exp\left\{-2\frac{\Omega}{c}\int_{r_s}^{r_{\sigma 2}}\left|g^2(r)\right|^{0.5}dr\right\}, \qquad (4.21)$$
$$\beta_{12} = \exp\left\{-2\frac{\Omega}{c}\int_{r_{\sigma 1}}^{r_{\sigma 2}}\left|g^2(r)\right|^{0.5}dr\right\}.$$

Finally, after determining the directivity coefficients, the power spectral directivity of an axisymmetric jet ($D_{22}^{(M)} = D_{33}^{(M)}$ and $D_{12}^{(M)} = D_{13}^{(M)}$) can be expressed as:

$$\overline{p_{Self}^2}(R,\theta,\Omega) \sim \int_{\vec{y}} \int_{-\infty}^{+\infty} \{D_{11}^{(M)} + 2C_1 D_{22}^{(M)} + 4(C_2 + 2C_4) D_{12}^{(M)} + 2(C_3 + 2C_5) D_{23}^{(M)}\} \Lambda_M e^{j\Omega\tau} d\tau d\vec{y} \quad , \tag{4.22}$$

$$\overline{p_{Shear}^2}(R,\theta,\Omega) \sim \int_{\vec{y}} \int_{-\infty}^{+\infty} \{C_4 D_{11}^{(M)} + (C_1 + C_5) D_{12}^{(M)}\} \Lambda_D e^{j\Omega\tau} d\tau d\vec{y} \, . \tag{4.23}$$

where,

$$\Lambda_M = \frac{(\rho_0 / \rho)^2}{(4\pi R c c_0)^2 (1 - M_0 \cos\theta)^2 (1 - M_c \cos\theta)^2} I_{1111} , \tag{4.24}$$

$$\Lambda_D = \left(\frac{2dU/dr}{\Omega} \frac{1 - M_c \cos\theta}{1 - M_0 \cos\theta} \right)^2 \Lambda_M \quad . \tag{4.25}$$

Source and observer frequencies are related through a modified convection factor, Eq. (4.26), where α_c is an empirical convection constant determined by [111] as equal to 0.55 by comparison of predicted spectra with noise data. M_c is the convective Mach number.

$$\Omega = \omega \sqrt{(1 - M_c \cos\theta)^2 + (\alpha_c k^{0.5} / c_0)^2} \, . \tag{4.26}$$

The axial quadrupole source component according to [111] is given by the following relation:

$$I_{1111}(\Omega) = \left(\frac{\alpha_1}{\alpha_2}\right)^3 \frac{\sqrt{2}}{4} \rho^2 \frac{\partial^4}{\partial \tau^4} g^2(\tau)\, k^{7/2}\, \tau_0^3\, \Delta^2 \left(\frac{3}{2} - \beta\right)^{-13/2}, \tag{4.27}$$

where,

$$\Delta = \frac{L_2}{L_1}, \qquad \beta = (1 - \frac{\overline{u_2^2}}{\overline{u_1^2}}). \tag{4.28}$$

The total noise from the MGBK method is the summation of the self and shear-noise components that are calculated from Eq. (4.22) and Eq. (4.23), respectively.

4.3.3.1 Limitations

Although MGBK gives a rational means of calculating the noise of jet flows, some of the assumptions made in its derivation limit its applicability for certain problems. According to Almeida [30] the main limitations of the method can be described are:

- The sound-flow interaction assumes an inviscid flow linearised about a unidirectional transversely shear flow. Transitions to supersonic flow due to high frequency emission associated with shock waves impose limitations to use the methodology.
- In the case of heated jets at low exit velocities, additional dipole sources terms associated with the velocity fluctuations imbedded in transverse gradients of the mean flow density become important. The formulation does not account for density variations and there is a limitation for its use in heated flows.
- The numerical method is based on an axisymmetric turbulence hypothesis and its application is limited to those jet flows which are completely axisymmetric in nature.

The last section of this chapter presents the proposed new method for jet noise predictions which is called LRT. This method is developed in order to overcome some of the drawbacks from the MGBK method.

4.4 LRT Method

This section is devoted to a presentation of the novel method for jet noise prediction that is being proposed in this thesis. The method will be referred to throughout this work as LRT as the method is a combination of **L**ighthill's theory with **R**ay-**T**racing acoustics. In this section all the formulation and assumptions considered for the LRT method are presented. Prior to that we briefly review how the LRT method overcomes the limitations discussed in Section 4.3.3.1.

A lot of strategies for jet noise prediction have already been discussed here and there are many more options available in the literature. However, there was a lack of a mathematical formulation that could be applied for jet flows that are exhausted from arbitrary nozzle geometries; in other words there was a need for a method that does not require making any geometrical simplification of the problem such as symmetry, parallel flow or shear flows. This is what the LRT method is capable of doing. The method was developed in a way to be applicable to non-circular nozzles, offset nozzles, serrated nozzles and any novel design aiming at noise reduction. Moreover, the LRT method provides the ability to investigate the effects of refraction due to a very complex 3-dimensional flow by calculating the noise for any azimuthal or polar angle of interest. This is only possible because the method developed uses a geometric acoustic strategy to calculate the sound and mean flow interactions without any simplification. The ultimate goal of the LRT method is to be a relatively fast tool for noise prediction that can be used in an engineering context for the design of novel nozzles for jet noise reduction.

The starting point of the model is the formulation proposed by Jordan and Gervais [115] for the acoustic field generated by a jet flow:

$$P(\vec{y},\theta) = A\, I_{ijkl}\, dir(ijkl)\,, \tag{4.29}$$

where

$$A = \frac{\rho_0}{16\pi^2 c_0^2 R^2 (1 - M_c \cos\theta)^5}\,. \tag{4.30}$$

The fourth-order autocorrelation function for a unit volume of turbulence is:

$$I_{ijkl}(\tau) = \int \frac{\partial^4}{\partial \tau^4} \overline{v_i v_j v_k v_l}\, d^3\vec{r}\,, \tag{4.31}$$

and the source directional patterns can be calculated by

$$dir(ijkl) = \frac{1}{2\pi}\int_0^{2\pi} \left(\frac{x_i x_j x_k x_l}{x^4} \right) \quad d\varphi\,. \tag{4.32}$$

Figure 4.2 depicts the coordinate system adopted for the derivation of the LRT method. All the mathematical expressions are related to this system from now one.

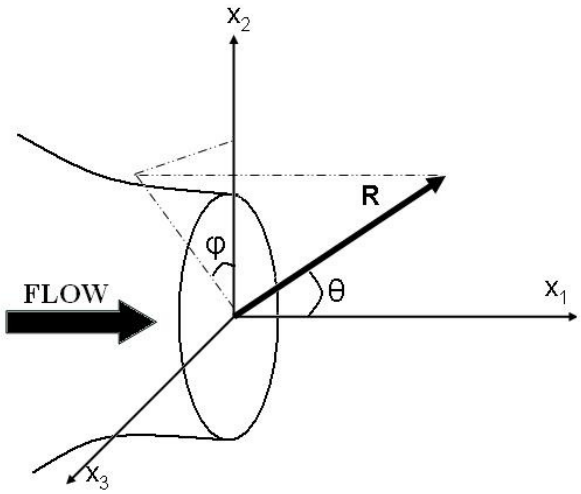

Figure 4.2 - Coordinate system adopted for the LRT derivation.

From Fig. 4.2 it is possible to write the following mathematical relations:

$$\begin{aligned} x_1 &= R\cos\theta \\ x_2 &= R\cos\varphi\sin\theta \\ x_3 &= R\sin\theta\sin\varphi \end{aligned} \quad . \tag{4.33}$$

And then the directivity patterns are given by:

$$\begin{aligned} &dir(1111) = \cos^4\theta, \\ &dir(1212) = dir(1122) = dir(1313) = dir(1133) = \frac{1}{2}\cos^2\theta\sin^2\theta, \\ &dir(2222) = dir(3333) = \frac{3}{8}\sin^4\theta, \\ &dir(2323) = dir(2233) = \frac{1}{8}\sin^4\theta. \end{aligned} \tag{4.34}$$

After carrying out some simple calculations the acoustic field generated by a jet flow can be written as:

$$P(\vec{y},\theta) = A(\cos^4\theta)I_{1111} + 4\left(\frac{1}{2}\right)A(\cos^2\theta\sin^2\theta)I_{1212} + 2\left(\frac{1}{2}\right)A(\cos^2\theta\sin^2\theta)I_{1122}$$
$$+\left(\frac{3}{8}\right)A(\sin^4\theta)I_{2222} + 4\left(\frac{1}{2}\right)A(\cos^2\theta\sin^2\theta)I_{1313} + 2\left(\frac{1}{2}\right)A(\cos^2\theta\sin^2\theta)I_{1133} .$$
$$+2\left(\frac{1}{8}\right)A(\sin^4\theta)I_{2233} + 4\left(\frac{1}{8}\right)A(\sin^4\theta)I_{2323} + \left(\frac{3}{8}\right)A(\sin^4\theta)I_{3333}$$

(4.35)

The next step is to define the fourth order autocorrelation function in order to determine the source strength and its contribution to the far-field noise. This will be addressed in the following section.

4.4.1 Source Modelling

The source modelling used in the LRT Method follows the concept also used by Khavaran and Krejsa [111] where a fourth-order space-time velocity correlation is expressed in terms of second-order correlations as shown in Eq. (4.36).

$$\overline{v_i v_j v_k' v_l'} = \overline{(v_i v_j)}\,\overline{(v_k' v_l')} + \overline{(v_i v_k')}\,\overline{(v_j v_l')} + \overline{(v_i v_l')}\,\overline{(v_j v_k')}\,, \tag{4.36}$$

where $\overline{(v_i v_j')}$ is the velocity correlation between two points $\vec{y}$ and $\vec{y}'$ separated by a vector $\vec{\xi}$ and a time-delay τ. Probably the first to introduce and experimentally examine this formulation for a homogeneous and isotropic turbulent flow was Uberoi [116]. Different types of correlation functions are available in the literature however the one introduced by Uberoi has been extensively used for jet noise predictions methods and it appears to reflect fairly well the underlying physics of the turbulence.

Considering the source correlation term due to a unit volume turbulence in Eq. (4.31) and repeated below for simplicity

$$I_{ijkl}(\tau) = \int_{\vec{\xi}} \frac{\partial^4}{\partial \tau^4} \overline{v_i v_j v_k v_l}\ d\vec{\xi}\,, \tag{4.31}$$

for $0 \le \left|\vec{\xi}\right| < \infty$. Substituting Eq. (4.36) into Eq. (4.31), we obtain

$$I_{ijkl}(\tau) = \frac{\partial^4}{\partial \tau^4} \int_{\vec{\xi}} [\overline{(v_i v_k^{'})}\,\overline{(v_j v_l^{'})} + \overline{(v_i v_l^{'})}\,\overline{(v_j v_k^{'})}]\, d\vec{\xi}\,. \tag{4.37}$$

The corresponding noise spectra for a source of frequency Ω is the Fourier transform of the autocorrelation function

$$I_{ijkl}(\Omega) = \frac{1}{2\pi} \int_{-\infty}^{+\infty} I_{ijkl}(\tau)\, e^{i\Omega\tau}\, d\tau\,. \tag{4.38}$$

To carry out with the integration of Eq. (4.37) and Eq. (4.38) it is convenient to assume space and time separation. This will be further discussed in the next section.

4.4.1.2 Separable Two-Point Correlation

Ribner [117] suggested one of the most convenient forms to express the two-point velocity correlation as:

$$Q_{ij}(\vec{\xi}, \tau) = R_{ij}(\vec{\xi})\, g(\tau)\,, \tag{4.39}$$

where, for homogeneous isotropic turbulence, the space factor R_{ij} can be written as given by Batchelor [118] as

$$R_{ij}(\vec{\xi}) = k\,[(f + \frac{1}{2}\varepsilon f')\delta_{ij} - \frac{1}{2} f' \frac{\xi_i \xi_j}{\xi}], \tag{4.40}$$

and $k = \frac{1}{2}(\overline{v_1^2} + \overline{v_2^2} + \overline{v_3^2})$ is the local turbulent kinetic energy, v_1 and $v_{2,3}$ being the stream-wise, and cross-stream (span-wise) turbulent velocities respectively, and f is function of $\vec{\xi}$ which can take different forms and $f' = \partial f / \partial \xi$. According to Azarpeyvand [108], the most common functions used for f are:

$$f(\xi) = e^{-\pi\left(\frac{\xi_1^2}{L_1^2} + \frac{\xi_2^2}{L_2^2} + \frac{\xi_3^2}{L_3^2}\right)}, \tag{4.41}$$

$$f(\xi) = e^{-\pi\left(\frac{\xi_1}{L_1} + \frac{\xi_2}{L_2} + \frac{\xi_3}{L_3}\right)}, \tag{4.42}$$

$$f(\xi) = e^{-\left(\frac{\xi_1}{L_1} + \frac{\xi_2^2}{L_2^2} + \frac{\xi_3^2}{L_3^2}\right)}, \tag{4.43}$$

$$f(\xi) = e^{-\sqrt{\left(\frac{\xi_1^2}{L_1^2}\right) + \left(\frac{\xi_2^2}{L_2^2} + \frac{\xi_3^2}{L_3^2}\right)^2}}, \tag{4.44}$$

$$f(\xi) = \exp\left(-\pi \frac{\xi^2}{L^2}\right), \tag{4.45}$$

where L_1, L_2, L_3 are length scales in the axial, radial and azimuthal directions, respectively, and $L(L_1,L_2,L_3,\xi)$ is defined by:

$$L(L_1, L_2, L_3, \vec{\xi}) = \sqrt{\frac{L_1^2 L_2^2 L_3^2 (\xi_1^2 + \xi_2^2 + \xi_3^2)}{L_2^2 L_3^2 \xi_1^2 + L_1^2 L_3^2 \xi_2^2 + L_1^2 L_2^2 \xi_3^2}} \,. \tag{4.46}$$

These formulations all require knowledge of the fluid dynamics, including turbulence, of the flow which one can obtain by measurements or by means of a CFD turbulence model, such as RANS.

The LRT method uses the formulation presented in Eq. (4.45) for the function *f*, which is the same as used in [111], when isotropic turbulence is considered. This formulation makes $f(\xi)$ decrease to zero for large ξ with sufficient rapidity to make $\int_0^\infty \xi^m f(\xi) d\xi$ converge for $m \geq 0$.

Substitution of Eq. (4.39) and Eq. (4.40) into Eq. (4.37) will give the general expressions for quadrupole sources assuming isotropic turbulence:

$$\begin{aligned}
&I_{1111}(\tau) = \rho^2 \frac{\partial^4}{\partial \tau^4} g^2(\tau) \frac{(\overline{u_1^2})^2 L^3}{2\sqrt{2}} \\
&I_{2222} = I_{3333} = I_{1111} \\
&I_{1122} = I_{1133} = I_{2323} = \frac{1}{8} I_{1111} \\
&I_{1212}(\tau) = I_{1313} = I_{2323} = \frac{7}{16} I_{1111}
\end{aligned} \,, \tag{4.47}$$

where the *L* is the turbulent length scale. (More discussion on the turbulent length scale will be presented in Section 4.4.2).

As already stated, Eq. (4.47) represents the general expressions for the quadrupole sources assuming isotropic turbulence. However, the LRT method has also the option of using an axisymmetric turbulence formulation. All the mathematical steps for the axisymmetric turbulence can be found in [111] and will not be repeated here. Eq. (4.48) presents only the

final result for the general expression for quadrupole sources with axisymmetric turbulence modelling:

$$
\begin{aligned}
&I_{1111}(\tau) = \rho^2 \frac{\partial^4}{\partial \tau^4} g^2(\tau) \frac{(\overline{u_1^2})^2 L_1^3 \Delta^2}{2\sqrt{2}}, \\
&I_{2222}(\tau) = I_{3333} = C_1 I_{1111}\ , \\
&I_{1122}(\tau) = I_{1133} = C_2 I_{1111}\ , \\
&I_{2233}(\tau) = C_3 I_{1111}\ , \\
&I_{1212}(\tau) = I_{1313} = C_4 I_{1111}\ , \\
&I_{2323}(\tau) = C_5 I_{1111}\ .
\end{aligned}
\tag{4.48}
$$

where the weight coefficients, C_i are given by:

$$
\begin{aligned}
&C_1 = \frac{3}{2}\beta^2 + \frac{1}{32}\left[9(\Delta+\Delta^{-1})^4 - 48(\Delta+\Delta^{-1})^2 + 80\right] - \frac{\beta}{4}(6 - \Delta^2 + 3\Delta^{-2})\ , \\
&C_2 = \frac{1}{8}\ , \\
&C_3 = \frac{1}{8}\left[\frac{3}{4}(\Delta+\Delta^{-1})^4 - 4(\Delta+\Delta^{-1})^2 + 7 - 2\Delta^2 + 4\beta^2 + 2\beta(\Delta^2 - 2 - \Delta^{-2})\right], \\
&C_4 = \frac{1}{16}(5 + 2\Delta^{-2} - 8\beta)\ , \\
&C_5 = \frac{1}{2}(C_1 - C_3)\ ,
\end{aligned}
\tag{4.49}
$$

In the limiting case of an isotropic turbulence, $\Delta = 1$, $\beta = 0$, and coefficients C_i (i = 1,…,5) reduce to those given by Eq. (4.47).

After analyzing the space factor of the correlation, it is now necessary to consider the temporal factor, $g(\tau)$, which gives the temporal decay of the correlation. There are different ways to model $g(\tau)$ but the best results were obtained by using the Gaussian form, presented in Eq. (4.50) below:

$$g(\tau) = \exp\left\{-\left(\frac{\tau}{\tau_0}\right)^2\right\} \quad , \tag{4.50}$$

where τ_0 is a characteristic time scale of the turbulence. (More detailed information of the time scale of the turbulence will be present in section 4.4.2).

The integration of the temporal part $g^2(\tau)$ over τ, which appears upon substituting Eq. (4.39) in Eq. (4.38), can be simplified using the following relation

$$\langle G \rangle = \int_{-\infty}^{+\infty} \frac{\partial^4}{\partial \tau^4} g^2(\tau) e^{j\Omega\tau} d\tau = \Omega^4 \int_{-\infty}^{+\infty} g^2(\tau) e^{j\Omega\tau} d\tau \,. \tag{4.51}$$

Using the Gaussian function for the temporal factor, as shown in [108], leads the following relation for $\langle G \rangle$,

$$\langle G \rangle = \frac{\sqrt{2\pi}}{2} \tau_0 \Omega^4 e^{-\frac{1}{8}\Omega^2\tau_0^2} \,. \tag{4.52}$$

Substitution of Eq. (4.52) and Eq. (4.47) in Eq. (4.39) and finally into Eq. (4.37) yields,

$$I_{1111}(\tau) = \frac{\sqrt{\pi}}{4} L^3 \rho^2 k^2 \tau_0 \Omega^4 \exp\left(-\frac{1}{8}\Omega^2\tau_0^2\right). \tag{4.53}$$

At this point it becomes necessary to establish the relationships between turbulence and noise generation mechanism. This information can be obtained by using a proper turbulence model, such as RANS. Section 4.4.2 will present the most important characteristics of turbulence that links with the noise prediction method.

4.4.2 Turbulent Length and Time-Scales

Different models for turbulent length scales have been developed during the years, such as the works of Harper-Bourne [119], Self [120] and Morris and Boluriaan [121]. Most probably the length scale associated with the turbulence decay rate is still the most widely used in the literature and it is given by

$$L = c_l \frac{k^{3/2}}{\varepsilon}, \tag{4.54}$$

k being the turbulent kinetic energy, ε the dissipation of turbulent energy and c_l is a calibrating constant. The turbulence characteristics frequency Ω_0, which is the inverse of the characteristic time-delay τ_0, relates to k and ε as

$$\tau_0 = \frac{1}{\Omega_0} = c_\tau \frac{k}{\varepsilon} \qquad \rightarrow \qquad \varepsilon = c_\tau \frac{k}{\tau_0}. \tag{4.55}$$

Therefore the turbulent-length scale can be written as

$$L = \frac{c_l}{c_\tau} k^{1/2} \tau_0. \tag{4.56}$$

The turbulent energy transfer time-scale (TET) presented in Eq. (4.57) has been chosen to model the turbulent time-scale (τ_0) in the LRT method [108]:

$$\tau_0 \approx \alpha_T c_\tau \frac{k}{\varepsilon}\left(\frac{\Psi}{L}\right)^{2/3}. \tag{4.57}$$

Here Ψ denotes the size of the eddy, which can be either determined from experimental results or can be estimated from the shear layer thickness. The quadrupole source for an axisymmetric turbulence used in the LRT method can now be written as:

$$I_{1111}(\Omega) = \frac{\sqrt{\pi}}{4}\left(\frac{c_l}{c_\tau}\right)^3 \Delta^2 \left(\frac{3}{2}-\beta\right)^{-13/2} \rho^2 \tau_0^4 \Omega^4 \, k^{7/2} \exp\left(-\frac{\tau_0^2 \Omega^2}{8}\right) . \quad (4.58)$$

There are two calibration coefficients in Eq. (4.58), c_l and c_τ, which need to be defined based on the experimental data. Instead of working directly with these two coefficients they can be transformed to only one calibration coefficient, α_T, as presented below:

$$\alpha_T = c_\tau c_l^{2/3} \qquad \rightarrow \qquad c_\tau = \frac{\alpha_T}{c_l^{2/3}} , \quad (4.59)$$

which leads to the forth-order correlation function that is used in the LRT method:

$$I_{1111}(\Omega) = \frac{\sqrt{\pi}}{4}\frac{c_l^5}{{\alpha_T}^3}\Delta^2 \left(\frac{3}{2}-\beta\right)^{-\frac{13}{2}} \rho^2 \tau_0^4 \Omega^4 \, k^{7/2} \exp\left(-\frac{\tau_0^2 \Omega^2}{8}\right) . \quad (4.60)$$

The modified convection factor, Ω, is calculated by using Eq. (4.26) already described in the MGBK method, which is repeated here for simplicity.

$$\Omega = \omega\sqrt{(1-M_c\cos\theta)^2 + (\alpha_c k^{0.5}/c_0)^2} . \quad (4.26)$$

The convection Mach number (M_c), Eq. (4.61), is expressed as a function of the weighted average of the local Mach number (M_0), given by Eq. (4.62), and the nozzle exit Mach number (M_j), given by Eq. (4.63).

$$M_c = 0.5M_0 + 0.3M_j, \tag{4.61}$$

$$M_0 = \frac{v_{1_i}}{c_i}, \tag{4.62}$$

$$M_j = \frac{U_j}{c}. \tag{4.63}$$

Rewriting Eq. (4.35) with all the mathematical operations shown before, the acoustic field on the far-field generated by a jet flow is calculated by the LRT method as:

$$\begin{aligned} P(\vec{y},\theta) = {} & A(\cos^4\theta)I_{1111} + 2A(\cos^2\theta\sin^2\theta)C_4I_{1111} + A(\cos^2\theta\sin^2\theta)C_2I_{1111} \\ & + \left(\frac{3}{8}\right)A(\sin^4\theta)C_1I_{1111} + 2A(\cos^2\theta\sin^2\theta)C_4I_{1111} + A(\cos^2\theta\sin^2\theta)C_2I_{1111}. \\ & + 4A(\sin^4\theta)C_3I_{1111} + 2A(\sin^4\theta)C_5I_{1111} + \left(\frac{3}{8}\right)A(\sin^4\theta)C_1I_{1111} \end{aligned} \tag{4.64}$$

Up to now, the sound and mean flow interactions have not been considered in the derivation of the LRT method. Section 4.4.4 will address this problem.

4.4.4 Coupling the refraction effects in the LRT

To account for the refraction due to the interaction of the mean flow with the radiated sound a method based on a Ray-Theory is used. This is in contrast to the work of Balsa for the high-frequency Green's function for the axisymmetric Lilley's equation.

As already discussed previously, the idea of using geometrical acoustics for jet noise studies is not something new. Most of the applications have been done to analyze the effects of scattering due to turbulence fluctuations on the shear layer, investigation of the zone of silence as well as the caustics of geometrical acoustics. However, in this thesis, the Ray-Tracing technique developed is applied in a way that the sound amplification or reduction due to refraction is taken into account on the source model when calculating the final far-field noise prediction. The major advantage of this methodology is that no simplification regarding geometry of the nozzle or nature of the jet flow needs to be considered and therefore overcoming one of the biggest limitation of the MGBK method.

Chapter 3 presented and discussed the main features of the Ray-Tracing (RT) Theory together with the numerical strategies used to calculate the propagation effects on the LRT code. The main output of the RT is the variation of Sound Pressure Level (SPL) on the farfield due to the refraction effects, which is given by (ΔSPL_{RT}),

$$\Delta SPL_{RT} = 10\log\left(\frac{p_{jet}^{\,2}}{p_{ff}^{\,2}}\right), \tag{4.65}$$

where p_{ff} is the pressure due to the source without the jet refraction effects or a free field pressure and p_{jet} is the pressure due to the source in the jet flow. Another way to write Eq. (4.65) is,

$$p_{jf} = p_{ff} \cdot 10^{(0.1 \cdot \Delta SPL_{RT})}. \tag{4.66}$$

Finally, the acoustic field that contains the refraction effects is obtained by integrating Eq. (4.64) with Eq. (4.66) which yelds,

$$P(\vec{r}, \theta) = \int p(\vec{y}, \theta) \cdot 10^{(0.1 \Delta SPL_{RT})} d\vec{y}\,. \tag{4.67}$$

The next section will present an overview of the calculation procedure for the LRT methodology.

4.4.5 Calculation Procedure

After presenting the mathematical details of the LRT method, this section introduces the computational procedure for noise predictions using the new methodology. A block diagram of the computation sequence for the LRT method is given in Fig. 4.3 as an outline of the methodology.

Assuming the nozzle geometry is defined and that the operational conditions of the jet are known, the first step required for the LRT method is to perform a CFD-RANS based calculation which will provide all the input information needed to calculate the noise in the far-field, such as mean velocity field, temperature, sound speed and turbulence quantities.

With the mean flow properties determined the next step is to generate the point sources which constitute a discretization of real continuum jet source. This procedure is necessary to identify the source positions that will be used in the Ray-Tracing code. Based on the local Mach number of the computation domain, the numerical technique will identify the most important sources that will be affected by refraction.

From each point source so defined, the Ray-Tracing code will launch a large number of rays and then determine their propagation path. The RT technique calculates the noise attenuation or amplification in the far-field. (The RT code is the one that consumes most of the computational time for the LRT method).

Knowing the variation of Sound Pressure Level (ΔSPL) in the far-field due to the refraction effects, the final step is to run the source model of the LRT method which will generate the jet free noise spectrum at each observer angle in terms of power spectra density or also in 1/3-octave band frequency of interest. The contributions from each volume element are summed on a mean-square pressure basis, assuming that individual volume elements are uncorrelated with each other. This provides the predicted total sound pressure level as seen by an observer in the far field.

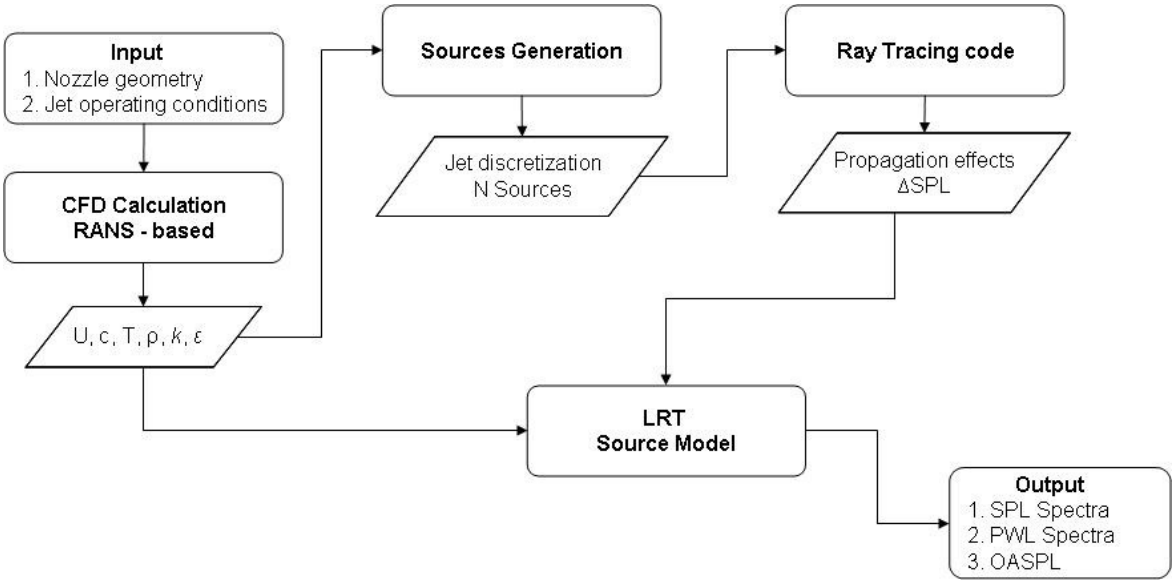

Figure 4.3 - Block diagram of the computational sequence of the LRT method.

Chapter 5: Numerical Results: Single stream jet flow

The objectives of this chapter are manifold. First, it will present a validation of the LRT method by comparing LRT noise predictions for a single jet flow against both experimental data and predictions using the well-know MGBK method. As will be shown, the LRT method gives considerably improved predictions for the rear and forward arcs compared to MGBK. Second, the ability of the LRT method to handle different nozzle geometries and nozzle operation conditions is demonstrated by studying a wide range of Mach number flows with temperature ratios varying from isothermal cases (TR=1.0) to extremely hot flows (TR=2.5). In addition, the effect of the mean flow on the propagation of the sound waves is considered and the Ray-Tracing results are discussed. These results provide the ability to roughly visualize (for what is believed to be the first time) the shape of the zone of silence for high speed jets. Finally, an investigation of the turbulent calibration constants used in the LRT method is presented.

The results presented in this chapter are divided into three sections. The first one covers the comparison of the LRT method with the experimental data from the JEAN project which is widely cited in the literature. The second section explores the application of the proposed methodology for a more recent and reliable noise data base collected during the SYMPHONY project in 2010. The third and final section investigates the turbulent calibration constants that are present in the LRT method.

5.1 Mach 0.75 isothermal jet – Validation case

In order to validate the methodology proposed in this thesis, results for a Mach number 0.75 isothermal jet case is given. The jet chosen is a very well-know case available in

the open literature. A vast number of papers focused on this particular flow condition can be easily found which provide detailed information regarding mean flow properties of the jet as well as far-field noise data to corroborate with the validation procedure. In addition, the MGBK method is also applied to compare with the predictions obtained by the LRT method. The details of the methodology are described in the following sections.

5.1.1 Experimental Database - JEAN

The experimental acoustic data used in this section were collected from the JEAN (Jet Exhaust Aerodynamics & Noise) EU Research Programme – FP5 Contract No. G4RD-CT-2000-00313. Experiments for a single flow jet were carried out by Jordan *et al.* [122] at the MARTEL facility at CEAT (Centre d'Etudes Aero-dynamiques et Thermiques) Universit de Poitiers. It is important to highlight here that during the JEAN project three different jet Mach numbers were tested. However, in this work we are using only the Mach number 0.75 isothermal jet condition to validate the LRT method.

5.1.2 Numerical procedure

As presented in the previous chapter, the basic input information for the LRT method is the mean properties of the jet flow. For this requirement, a RANS based CFD calculation was performed for the validation case and the most important parameters are described below.

5.1.2.1 CFD Results

The nozzle geometry used in the experiments has a diameter of 50 mm with a smooth contraction and a sharp lip as depicted in Figure 5.1. The nozzle operational conditions for the Mach number 0.75 jet are presented in Table (5.1).

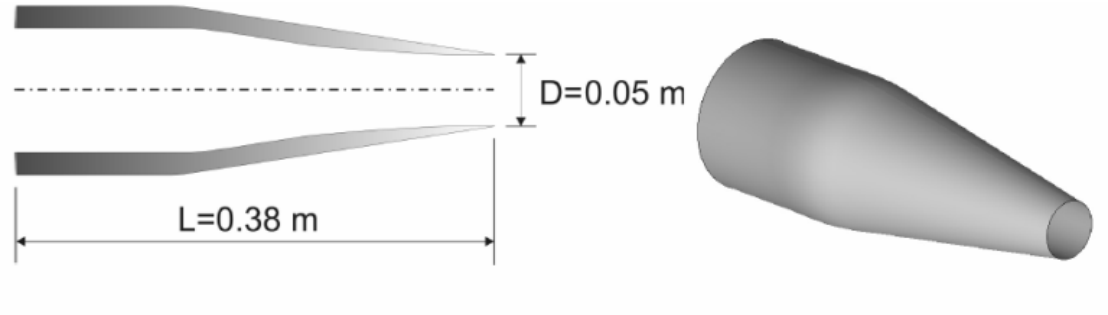

Figure 5.1 - Geometry for the Mach number 0.75 JEAN case. Modified from [30].

Table 5.1 - Nozzle operational condition.

Case	U_j/c_∞	T_j/T_0	U_j (m/s)	c_∞ (m/s)	P_j (Pa)	ρ_∞ (kg/m^3)	P_0 (Pa)	T_0 (K)
1	0.75	1.0	253.31	337.75	144400	1.225	99670	283.15

The computational grid used for the 3-dimensional RANS simulations is shown in Fig. 5.2, which has approximately 600x10^3 elements. Fig. 5.2(b) illustrates the clustering of points near the shear layer of the jet. This mesh was determined as the optimum mesh after a mesh sensitivity studied performed.

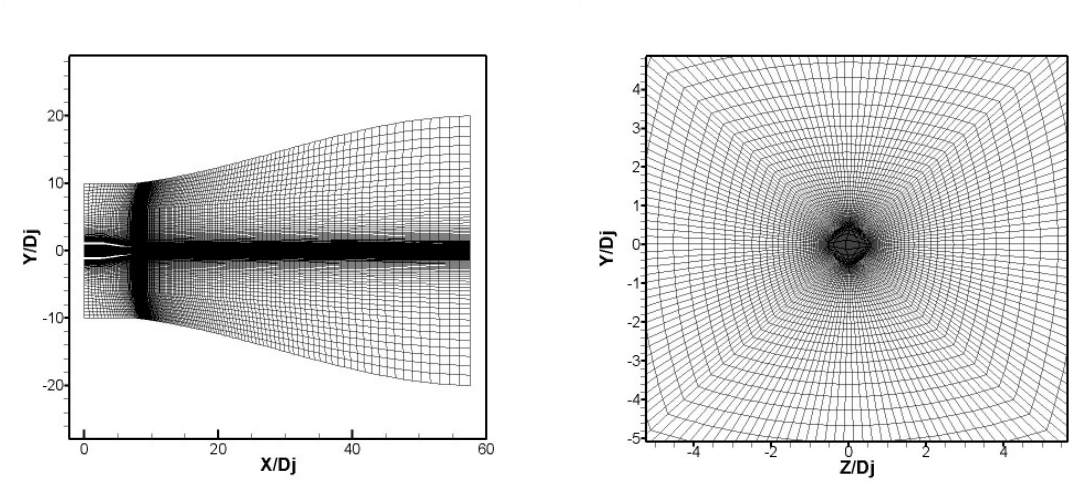

(a) (b)

Figure 5.2 - Computational grid in (a) xy-plane and (b) yz-plane.

A non-linear k-ε turbulence model, named k-ε cubic, proposed by Goldberg *et al.* [123] was applied in the present work. The jet boundary condition was

modelled as a pressure inlet with specified values for total pressure and total temperature as presented in Table (5.1). This turbulence model is available on the CFD++ commercial code from Metacomp Tech and it has been extensively used for some years, not only for jet noise predictions [124, 125] but also for automobile aeroacoustics [126].

Figure 5.3 presents the Mach number distribution, turbulent kinetic energy distribution and the jet centreline velocity decay obtained from the CFD method. The turbulent kinetic energy is compared for three different radial positions, showing that the peak value is distributed along the lipline of the jet ($Y/D_j = 0.5$). The centreline velocity decay from the RANS calculations is compared against the experimental data [127].

As can be seen in Fig. 5.3(c), there is an over-prediction of the jet's potential core length. This is a result mainly of the turbulence modelling used. The turbulence models are developed by assuming that the turbulence is in a state where certain simplifying conditions apply and therefore they are in a strict sense limited by these simplifications and typically contain one or more coefficients that cannot be determined theoretically. It is therefore necessary to calibrate these models using, for example, experimental data, both to validate the underlying assumptions and to determine the coefficients. The disadvantage of this approach is that the flow process used to calibrate the coefficients will not always represent the physics of more complex flows accurately and therefore discrepancies may be expected.

The problem of using a particular turbulence model to correctly predict the velocity decay for round jets is well known. The first to realize and propose modifications to try to overcome this drawback was Pope [128] in which he refers to this problem as a round-jet anomaly. Pope's explanation was based on the presence of vortex stretching in the flow region that leads to greater dissipation and lower effective viscosity especially for axisymmetric jets. Pope proposed modifications to the constants of the dissipation equation to model this behaviour. Nalassamy [129] presents an extensive survey of turbulence models

applied for jet noise computation utilizing computational fluid dynamics of the turbulent jet flow field. The main conclusion was that anisotropic turbulence characteristics would substantially improve the confidence levels in jet flow predictions. Knowing that there is still a lack of turbulence models for turbulent jet flows, this work uses the state-of-art turbulence models available on CFD commercial codes.

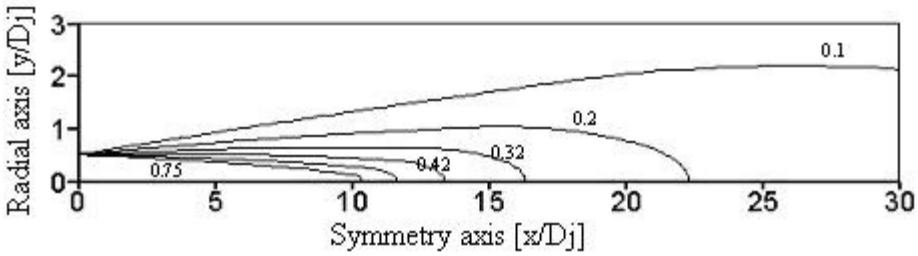

(a) Mach number distribution.

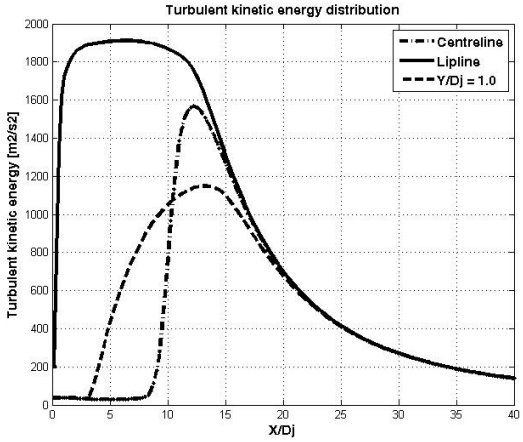

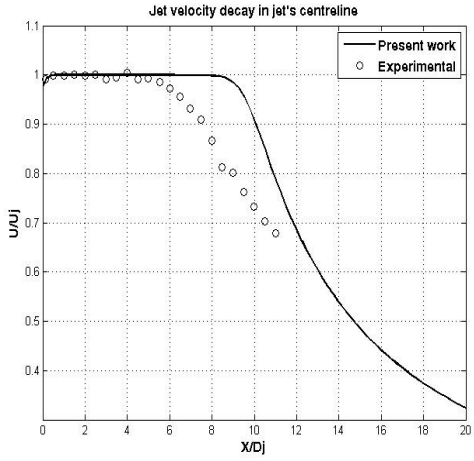

(a) Turbulent kinetic energy distribution. (c) Centreline velocity decay.

Figure 5.3- Fluid dynamics results from the RANS CFD simulation of the Mach number 0.75 jet.

Once the mean flow values are obtained it is possible to apply the noise prediction method. Far-field noise predictions calculated with the LRT method are presented in the next

subsection. The results are compared against the available experimental data and also with the predictions of the total noise obtained with the MGBK method.

5.1.2.2 Far-field noise predictions

The noise predictions for the Mach number 0.75 jet are shown in Fig. 5.4. The results show the strength of the LRT for calculating the noise directivity for single stream jets. All the turbulent constants required in the method have been adjusted to give agreement with data at 90 degrees. The results are presented for the angles outside the zone of silence, where the refraction effects due to the mean flow are calculated from the Ray-Tracing code.

As can be seem in Fig 5.4, for ninety degrees the differences between LRT and MGBK predictions are negligible and both methods are able to capture the peak frequency and also the shape of the spectra in good agreement with experiments. Going to the rear angles, close to the zone of silence region, where the refraction effects start to play an important rule, the MGBK method slightly over-predicts the measurements but the results still have reasonable agreement. However, going into angles higher than 90 degrees, the MGBK code starts to over predict the noise by more than 4dB but the LRT method preserves very good agreement with the experiments. This is mainly due to the improvements the LRT has in calculating the refraction effects with the Ray-Tracing code instead of using the shielding functions from the high-frequency assumption derived from Lilley's equation which is used by the MGBK.

To better understand these improvements on the far-field noise predictions that the LRT method provides when compared to the MGBK, it is necessary to evaluate the refraction effects calculated by the Ray-Tracing code. Figure 5.5 depicts the 3-dimensional results of the calculated ΔSPL for different downstream observer locations. In this case, the RANS solution of the jet flow was used as the input for the RT code in order to calculate the refraction effects from the jet sources propagation to the observer angles. For positives values of ΔSPL it means

that the noise from the equivalent point source is being amplified due to the mean flow and negative values of ΔSPL means that the noise is being attenuated due to the mean flow. These results are strongly dependant on the polar angle that is being analyzed and also on the local position of the source inside the jet. The ability of the Ray-Tracing Theory to calculate the flow-acoustics interactions from a real 3D spreading jet overcomes the main simplification of the generalized high frequency shielding theory derived by Balsa *et al.* [130]. In this theory, they simplified the problem by assuming the flow as a parallel axisymmetric jet-like sheared flow in order to derive the shielding functions that are used on the MGBK method.

Another way to analyze the refraction effects is presented in Fig. 5.6. This figure depicts the results of ΔSPL on a plane passing through the jet centreline for different polar angles relatively to jet axis to an observer located at $50D_j$. For the shallow angles to the jet axis, i.e. zone of silence region (40º and 50º), there is a very large noise attenuation which will greatly affect the sound in the far-field. As already mentioned, this is attributed to the shrouding effect of the mean flow. At 90º the flow-acoustics interaction are negligible explaining once more the agreement of the LRT method with the MGBK.

For completeness, Fig. 5.7 shows the sources used in the Ray-Tracing code for the validation case. The sources are distributed in space following the spreading rate of the jet so that a higher density of sources is used near the high velocity gradients in the flow, i.e. shear layer. The domain used to distribute the sources is shown in Fig. 5.7(a) which goes from the nozzle exhaust position up to $18D_j$ downstream covering the most important source region of this kind of jet flow. Fig. 5.7(b) depicts the radial distribution of the sources near the nozzle position.

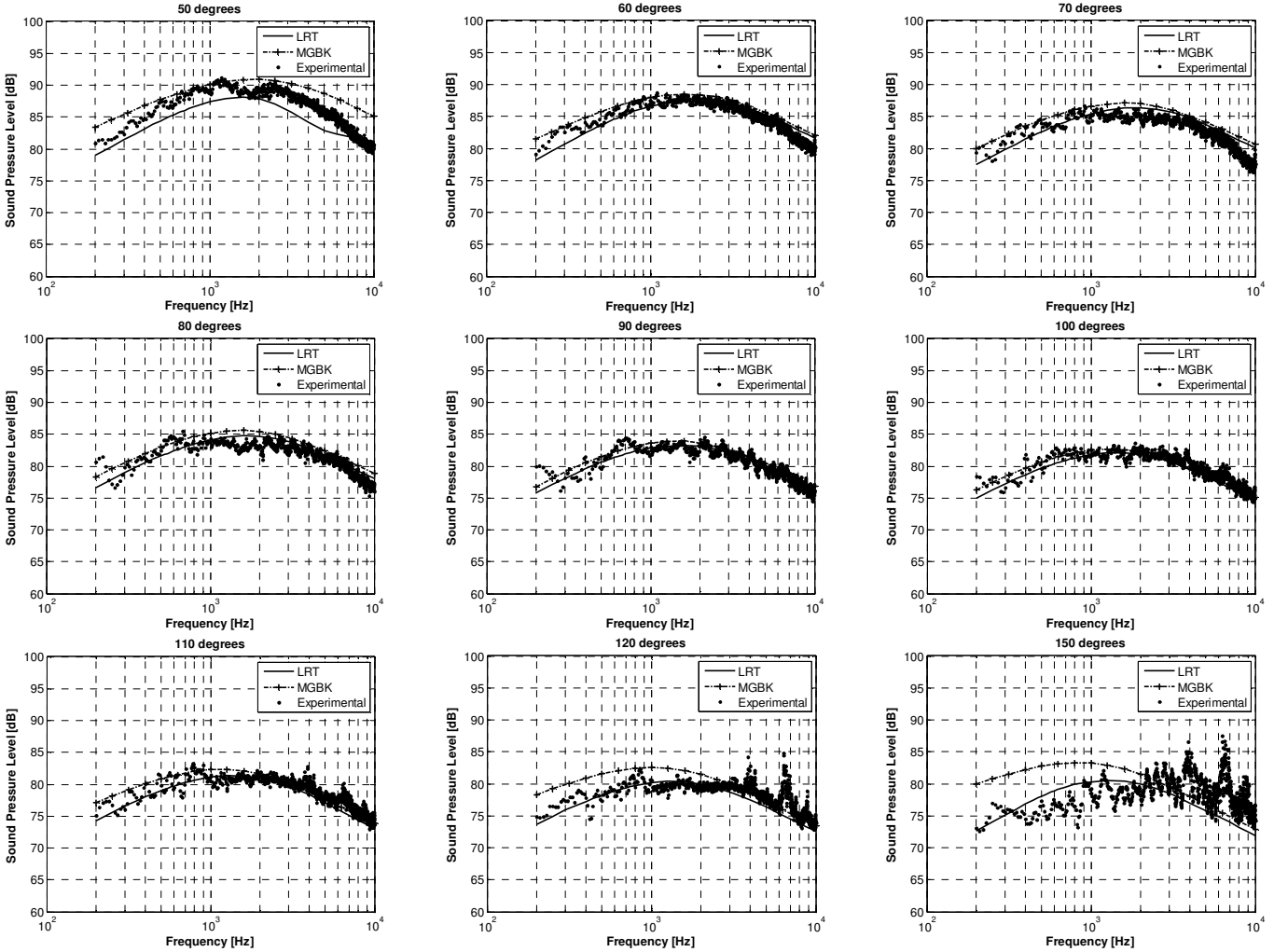

Figure 5.4 - Comparison of experimental narrowband data with predicted spectral density at different angles to jet axis. $R=50D_j$ and $M_j=0.75$.[9]

[9] Experimental results obtained from Jordan *et al.* [122].

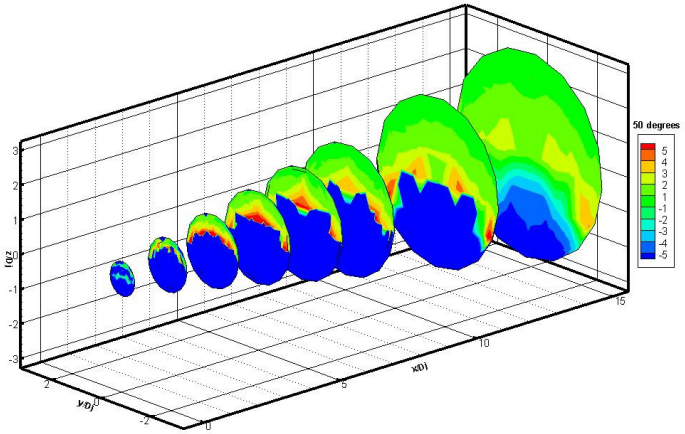

(a) Polar angle = 50 degrees

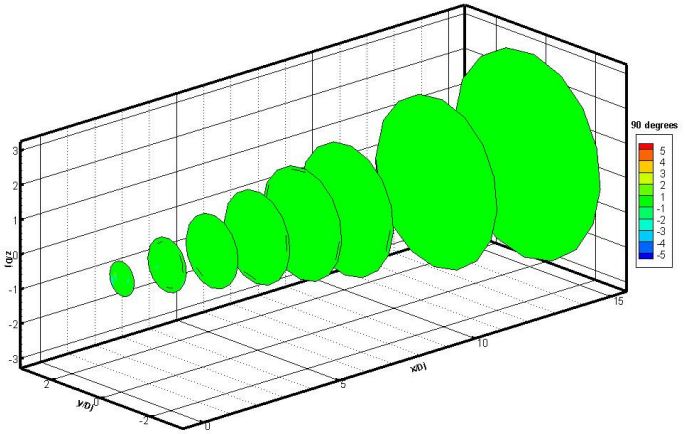

(b) Polar angle = 90 degrees

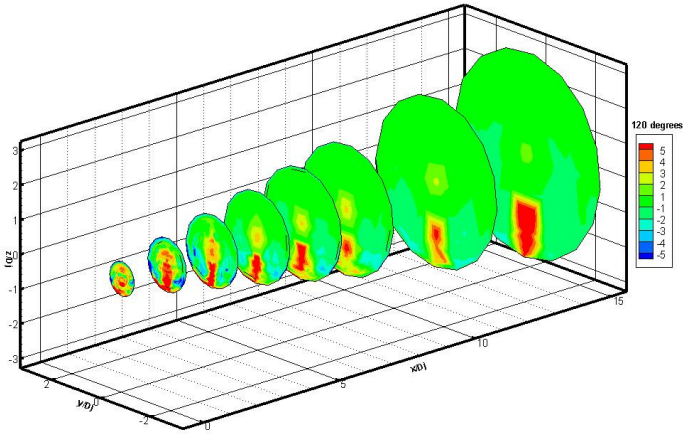

(c) Polar angle = 120 degrees

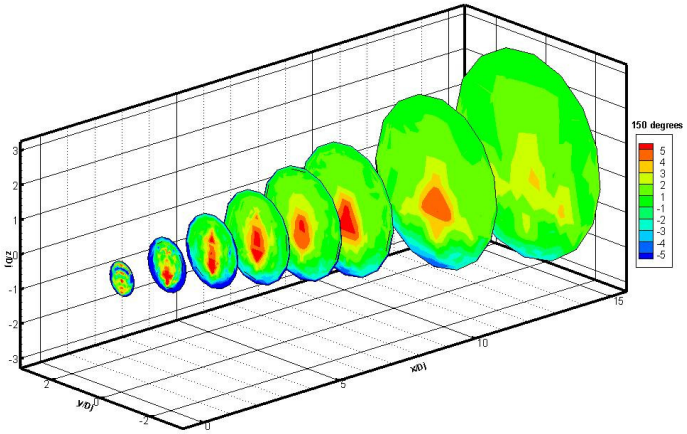

(d) Polar angle = 150 degrees

Figure 5.5 - ΔSPL (dB) calculated from Ray-Tracing code for azimuthal angle 90 degrees in different downstream locations. R = $50D_j$ and $M_j = 0.75$.

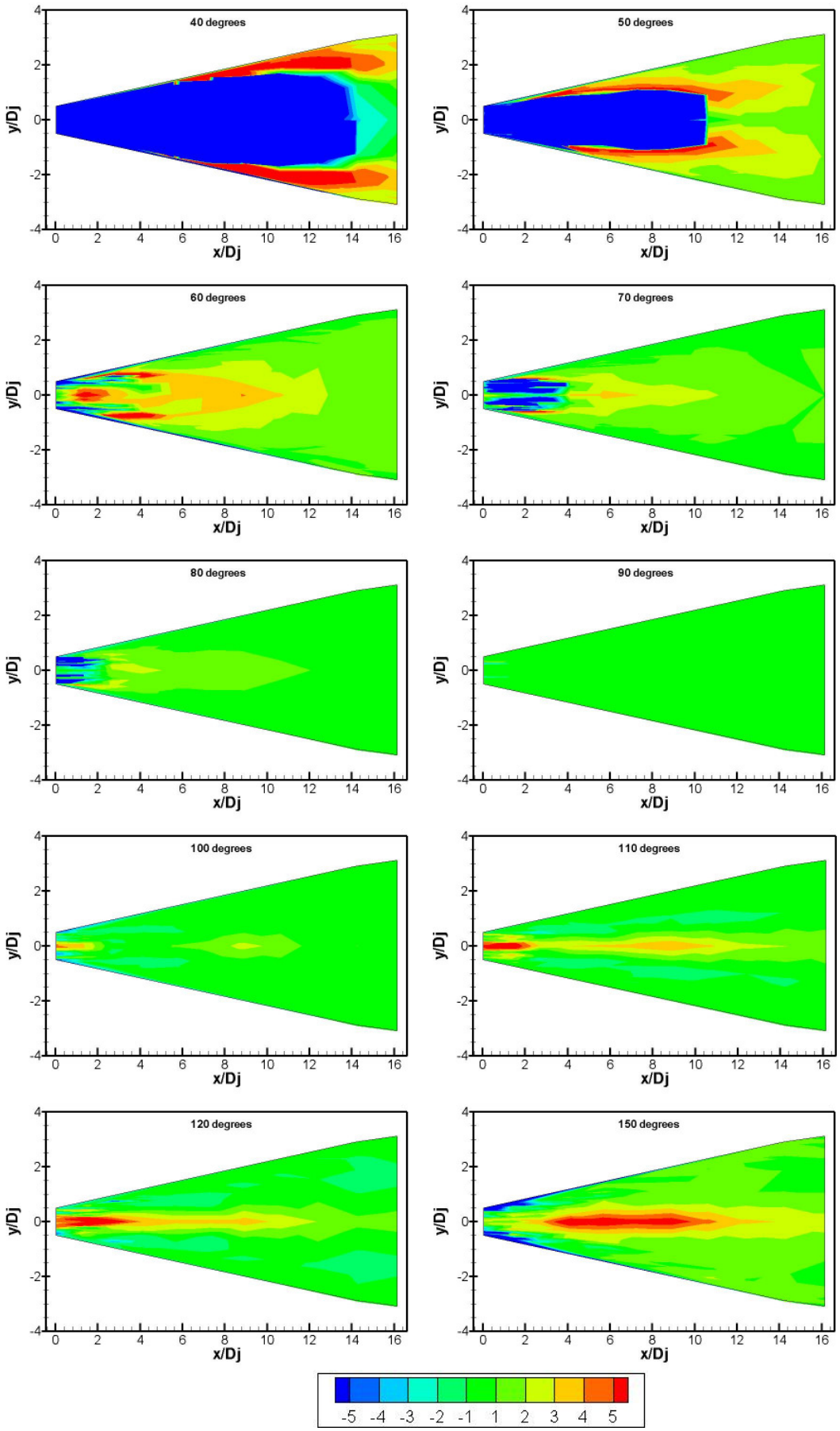

Figure 5.6 - ΔSPL (dB) calculated from the RT code for different polar angles.

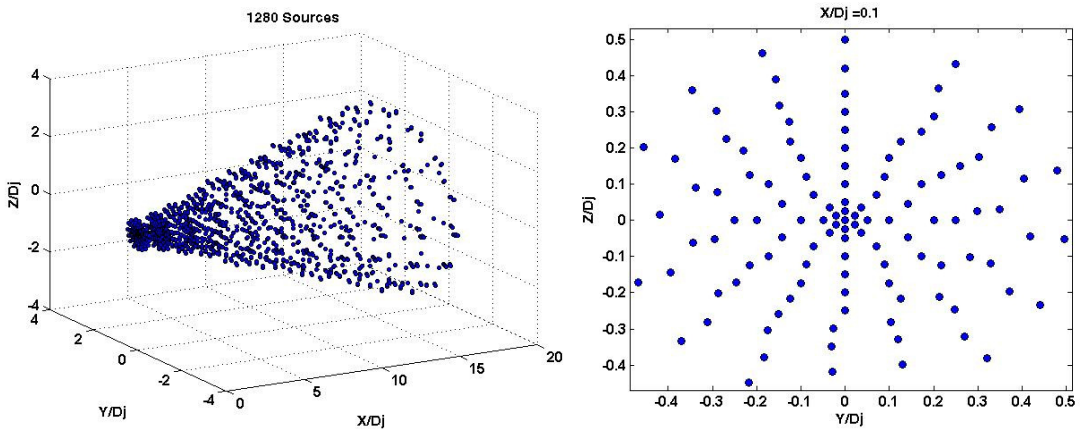

(a) (b)

Figure 5.7 - (a) 1280 sources distributed in the jet field. (b) Radial distribution of the sources near the nozzle.

Although the JEAN data has been of great value in the past and provided very good insights; an important observation needs to be made about the experimental data from [127]. The experiments were carried out in an open jet rig with the jet placed in a vertical orientation, with the discharge pointed down which could be one of the reasons for the reflections presented on the measured data, especially at high frequencies. In addition, the microphones located at 120 and 150 degrees were placed very near the combustor of the test rig which also caused the atypical behaviour of the experimental data at high frequencies. As Ray-Tracing by definition is a high-frequency approach of geometrical acoustics and also because the flow-acoustics interactions are more pronounced in the forward and rear arc of the jet, we chose to use another noise database in alternative to the JEAN database

This work had the opportunity to use more recent jet noise data collected during a project called SYMPHONY. From now on, this chapter on single stream jets will explore the use of the LRT using this more reliable data.

5.2 Single-Stream Jets: SYMPHONY Project

A nozzle with D_j = 101.6 mm was used for the single jet flow noise measurements and aerodynamic numerical simulation. Fig. 5.8 depicts a general description of the geometry.

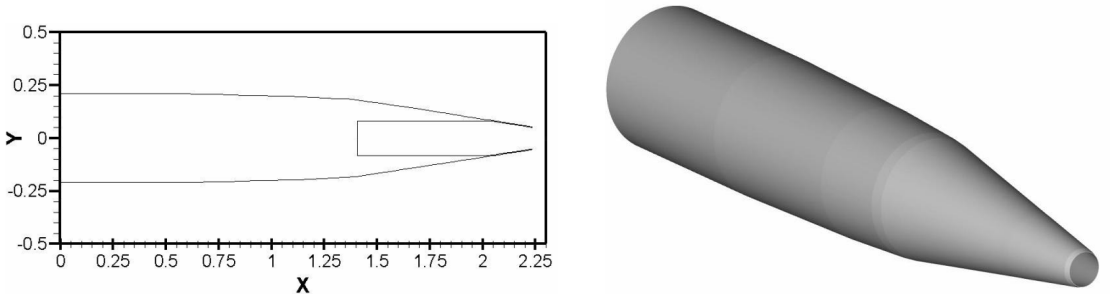

Figure 5.8 - Nozzle geometry for the single stream jets from SYMPHONY.

Table 5.2 presents the flow conditions for the single flows cases investigated in this work. For each case, a RANS CFD simulation was performed to determine the mean flow properties which are necessary as input information to the LRT method. Details of the CFD numerical procedures are presented in Appendix A.

Three different Mach numbers were analyzed with different temperatures ratios (*TR*), defined as the ratio between the static temperature in the nozzle exit plane (T_j) with the static temperature of the ambient air (T_0). A TR equal to one is usually called an unheated or an isothermal jet. The ability of the LRT to account for the effects of the jet's temperature on the far-field noise is addressed for the cases with TR higher than one. All the cases in this section are generally referred to as static conditions since the ambient atmosphere into which the jet is exhausting is quiescent.

Table 5.2 - Single stream jets operating conditions from SYMPHONY.

Case	Mach number	TR	T_j [K]
1	0.50	1.00	288.0
2	0.50	1.25	360.0
3	0.50	1.50	432.0
4	0.50	2.00	576.0
5	0.50	2.50	720.0
6	0.75	1.00	288.0
7	0.75	1.50	432.0
8	0.75	2.00	576.0
9	0.75	2.50	720.0
10	1.00	1.00	288.0
11	1.00	1.25	360.0
12	1.00	1.50	432.0
13	1.00	2.00	576.0
14	1.00	2.50	720.0

5.2.1 Experimental data base

The noise tests of the SYMPHONY project, more specifically, of the package called "WP3 Advanced Nozzle System" were conducted at the Noise Test Facility (NTF) at QinetiQ. The NTF is a large high-quality anechoic chamber specifically designed for model scale exhaust noise research. The facility has internal dimensions of 27 m long by 26 m wide by 15 m high, making it suitable for far-field noise measurements, see Fig. 5.9. Twenty two thousand non-reflective wedges line the chamber, rendering it anechoic down to frequencies of 90 Hz, and positive ventilation prevents hot gas recirculation thereby providing stable noise propagation paths.

Recently enhanced to facilitate larger scale nozzle testing, the test rig protrudes into the chamber at a nominal height of 9 m. Core and bypass air flows are supplied by a centrifugal compressor, to a maximum combined mass flow of 15 kg/s at 3 bars. The core air

is then heated to jet exhaust temperatures using an Avon combustion can, specially modified to burn LPG, whilst bypass temperatures are controlled by mixing in cooler air from a heat exchanger system. The test models are mounted onto a sting assembly which is cantilevered into the centre of the 1.8 m diameter open jet used for flight simulation up to M = 0.33. The airflow for this is supplied by a very large blower (350 kg/s) through an extensive silencing arrangement such that the noise produced by the flight stream is effectively only due to that of the fundamental jet mixing. Typically, the test model protrudes from the flight simulation nozzle by about 1 nozzle diameter thereby enabling measurements to be made in the forward arc of the jet. Target test conditions are corrected for day conditions, such that the acoustic Mach number remains constant (i.e. the ratio of the jet velocity to the ambient speed of sound is kept constant, and the ratio of the square roots of the jet temperature and the ambient temperature is kept constant. When the flight stream is being used, 'ambient' is taken to be the value in the flight-stream).

The aerodynamic data, in the form of multiple total pressure and temperature measurements are acquired in real-time, from probes upstream of the nozzle. This data is used to compute continually updated online conditions, which are matched to the corrected target conditions. Accurate pressure measurements are ensured by regular weekly calibration.

Mass flow measurements are conducted during the test using real-time measurements from Venturi meters. These are installed in the core and bypass supply pipe work upstream of the nozzle assembly.

Dedicated suction surfaces feature on the sting assembly, as shown in Fig. 5.10, to minimise adverse aerodynamic effects inherent in the cantilevered design. The system addresses:

- The boundary layer growth along the axial length of the drum.

- The corner vortices generated at the interface between the drum and aerofoil, on the upper and lower surfaces of the rig.
- The thickness of the wake from the cantilevered aerofoil section, in the area local to the nozzle exit.

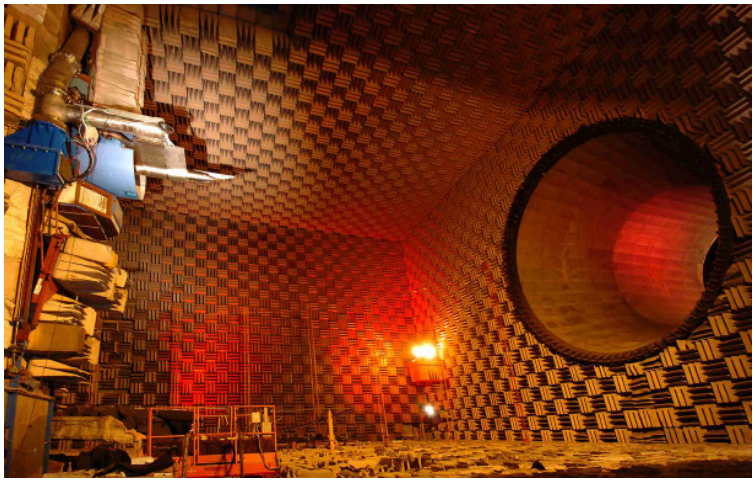

Figure 5.9 - Internal view of the QinetiQ noise test facility showing the rig assembly, anechoic chamber and exhaust collector (courtesy QinetiQ).

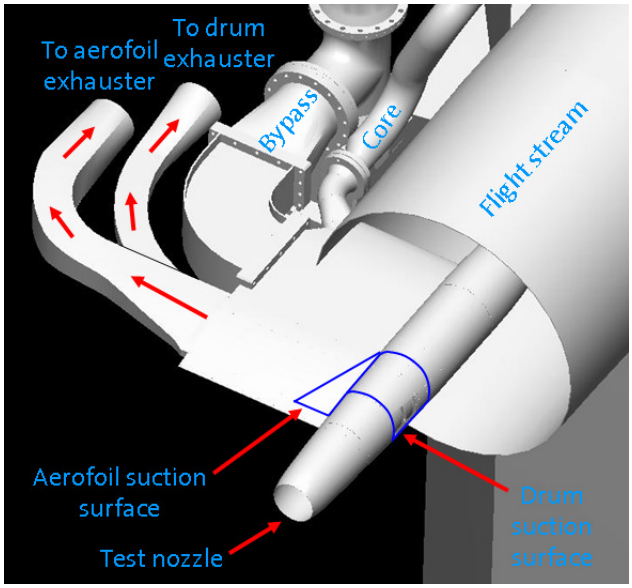

Figure 5.10 - BLSS system layout (courtesy QinetiQ).

Different configurations of microphones arrays are possible at the NTF. The results presented here are from a far-field array configuration at 12 meters from the nozzle, approximately $120D_j$. All microphones used are ¼" B&K type 4939 with the grids removed aligned to point at the nozzle exit. The far-field data is presented as 1m loss-less data corrected for background noise.

5.2.2 Refraction effects and far-field noise predictions

Figure 5.11 and Fig. 5.12 present the results of ΔSPL calculated using the Ray-Tracing code for a fixed Mach number flow with different temperature ratios. The results are presented for various angles varying from 40 to 120 degrees. In the first figure, it is possible to visualize the effect of increasing the temperature of the jet on the critical angle of the zone of silence. As the temperature ratio increases the region of sources that contribute to the reduction of sound also increases, i.e. the critical angle is changing and moving forward. This is a result of the higher sound speed gradient in the flow which contributes to increased blockage of rays going to the shadow angles. In the second figure, angles from 90 to 120 degrees are shown. For the isothermal case, the ΔSPL is approximately zero at 90 degrees as expected; the same is not true for hot jets where the refraction effects can modify the far-field noise predictions with regions of attenuation and also amplification of noise. Similar results were also found in the work of Morfey and Szewczyk [131].

Figure 5.13 presents the 3-dimensional results of ΔSPL which shows the same results as before but in a way that allows the visualization of the shape of the zone of silence and how it varies as a function of the jet's temperature. Another improvement of the LRT code can also be seen in this figure where it is possible to see that the refraction is not totally symmetric as assumed by the shielding functions of the MGBK method.

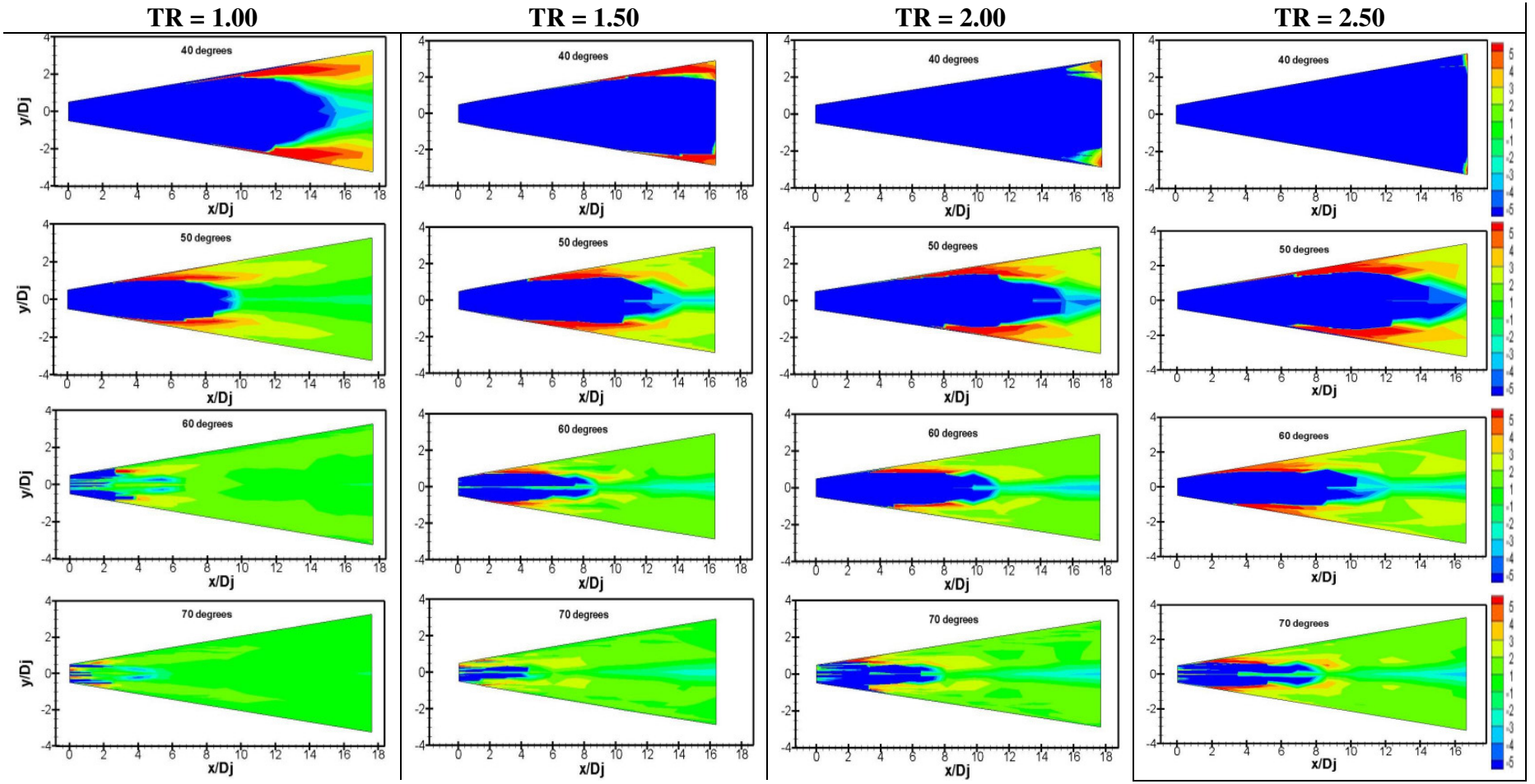

Figure 5.11 - Effect of *TR* on the refraction calculated by the RT code in ΔSPL (dB) for the rear arc of the jet.

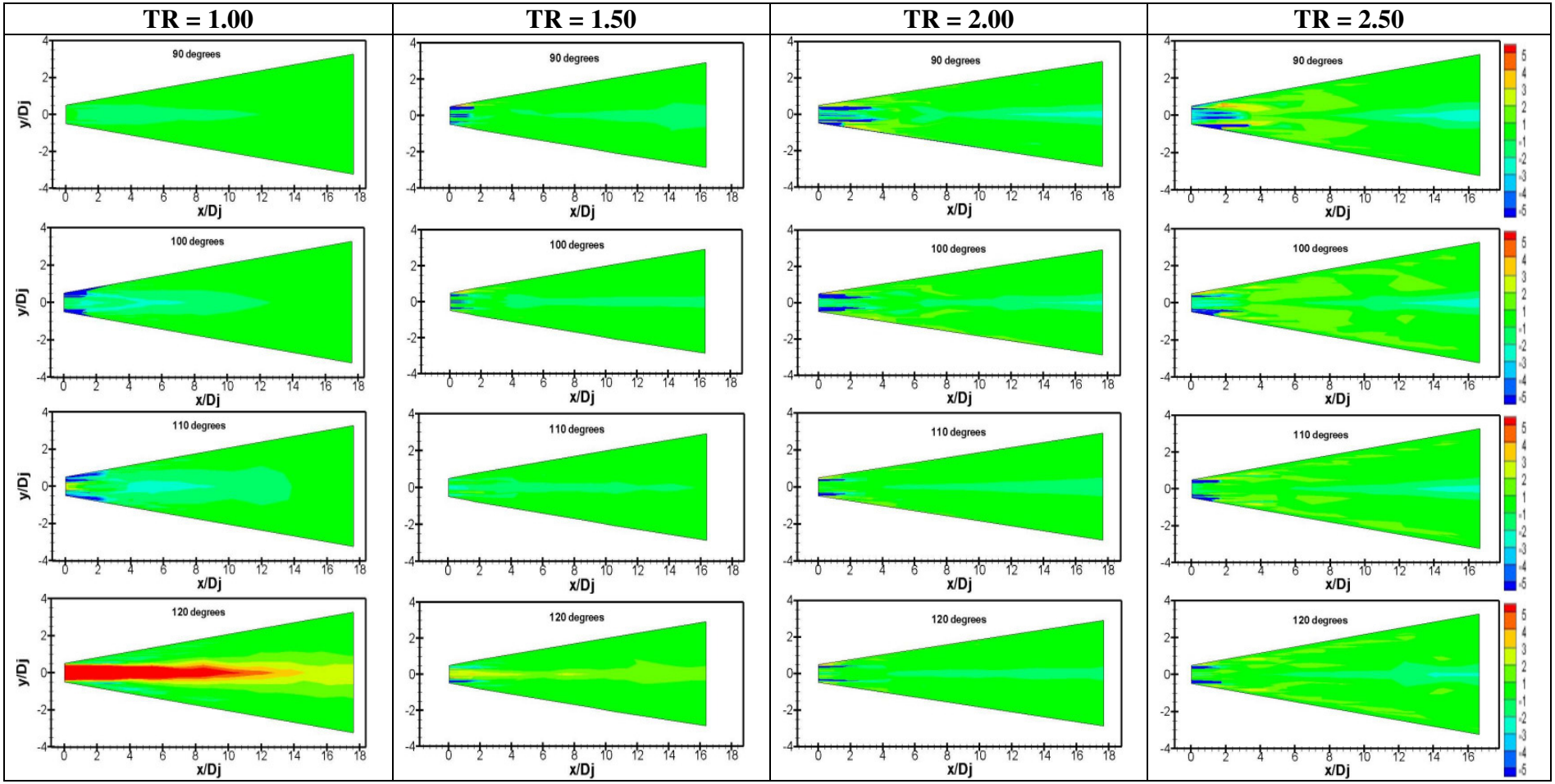

Figure 5.12 - Effect of *TR* on the refraction calculated by the RT code in ΔSPL (dB) for the forward arc of the jet.

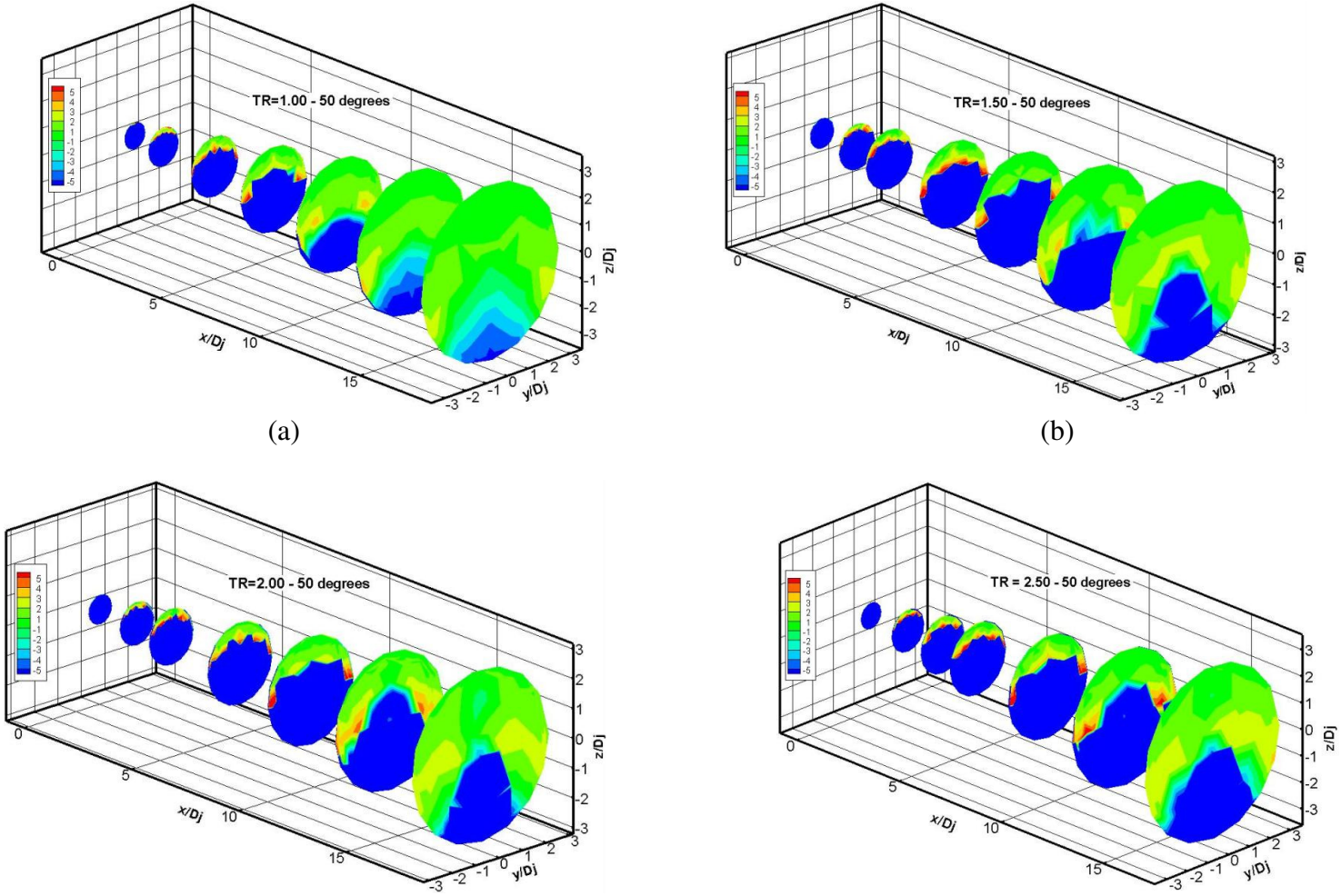

(a) (b)

(a) (b)

Figure 5.13 - 3-dimenstional results of flow-acoustics interactions from Ray-Tracing calculation in ΔSPL (dB).

With the refraction effects calculated for each of the 14 cases it is now possible to proceed with the far-field noise calculations by applying the LRT method. The noise predictions are presented in the next sections.

5.2.2.1 Ninety Degrees Predictions

The noise radiation at 90 degrees to the jet axis is an important point for most of the predictions models. At this angle the mean flow-acoustic interaction, i.e., convection and refraction are negligible. Therefore, it is at this angle that the specification of the source and its assumed relationship to the turbulence model is best assessed. Due to the reasons discussed above, the turbulent calibration coefficients of the model are chosen to match the peak frequency and noise levels at 90 degrees. The method must be able to characterize the spectrum shape and noise levels at this point. Figure 5.14 presents the noise spectra predictions at 90º for the jet conditions presented in Table (5.2).

The results show a good agreement in the peak frequency for the whole range of Mach numbers and temperature ratios. For the jet exhausting at Mach number 1.00 the predictions show an excellent agreement for the entire range of frequencies on the spectrum and also for the cases at high temperatures. The same results can be found for the Mach number 0.75 jet but with a slight over-prediction at the very high frequency at temperature ratio equal 2.50. Going to the low Mach number case (M=0.50) it is possible to verify a more pronounced effect of the temperature on the model. For temperature ratios higher than 2.0 a discrepancy of the predictions at high frequencies can be observed for the Mach number 0.5 jet although the model is able to capture the noise increase at low frequencies.

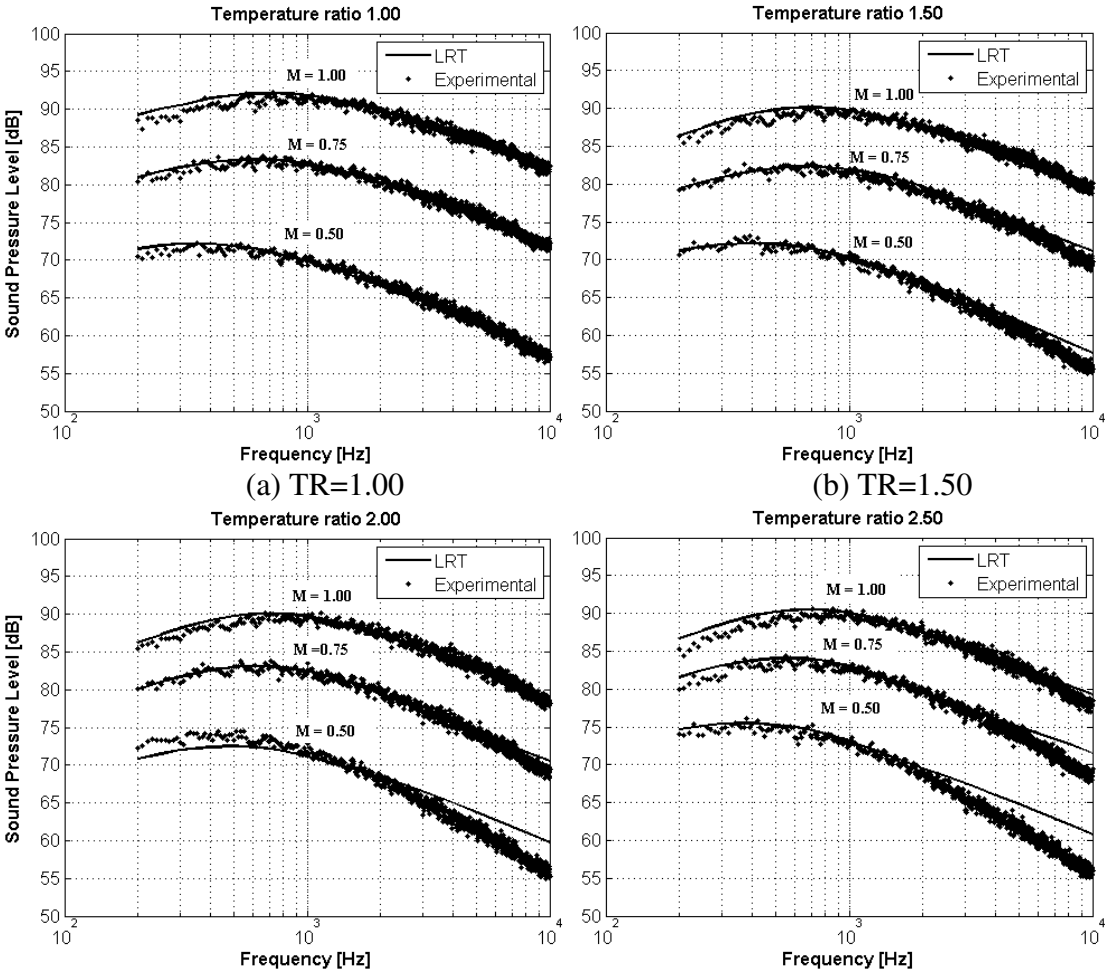

(a) TR=1.00 (b) TR=1.50

(c) TR=2.00 (d) TR=2.50

Figure 5.14 - Ninety degrees noise predictions using the LRT method.

These results show that the dipole sources present in the hot jets are only important for relatively low Mach number flows and therefore the quadrupole sources dominates the spectra for high speed jets even for very hot conditions (TR>1.5). In addition, the Ray-Tracing code also improves the predictions of the LRT method for hot jets by taking into account the effect of the sound speed gradients in the flow and also the density variation from the source position (inside the jet) to observer point (in the far-field)[10].

[10] The energy conservation in the Ray-Tracing Theory is maintained by applying the Blokintzev invariant on the ray-tube.

5.2.2.2 Noise directivity

After the calibration of the model at ninety degrees, the LRT method is used to calculate the noise for the other angles of interest which give important information about the directivity of the noise. The figures that follow present the predictions for the three Mach number jets with temperature ratio equal 1.0. All the results are presented for the region outside the zone of silence.

Figure 5.15 depicts the prediction for the Mach number 0.50 jet. The results show good agreement with the experimental data for all angles.

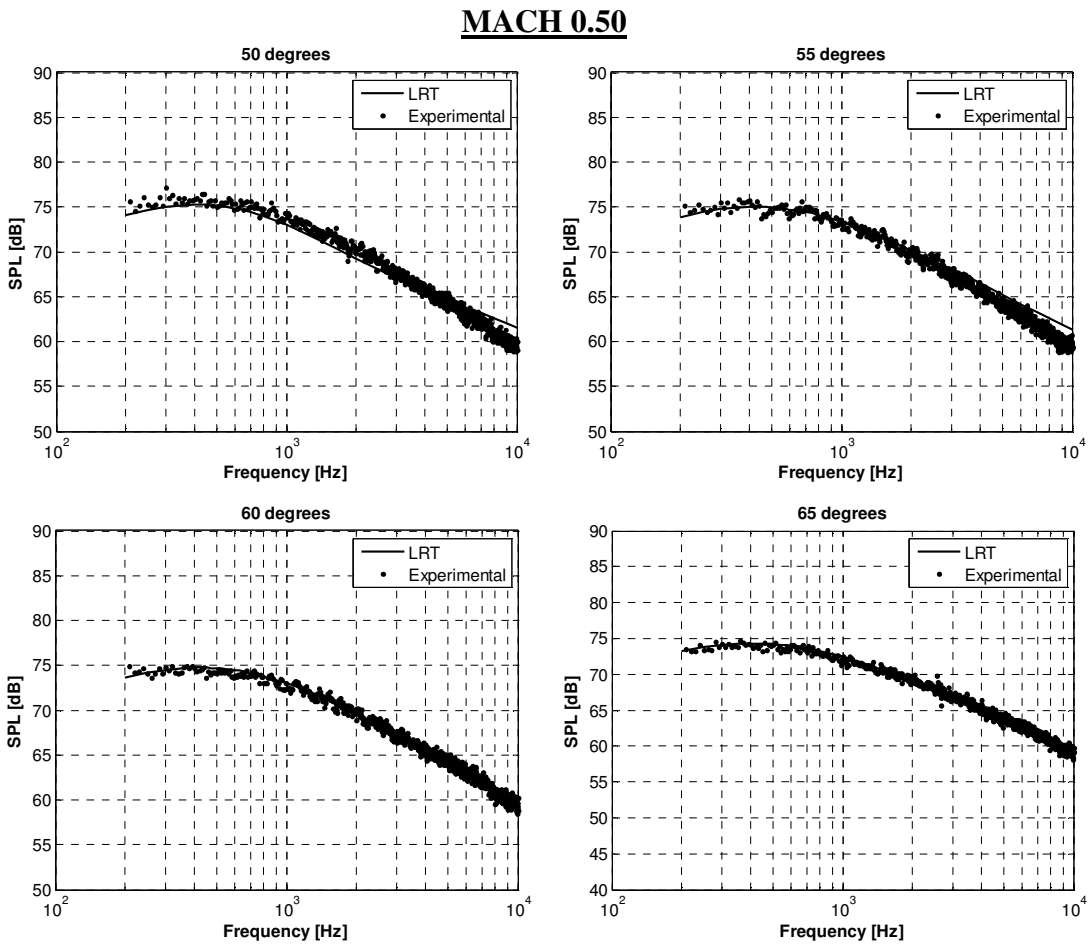

Figure 5.15 – (cont. over).

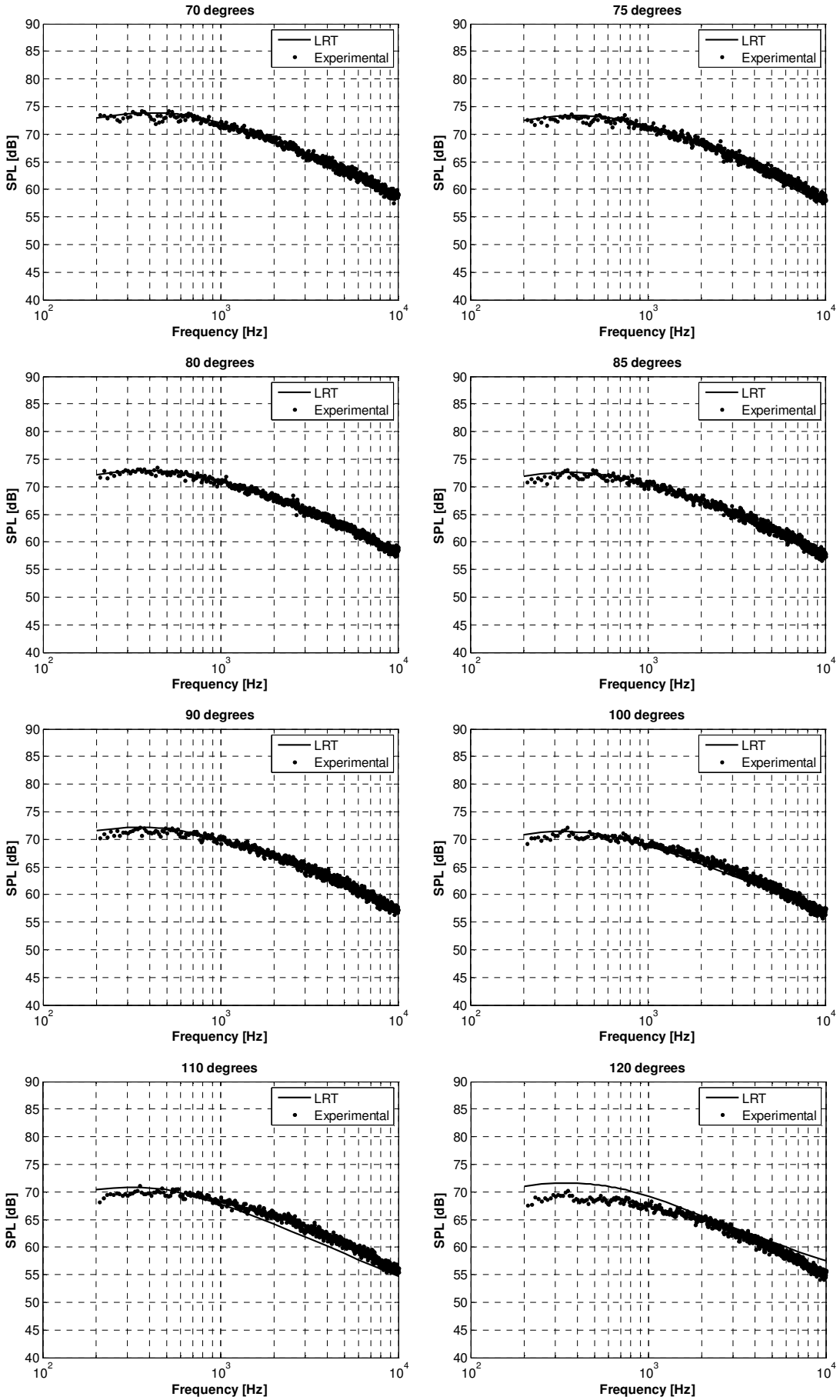

Figure 5.15 - – Far-field noise directivity results using the LRT – $M = 0.50$ and TR=1.00.

Figure 5.16 shows the predictions for the Mach number 0.75 jet. As can be seen, the method captures the peak frequency and also the shape of the spectrum with impressively good agreement with the experimental data.

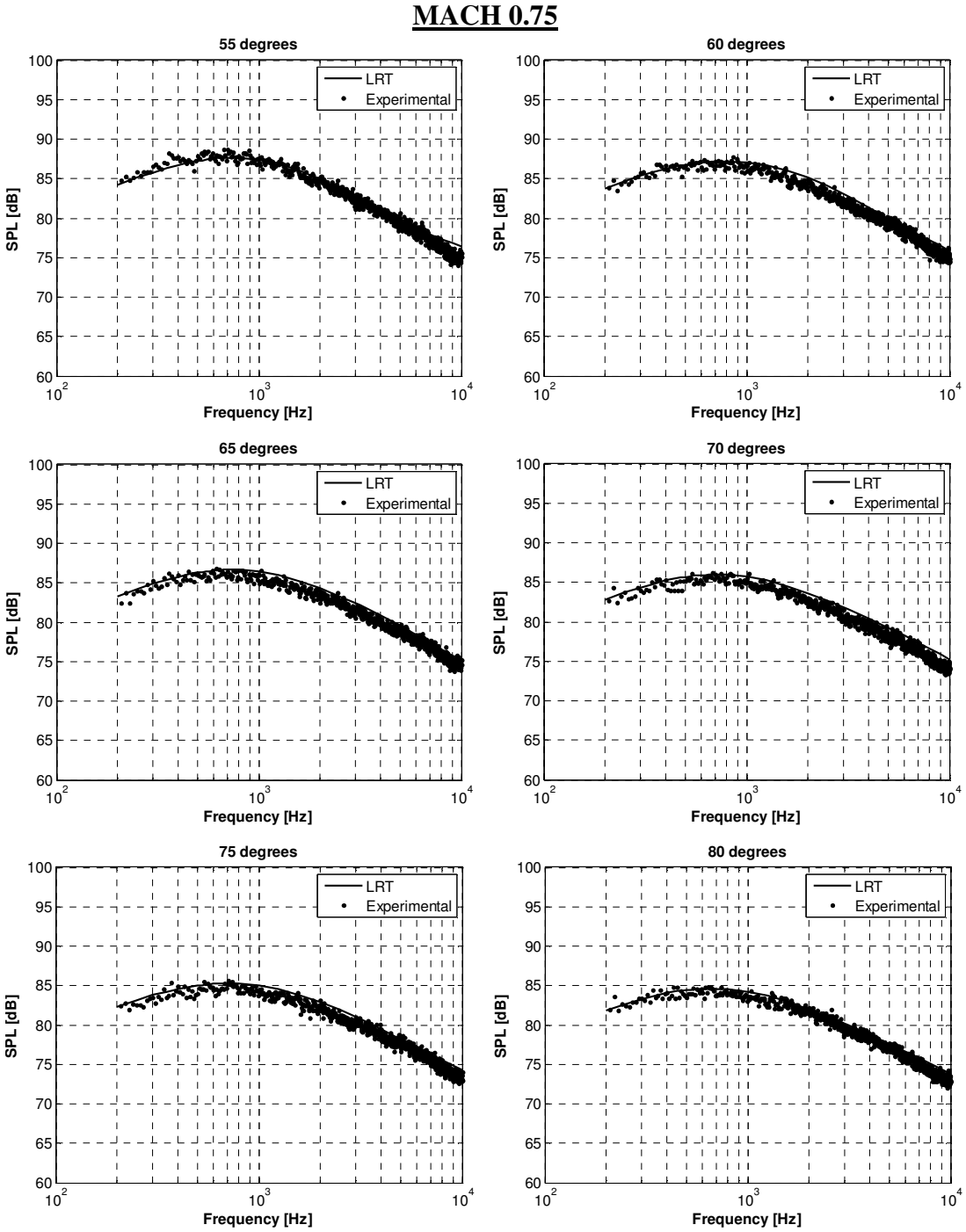

Figure 5.16 – (cont. over).

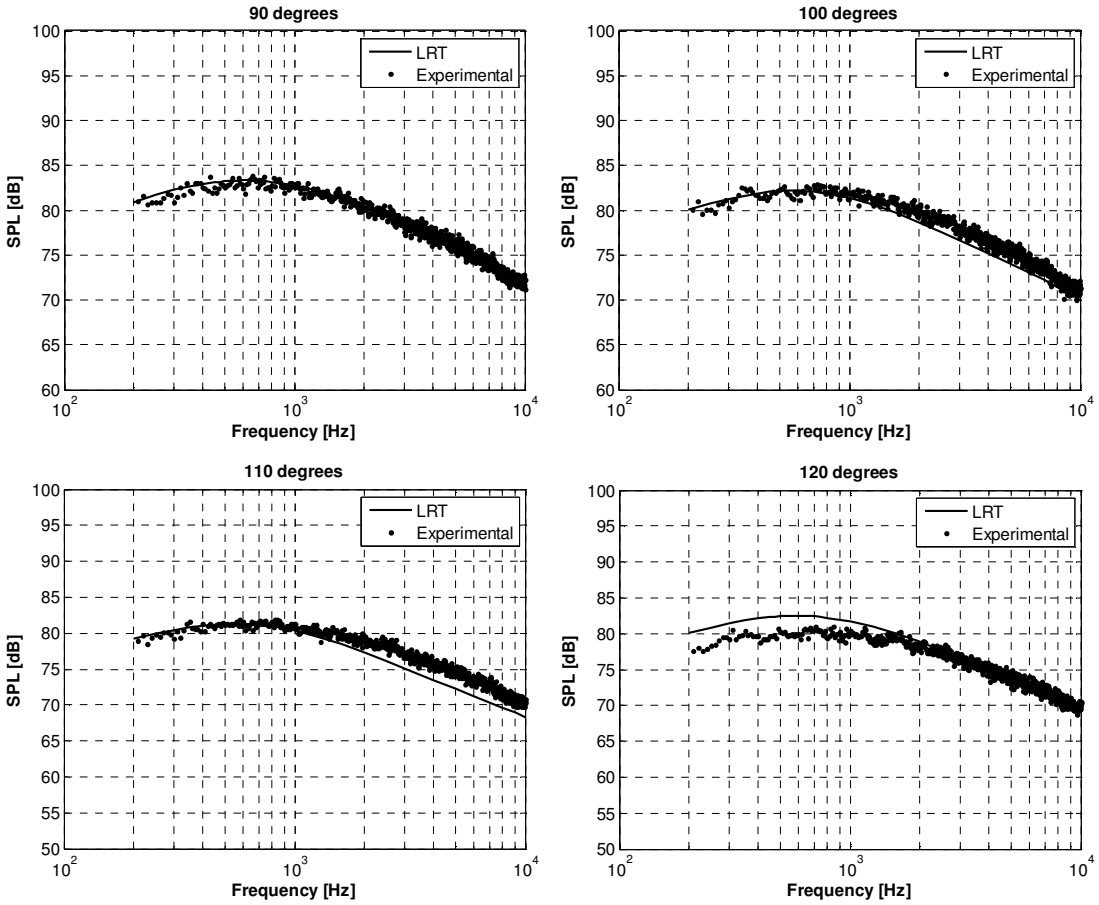

Figure 5.16 – Far-field noise directivity results – M = 0.75 and TR=1.00.Figure 5.16

The last results for the predictions of the Mach number 1.00 jet are presented in Fig. 5.17. Even for such high Mach number, the predictions from LRT have a reasonable agreement with the data. There is an under-prediction for the forward angles, relative to jet axis, which is due to the Doppler correction adopted in the calculations.

MACH 1.00

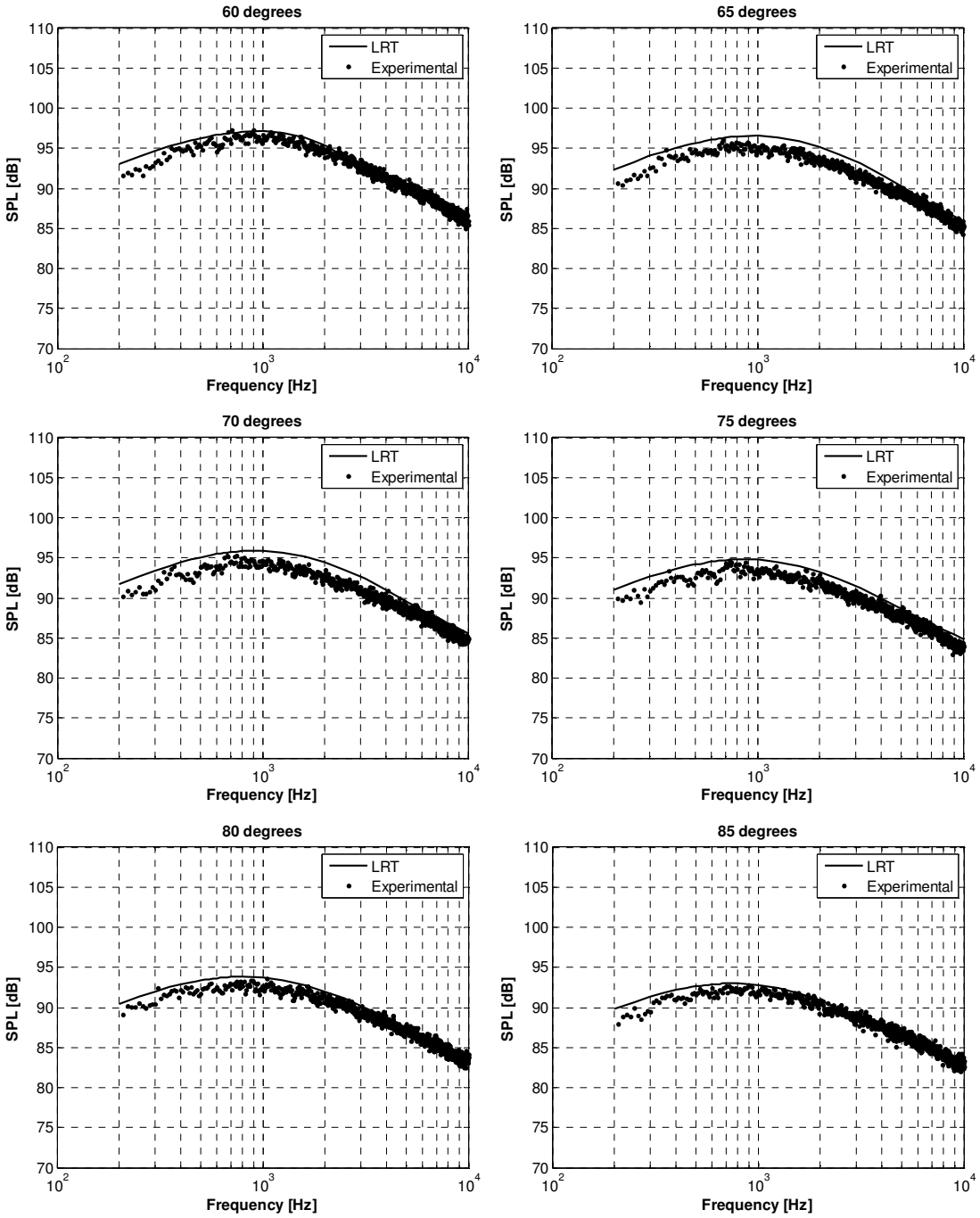

Figure 5.17 – (cont. over).

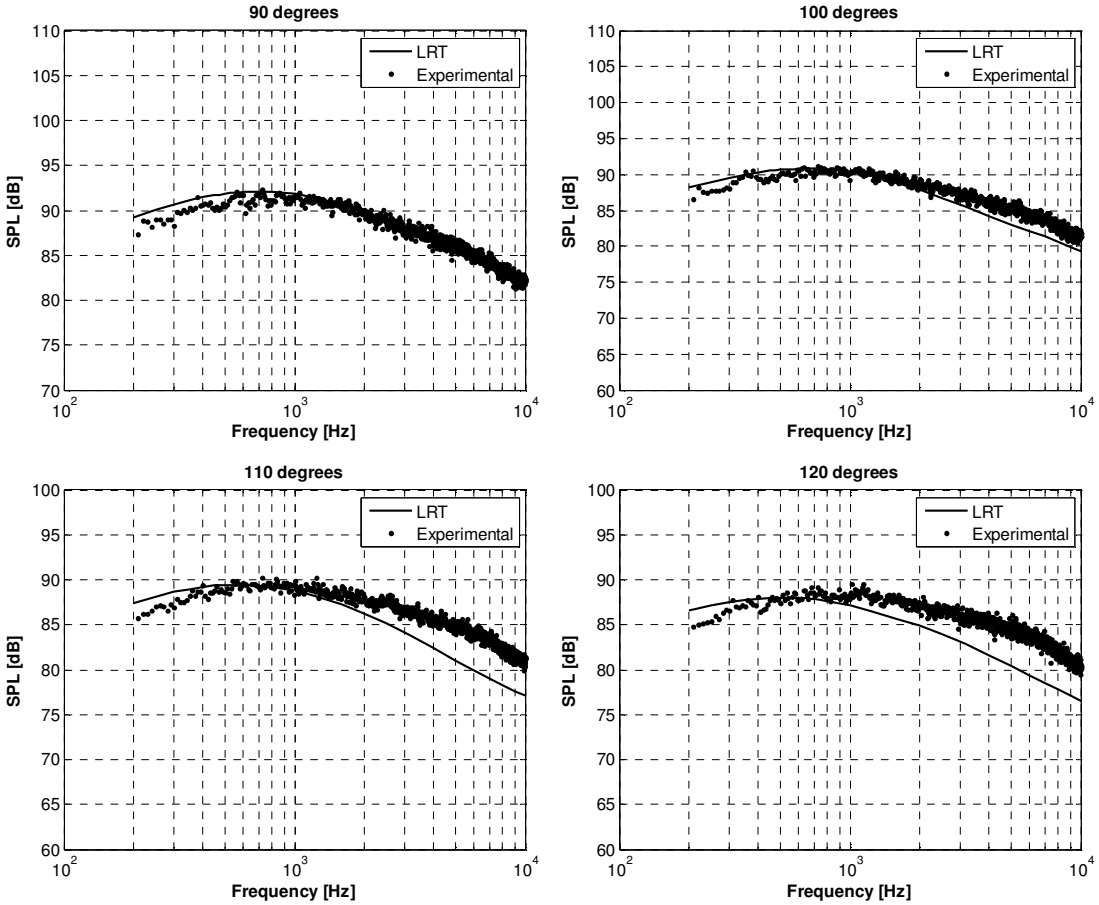

Figure 5.17 – Far-field noise directivity results – M = 1.00 and TR=1.00.

5.2.2.3 Overall Sound Pressure Level (OASPL)

A large number of conditions for the single stream jet were analyzed and therefore a huge amount of data was generated. To be able to show the predictions for most of the cases, this section presents the results in terms of OASPL. The results are presented for angles varying from 30 to 120 degrees for each nozzle operation condition presented in Table (5.2). It should be noted that OASPL is greater than any individual sound pressure level because it represents the intensity of the spectrum as a whole. Figure 5.18 presents the results for the Mach number 0.50 jet. As can be seen the predictions from the LRT method have a very good agreement for the angles outside the zone of silence. As we move to shallow angles, lower than the critical angle (θ_c) of the jet, the predictions start to rapidly fall. This behaviour was

expected from the nature of the Ray-Tracing technique that was used. An interesting result from the OASPL plots is that they show in a clear way the variation of the critical angle as a function of the jet's temperature. Variation to up to 10 degrees is seen for temperature ratio equal 2.00 compared to the isothermal jet.

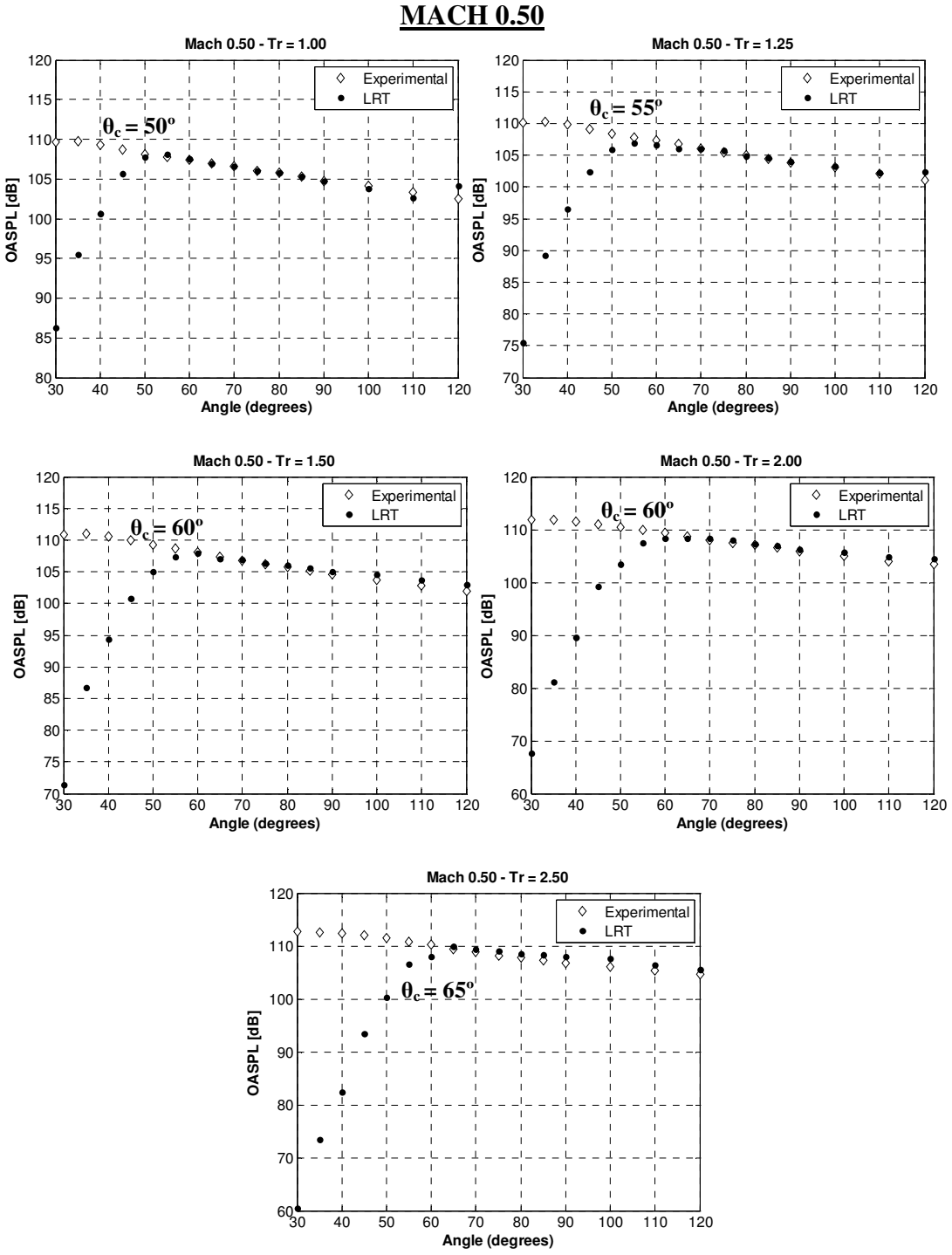

Figure 5.18 - OASPL predictions for the Mach 0.50 jet for different temperature ratios.

The results from the Mach number 0.75 jet are shown in Fig. 5.19. Once more, the predictions from the LRT have good agreement for the angles outside the zone of silence. The same behaviour as before can be noted where the critical angle moves from 55º at *TR*=1.00 to approximately 70º at *TR*=2.50.

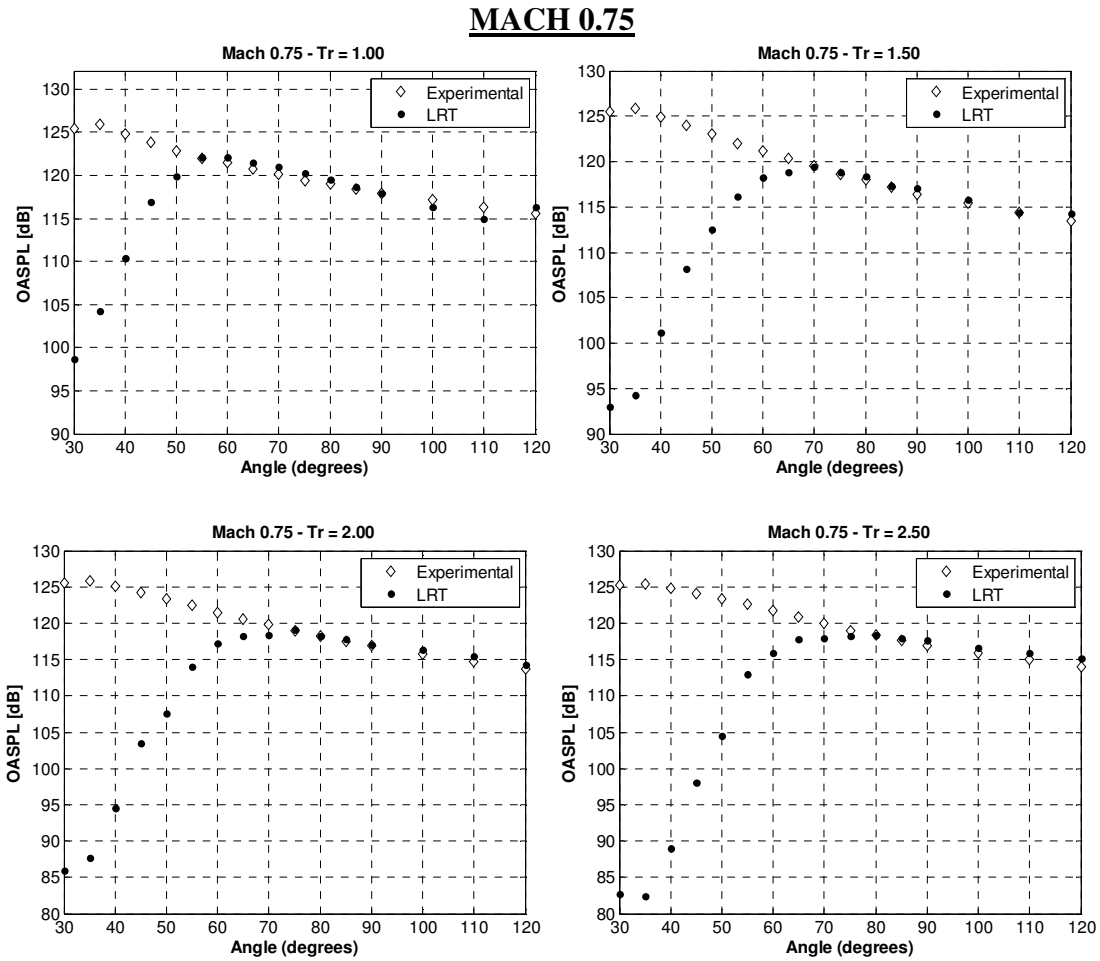

Figure 5.19 - OASPL predictions for the Mach 0.75 jet for different temperature ratios.

The results for the Mach number 1.0 jet are presented in Fig. 5.20. As can be seen, at 90º the predictions show a perfect agreement with experiment data however, when we move to higher angles, where the flow-acoustics interaction is more pronounced there is an under-prediction by the LRT method. This result was expected as the Doppler correction that was implemented in the method considers the flow as being subsonic and therefore a singularity at

Mach=1.00 would need additional treatment. As already explained, for high TR jets these effects are enhanced which negatively affects the predictions for angles different from ninety degrees. Therefore, results for the isothermal condition only are presented.

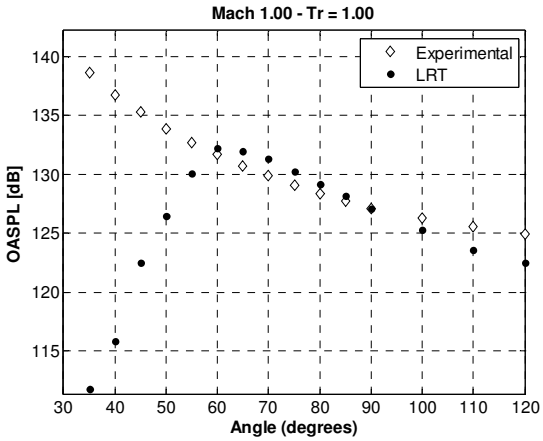

Figure 5.20 - OASPL predictions for the Mach 1.00 jet and temperature ratio 1.00.

After applying the proposed method for a range of Mach number flows and also for different temperatures, the last test is to analyze the applicability of the LRT when a flight condition is present. The next section is devoted to this task.

5.2.2 Simulated Flight Condition

Experimentally, it has been found that a jet in forward flight emits less noise than the same jet in a static condition. The decrease in noise intensity can be quite substantial and therefore the simulated flight condition constitutes a very important issue for industry.

The standard practice to quantify the effect of forward flight on jet noise in a laboratory is to put the jet inside an open wind tunnel and measure the emitted noise by microphones mounted outside [132]. However, such experiments are expensive and very difficult to control. During the 1970s and early 1980s, two semi-empirical methods were established for predicting the effects of forward flight on the noise of high-speed jets. One

method was the so-called relative velocity exponent [133] and the other was a scaling method [134]. With the improvements of noise measurements and the better insight into the nature and characteristics of jet turbulence new methods based on computational aeroacoustics are now possible.

The objective of this section is to apply the LRT method to a very high-speed jet with a simulated flight condition in order to verify the applicability of the model to capture the main features of the noise spectra. The nozzle operation condition is the same as the Case 10 presented in Table (5.2) but now, instead of a static ambient, here was imposed on the CFD parameters a velocity on the far-field boundary condition in order to simulate a forward flight condition. Figure 5.21 shows the measured and calculated jet noise spectra for the Mach number 1.00 jet with flight stream equal to 102 m/s (M = 0.3). As can be seen the noise reduction is nearly uniform across the entire frequency range of the spectrum.

The effects of forward flight on the mean flow of a high-speed jet are relatively well known. The presence of an outside flow reduces the shear gradient across the mixing layer of the jet. This then leads to a reduction in the jet spreading rate. With a smaller spreading rate, the potential core of the jet is lengthened as depicted in Fig. 5.22. The changes in the mean flow due to forward flight, in turn, also alter the turbulence and the source of noise in the jet. Figure 5.23 shows the turbulence kinetic energy (TKE) reduction that can be achieved when a jet is operating with a flight condition. The TKE reduction is presented at two different locations: at the centreline of the jet and at the lipline of the nozzle. These aerodynamic results were calculated by the RANS CFD simulation.

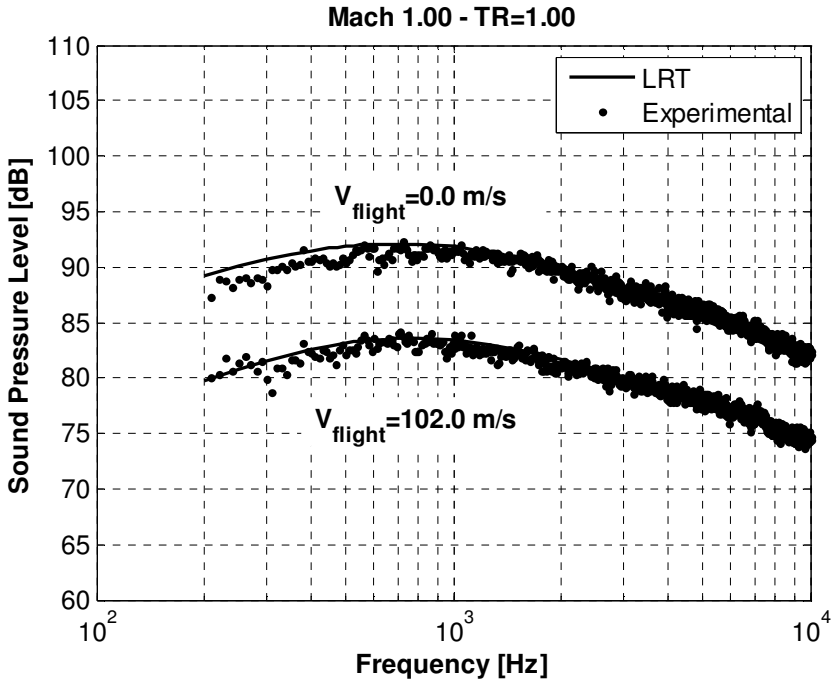

Figure 5.21 - LRT predictions for flight condition.

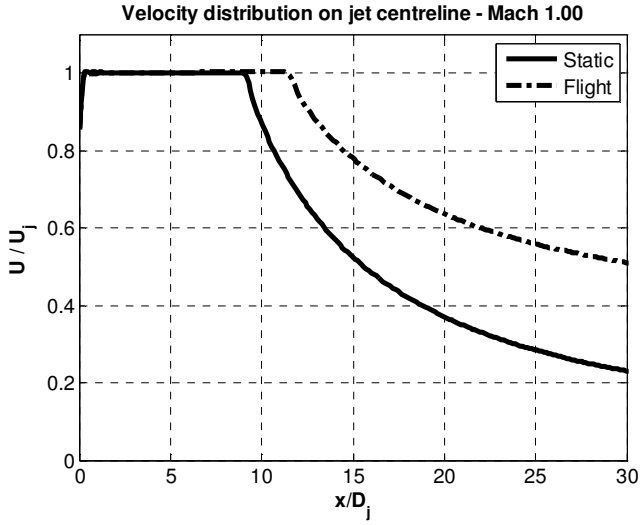

Figure 5.22 – Jet centreline velocity decay comparing static vs. flight condition at Mach 1.00.

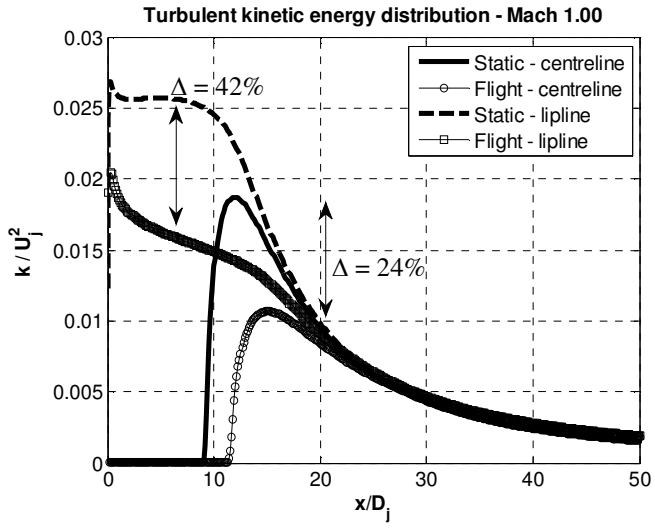

Figure 5.23 – Turbulent kinetic energy reduction with flight condition at the centreline of the jet and the lipline of the nozzle.

The noise comparisons between theoretical predictions and experiments show very good agreement suggesting that the basic theoretical model is valid and that the model theory contains the essential physics of sound generation by a turbulent shear flow.

5.3 Turbulent Calibration Constants

The use of turbulent calibrations constants on noise prediction methods is not restricted to the LRT method. For instance, Tam and Auriault's Method [135] and also the MGBK method use this artifice in other to establish the relationship between turbulence and noise, more specifically the relationship between source and the turbulence model solution of the turbulent flow.

The equations for the turbulent length scale, Eq. (5.1), and time scale, Eq. (5.2), used by the LRT method are repeated in this section in order to facilitate the discussions of the results.

$$L = c_l \frac{k^{3/2}}{\varepsilon} \tag{5.1}$$

$$\tau_0 \approx \alpha^T \frac{k^2}{D_j^{2/3} \varepsilon^{5/3}} \tag{5.2}$$

where,

$$\alpha^T = c_\tau c_l^{2/3} \tag{5.3}$$

As already mentioned, the calibration coefficients are empirically chosen to match the experimental peak frequency and noise spectra at 90 degrees where flow-acoustics interactions are negligible. In the LRT method, c_τ is responsible for capturing the peak frequency in the spectra whereas c_l affects the magnitude of the predictions.

The purpose of the prediction method proposed here is to be able to handle different nozzle geometries and operation conditions. However, there is a need to empirically define the calibrations constants based on experimental data. This could lead to a limitation of the method. In order to overcome this limitation, a large number of simulations were performed varying the nozzle operation conditions with the aim of defining a first approximation of these coefficients based on the jet's condition.

Figure 5.24 shows the values for the calibration coefficients of the LRT method as a function of total temperature and velocity of the jet for two different Mach numbers. As can be seen the time scale coefficient, c_τ, does not change significantly for any of the cases and can be considered constant and equal to 0.44. On the other hand, the length-scale coefficient, c_l, shows a strong dependence on the jet's condition.

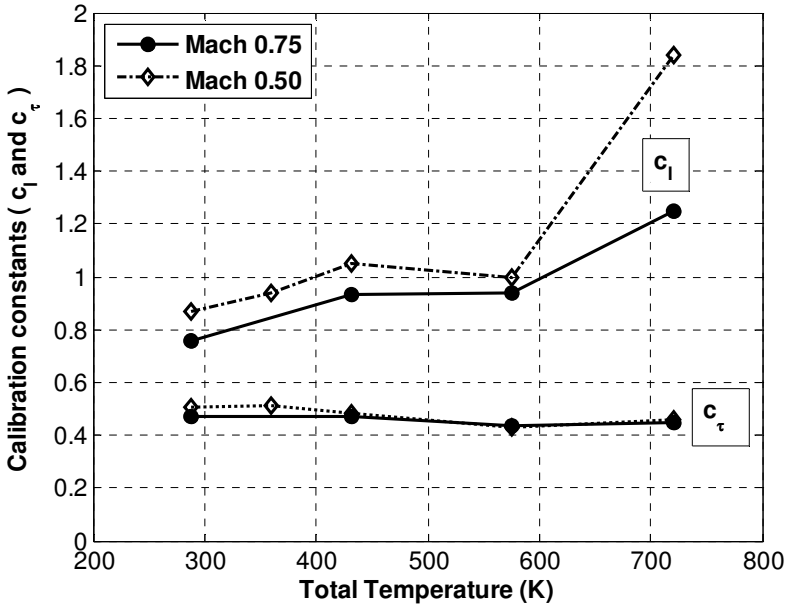

Figure 5.24 - Calibration coefficients for single stream jets.

Chapter 6: Dual stream jets: Coaxial nozzles

After presenting the results for single stream jets, this chapter investigates the applicability of the LRT method for predicting the noise from dual-stream jets, also called coaxial nozzles. A large number of jet operation conditions and coplanar nozzle diameters were investigated using the LRT method and comparisons were made between numerical predictions and experimental data. The results show good agreement for a considerable range of nozzles and velocity ratios.

This chapter is divided into four main sections. First, a brief introduction into coaxial turbojet engines together with a description of the source-production regions is presented. The next section is devoted to the experimental noise database used to benchmark the LRT predictions as well as presenting the coplanar nozzles and the jet operation conditions investigated. The numerical predictions are presented in the following section showing noise directivity, OASPL, influence of area ratio and velocity ratio, and noise source distribution as a function of frequency and position relative to the jet exit. Finally, the last section is devoted to presenting the noise predictions for a short cowl nozzle operating in an extreme condition, with a high subsonic speed jet, flight stream condition and thermal effects.

6.1 Experimental noise database

The experimental data used in this chapter were measured in the anechoic chamber of the Noise Test Facility (NTF) at QinetiQ (Farnborough, UK). A series of jet noise measurements were made in 1989 and 1993 on coplanar coaxial nozzles over a range of fully expanded jet velocities compatible with those of aero-engine exhausts. This provided a large set of data for validating the LRT method for different jet operation conditions. The

measurements were performed in the geometric far-field and the noise levels were adjusted for spherical spreading to yield a level at 6 metres polar in a loss-less atmospheric condition. All the results are presented in terms of one-third octave bands and they are available from 30 degrees to 130 degrees from the jet axis – see Fig. 6.1.

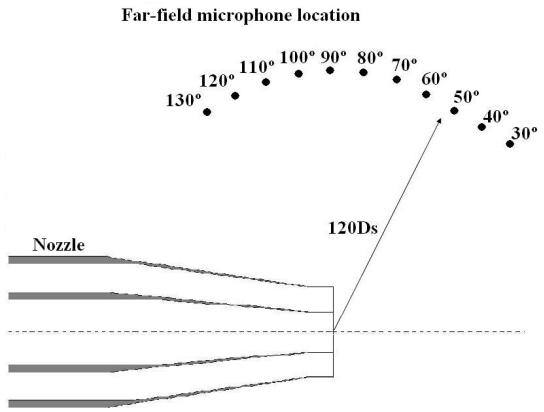

Figure 6.1 - Far-field microphone location, as measured at the NTF.

6.2.1 Nozzle geometries

The exit core diameter (D_p) of 33 mm and 43 mm in exit diameter and the bypass diameter (D_s) of 58 mm and 75 mm respectively are shown in the different area ratio configurations in Fig. 6.2. These geometries were used in the CFD calculations to generate all the mean flow and turbulent input information required by the LRT method. More detailed information of the geometries is presented in Appendix B of this thesis.

6.2.2 Flow conditions

Table 6.1 presents the flow conditions for the coaxial jets investigated in this chapter. Three different area ratios (AR) and a range of velocity ratios (VR) were considered. In all cases described below, both primary and secondary streams were running in an unheated

condition, i.e. the static temperature of the jets are equal to the ambient temperature. The same numerical procedure for the single stream jet predictions were applied for the coaxial noise investigation. For each of the 20 cases presented in Table (6.1) a RANS based CFD calculation was conducted in order to obtain all the mean flow and turbulent data necessary for the LRT prediction method. The acoustics results are presented in the next section.

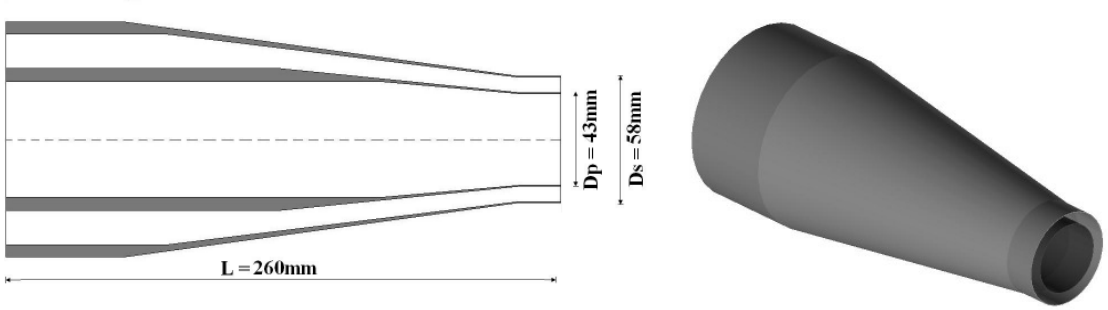

(a)

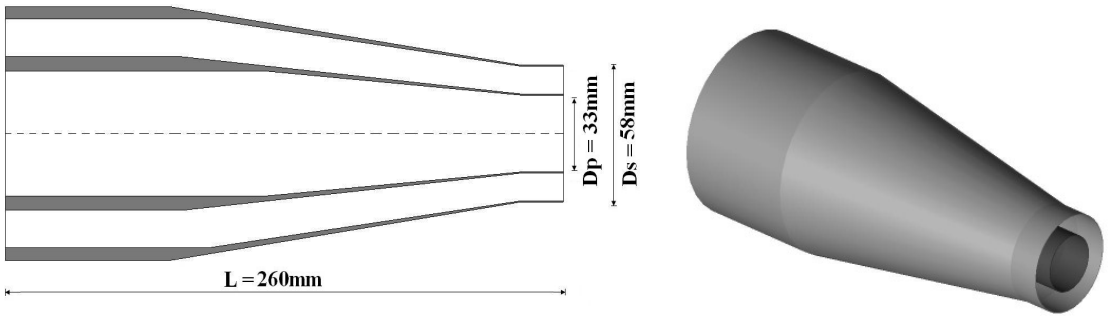

(b)

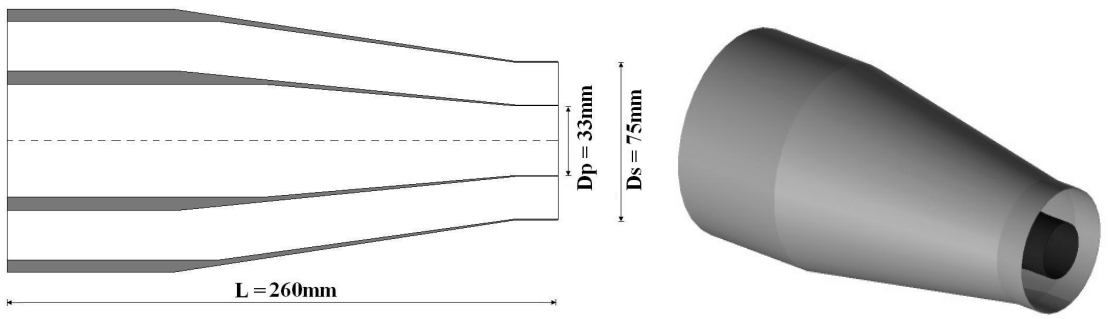

(c)

Figure 6.2 - Coplanar coaxial nozzles geometries used in this chapter: (a) *AR*=0.87; (b) *AR*=2.00; and (c) *AR*=4.00.

Table 6.1 - Jet operation conditions for the coaxial studies.

AR	Case	VR	Mach number Primary Stream	Mach number Secondary Stream
0.87	Coax1	0.63	0.65	0.40
	Coax2	0.79	0.65	0.50
	Coax3	1.26	0.65	0.84
	Coax4	0.63	0.84	0.50
	Coax5	1.00	0.84	0.84
	Coax6	0.79	0.50	0.40
	Coax7	1.00	0.50	0.50
2.00	Coax8	0.63	0.65	0.40
	Coax9	0.79	0.65	0.50
	Coax10	1.16	0.65	0.84
	Coax11	0.63	0.84	0.50
	Coax12	1.00	0.84	0.84
	Coax13	1.00	0.50	0.50
4.00	Coax14	0.63	0.65	0.40
	Coax15	0.79	0.65	0.50
	Coax16	1.26	0.65	0.84
	Coax17	0.63	0.84	0.50
	Coax18	1.00	0.84	0.84
	Coax19	0.79	0.50	0.40
	Coax20	1.00	0.50	0.50

6.3 LRT Predictions

This section presents the LRT results for the noise investigation of the coaxial cases described in Table (6.1). The refraction effects, calculated by the Ray-Tracing code and the far-field noise predictions are addressed here.

6.3.1 Refraction effects

The effects of the mean flow on the noise propagation through the jet are presented here. Figure 6.3 shows an example of source distribution used in the Ray-Tracing code. The sources are distributed in space following the spreading rate of the jet. The domain used to distribute the sources is shown in Fig. 6.3(a) which goes from the nozzle exhaust position down to $25D_j$ downstream covering the most important source regions. Figure 6.3(b) depicts the radial distribution of the sources near the nozzle exit. Here, D_j corresponds to the secondary nozzle diameter.

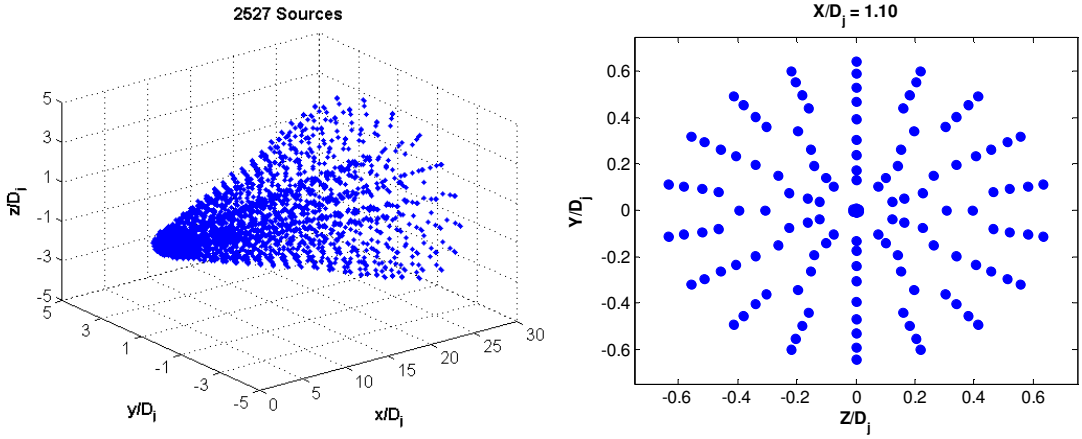

(a) (b)

Figure 6.3 - (a) 2527 sources distributed in the jet field. (b) Radial distribution of the sources near the nozzle exit.

Figure 6.4 presents the results from the LRT method for six different cases. The refraction effects for the 3-dimensional jets are shown as ΔSPL in the far-field for an observer polar angle equal to 50 degrees. From these results, it is possible to verify slight differences from case to case related to the shape of the zone of silence (represented roughly by the blue color on the plots). Comparing the same nozzles but with different *VR*, for example Coax1 and Coax2, no significant modifications can be seen. On the other hand, the length on the downstream direction of the zone of silence slightly increases with the increase of the *AR* of

the jet (cases Coax2 and Coax15) From Fig. 6.5 it is possible to verify that most of the sources that are affected by the mean flow are located in the first $12D_j$ region, where D_j is the diameter of the secondary nozzle. This is mainly due to the presence of the potential core of the primary jet that behaves like a shielding region to the acoustic waves.

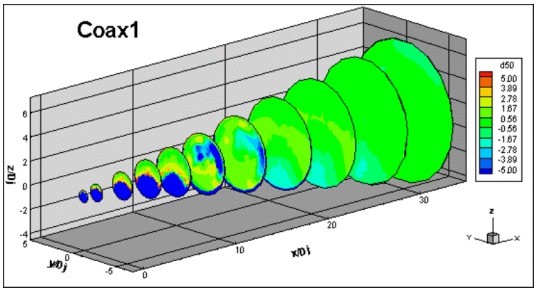

(a) Coax1 case.

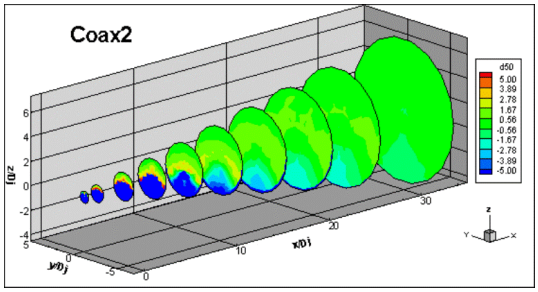

(b) Coax2 case.

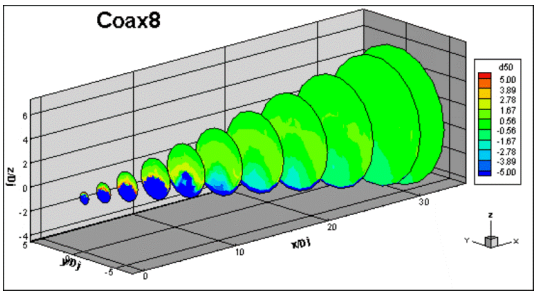

(c) Coax8 case.

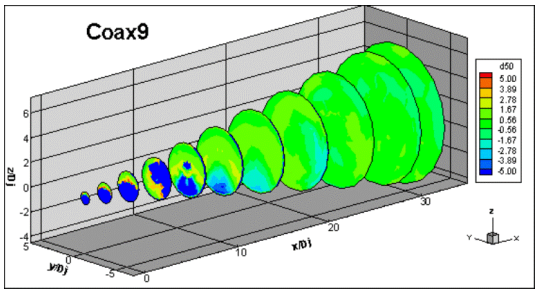

(d) Coax9 case.

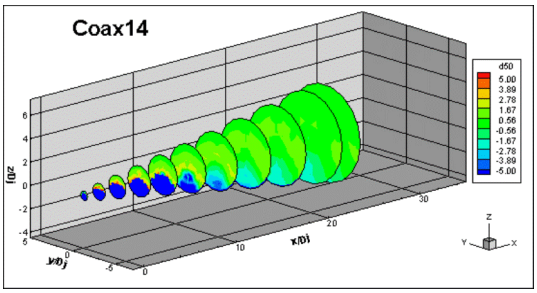

(e) Coax14 case.

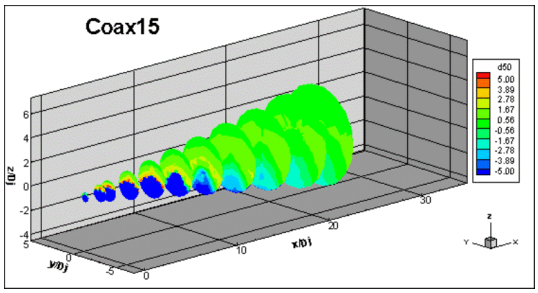

(f) Coax15 case.

Figure 6.4 – Ray-Tracing results in ΔSPL (dB) for a far-field observer located at 50 degrees polar angle.

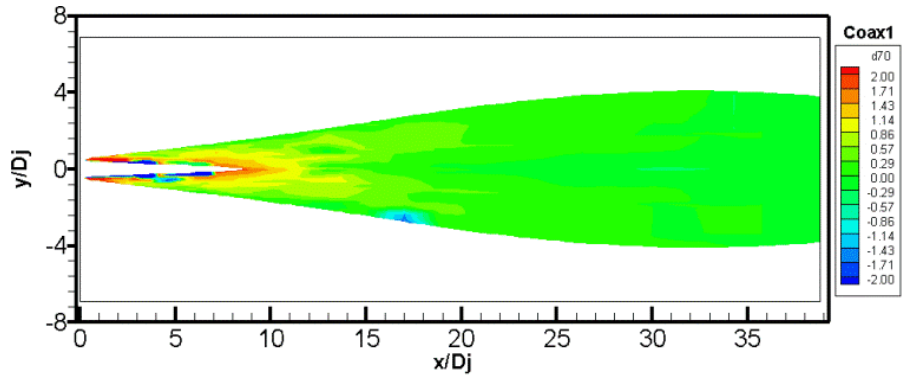

(a) Coax1 case – $VR = 0.63$.

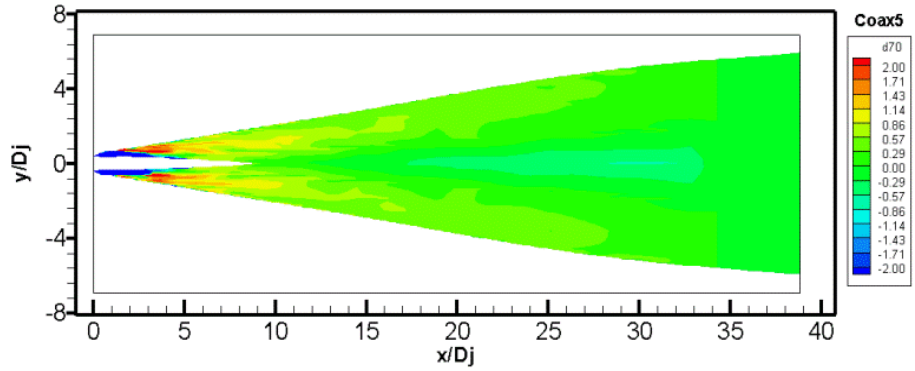

(b) Coax5 case – $VR = 1.00$.

Figure 6.5 – Cut-plane showing the refraction effects in ΔSPL (dB) at 70 degrees polar angle.

In addition to the potential core influence on the refraction, there is also the effect of the presence of gradients of sound speed and flow velocity in the initial and interaction regions of the coaxial jet. These two quantities are important parameters in the Ray-Tracing theory, as already discussed in Chapter 4. Figure 6.6 presents the profiles of speed of sound for two different locations in the downstream direction to the nozzle ($8D_j$ and $20D_j$) calculated by CFD. It is clear that the gradients experienced by the rays (acoustic waves) are higher in the region near the primary potential core of the coaxial jet than those in the mixed-flow region.

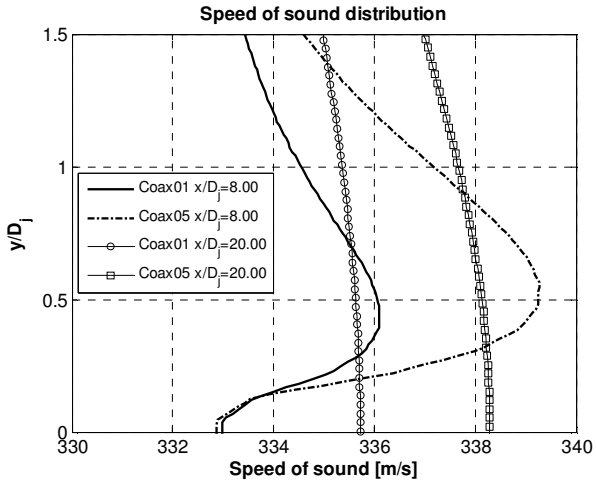

Figure 6.6 – Speed of sound profiles in the radial direction for two different positions downstream the nozzle for Coax1 and Coax5 cases.

6.3.2 LRT noise predictions

The first results that are presented is a noise comparison between two different cases of area ratio 2 with velocity ratios of 0.63 and 1.00. Coplanar flows with velocity ratio about unity behave very similarly to an equivalent single stream jet. Therefore, by means of this comparison it is possible to verify the noise decrease for the coplanar case with velocity ratio less than unity – see Fig. 6.7.

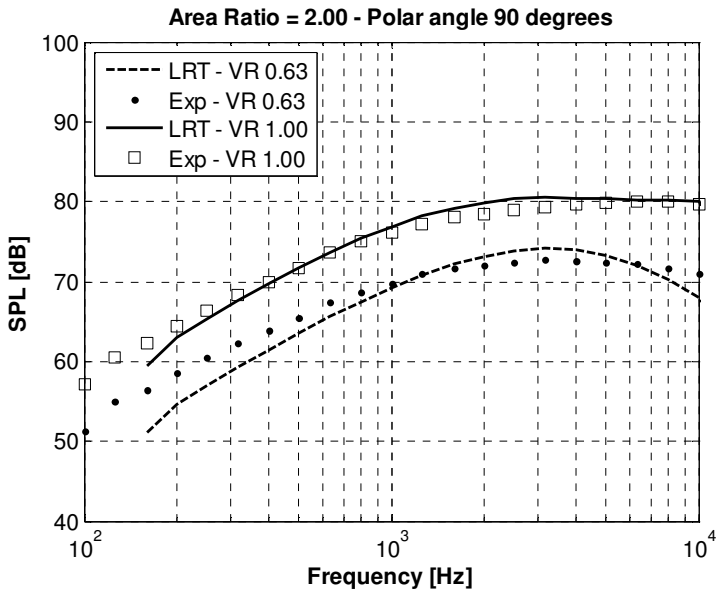

Figure 6.7 - Noise comparison between coaxial jets with VR=0.63 and VR=1.00

This noise decrease can be easily understood by investigating the mean flow quantities of both cases, as presented in Fig. 6.8. By reducing the velocity ratio of the coplanar nozzle it is possible to verify a modification of the velocity distribution on the radial directions of the jet. This implies in a reduction on the strength of the sources in the primary and secondary shear layers, as shown on the turbulent kinetic energy distribution in the same figure.

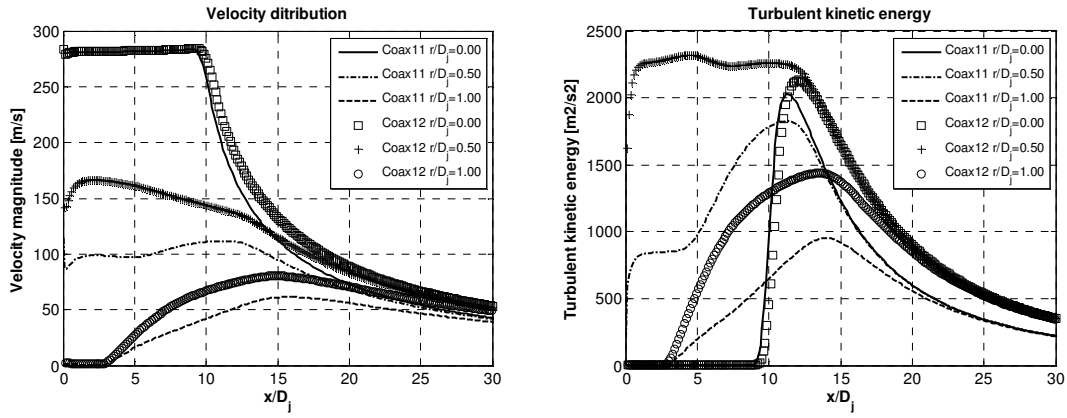

Figure 6.8 – CFD results of mean flow properties at different radial positions for Coax11 and Coax12 cases.

The LRT method was able to calculate the noise for both cases with fairly good agreement with the experimental data. This gives us the confidence to use the new methodology for further investigations on aspects of noise generation in isothermal coaxial jets. In this context, it is possible to analyze the sources distribution inside the jet by dividing the computational domain into different parts and calculating the contribution of each part to the far-field noise. This is attempted here for the same two cases (VR = 0.63 and VR = 1.00) presented above. We divided the domain into Part I, Part II and Part III as shown in Fig. 6.9. Part I contains the computational cells in the first 4 D_j region, Part II contains the cells from 4 D_j to 10 D_j and Part III the cells from 10 D_j to 25 D_j, where D_j in this specific case refers to the secondary jet diameter. In other words, Part I represents the initial region, Part II the interaction region and Part III the mixed-flow region as illustrated in Fig. 2.7.

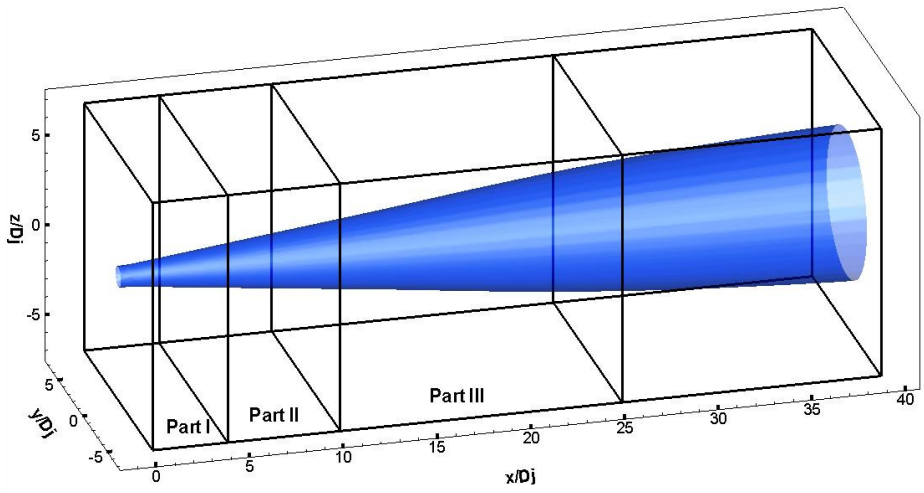

Figure 6.9 - Computational domain divided in three parts for source distribution investigation.

Figure 6.10 shows the noise results for the three parts of the domain separately and the total noise for the Coax11 and Coax12 cases. As can be seeing, each part contributes in a different way to the far-field noise. Part III, located in the mixed flow region, is the main contributor to the low frequency noise and then its importance dramatically reduces as we go to higher frequencies. Part II contains most of the main sources as it comprises a significant part of the secondary-ambient shear layer and also the region of the end of the primary potential core. Part I starts to play an important role only for the high frequency noise due to the small scale turbulence structures present in this region. Looking at the noise spectra in Fig. 6.10 and the computational domains in Fig 6.9 we are also reassured that the important noise sources contributing to the far-field noise on a jet flow are located between 0 to $25D_j$.

Another interesting way to investigate jet noise is to look at the source distribution of the jet for each specific frequency. The mathematical basis is the same as presented in Chapter 4: we take the overall intensity as an integral over the axial extent of the jet. Figure 6.11 shows a comparison of the noise distribution for different frequencies for cases Coax11 and Coax12. It is clear to observe that the high frequency noise intensity is higher for

the Coax12 case ($VR = 1.00$) and as we decrease the velocity ratio to 0.63 (Coax11) the sources are shifted further downstream the nozzle.

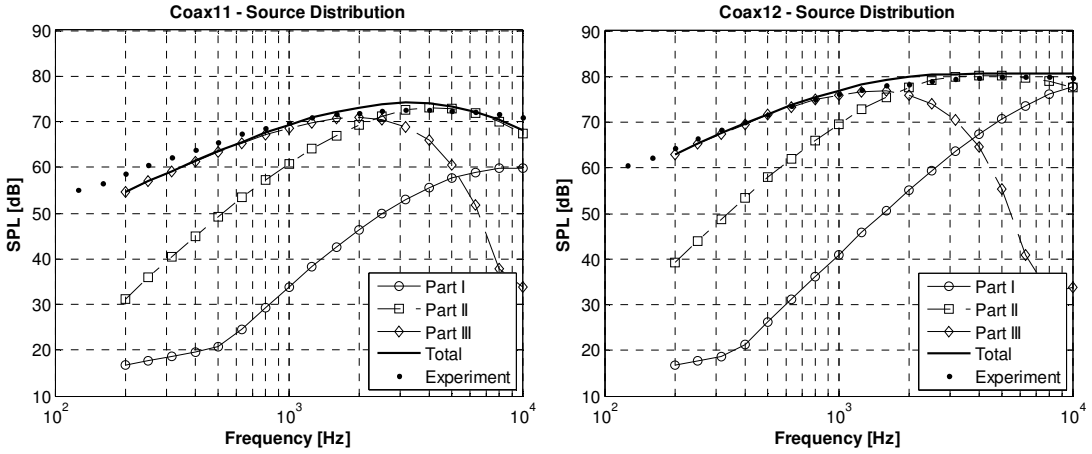

Figure 6.10 Sources distribution for the Coax11 (VR = 0.63) and Coax12 (VR = 1.00) cases.

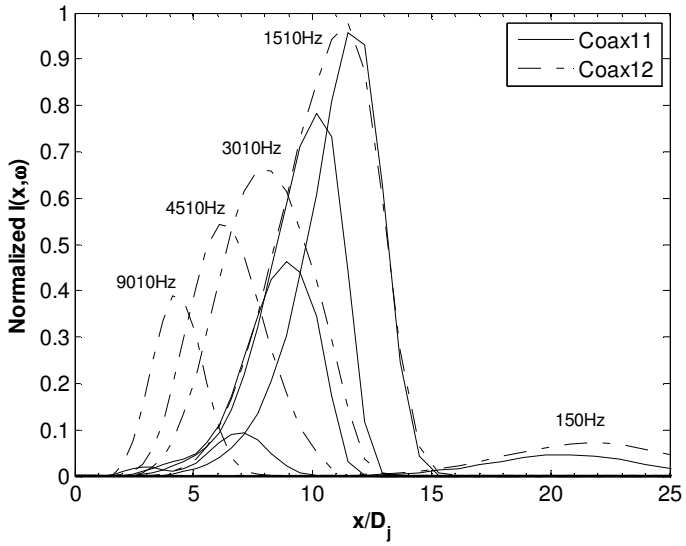

Figure 6.11 – Predicted noise distribution at each frequency using the LRT method for 90 degrees, $AR = 2.00$; $Mp = 0.84$.

These results are not new, Fisher *et al.* [29] presented a very detailed explanation of source distribution in coaxial jets for developing his semi-empirical method, the so-called Four Source Model. However, the aim here is to show the LRT method's ability to provide

important information about jet noise that can be used for developing new techniques for noise reduction.

The next results will present the predictions of the directivity noise for different cases, varying the velocity ratio and also the area ratio of the coplanar jets. The results are presented in terms of one-third octave bands and each case is referred to the ones described in Table (6.1). First, Fig. 6.12 presents the results for the Coax1 case with area ratio 0.87 and velocity ratio 0.63. Fig. 6.13 presents the results for the Coax2 case with area ratio 0.87 and velocity ratio 0.79.

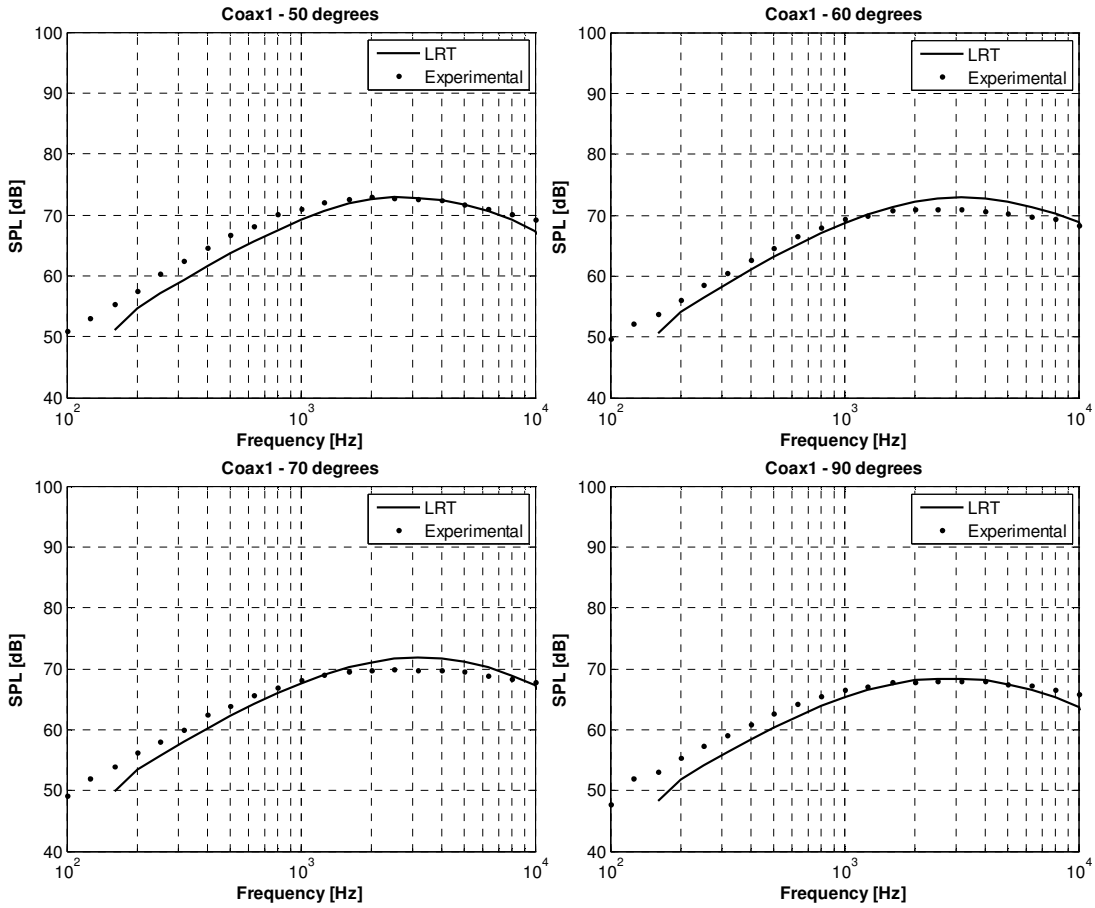

Figure 6.12 – (cont. over).

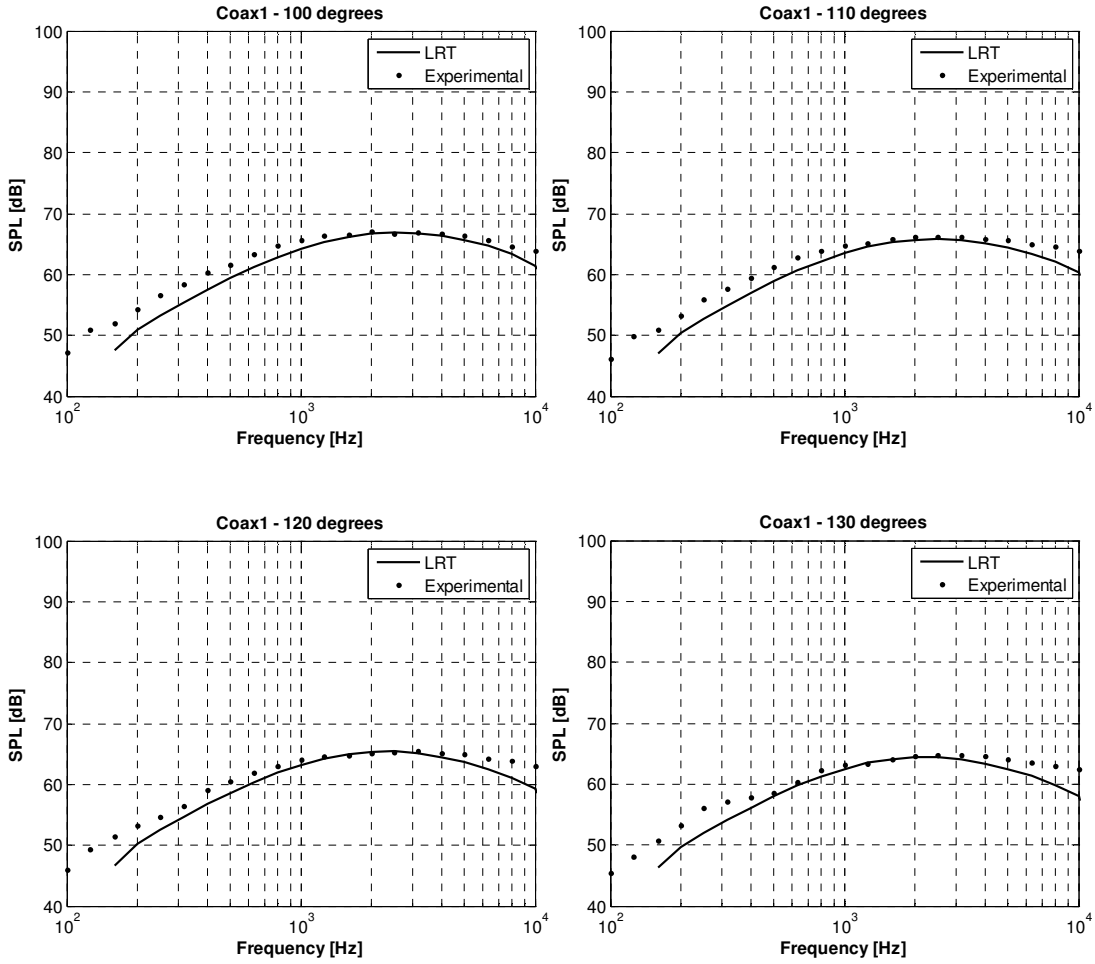

Figure 6.12 - LRT noise predictions for different polar angles for the Coax1 case, $VR = 0.63$; $AR = 0.87$.

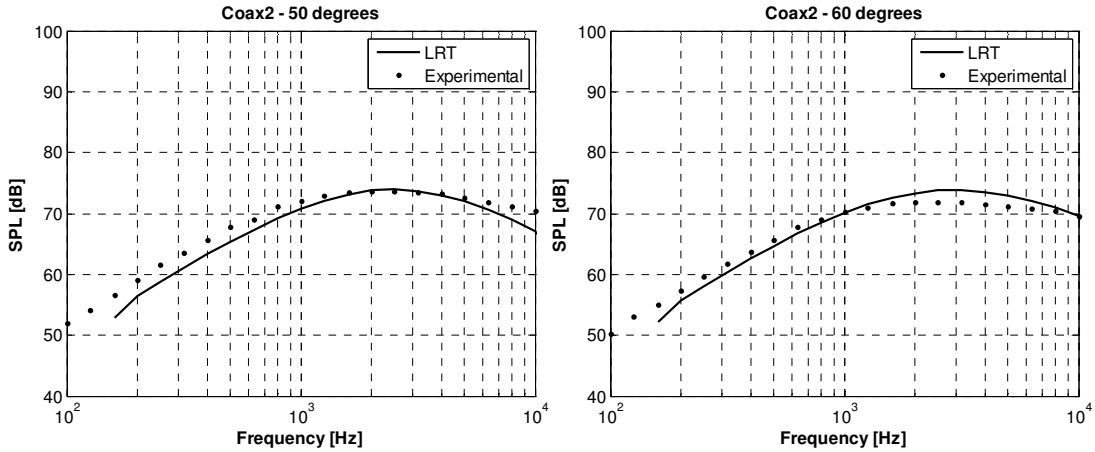

Figure 6.13 – (cont. over).

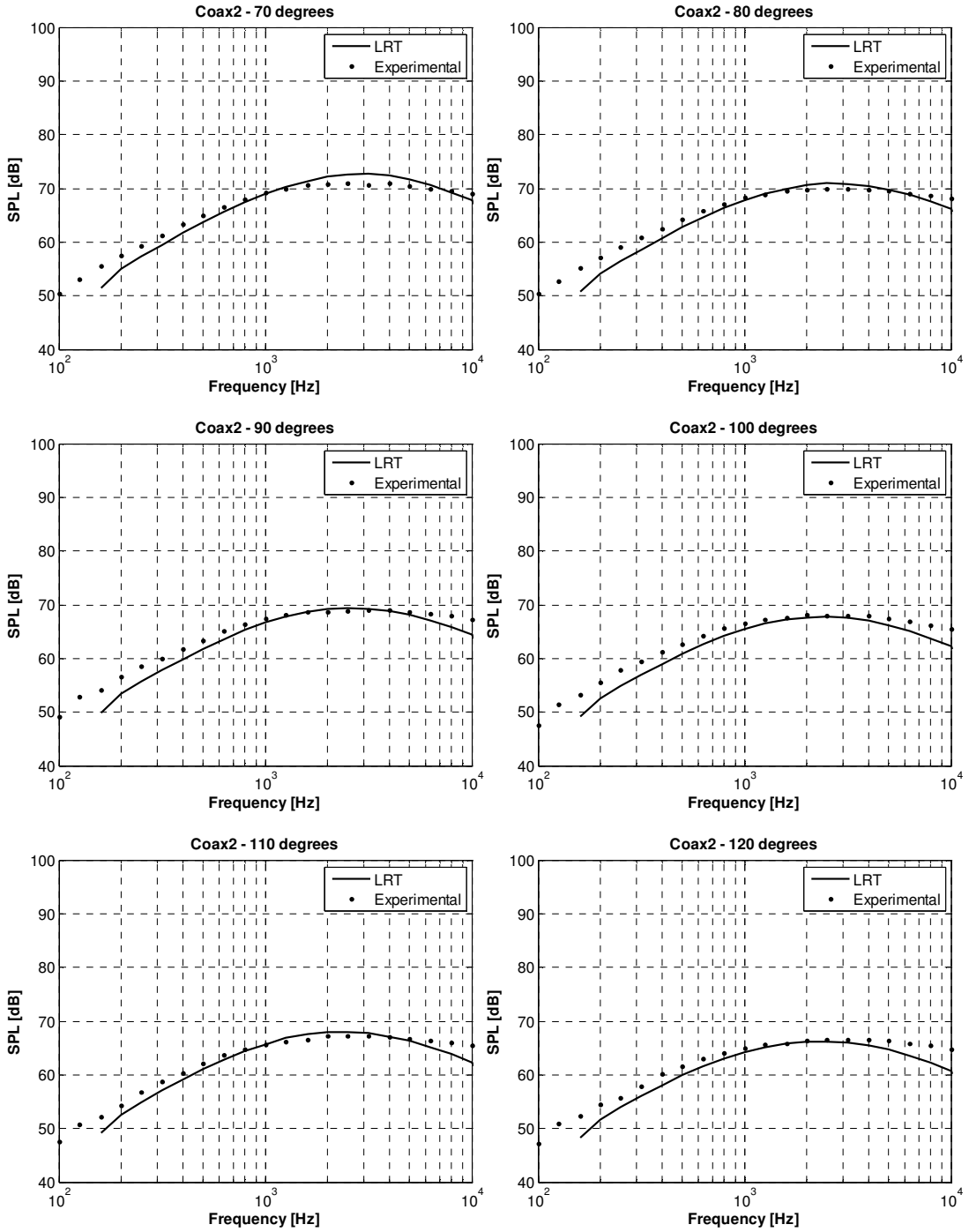

Figure 6.13 - LRT noise predictions for different polar angles for case Coax2, *VR* = 0.79; *AR* = 0.87.

Fig. 6.14 presents the results for the Coax5 case with area ratio 0.87 and velocity ratio (VR) 1.00.

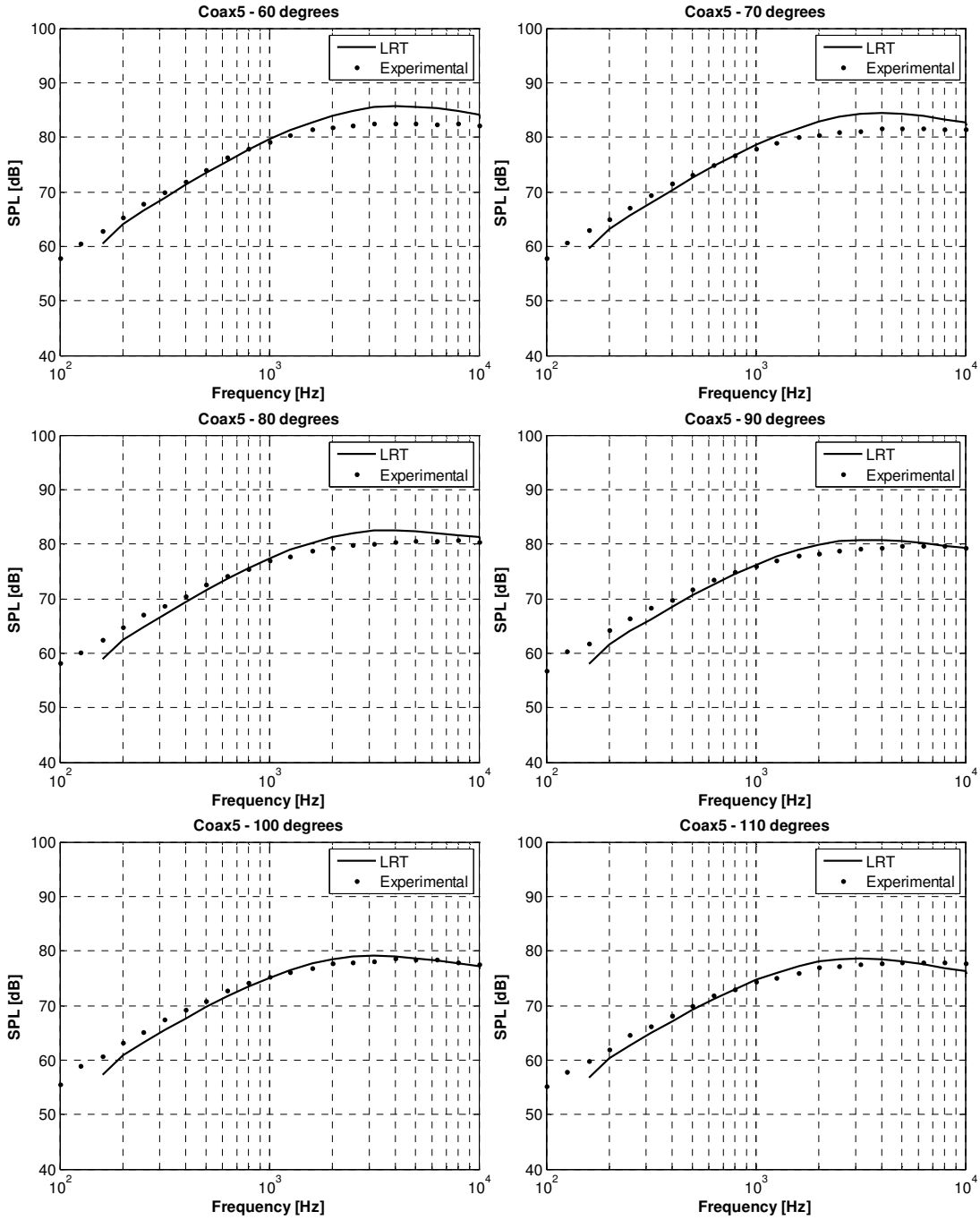

Figure 6.14 – (cont. over).

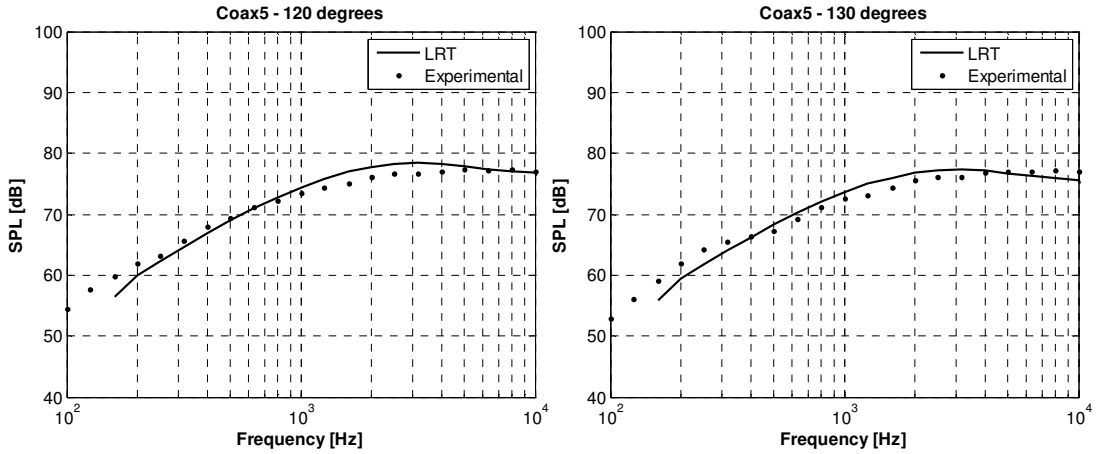

Figure 6.14 - LRT noise predictions for different polar angles for the case Coax5, *VR* = 1.00; *AR* = 0.87.

Fig. 6.15 presents the results for the Coax8 case with area ratio 2.00 and velocity ratio 0.63.

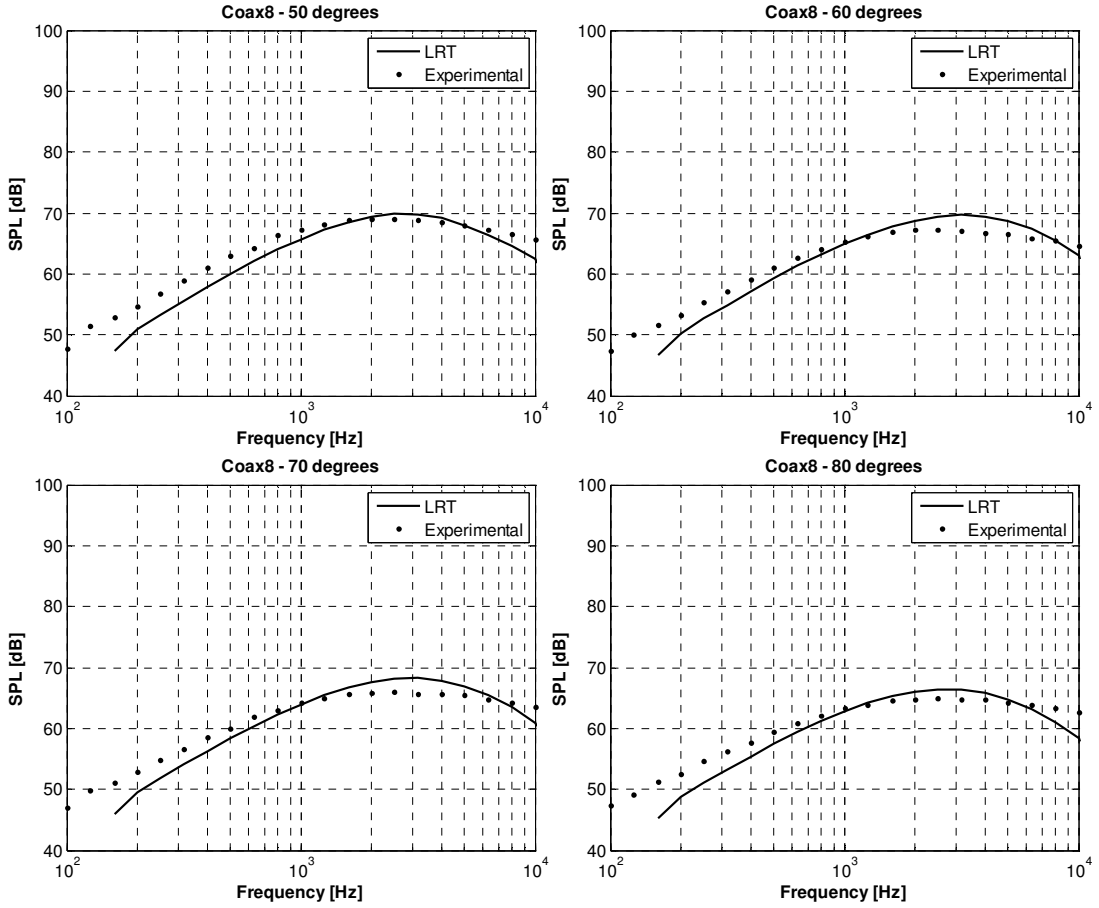

Figure 6.15 – (cont. over).

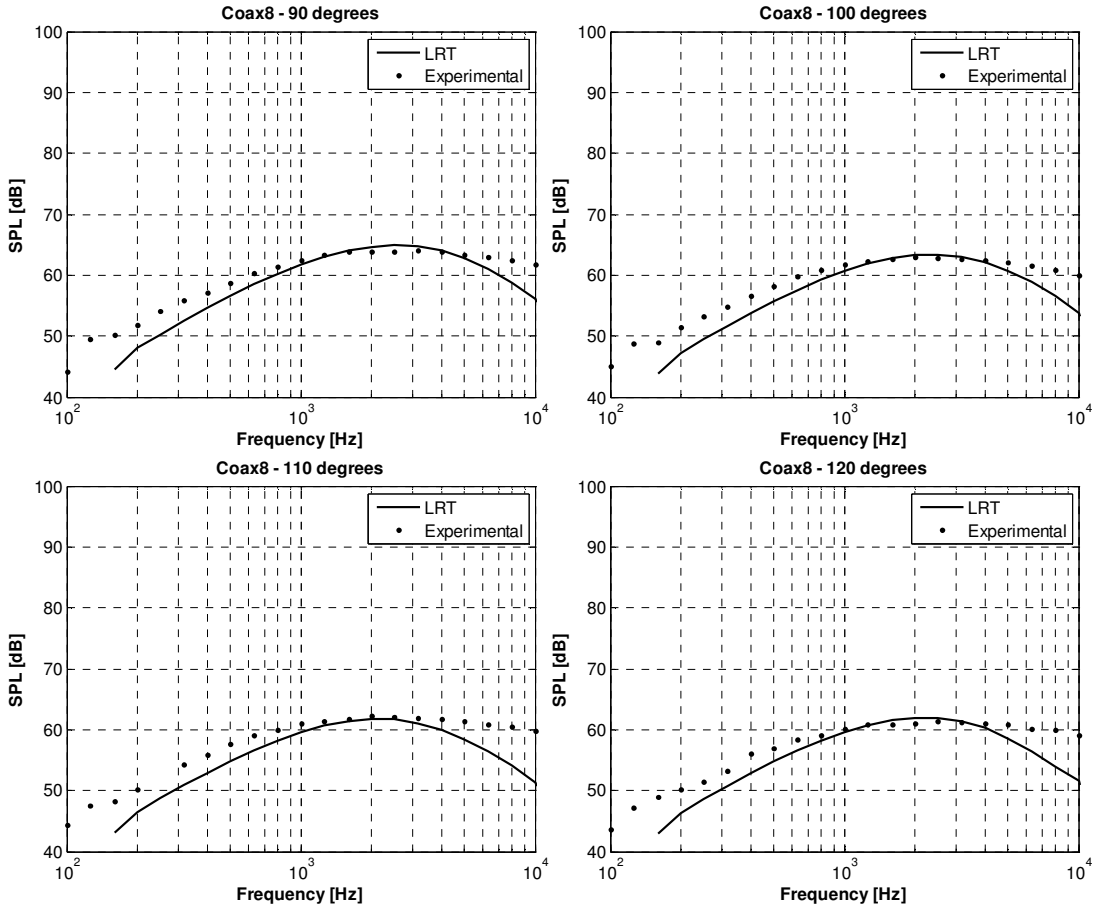

Figure 6.15 - LRT noise predictions for different polar angles for the case Coax8, $VR = 0.63$; $AR = 2.00$.

Fig. 6.16 presents the results for the Coax15 case with area ratio 4.00 and velocity ratio 0.79.

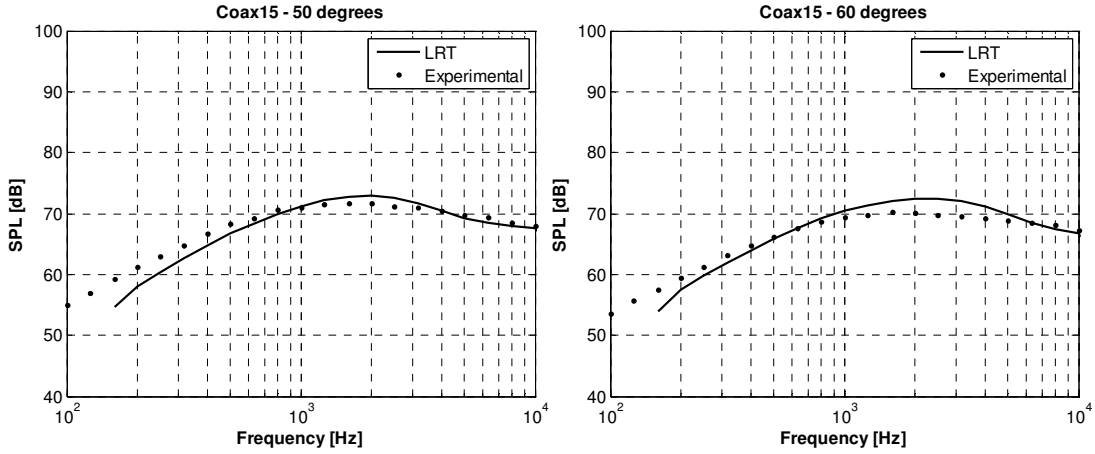

Figure 6.16 – (cont. over).

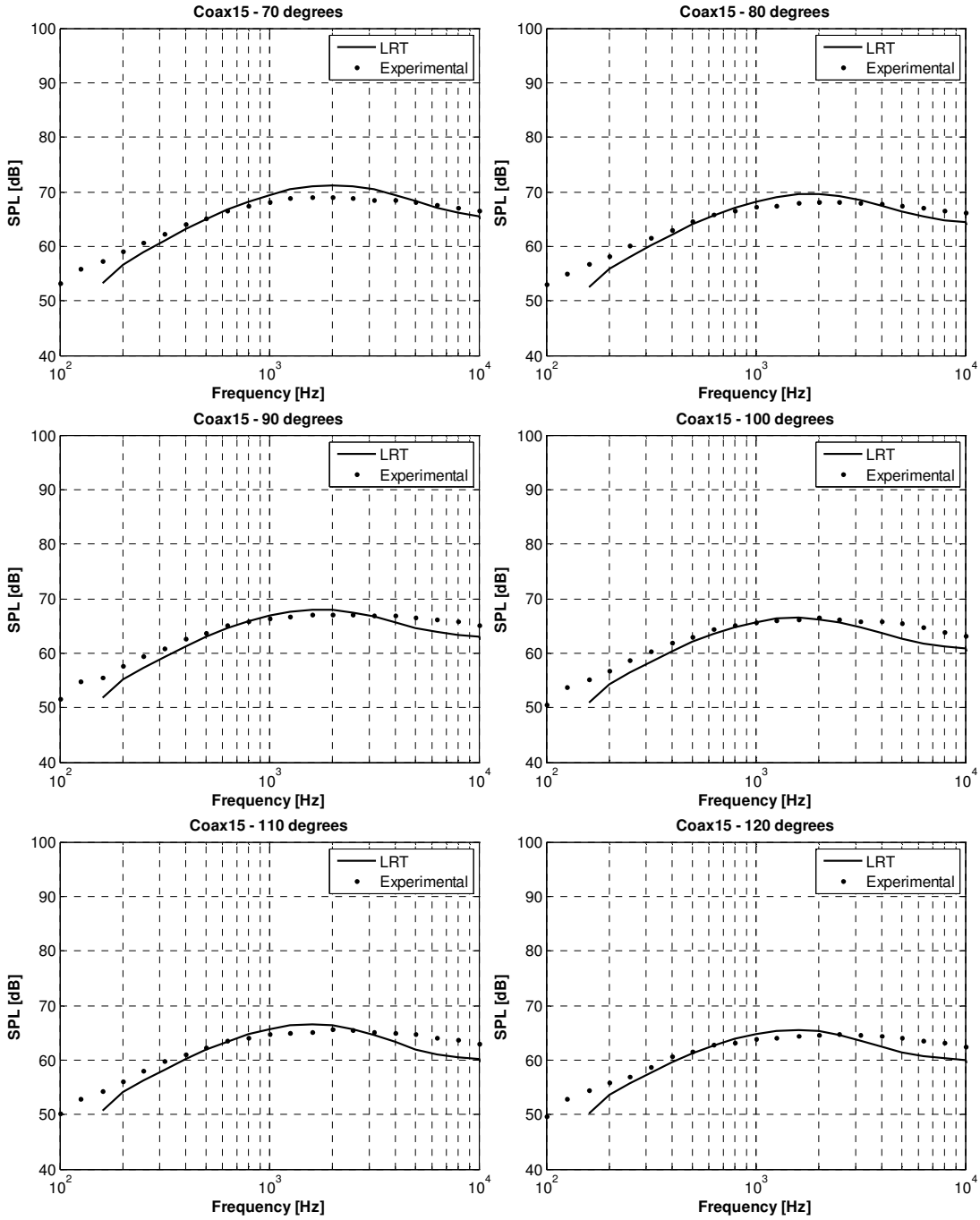

Figure 6.16 - LRT noise predictions for different polar angles for the case Coax15, $VR = 0.79$; $AR = 4.00$.

From all the results presented in this section the LRT method provided reasonable agreement for nozzles with different area ratios, velocity ratios and different Mach numbers. The variation of these parameters affects considerably the flow structure of the jet hence changing the noise sources and propagation for each case. Therefore, it is reasonable to

conclude that the LRT method was able to model the noise sources and calculate the refraction effects giving a fair agreement with the experimental data.

6.3.3 Overall Sound Pressure Level

To be able to show the predictions for most of the cases, this section presents the results in terms of OASPL, which are depicted in Fig. 6.17. The results are presented for angles varying from 30 to 120 degrees. It should be noted that OASPL is greater than any individual sound pressure level because it represents the intensity of the spectrum as a whole. For jet operation condition and nozzles refer to Table (6.1).

The LRT predictions show a good agreement for all angles outside the zone of silence region, indicated by the critical angle (θ_c) on the Fig. 6.17. There is no significant modification on the directivity of noise when velocity and area ratios are modified, at least for the range investigated in this thesis.

6.3.4 Effects of velocity ratio

In order to investigate the effects of the velocity ratio for each fixed area ratio this subsection presents comparisons of the LRT predictions for the jet cases ranging from $VR = 0.63$ to $VR = 1.26$. Figure 6.18 shows the results for the nozzle of area ratio 0.87. Figure 6.19 shows the results for the nozzle of area ratio 2.00 and Fig. 6.20 presents the results for the nozzle of area ratio 4.00. For the smaller AR nozzle, there is not a considerable noise difference when varying the VR from 0.63 to 0.79. As the AR of the nozzles is increased, the difference on the noise levels from the aforementioned VR becomes more pronounced whilst, no significant variation of the peak frequency can be observed. As expected, the noise from the cases with VR of 1.26 is consistently higher than the other VR cases due to the higher turbulence energy produced by the shear-layer formed between the

secondary jet and the ambient field in this condition. Also for VR = 1.26 cases, due to the increase of the mass flow of the outer jet, which is a direct consequence of increasing the secondary nozzle diameter, modifications on the flow turbulent structures occur, affecting mostly the interaction and the mixed-flow region of the jet. These phenomena can be confirmed when looking at the low and mid-frequency range of the noise spectra, for the highest VR cases. As can be seen in this figure, the noise increase is concentrated for these frequencies whereas only minor changes on the high frequencies are observed. The LRT method was able to model the noise generation and propagation fairly well for the whole range of cases investigated.

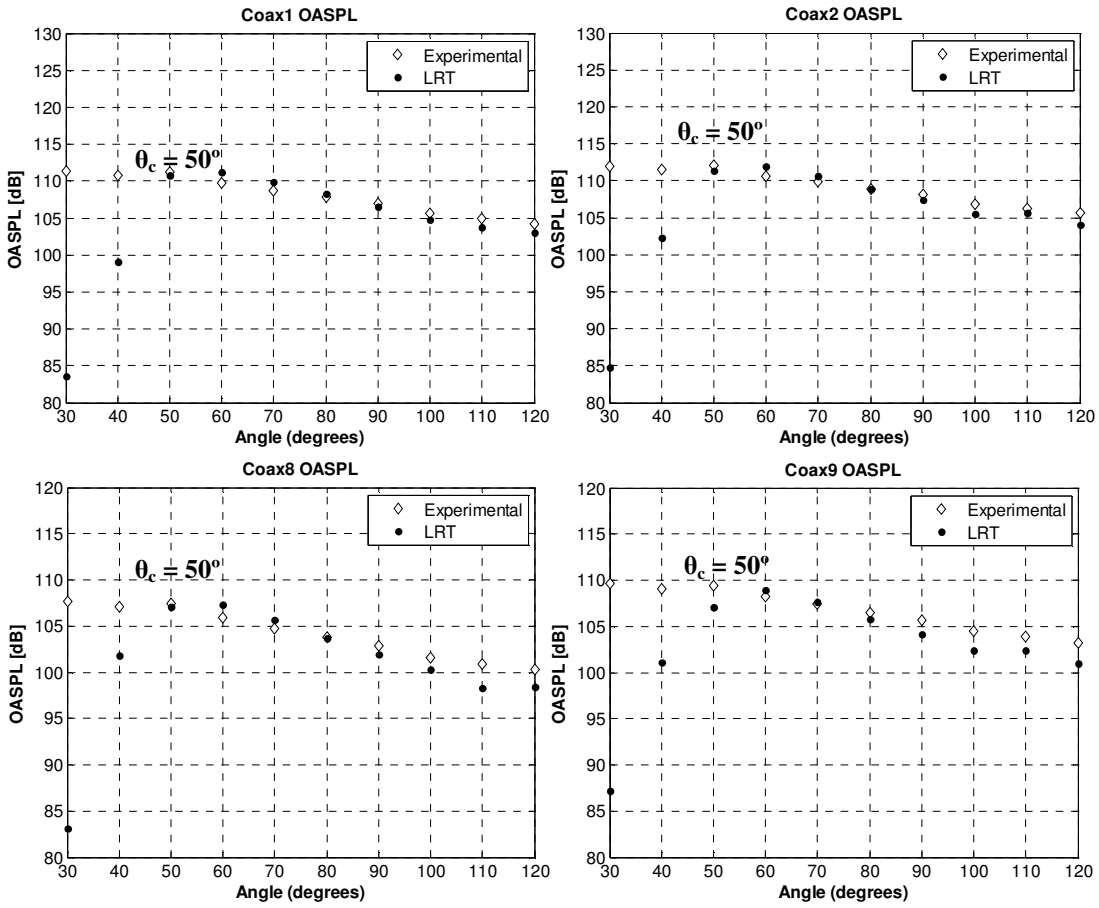

Figure 6.17 – (cont. over).

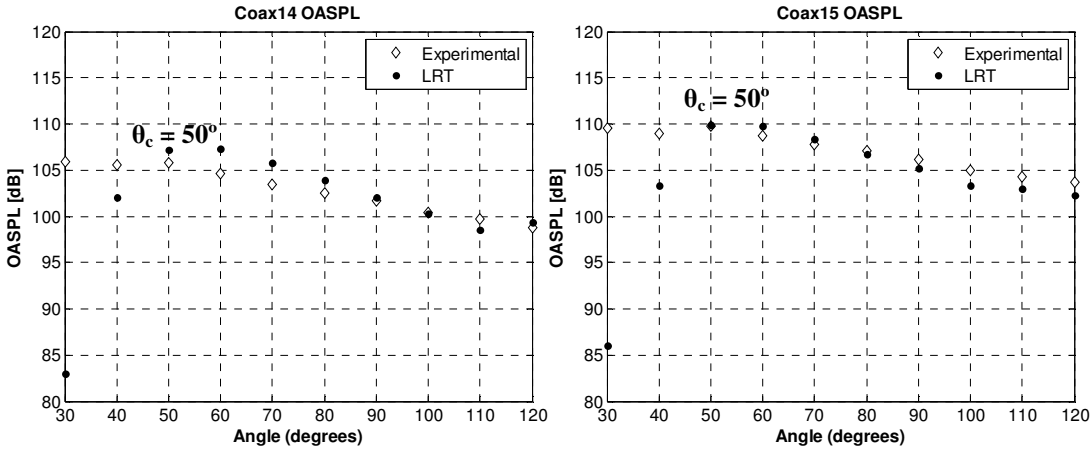

Figure 6.17 - OASPL results for the coplanar nozzle with different velocity and area ratios.

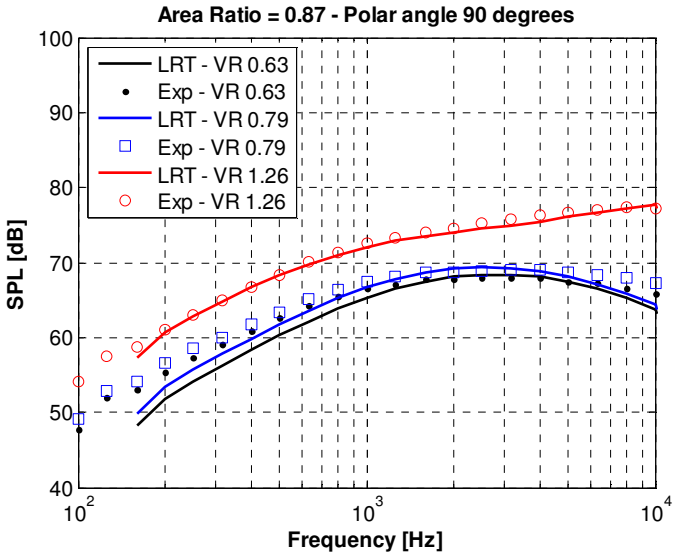

Figure 6.18 - Investigation of velocity ratio effect on the far-field noise using the LRT method for polar angle 90 degrees. *AR* = 0.87.

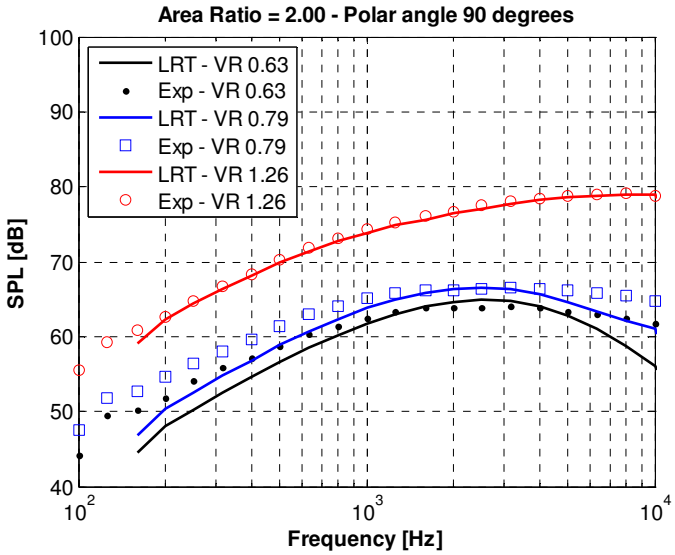

Figure 6.19 - Investigation of velocity ratio effect on the far-field noise using the LRT method for polar angle 90 degrees. *AR* = 2.00.

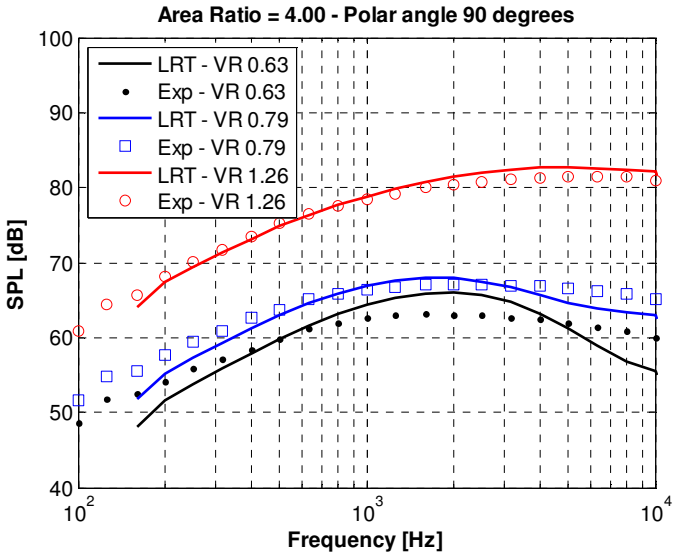

Figure 6.20 - Investigation of velocity ratio effect on the far-field noise using the LRT method for polar angle 90 degrees. *AR* = 4.00.

The next and last section of this chapter presents the noise predictions for a different nozzle configuration. The objective is to apply the LRT method for a short-cowl nozzle operating in a severe flow condition.

6.4 Short-cowl nozzle predictions

Short-cowl coaxial jets were also investigated during the SYMPHONY project. A large number of noise measurements were conducted at the NTF in QinetiQ during 2010. This data will be used here to corroborate the LRT predictions for one jet operation condition.

Figure 6.21 depicts the short-cowl nozzle geometry used in the numerical simulations. The internal diameter of the core is equal to 100.8mm and the bypass diameter is 185.7mm. Table 6.2 presents the operation conditions of the primary stream (core) and the secondary stream (bypass) together with the ambient environment which simulates a flight condition. The temperature ratio between the core and bypass flow is equal to 2.00.

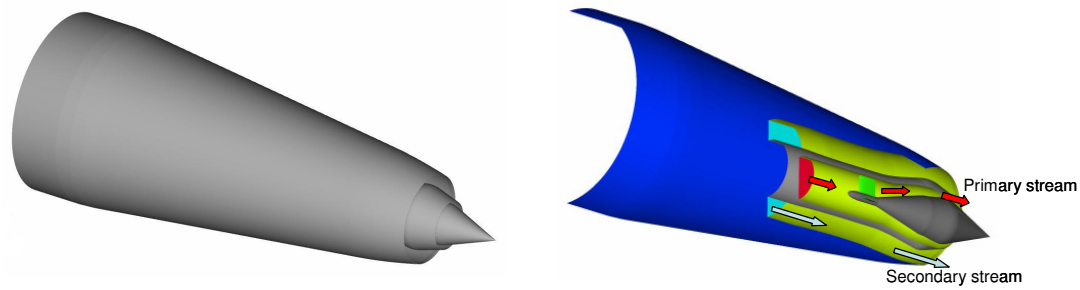

(a) (b)

Figure 6.21 – Short-cowl coaxial nozzle of area ratio equal to 5.5: (a) 3D geometry used on the CFD calculations; (b) cut-plane of the coaxial nozzle.

Table 6.2 - Jet operation conditions for the short-cowl nozzle.

Core Conditions		**Bypass conditions**		**Flight stream**
Vel.(m/s)	**Tot. Temp. (K)**	**Vel.(m/s)**	**Tot. Temp. (K)**	**Vel. (m/s)**
377.8	728.7	292.3	359.3	102.0

Figure 6.22 shows the LRT noise predictions for the short-cowl nozzle. The results are presented for twelve different polar angles from 50 to 120 degrees in terms of narrow band spectra. The experimental data presented here are collected by a far-field microphone array configuration at 12 meters from the nozzle exit, approximately $120D_j$. All microphones used

are ¼" B&K type 4939 with the grids removed aligned to point at the nozzle exit. The noise data is presented as 1m loss-less data corrected for background noise.

Considering that the jet operational conditions for the short-cowl nozzle were extremely complicated, with high temperature ratio, very high jet speed and, with the presence of a flight stream, the predictions from the LRT method are fairly good and hence show the potential of the methodology for noise calculations. The case investigated in this section will be used as a baseline in the next chapter where non-axisymmetric flows will be addressed.

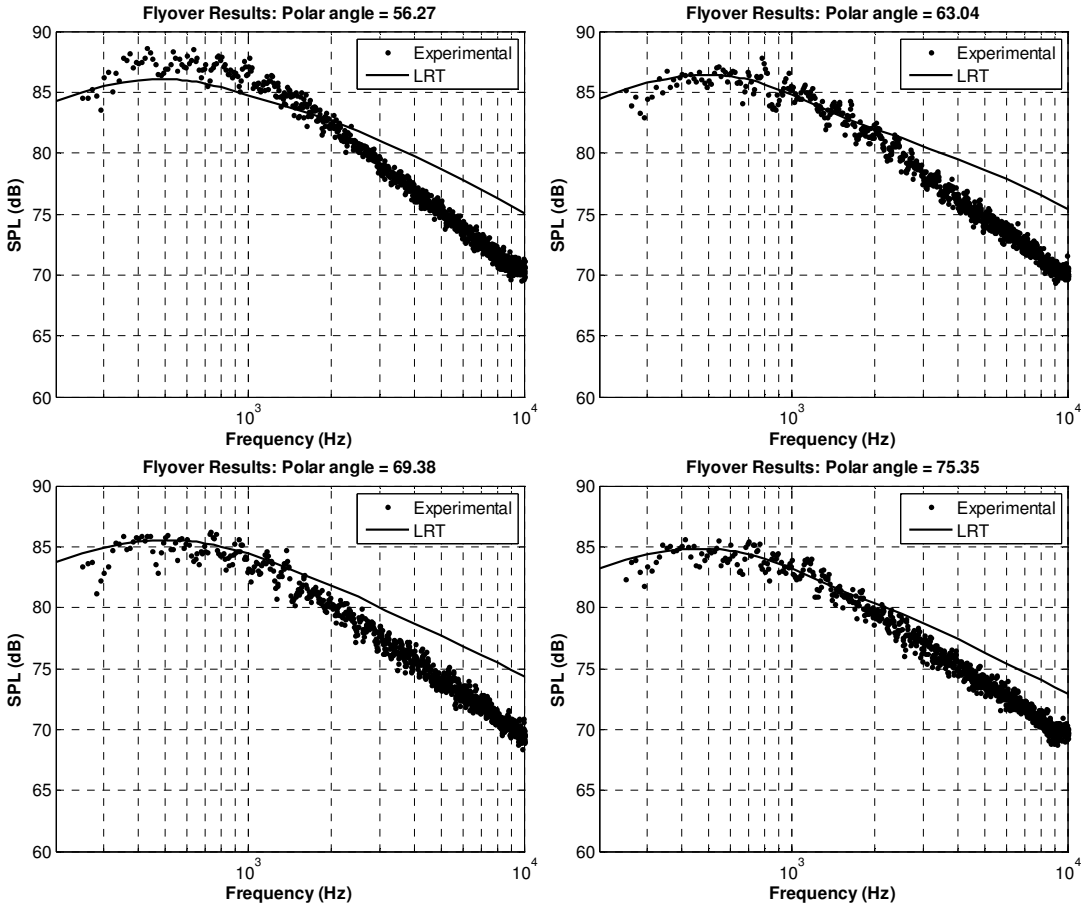

Figure 6.22 – (cont. over).

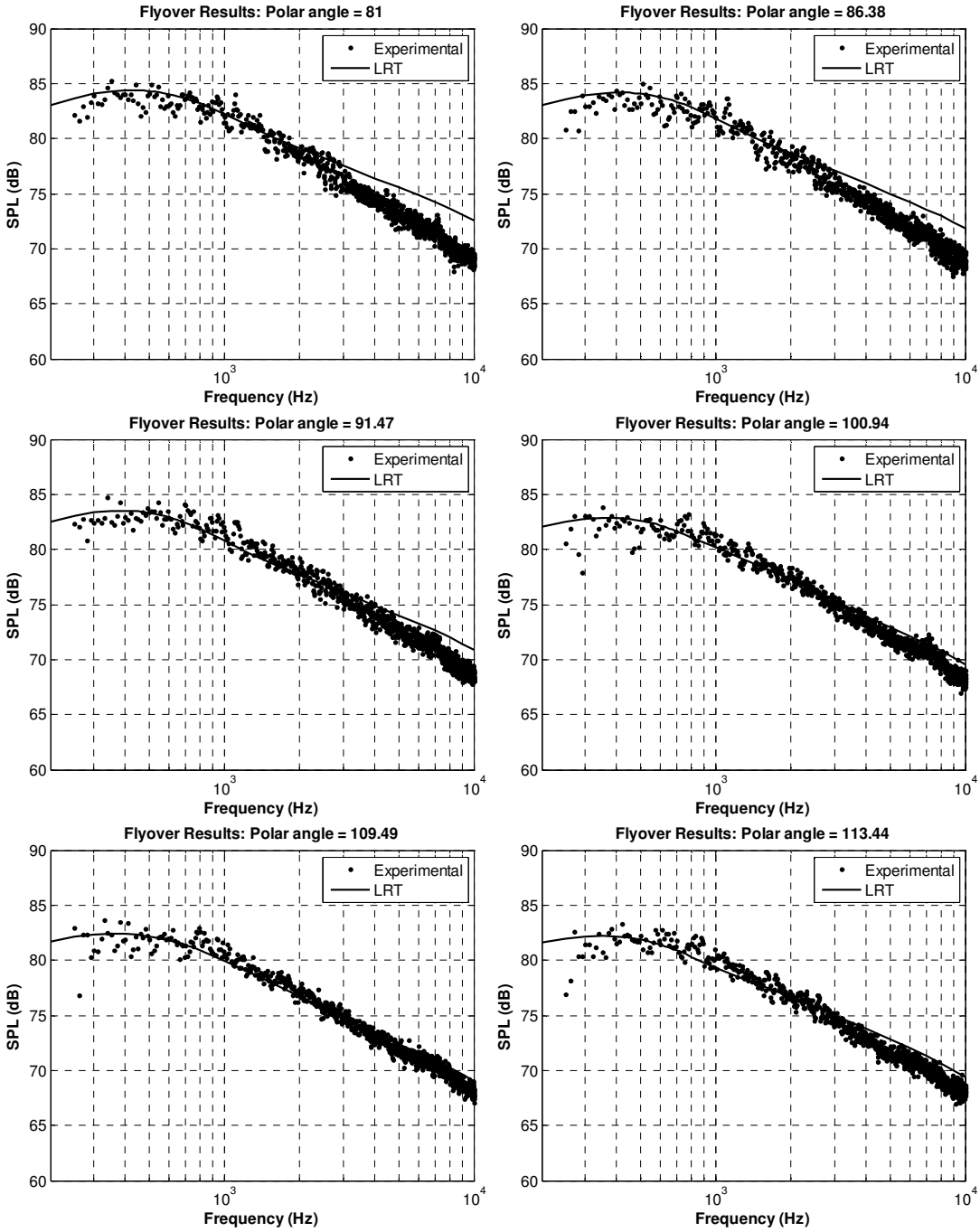

Figure 6.22 – (cont. over).

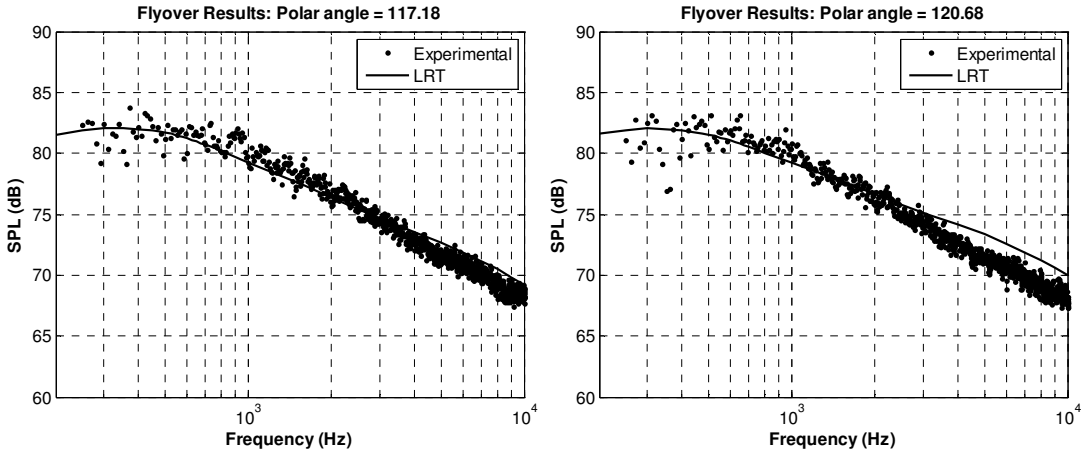

Figure 6.22 – Short-cowl nozzle predictions using the LRT method for different polar angles.

Chapter 7: Complex jet flows from asymmetric nozzles

The efforts to first understand and then reduce jet noise in the scientific community over the last decades are remarkable. Many achievements have been accomplished by modifying somewhat the source generation mechanism by introducing mixing devices on the flow, such as chevrons, and also by introducing novel nozzles design concepts, with the aim of modifying the directivity of the jet noise. On the other hand, the complexities related to the fluid-dynamics structures present in the flow from these noise-improvements-devices are substantial. Hence, simplifications that are usually assumed on most of noise predictions methods, such as axisymmetry, are no longer suitable due to the complexity of the flow generated by modern nozzle geometries. Therefore, this brings the requirement for more advanced noise prediction tools. In this context, this chapter presents the application of the LRT method to predicting the noise from complex asymmetric nozzles and also the effects of the pylon interaction with the jet. The main objective is to investigate the ability of the proposed method to capture the modifications on the noise generation and propagation mechanisms when non-axisymmetries are present on the problem.

7.1 Numerical Predictions using the LRT method

After presenting a general overview of the possible applications of complex jet flows in the aeronautics industry, this section shows the LRT noise predictions for two different asymmetric jet flows. The results are presented for various numbers of polar angles and also for two different arrays of microphones which are called as sideline and flyover arrays, see Fig. 7.1. The objective of looking of two different microphone arrays is to analyse the azimuthal dependence of the noise radiated to the far-field by these complex jet flows. The

nozzle geometries and the experimental data used here are part of the SYMPHONY project. The experimental tests were conducted at the NTF at QinetiQ.

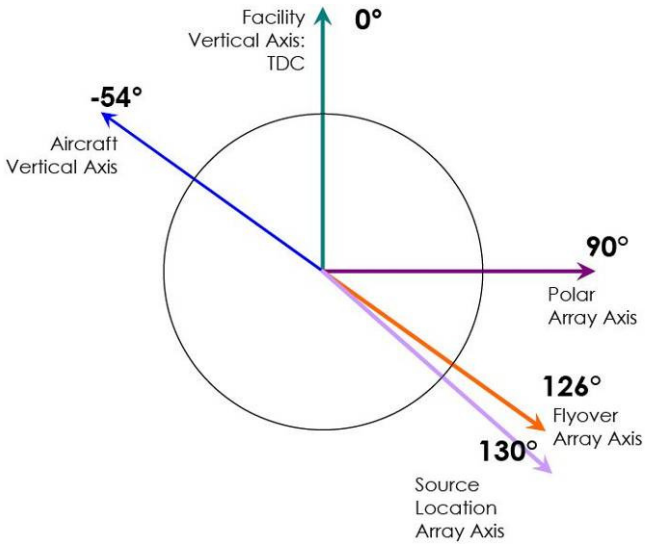

Figure 7.1 – The azimuthal array microphone angles convention at the NTF.

The results from LRT method are presented in this chapter in two different forms: "LRT – NoRefraction" and "LRT". The first form refers to the application of the LRT method without taking into account the refraction effects calculated by the Ray-Tracing, which in theory, corresponds approximately to the results that would obtain if Lighthill's Acoustic Analogy were applied. This can be easily implemented using the LRT code by simply considering the ΔSPL from the RT as equal to zero for the entire source region inside the computational domain. The second form represents the results from the typical LRT methodology, which accounts for the propagation effects throughout the jet flow. The main objective of showing the results in this way is to emphasize the importance of calculating the refraction effects on the final noise prediction. This is especially true when asymmetries are present in the problem, which is the case for the investigations carried out in this chapter.

The same procedure for running the LRT method for the single (Chapter 4) and coaxial (Chapter 5) jet cases was applied in this chapter for the complex jet cases.

Aeroacoustics predictions and mean flow quantities for each case will be presented. The CFD calculations were performed with the commercial code Fluent using a k-ε turbulence model.

7.1.1 LRT predictions for the offset nozzle

Figure 7.2 depicts the offset nozzle. It has the same characteristics as the short-cowl coaxial nozzle presented in Chapter 6 (Section 6.4) but the position of the core nozzle is different. In this case, the core is offset 7.7% (relative to the secondary nozzle diameter) down from the jet centreline. This results in a relatively strong asymmetry in the flow. The geometry presented in Fig. 7.2 was used for the CFD calculation to obtain the mean flow properties by means of a RANS simulation and then the results used as input for the LRT method.

The jet operation condition that is being investigated is described in Table (7.1). As can be seen this condition is relatively extreme, with a high temperature ratio (~2.0) between the core and the bypass streams. This generates a significant temperature gradient and therefore density and sound speed variations inside the jet flow that strongly affects the sound propagation, i.e. the refraction effects can be enhanced. In addition, the presence of a flight stream condition is also considered in the calculation.

Figure 7.3 presents the CFD result for the velocity magnitude of the jet flow for different positions downstream the nozzle. In this figure, it is possible to verify the spreading of the jet and how it is affected by offsetting the core relatively to the by-pass region. Figure 7.4 and Fig. 7.5 shows contours results of mean flow properties for the offset nozzle indicating the asymmetry on the flow.

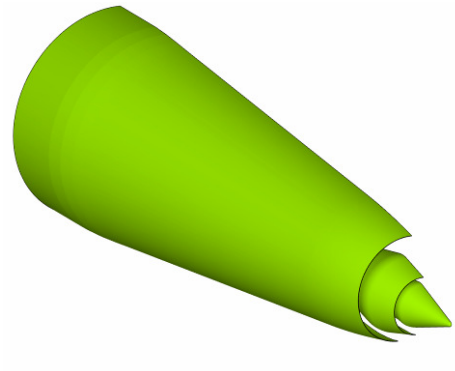

(a) A 3D view of the surface model.

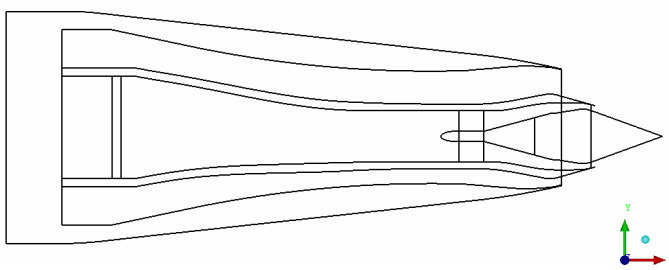

(b) XY plane.

Figure 7.2 Offset geometry been investigated by the LRT method.

Table 7.1 - Jet operation conditions for the offset nozzle.

Core Conditions		**Bypass conditions**		**Flight stream**
Vel.(m/s)	**Tot. Temp. (K)**	**Vel.(m/s)**	**Tot. Temp. (K)**	**Vel. (m/s)**
377.8	728.7	292.3	359.3	102.0

The propagation results obtained by the Ray-Tracing code for the offset nozzle are now presented. Figure 7.6 presents the calculation of ΔSPL, due to sound refraction, for different polar angles. In the forward arc (63.04º) there is a region on the upper side of the jet centreline where the noise is being attenuated due to refraction caused mainly by the potential core. At 92º a slight effect of refraction can be observed for the sources located up to $4Dj$. On the other hand, in the rear arc (123.68º) there is a sound amplification region for the sources

located between the shear layer and the potential core. These results were calculated for observers located on the sideline array. The 3-dimensional contours are shown in Fig. 7.7.

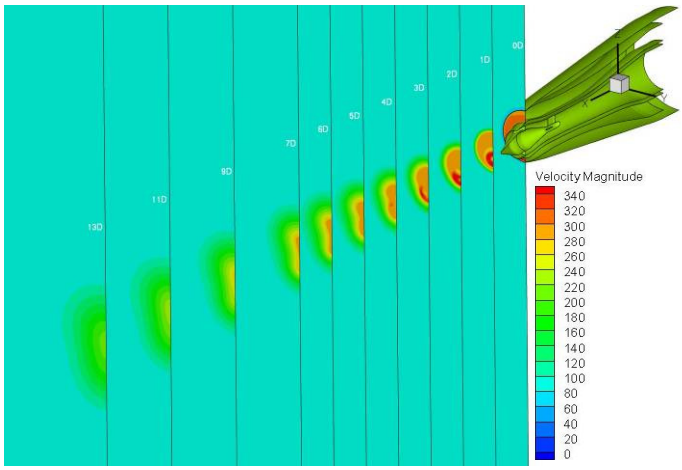

Figure 7.3 - CFD results of the offset nozzle for velocity magnitude in different positions relatively to the jet's diameter.

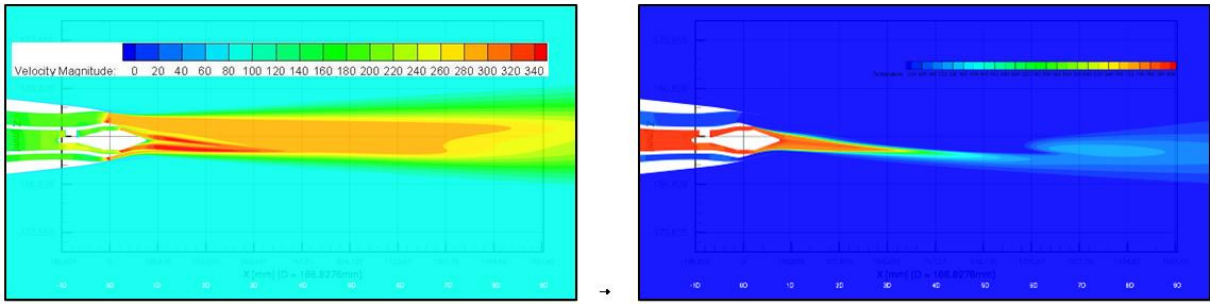

(a) Velocity distribution. (b) Temperature distribution.

Figure 7.4 – Contours of mean flow properties obtained from a RANS simulation for the offset nozzle.

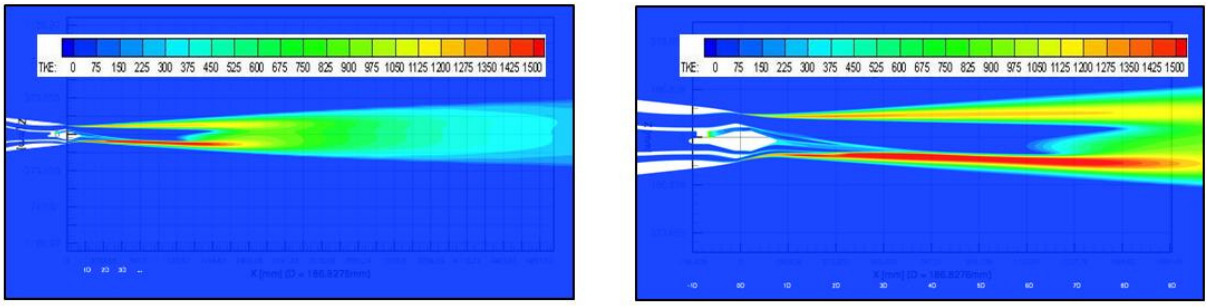

(a) TKE distribution. (b) Zoom view near the nozzle.

Figure 7.5 – Contours of turbulent kinetic energy (TKE) for the offset nozzle.

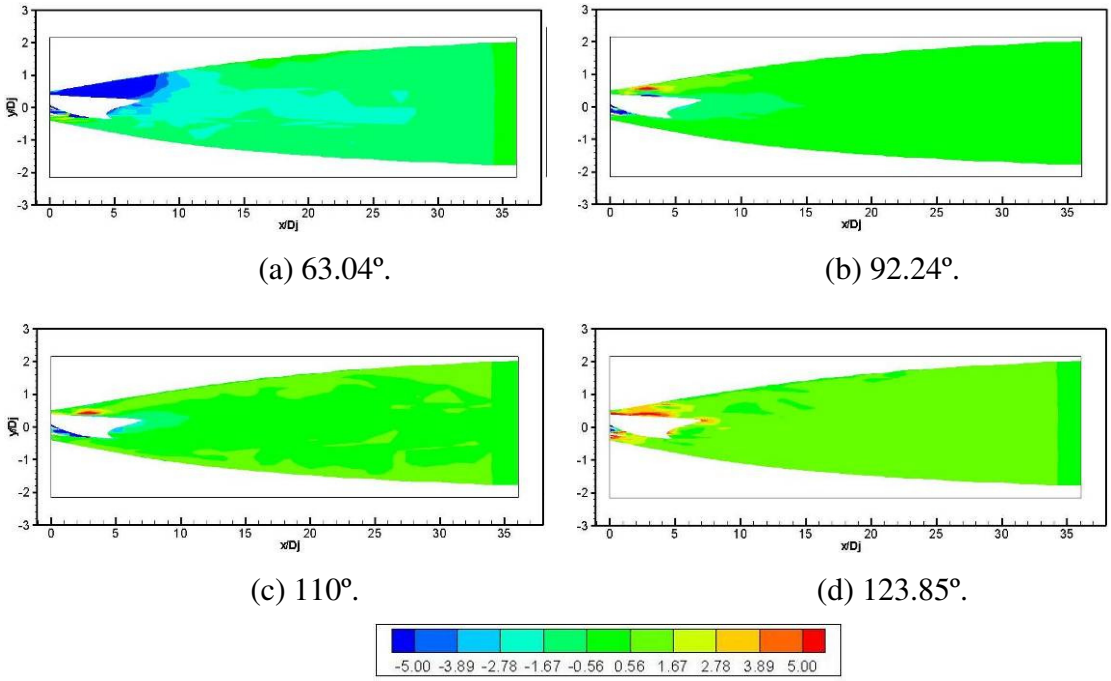

(a) 63.04º. (b) 92.24º.

(c) 110º. (d) 123.85º.

Figure 7.6 - ΔSPL (dB) calculated from the Ray-Tracing method for the offset nozzle at four polar angles.

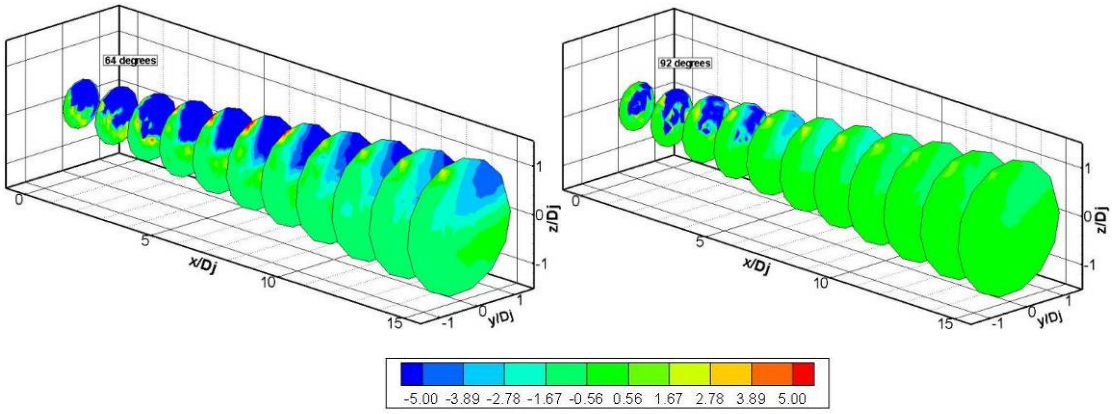

(a) 63.04º. (b) 92.24º.

Figure 7.7 – 3D Ray-Tracing results in ΔSPL (dB) for the offset nozzle.

In order to demonstrate the Ray-Tracing capability for noise propagation, five different point sources, modelled as monopoles, were positioned inside the jet flow region at x/D_j = 1.50, as depicted in Fig. 7.8. The results for the ΔSPL on the far-field, for each of these sources, are presented in Fig 7.9 as a function of polar and azimuthal angles.

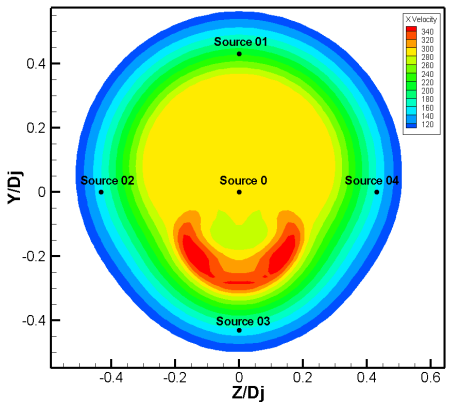

Figure 7.8 - Point sources positions on the jet flow field. Contour plot of velocity at $x/D_j = 1.50$.

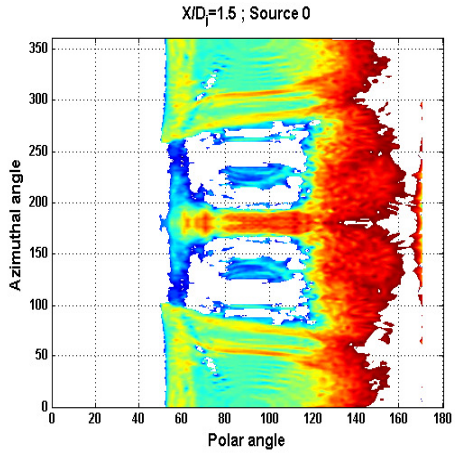

(a) Source 0.

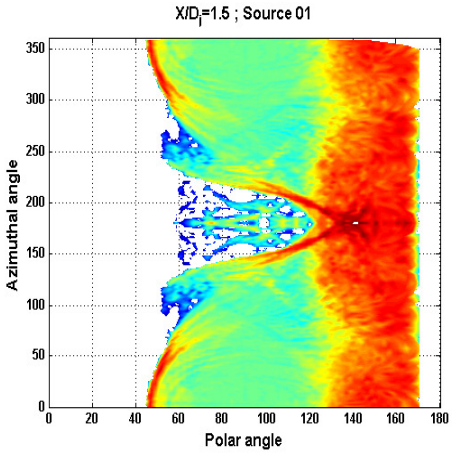

(b) Source 01.

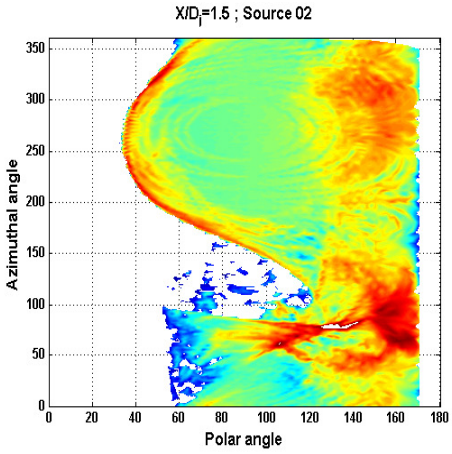

(c) Source 02.

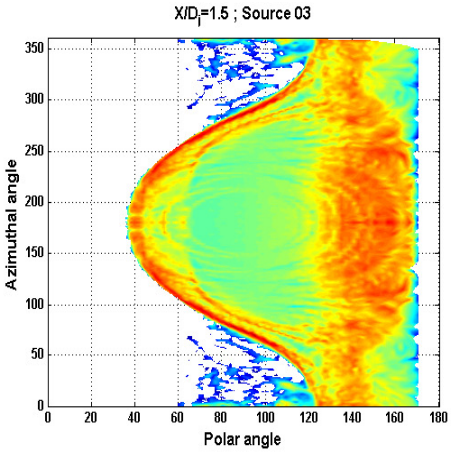

(d) Source 03.

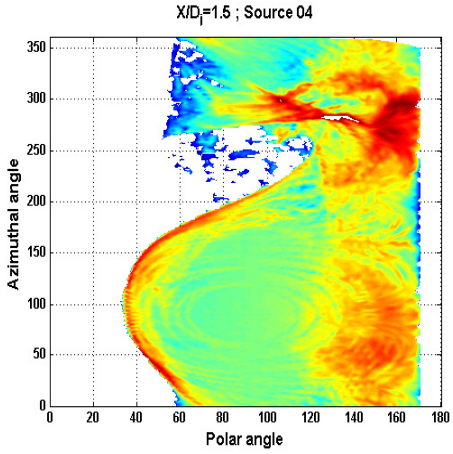

(e) Source 04.

Figure 7.9 - Ray-Tracing results in ΔSPL (dB) for different sources located on the offset nozzle flow field at x/D_j = 1.50.

The noise predictions from the LRT method for the offset nozzle are now discussed. The results are shown comparing the two predictions from the LRT (LRT–NoRefraction and LRT, as explained previously) with the experimental data for the sideline array at different polar angles, see Fig. 7.10.

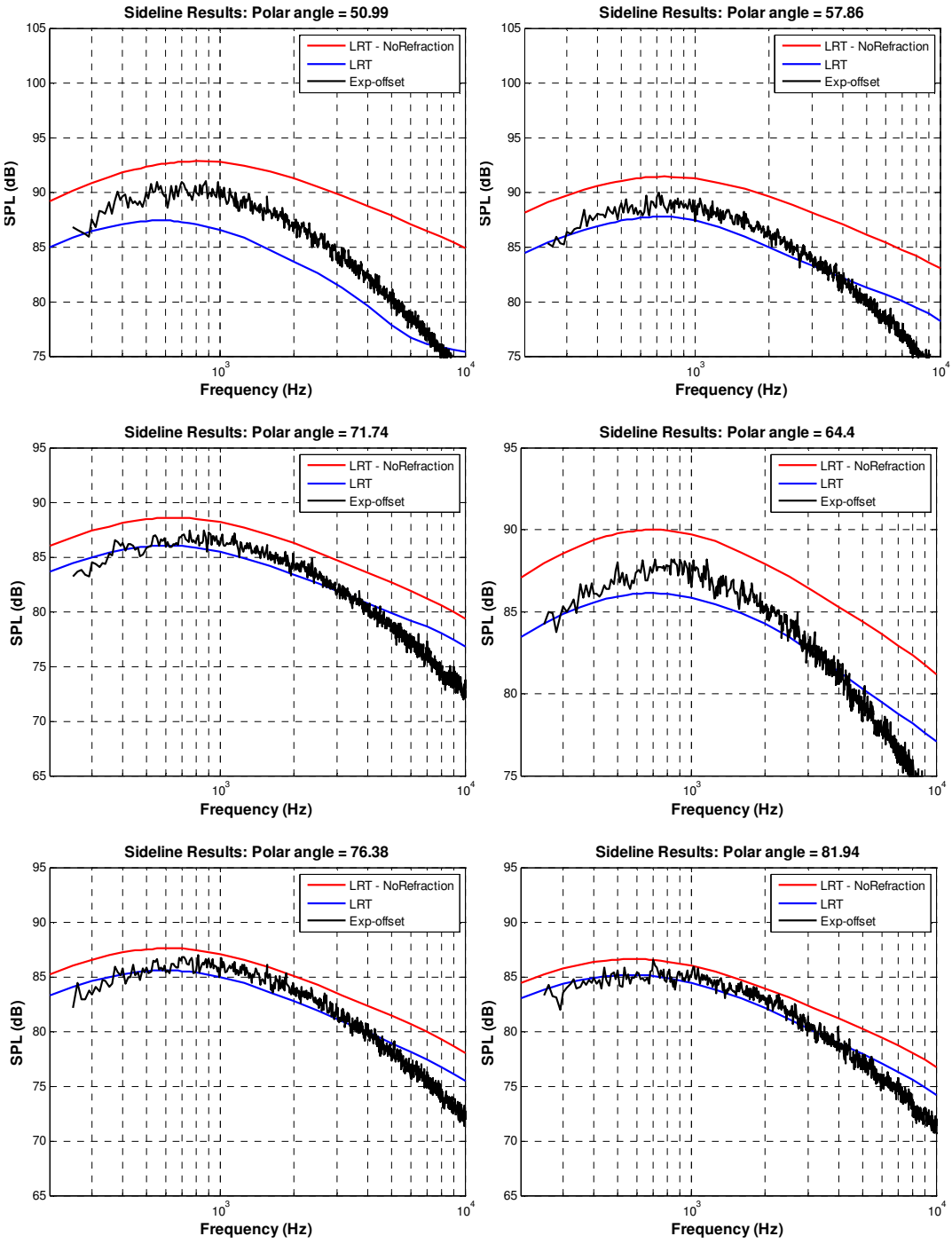

Figure 7.10 – (cont. over).

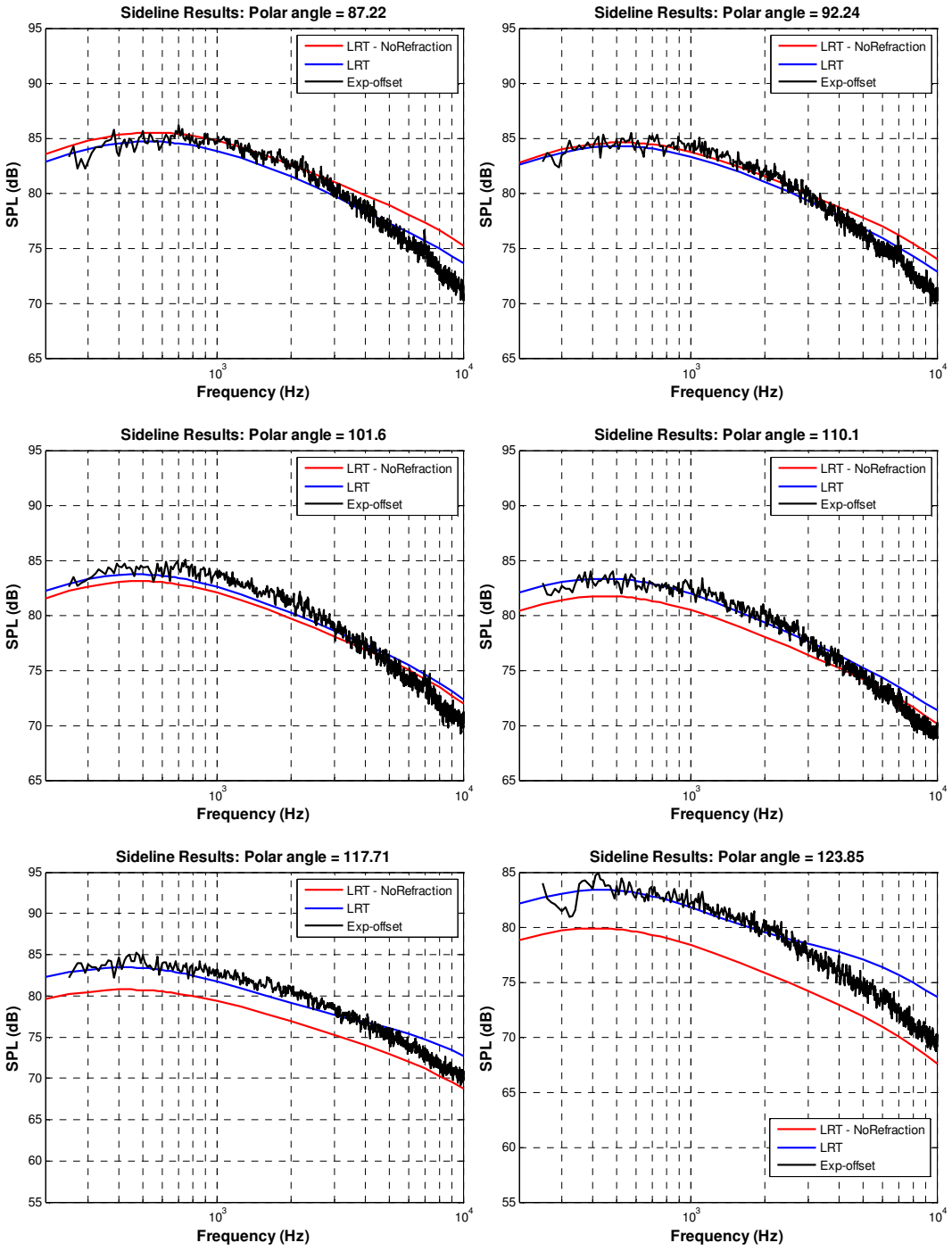

Figure 7.10 – Offset LRT noise predictions for different polar angles with and without the refraction effects calculated by the Ray-Tracing.

The results from the LRT method presented in Fig. 7.10 show fairly good agreement with the experimental data in the forward and rear arc angles. It is evidently the improvements on the noise predictions when the refraction effects are accounted for with the LRT method.

As can be seen the LRT method correctly computes both the attenuation of the sources, especially in the forward arc, and the amplification of the sources in the rear arc. This demonstrates the importance of considering flow-sound interactions for predicting the noise from complex jet flows.

7.2.2 Short-cowl axisymmetric coaxial vs. offset noise predictions

This section presents the flow-field and noise modifications when offsetting the core stream from an axisymmetric coaxial nozzle. The results from the short-cowl coaxial nozzle presented here are the same of the coaxial axisymmetric nozzle that was already presented in Chapter 6 (Section 6.4). For simplicity, from now on the axisymmetric geometry will be called the baseline nozzle. For both geometries the jet operating conditions simulated were the same as the ones presented in Table (7.1).

Figure 7.11 and Fig. 7.12 present the CFD mean flow properties for the baseline and the offset nozzles. Comparing the contours of velocity distribution (Fig. 7.11), there is a strong effect on the potential core of the offset nozzle, which in this case breaks down around $6D_j$ whereas in the baseline nozzle it breaks down around $8.5D_j$. It is also possible to identify that for the offset nozzle, there are two shear layers formed with different lengths. Contours of turbulent kinetic energy are shown in Fig. 7.12. Offsetting the flow slightly reduced the turbulence on the upper side of the nozzle when compared to the baseline nozzle. However, the turbulence on the lower side of the jet plume is considerably increased over that of the baseline changing therefore the location of the peak energy of the flow. It is also important to emphasize that from these results, it is possible to confirm that the CFD simulations conducted in this thesis show the same asymmetry characteristic in the flow, as presented previously, when offsetting the fan flow.

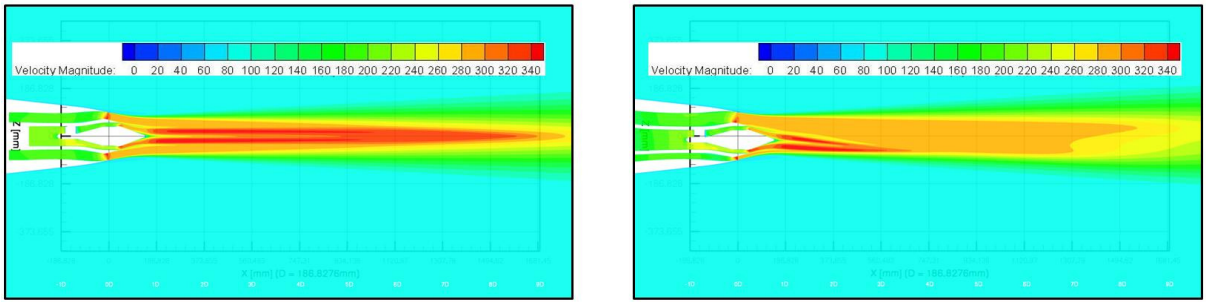

(a) Baseline nozzle. (b) Offset nozzle.

Figure 7.11 – Numerical results of the velocity distribution for the coaxial and the offset nozzles.

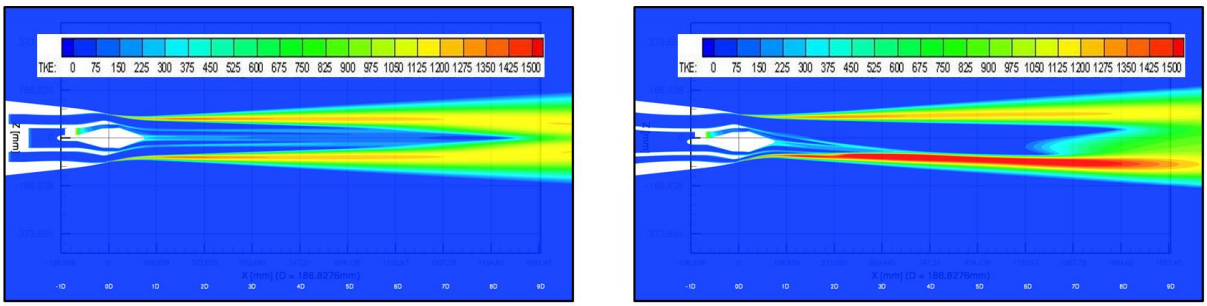

(a) Baseline nozzle. (b) Offset nozzle.

Figure 7.12 – Numerical results of the turbulent kinetic energy for the coaxial and the offset nozzles.

The noise predictions from the LRT method for both nozzles are compared for different polar angles, at the sideline array, and the results are shown in Fig. 7.13. All the experimental data used here were obtained during the SYMPHONY project at QinetiQ's anechoic chamber.

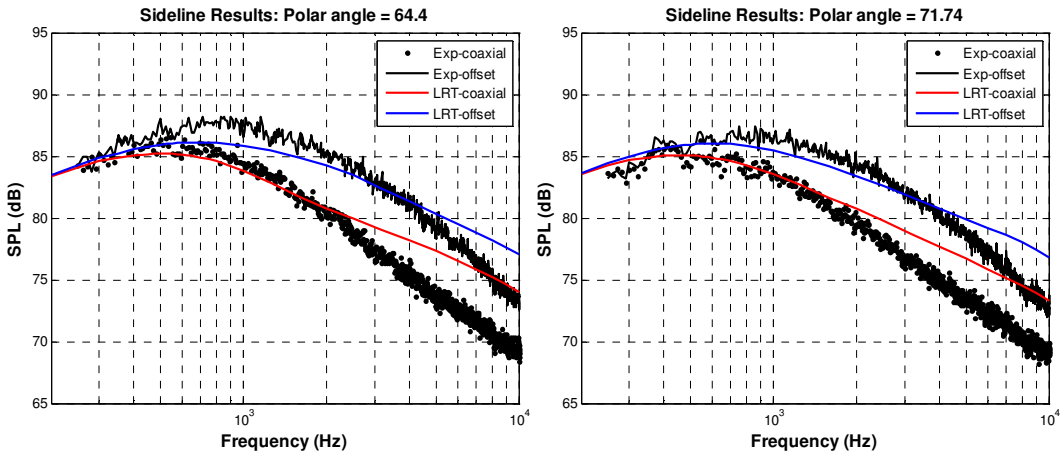

Figure. 7.13 – (cont. over).

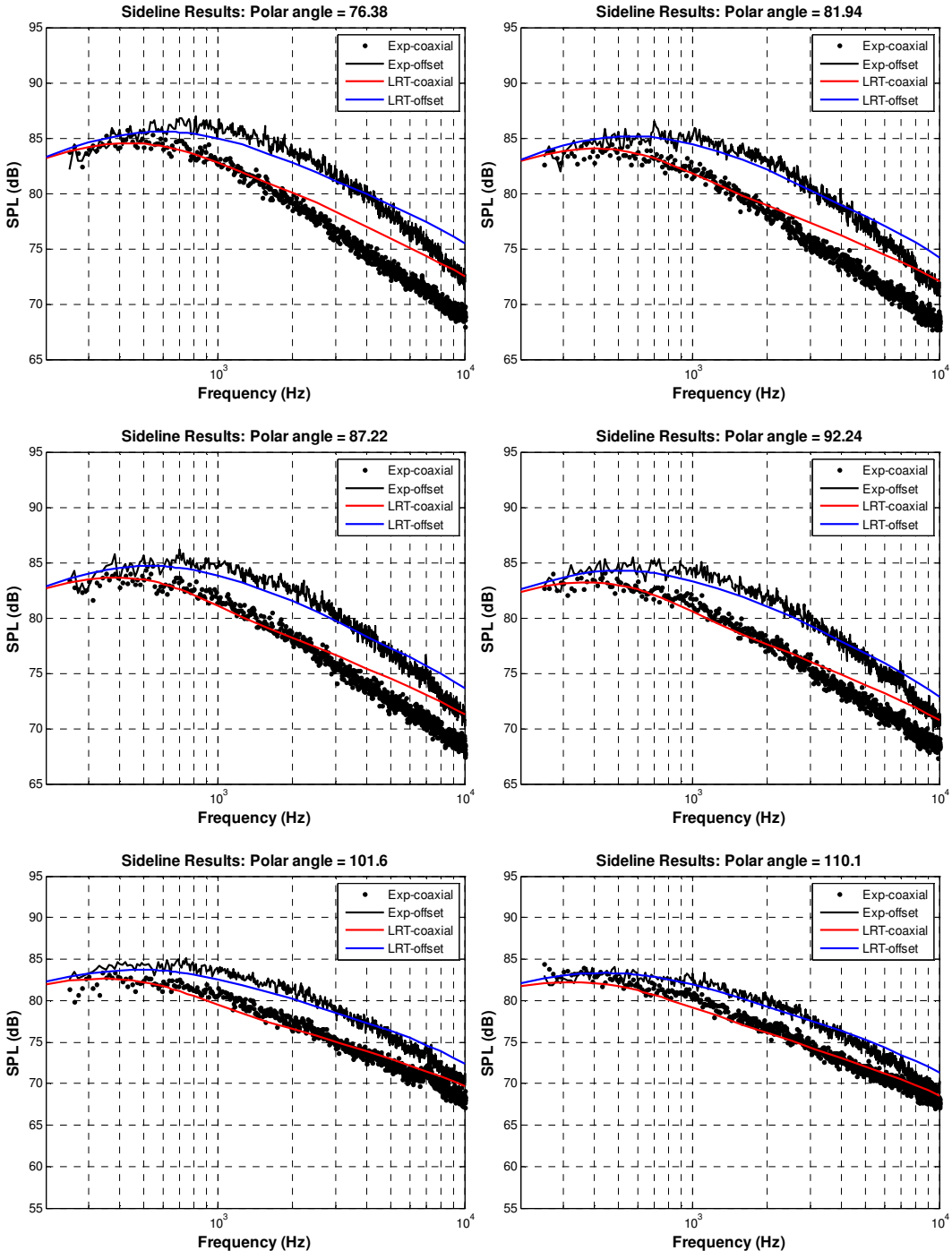

Fig. 7.13 – (cont. over).

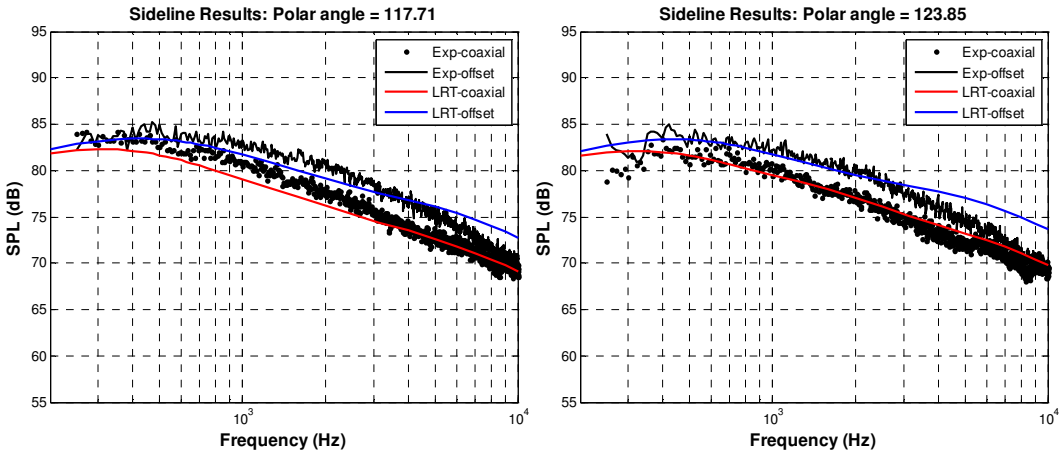

Figure 7.13 - Noise comparisons between the offset nozzle and the axisymmetric coaxial nozzle using the LRT method.

The LRT predictions for both cases presented above (coaxial axisymmetric and offset nozzle) can be considered to be fairly good when compared to the experimental data.

It can be noted from Fig. 7.13, that there was a noise increase on the whole spectra for the offset nozzle. Also the peak frequency moved to higher frequencies. This noise increase by the offset nozzle was not totally expected by the SYMPHONY participants and, it generated long discussions to try to understand what went wrong. Unfortunately, no consensus has been achieved by the time of writing. However, looking at the literature, something similar has already reported by Brown *et al.* [53] during the Offset Stream Technology programme. According to this work, an offset stream jet is less effective at reducing noise when the effect of flight is considered. Furthermore, these authors report that the jet offset using a S-duct (that is similar to the offset nozzle investigated in this thesis) showed a small reduction in noise relative to the baseline jet in the static case. However, it had an increase in noise relative to the baseline jet when the flight effect was added, which is the same operation condition that was investigated here. Another possibility is related to possible undesired variations on the nozzle walls. Birch [60] affirms that where asymmetric flows are concerned, they are extremely sensitive to small nozzle deformations and that this can influence the far-field noise radiated from them. Perhaps, the most probably correct

answer to this question is that there are still open issues on jet noise and that more dedicated research is necessary.

Apart from the unexpected noise increase for the offset nozzle, is important to highlight that the effects caused by the complex modifications on the sources and on the sound propagation were satisfactory captured by the LRT method. Therefore, the objective of the current effort was achieved.

7.2.3. PAA investigation with LRT method: jet-pylon configuration

Figure 7.14 depicts the geometry of the jet-pylon configuration investigated here. The jet nozzle in this case is similar to the short-cowl coaxial nozzle presented in Chapter 6 (Section 6.4) but with the addition of the pylon on the model. The geometry presented in Fig. 7.14 was used for the CFD calculation to obtain the mean flow properties by means of a RANS simulation and then these results were used as input for the LRT method.

The jet operation condition for this case is presented in Table (7.2). Just as in the offset case, the jet-pylon interaction case is investigated at a severe flow condition with the presence of high temperature ratios and flight stream condition.

To understand how jet-pylon interactions affect jet noise, it is first necessary to understand how these interactions change the jet flow. Figure 7.15, depicts the CFD results for the velocity magnitude at different positions downstream the nozzle. From this figure it is possible to visualize the effects of the pylon on the mean flow properties of the jet, such as the spreading rate of the jet to the far-field.

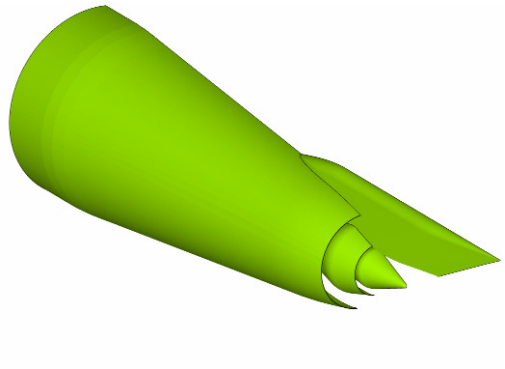

(a) 3D view of the jet-pylon configuration.

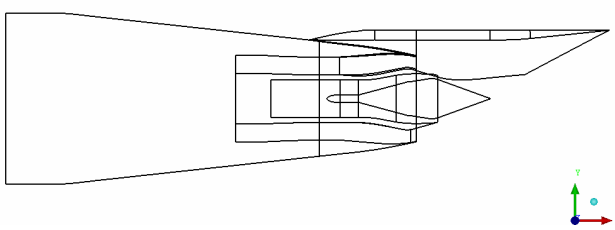

(b) XY plane of the jet-pylon configuration.

Figure 7.14 - Geometry of the jet-pylon configuration been investigated by the LRT method.

Table 7.2 - Jet operation conditions for the jet-pylon configuration.

Core Conditions		**Bypass conditions**		**Flight stream**
Vel.(m/s)	**Tot. Temp. (K)**	**Vel.(m/s)**	**Tot. Temp. (K)**	**Vel. (m/s)**
377.8	728.7	292.3	359.3	102.0

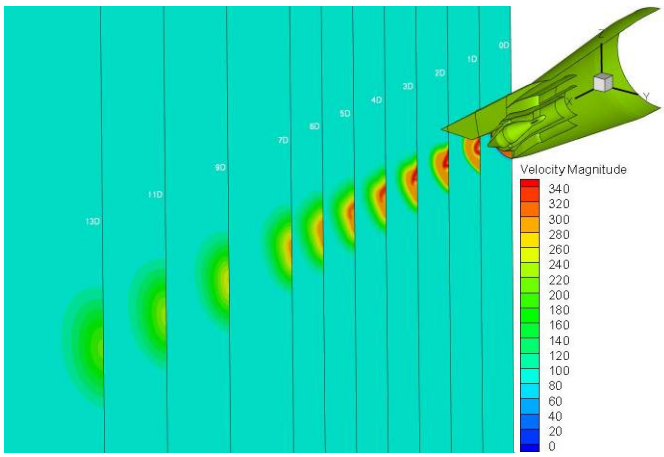

Figure 7.15 - CFD results of the jet-pylon configuration for velocity magnitude in different positions relatively to the jet's diameter.

Figure 7.16 and Fig. 7.17 also show a comparison of the RANS calculations from the baseline coaxial and the jet-pylon configuration. From these numerical results, it is possible to verify that for the coaxial axisymmetric nozzle there are two shear layers, one formed between the core flow and the fan flow, and the second between the fan flow and the external flow. As we go farther downstream, these shear layers merge to form a stronger shear layer with higher turbulence, located approximately at the centreline of the jet. When the pylon is added, the results show a significant modification on the flow structure, with the presence of strong asymmetries. The peak turbulence is now moved upstream from the jet centreline, downstream of the trailing edge of the pylon, and there is also an increase on the jet mixing which reflects in a shorter potential core.

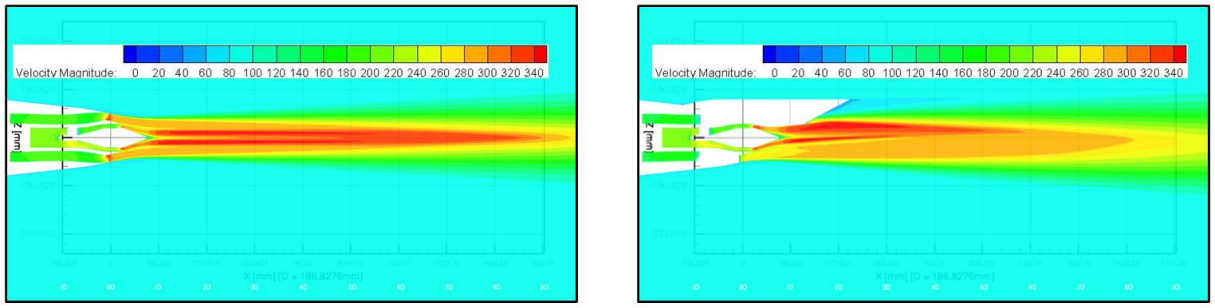

(a) Baseline nozzle. (b) Jet-pylon configuration.

Figure 7.16 – Numerical results of the velocity distribution for the coaxial nozzle and the jet-pylon configuration.

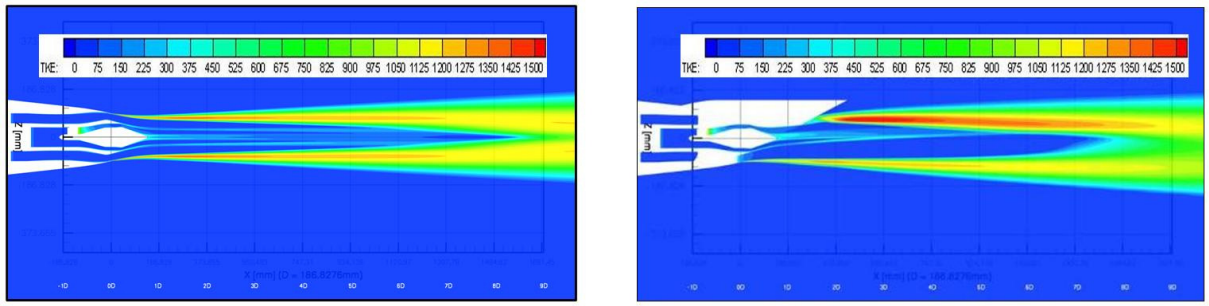

(a) Baseline nozzle. (b) Jet-pylon configuration.

Figure 7.17 – Numerical results of the turbulent kinetic energy for the coaxial nozzle and the jet-pylon configuration.

The propagation results obtained by the Ray-Tracing method for the jet-pylon configuration are now discussed. Figure 7.18 presents the calculation of ΔSPL, due to sound refraction, for two specific polar angles, 63º and 124º. These positions were carefully selected to demonstrate the importance of the sound-flow interactions when predicting jet noise from asymmetric configurations. At the forward arc position (63º), there is a considerable region upstream of the potential core where the sources are being attenuated by the refraction effects. This region, in particular, is a strong source region for the high frequency noise. This is due to the modification on the flow field caused by the addition of the pylon, which concentrates the peak turbulence there; see Fig. 7.17(b). As will be seen by the results of noise prediction spectra, if the attenuation caused by this region is not considered in the calculation there will be over-predictions of the noise in the far-field at this polar angle. However, when the rear arc (124º) is considered, the refraction effects are not as aggressive as at 63º, but there is a slight amplification region near the nozzle, upstream of the potential core. Once again, if this amplification is not taken into account in the noise calculations, there will be, to some extent, under-predictions in the far-field noise for this particular polar angle, this will be demonstrated in the noise results that follow.

Similarly to the offset nozzle, Fig. 7.19 shows five different point sources positioned in the jet flow that will be used to evaluate the Ray-Tracing results for the jet-pylon configuration. Figure 7.20 show the results for the ΔSPL calculated in the far-field as a function of polar and azimuthal angles for each of the point sources presented in Fig. 7.19.

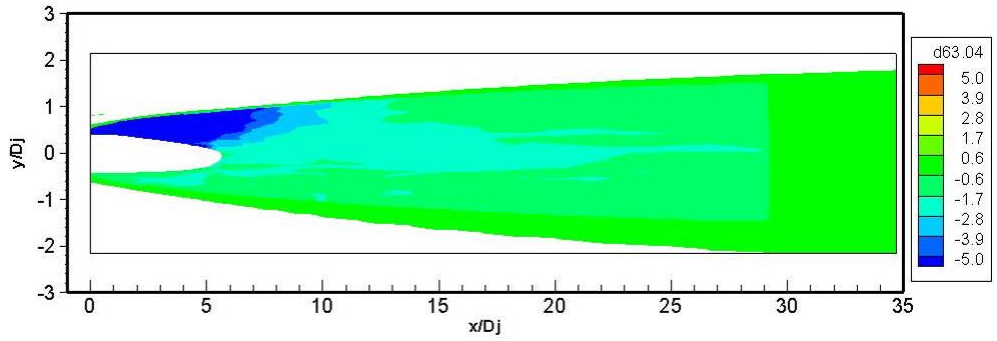

(a) Δ*SPL* (dB) calculated from the Ray-Tracing method for a probe at 63º.

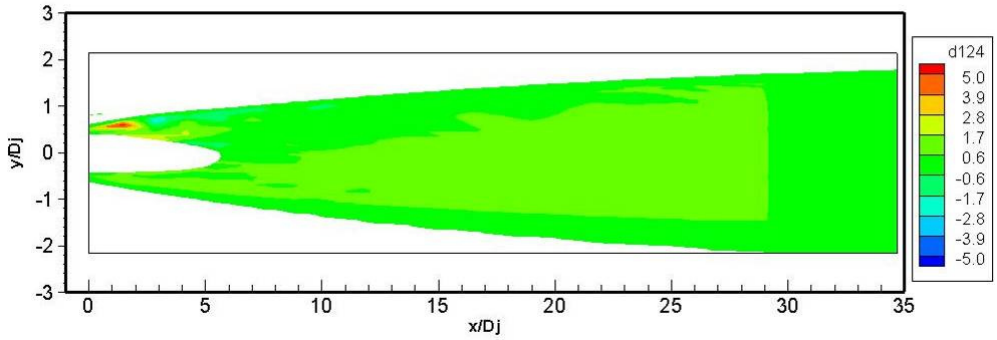

(b) Δ*SPL* (dB) calculated from the Ray-Tracing method for a probe at 124º.

Figure 7.18 – Contour plots of calculated ΔSPL for two different polar angles.

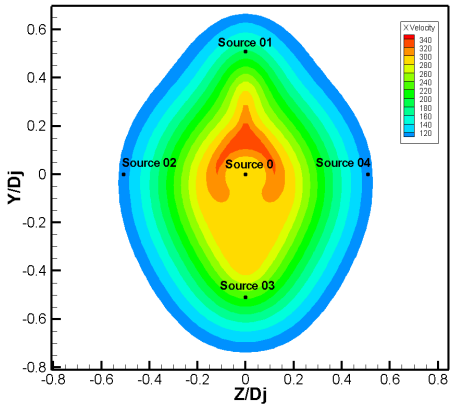

Figure 7.19 - Point sources positions on the jet flow field showing the contour plot of velocity at $x/D_j = 1.45$.

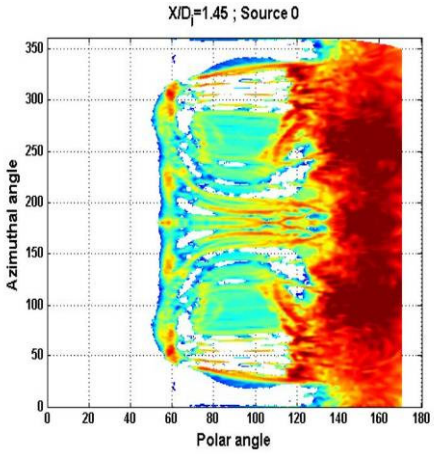

(a) Source 0.

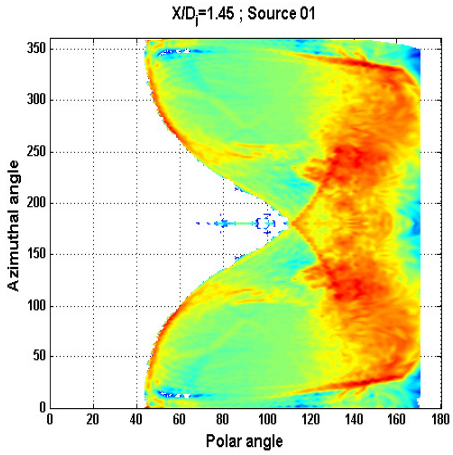

(b) Source 01.

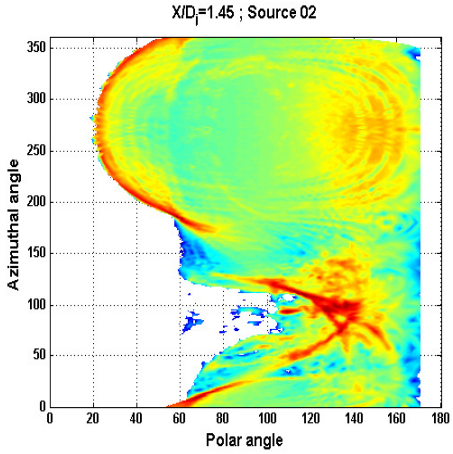

(c) Source 02.

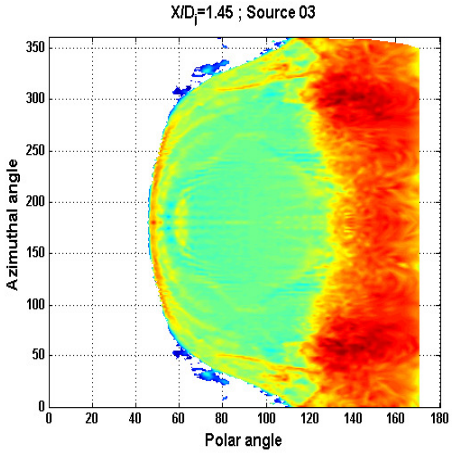

(d) Source 03.

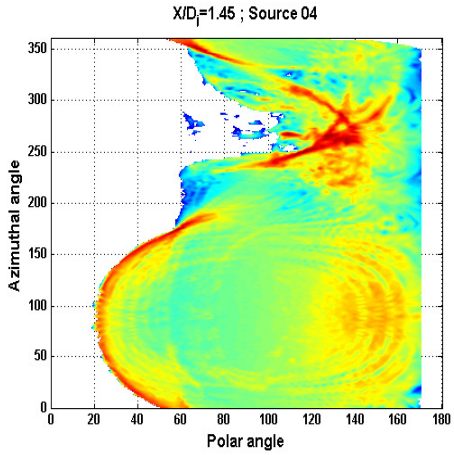

(e) Source 04.

Figure 7.20 - Ray-Tracing results in ΔSPL (dB) for different sources located on the jet-pylon configuration at x/D_j = 1.45.

The LRT noise predictions for the jet-pylon configuration, at different polar angles, are now presented. The results are shown for the sideline array, considering the angles definition described in Fig. 7.1. In the same way as described before, the predictions from the LRT method are presented in two different forms: "LRT – NoRefraction" and "LRT". Figure 21 presents the LRT noise predictions and the experimental data.

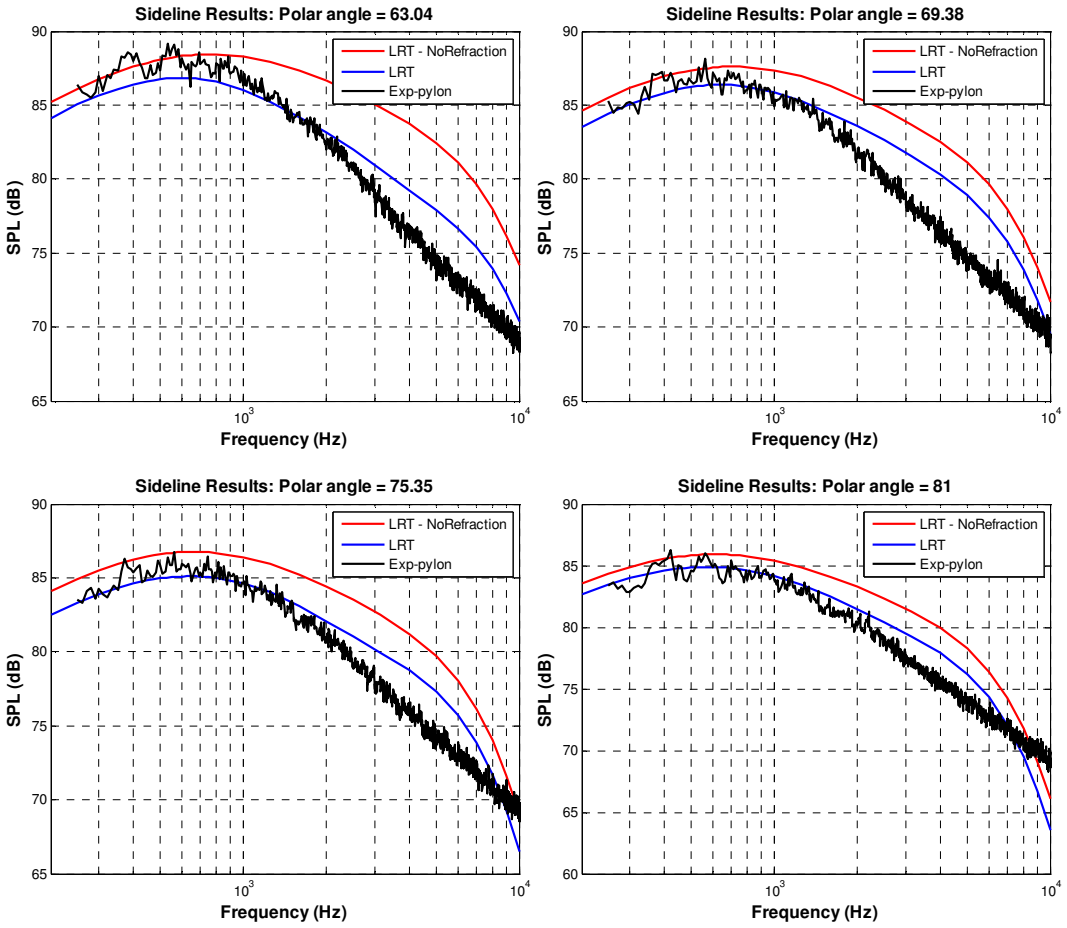

Figure 7.21 - (cont. over).

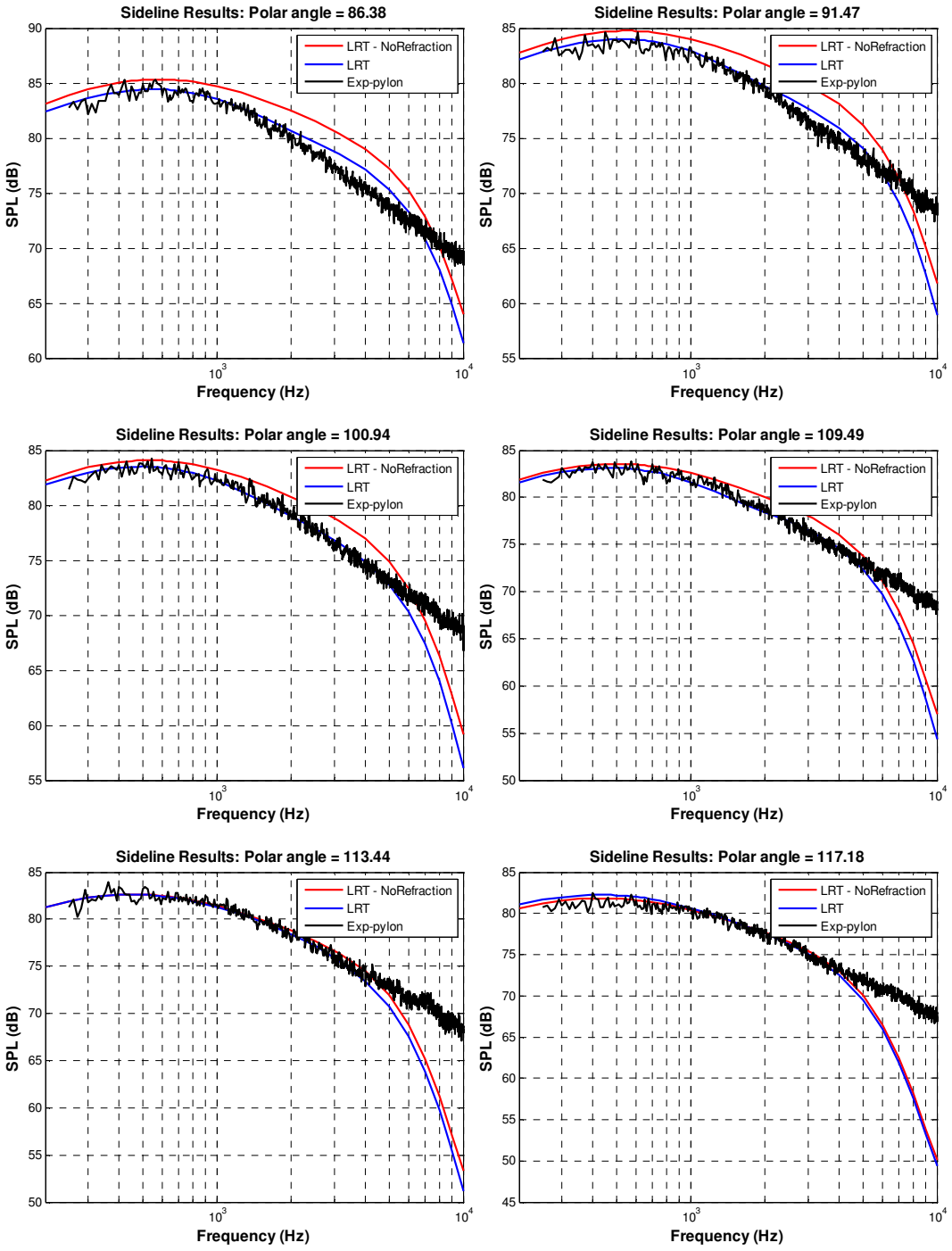

Figure 7.21 - (cont. over).

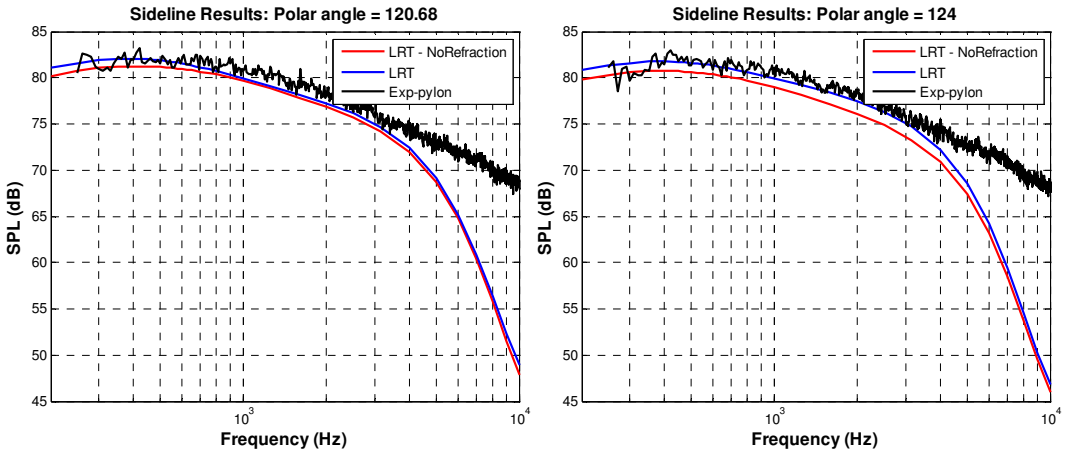

Figure 7.21 - LRT noise predictions for different polar angles with and without the refraction effects calculated by the Ray-Tracing for the jet-pylon configuration.

As can be seen from the above results, the LRT provide reasonable predictions for the noise generated by the complex asymmetric jet-pylon configuration. It is remarkable the effects of refraction on this problem, especially for the forward arc. Comparing the results of the typical LRT with the "LRT – NoRefraction" for polar angles 63º and 124º, it is possible to verify that the LRT method correctly took into account both the noise attenuation and the amplification regions when predicting the total noise on the far-field – see Fig. 7.18.

From Fig. 7.21 it is possible to verify a cut-off frequency in the noise predictions using the LRT method, which is around 5 kHz. This arises because, in this investigation, only the effects of the pylon on the mean flow field are considered. Therefore, this rapid drop off in the high frequency spectra was expected due to the reduced computational domain used for the LRT predictions. As the Ray-Tracing code developed in this thesis does not take into account the presence of solid surfaces on the computational domain, there was a need to reduce the size of it in order to exclude the pylon surface from the calculations, as depicted in Fig. 7.22. As a result, the sources that are located close to the nozzle, which contribute mostly to the high frequency noise, were not considered in the calculation. However, if the code is

improved, in a future work for instance, to include the missing part of the jet, it is quite clear that the predictions should be very reasonable for the whole spectra.

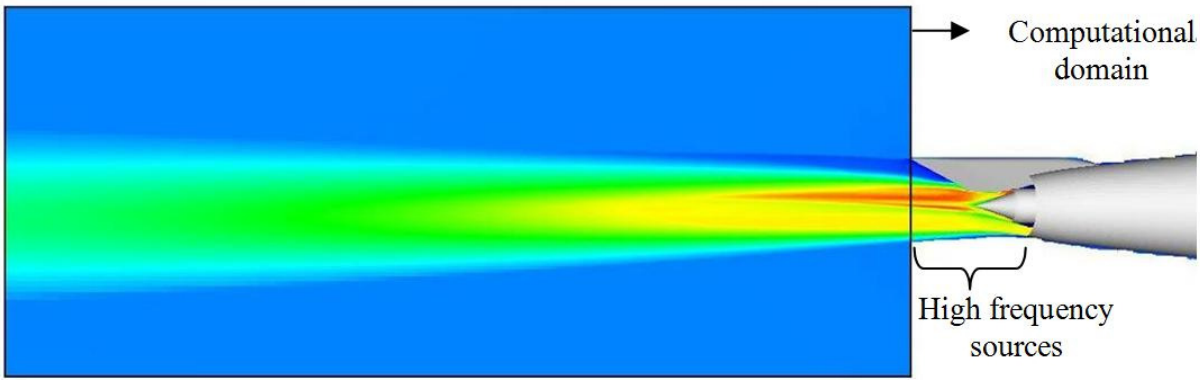

Figure 7.22 - Schematic of the computation domain used on the LRT method for the jet-pylon configuration.

7.3. Summary

A novel method for 3D jet noise predictions was developed in this thesis, which is named the LRT method. This method can be classified as a RANS-based method which is fast enough to be used inside an industrial context for design purposes.

After validating the LRT method for single and coaxial nozzles, it was applied for complex non-axisymmetric cases, where strong asymmetries in the flow and sound propagation exist. Experimental data from the SYMPHONY programme measured at QinetiQ was used to evaluate the LRT predictions.

Considering that in the two cases investigated in this chapter (offset nozzle and jet-pylon configuration) the jet operational conditions were extremely complicated, with high temperature ratio, very high speed and, with the presence of a flight stream, it is fair to consider that the predictions from the LRT method show the potential of the methodology for noise calculations. Moreover, it is reasonable to conclude that the basic theoretical model

developed and proposed in this thesis is valid and the model theory contains the essential physics of sound generation and propagation by a fully 3D turbulent shear flow.

Chapter 8: Conclusions

In this thesis the problem of aircraft noise and its impact on society and the aviation industry have been introduced. As a result, the importance of understanding jet noise, which is the main source of aero-engine noise at the take-off condition, and for developing novel low-noise configurations has been highlighted. The requirement of this research was to understand and predict the aeroacoustic noise generated from complex asymmetric jets operating at high-speed velocities. This requires an understanding not only of noise sources generated by the turbulent jet, but also the propagation of the sound waves through an inhomogeneous flow. To this end, it was necessary to develop a new jet noise prediction method that provides the ability of calculating the noise from complex three-dimensional flows taking into account source identification and sound-flow interaction. At the same time, an important premise of the method developed was that it needed to be fast enough to be useful as an engineering prediction tool for industrial application.

In Chapter 3 and Chapter 4, the description of the new jet noise prediction method satisfying the aforementioned requirements, called LRT, was presented. LRT is a relatively fast jet noise prediction method based on Lighthill's Acoustic Analogy and it uses a Reynolds-Average Navier Stokes (RANS) computational fluid dynamics (CFD) simulation as input information. The sound-flow interaction is computed by applying a well-known geometric acoustic concept, which solves the Ray-Tracing equations. The Ray-Tracing code was developed in an elegant form that provides the change in the sound pressure level in the far-field due to sound refraction so that, these results could be used by the LRT source model to correct the prediction for an observer positioned far from the source region. Although limited to high frequency, using the ray technique to account for refraction by the jet has proven to be a powerful tool, in that it can provide solutions for realistic complex jet flow profiles. As the

LRT method has been formulated as a general three-dimensional method it has no restrictions of applicability regarding the type of flow field or nozzle geometry for noise predictions. In addition, the LRT can also be used to evaluate engine installation effects, such as jet-pylon interaction, which is another important and potential area for reducing aircraft noise. The LRT executable code is written in FORTRAN 90 and the pre- and post-processing tools are written in MATLAB.

In order to validate the new computational aeroacoustics method, Chapter 5 and Chapter 6 presented the results obtained from noise investigations for single and dual-stream jet flows. A large number of nozzles and jet operation conditions were simulated. The LRT predictions for the far-field noise show considerably good agreement with experimental data, which gave confidence in the new method. Apart from validating the LRT, Chapter 5 results show that the LRT method is able to produce better noise predictions than the well-known MGBK method developed by NASA, especially for shallow observer angles. This implies that the LRT provides a better simulation of sound directivity, for the angles outside the zone of silence, as it has the capability of accounting for the refraction effects generated by the sound-flow interaction. These results can be used to elucidate and help understanding the importance of the zone of silence for jet noise, especially when aircraft certification is regarded.

Chapter 7 presented the results of the ultimate test for the LRT method in which asymmetric flows were investigated. Predictions for an offset nozzle and for a jet-pylon interaction problem were conducted. First, numerical results from the LRT showed the major influence of refraction effects when predicting the noise in the far-field for complex jet flows, such as the one from an offset nozzle. Important verifications were achieved regarding flow field, turbulence generated noise and sound refractions. Comparisons between a coaxial axisymmetric nozzle with the offset nozzle and the jet-pylon interaction problem were shown

and the results were discussed. Considering that in the two asymmetric cases investigated (offset nozzle and jet-pylon configuration) the jet operational conditions were extremely complicated, with high temperature ratio, very high speed and, with the presence of a flight stream, it is fair to say that the predictions from the LRT method show the potential of the methodology for noise calculations of complex jet flows.

It is reasonable to conclude that the basic theoretical model developed and proposed in this thesis is valid and the model theory contains the essential physics of sound generation and propagation by a fully 3D turbulent shear flow. Moreover, the LRT method can be applied as an engineering tool for jet noise predictions inside an industrial development cycle.

Finally, as with most numerical methods, the LRT has some intrinsic limitations due to physical assumptions and mathematical strategies used in the method development, which can be listed as:

- The LRT predictions are only reliable for the angles outside the zone of silence of the jet. This is due to the geometrical acoustics method used in the LRT to model the sound refraction. In turn, the method predicts well the jet critical angle and also the shape of the zone of silence.
- Although the LRT method calculates the thermal effects on the sound propagation, which are present in heated jet cases, the method only models quadrupole sources, generated by the turbulent velocity. Dipole sources that are present in heated cases are not modelled in the LRT method at present.
- When new nozzle designs are envisaged, there is a need to calibrate the turbulent coefficients of the model with baseline experimental data. However, the LRT method has been calibrated using a large experimental data set for single stream jets, which generated a first model to determine these coefficients based on the jet operation

conditions. This is reasonable enough for applying the LRT method for qualitative investigations for any type of nozzles configurations.

8.1 Current and future investigations using the LRT method

At the Rolls-Royce UTC group, located at the ISVR, the LRT method is currently been applied for jet noise predictions inside the SYMPHONY programme. Additionally, new research projects are already planned which will further development the LRT approach for investigating the cone of silence. At Cambridge University (also in the UK), there is a group looking at the dipole source contributions and how to include them in the model.

8.2 Suggestions for future work

The improvement of computer resources in the last decade has been tremendous and there is no doubt that the computational aeroacoustics will also be greatly benefited from it. It is becoming more common to find direct noise computations, such as LES and DNS, of various engineering problems nowadays. However, when it comes to aeronautical applications where high Reynolds and Mach numbers are involved, like the jet noise problem, it is still prohibitively costly in an industrial design context. Therefore, there is still room for RANS-based noise predictions methods. In this context, there are many possibilities for future work regarding the improvement of the LRT method for jet noise predictions. Some recommended actions are listed below:

1 - Extension of the Ray-Tracing theory used in the LRT method by taking into account the possibility of complex ray contributions. This can be done by applying the complex ray theory where the complete solution of the eikonel equation (complex and real part) is considered. The theory of complex rays is useful for investigating propagation of acoustic

waves, particularly those originated from the downstream low frequency sources, into the zone of silence of the jet.

2 - Extension of the Ray Tracing theory used on the LRT method to calculate reflection and diffraction of the sound. These are necessary when one or more solid surfaces are required to be taken as part of the computational domain of the problem under investigation.

3 - Develop a noise model for dipole sources that arise as a result of density variations in the flow field. This will be useful to improve the noise predictions especially for low Mach number and high temperature jets.

4 - Further investigation of the turbulence calibration coefficients involved in the current model to better understand their variation with the mean flow properties of the jet, such as thrust, maximum jet velocity, and kinetic turbulent energy.

5 - Using the LRT method for more asymmetric jet cases, such as chevron nozzles, beveled nozzles and for problems involving interaction of jet noise with an external body, i.e. jet-pylon, jet-wing, jet-flap, etc.

6 - Utilization of the LRT method in an automatic nozzle design optimisation software to further reduce the far-field noise by varying the nozzle design, with least thrust loss.

Appendix A – Numerical Procedures

This appendix describes the use of Computational Fluid Dynamics (CFD) as a numerical tool to calculate the mean properties of a jet flow by using a Reynolds Average Navier-Stokes (RANS) methodology. The mean flow and turbulence quantities are used as input information for the LRT method presented in Chapter 3 (Propagation Model) and Chapter 4 (Source Model).

In order to achieve good noise predictions with any RANS-based acoustic model, such as the LRT method, it is first necessary to have an accurate aerodynamic calculation of the flow. Therefore, this appendix aims to provide detailed information about the CFD procedures used throughout this thesis, such as turbulence model, computational domain, meshes, boundary conditions and relevant numerical parameters. The CFD results for each case analysed in this thesis have already been presented in each specific chapter.

A1. Single Stream Jets

Chapter 5 presented the validation of the LRT method for single stream jets for different flow operation conditions. These single jet investigation studies were part of the SYMPHONY project. Additional data regarding aerodynamic results will be presented and discussed in the next subsections together with numerical descriptions of the simulations conducted.

A1.1 Numerical details

The computational domain used in the RANS simulations for the single stream jets is presented in Fig. A.1. The size of the domain in the x and y directions were selected after initial tests in order to evaluate the influence of the downstream and transverse lengths in the flow-field when numerical boundaries are applied. The values showed below were used for

both static and flight ambient conditions as described in Chapter 5. Figure A.1 also shows the boundary conditions imposed for the CFD calculations and Table (A1) describes which method was used for modelling each of them. For more information of the flow properties refer to Table (5.2) in Chapter 5.

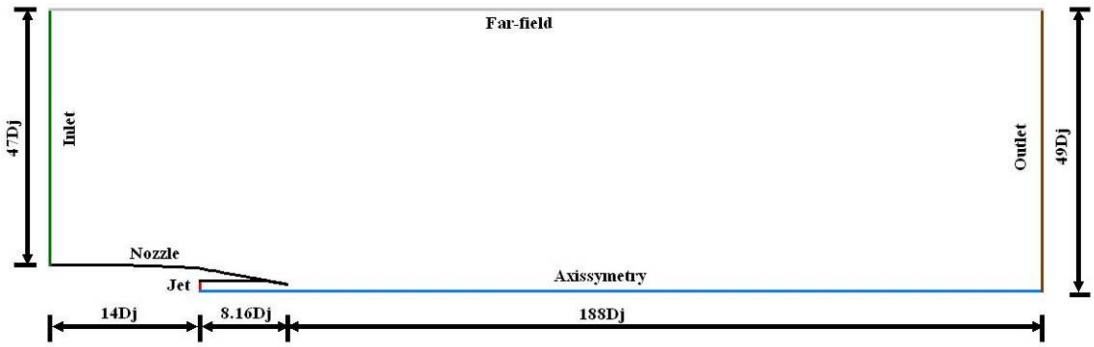

Figure A. 1 - Boundary

Figure A.1 – Boundary conditions for the single jets.

Table A1 - Boundary conditions from the single stream jet simulations.

Boundary Condition	Model - Fluent	Input information
Inlet	Pressure inlet	Pressure and temperature
Far-field	Pressure-far-field	Pressure and temperature
Outlet	Pressure outlet	Pressure and temperature
Axisymmetry	Axis	N/A
Jet	Pressure Inlet	Total Pressure and temperature
Nozzle	Wall	No slip/No motion

The commercial code FLUENT®, version 6.3.26 was used in all the simulations for the single stream jets. The steady-state coupled solver (density-based) in its 2D axisymmetric frame was employed. The governing equations were solved with a second order accuracy. The Standard k-ε model was used for modelling the turbulence. The final converged solution was obtained after approximately 6000 iterations. More detailed technical information regarding the numerical parameters used in the CFD code can be obtained in the FLUENT® documentation [136].

A1.2 Mesh Refinement

Figure A.2 depicts the grid used for the CFD simulations. It is a non-uniform structured Cartesian mesh with approximately 80,000 elements. Stretching factors are used in order to cluster a large number of closely spaced grid points in the shear layer region of the flow, where large gradients in the flow-field exist, extending its refinement at least until the end of the jet's potential core. Figure A.3 shows the mesh refinement near the nozzle and in the shear layer region.

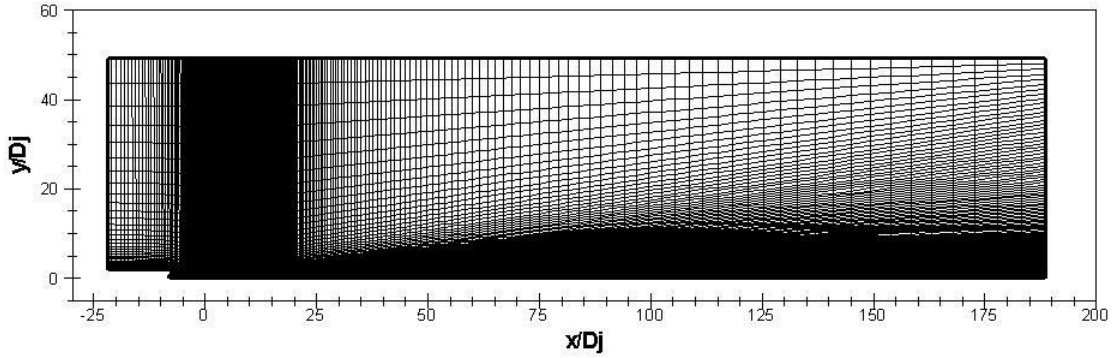

Figure A.2 – Mesh refinement over the whole domain – 80.000 quadrilateral cells.

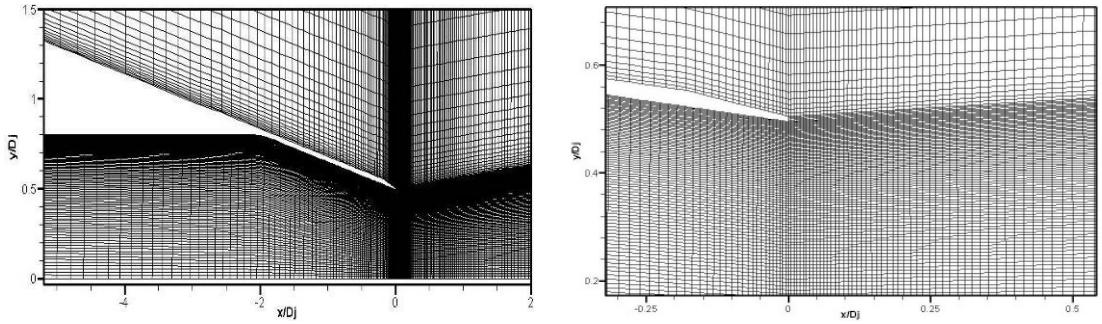

(a) Mesh refinement close to the nozzle. (b) Mesh refinement on the shear layer.

Figure A.3 – Zoom close to the nozzle exhaust to illustrate the mesh quality.

A2. Coaxial Jets

In Chapter 6, the LRT method was applied for predicting the noise from coaxial jets. Two kinds of nozzles were investigated: coplanar and short-cowl nozzles. For the coplanar

nozzles, three different area ratios and a large range of jet operation conditions were studied. The main numerical parameters used for these CFD simulations are presented below.

A2.1 Numerical details

The RANS simulations for the coplanar coaxial jets were conducted applying the CFD++ software developed by Metacomp Technologies, Version 8.1.1. This commercial software, which is a second-order accuracy code, provides the ability to handle multi-block meshes with various types of inter-block connectivity. It also uses implicit boundary condition treatments. CFD++ uses upwind formulations, including realizable Riemann solvers and it also solves the mass, momentum and energy equations in a coupled mode.

A non-linear k−ε closure turbulence model, named k−ε cubic model, which is available in the CFD++ was applied in this investigation. The cubic model accounts for Reynolds stress anisotropy and streamline curvature, including swirl effects. The formulation to obtain the Reynolds-stress tensor is defined via a tensorial expansion, cubic in the mean strain and vorticity tensors. The stresses are related to the mean strain and vorticity using the quadratic model of Shih [137] with the cubic extension proposed by Lien and Leschziner [138]. More details about the model are given in the work of Goldberg *et al*. [123].

Figure A.4 presents the boundary conditions imposed for the CFD calculations for the coplanar nozzles while Table (A2) describes which method was used for modelling each of them, where P is pressure and T is temperature. More technical details about the boundary conditions models used in this investigation can be found in the CFD++ User Manual [139]. The flow properties that are needed as input for the boundary conditions were already presented in Table (5.2) in Chapter 6.

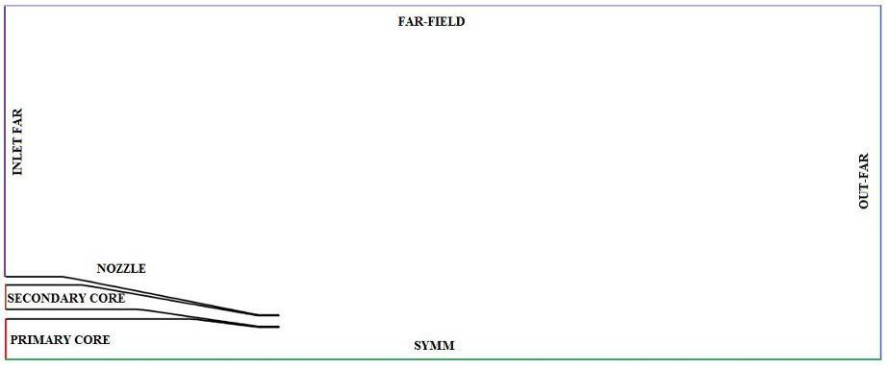

Figure A.4 – Boundary conditions imposed for the coplanar coaxial jets.

Table A2 - Boundary conditions for the coaxial stream jet simulations.

Boundary Condition	**Model – CFD++**	**Input information**
Inlet Far Far-Field Out-Far	Pres. Temp. inflow/outflow using inside velocity	P and T
Symm	Symmetry	N/A
Primary Core	Reservoir Ptot Ttot	Total P and Total T
Secondary Core	Reservoir Ptot Ttot	Total P and Total T
Nozzle	Adiabatic viscous wall function	N/A

A2.2 Mesh refinement

Figure A.5 depicts the grid used for the CFD simulations for the coplanar coaxial nozzles. It is a non-uniform structure Cartesian mesh with approximately 120000 elements. Similar to the single stream jet mesh, stretching factors are used in order to cluster a large number of closely spaced grid points in the shear layer region of the flow. Figure A.6 shows the mesh refinement near the nozzle. The number of necessary interations for achieving the converged solution is dependant on the nozzle area ratio and the jet operation condition.

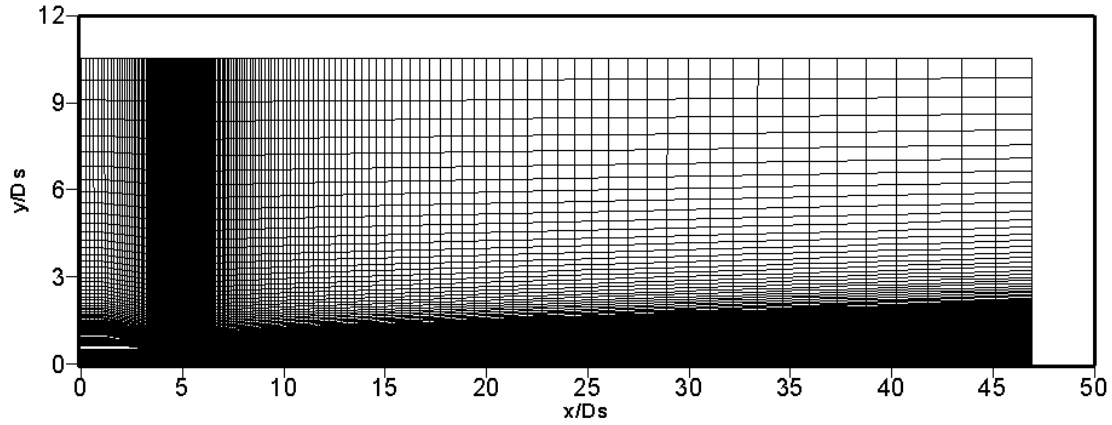

Figure A.5 – Computational domain for the coplanar coaxial axisymmetric nozzle.

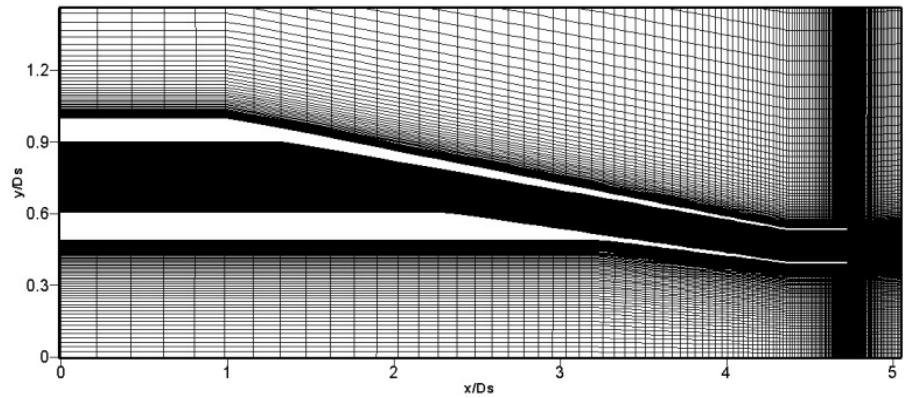

Figure A.6 – Mesh refinement close to the coplanar coaxial axisymmetric nozzle.

A2.3 Short-cowl nozzle

In addition to the coplanar coaxial nozzles, Chapter 6 also shows the application of the LRT method for a short-cowl nozzle. For this specific case, all the data used for noise predictions were generated within the SYMPHONY project. The following subsections will present detailed information regarding the computational procedures used for simulating the flow-field for this commonly used nozzle.

A.2.3.1 Numerical Details

Inside the SYMPHONY project all the CFD simulations were conducted using FLUENT®, Version 6.3.26. The steady-state coupled solver (density-based) in its 3D frame

was employed. The governing equations were solved with a second order accuracy and the Standard k-ε model was used for modelling the turbulence.

For the short-cowl coaxial nozzle, offset nozzle and jet-pylon configuration the same CFD methodology was applied. This means that, apart from the CFD code and its numerical parameters, the same computational domain and types of boundary conditions were used for all three cases. The boundary conditions imposed in the CFD calculations for the SYMPHONY simulations are shown in Fig. A.7 while Table (A3) describes which method was used for modelling each of them. For more information of the flow properties refer to the specific section of the geometry on this thesis.

Specifically, for the short-cowl coaxial nozzle the final RANS converged solution was obtained after approximately 7000 interactions. The next subsection presents the mesh used in the calculations.

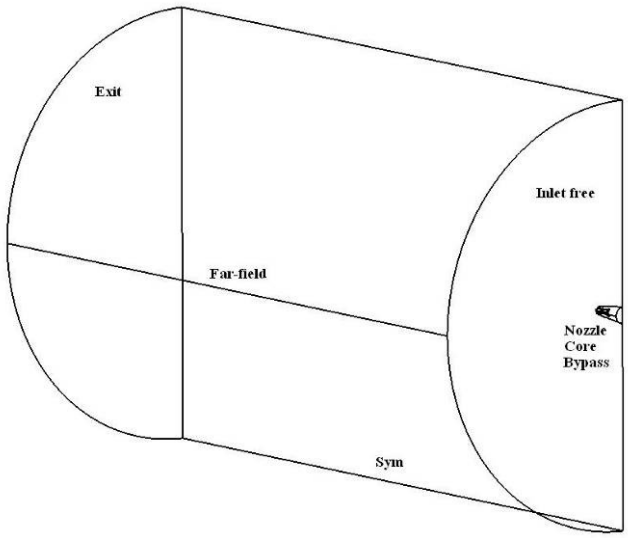

Figure A.7 – Boundary conditions used for the SYMPHONY geometries simulations.

Table A3. Boundary conditions for the SYMPHONY geometries simulations.

Boundary Condition	Model - Fluent	Input information
Inlet free	Pressure inlet	Pressure and temperature
Far-field	Pressure-far-field	Pressure and temperature
Exit	Pressure outlet	Pressure and temperature
Sym	Axis	N/A
Core	Pressure Inlet	Total Pressure and temperature
Bypass	Pressure Inlet	Total Pressure and temperature
Nozzle	Wall	No slip/No motion

A2.3.2 Mesh refinement

A 3D view of the computational mesh used for the short-cowl nozzle is depicted in Fig. A.8. It is a non-uniform structure grid with approximately 8.4×10^6 elements, formed predominantly by hexahedrons. Figure A.9 shows the cross-section of the computational domain and the mesh refinement close to the nozzle is show in Fig. A.10.

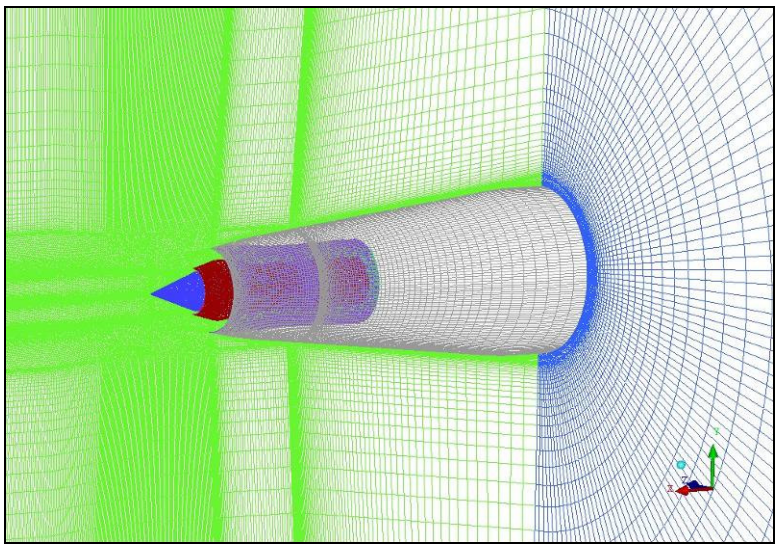

Figure A.8 – 3D view of the grid used for the short-cowl axisymmetric nozzle simulations – Total of 8.4×10^6 elements.

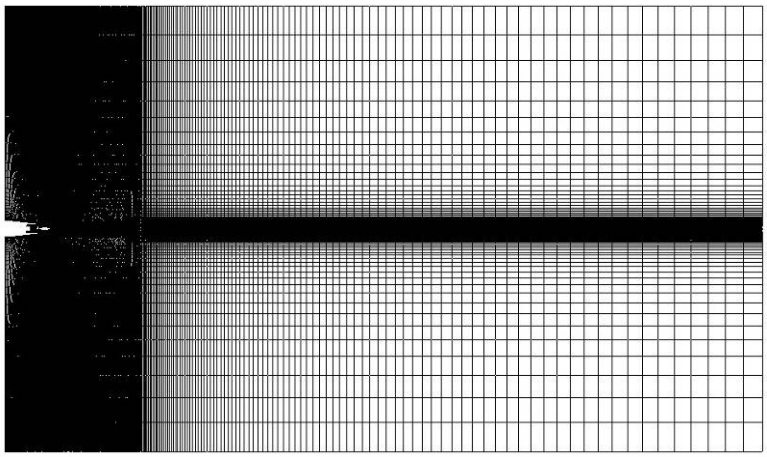

Figure A.9 – Cross-section of the computational domain in the 3D mesh for the short-cowl axisymmetric nozzle.

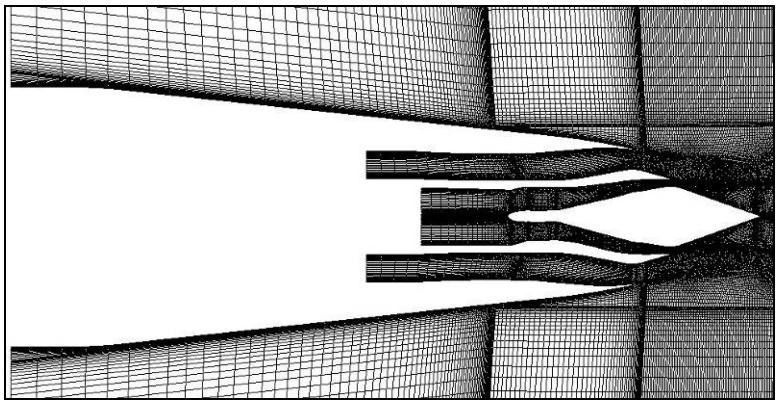

Figure A.10 – Mesh refinement close to the short-cowl axisymmetric nozzle.

A3. Asymmetric Jets – Complex flow

Chapter 7 presented the application of the LRT method to predicting the noise from a complex asymmetric offset nozzle and the effects of the pylon interaction with the jet. Similar to the short-cowl coaxial nozzle, Fluent was used in these flow-field calculations applying the same numerical parameters (equations and turbulence model), models of boundary conditions and computation domain. As the geometries are different for each case, the subsections that follow will present the mesh information as well as numerical details for both cases separately.

A3.1 Offset nozzle

A3.1.1 Numerical details and mesh refinement

A 3D view of the computational mesh used for the offset nozzle is depicted in Fig. A.11. It is a non-uniform structure grid with approximately 8.7×10^6 elements, formed predominantly by hexahedrons. Figure A.12 shows the cross-section of the computational domain and the mesh refinement close to the nozzle is show in Fig. A.13.

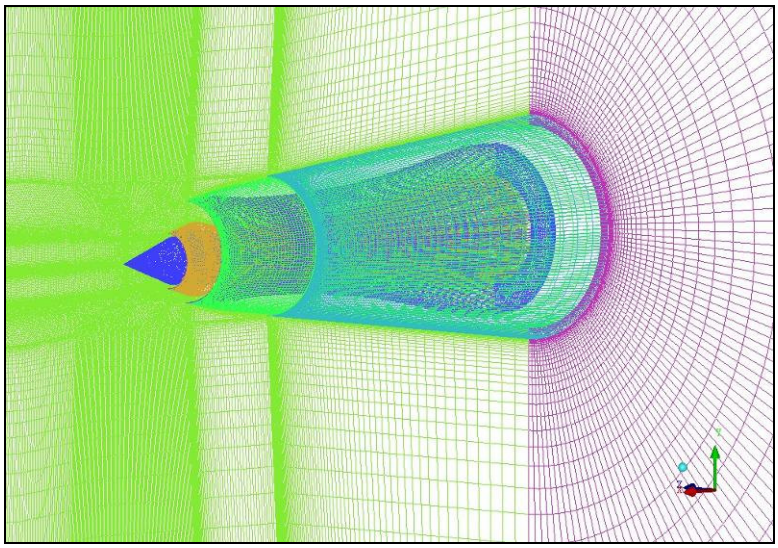

Figure A.11 – 3D view of the grid used for the offset nozzle simulations – Total of 8.7×10^6 elements.

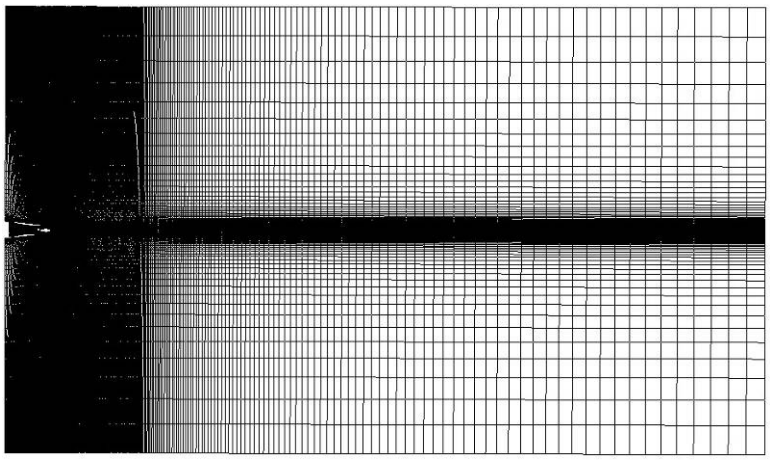

Figure A.12 – Cross-section of the computational domain in the 3D mesh for the offset nozzle.

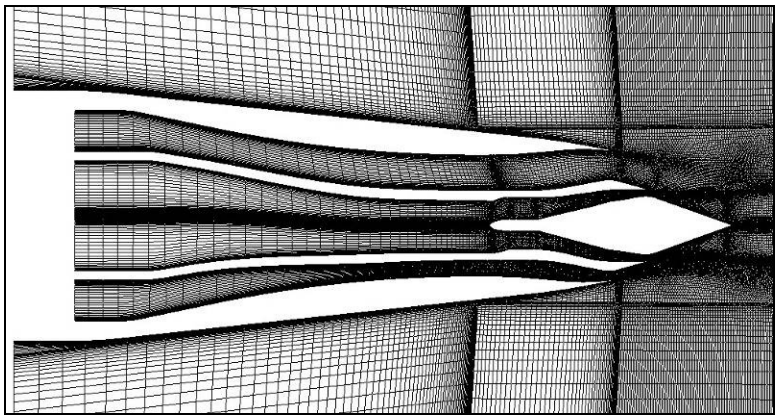

Figure A.13 – Mesh refinement close to the offset nozzle.

A3.2 Jet-pylon configuration

A3.2.1 Numerical details and mesh refinement

A 3D view of the computational mesh used for the jet-pylon configuration is depicted in Fig. A.14. It is a non-uniform structure grid with approximately 8.2×10^6 elements, formed predominantly by hexahedrons. Figure A.15 shows the cross-section of the computational domain and the mesh refinement close to the nozzle is show in Fig. A.16.

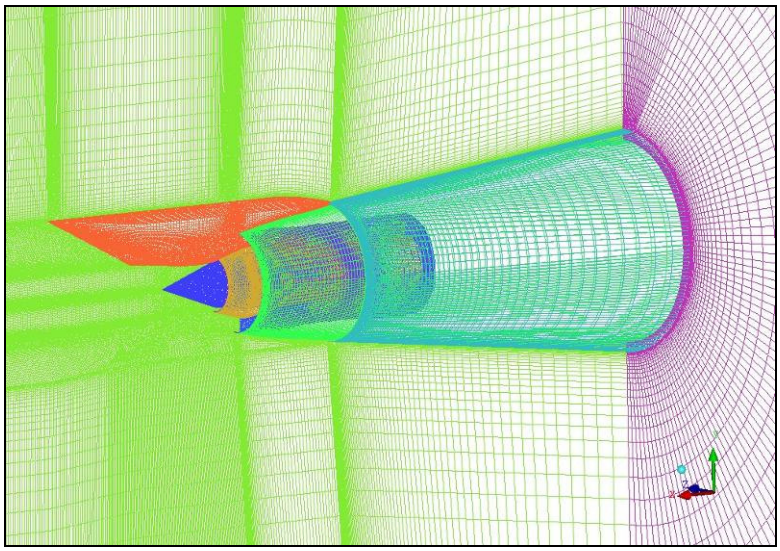

Figure A.14 – 3D view of the grid used for the jet-pylon simulations – Total of 8.2×10^6 elements.

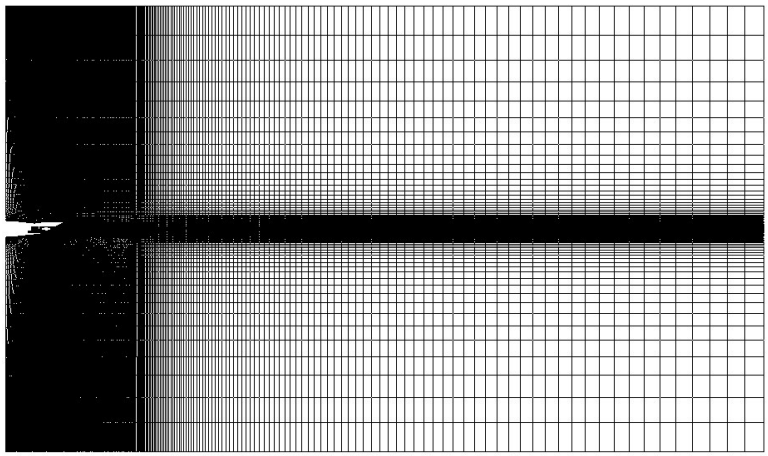

Figure A.15 – Cross-section of the computational domain in the 3D mesh for the jet-pylon configuration.

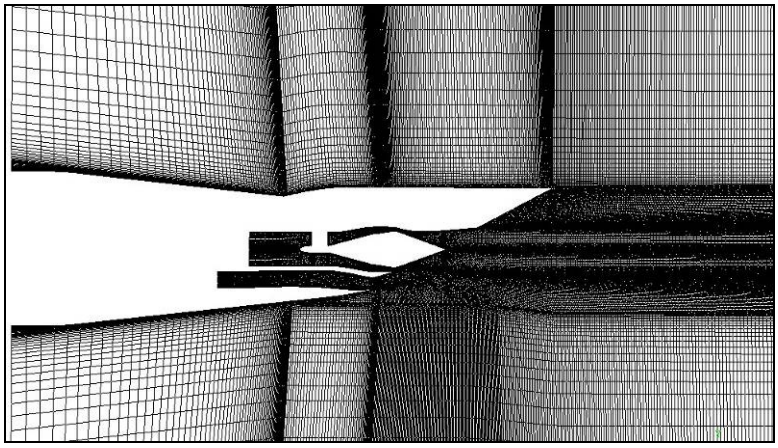

Figure A.16 – Mesh refinement close to the jet-pylon surfaces.

Appendix B – Coplanar Coaxial Geometries

The objective of this section is to present in more detail the nozzle geometries for the coaxial stream jet investigation presented in Chapter 6 of this thesis. The sketches of the individual nozzles are shown from Fig. B1 to Fig. B4 below. All the dimensions are given in millimetres.

These nozzles were used in a series of jet noise measurements made in 1989 and 1993 on coplanar nozzles in the NTF at QinetiQ. The United Kingdom Department of Industry under the Civil Aircraft Research and Development (CARAD) programme funded the work.

Figure B1 depicts the 33 mm nozzle used as the primary stream in configuration builds of area ratio 2 and area ratio 4.

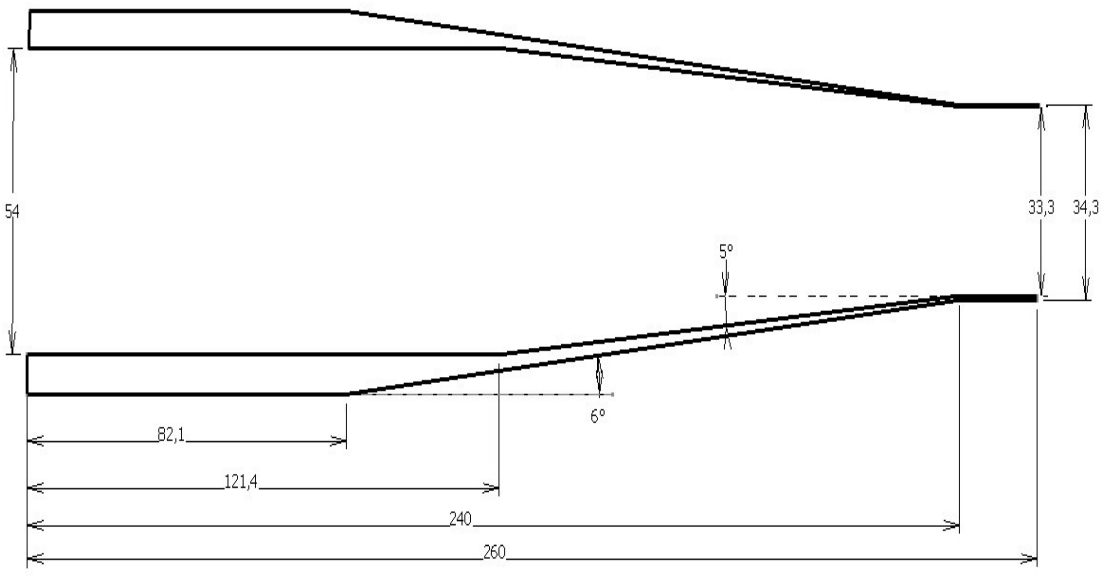

Figure B.1 - Sketch of the 33 mm nozzle used on the coaxial study.

Figure B2 shows the 43 mm nozzle used as the primary stream in configuration build of area ratio 0.87. Figure B3 presents the 58 mm nozzle used as the secondary stream in configurations build of area ratio 0.87 and area ratio 2.

Figure B4 depicts the 75 mm nozzle used as the primary stream in configuration build of area ratio 4.

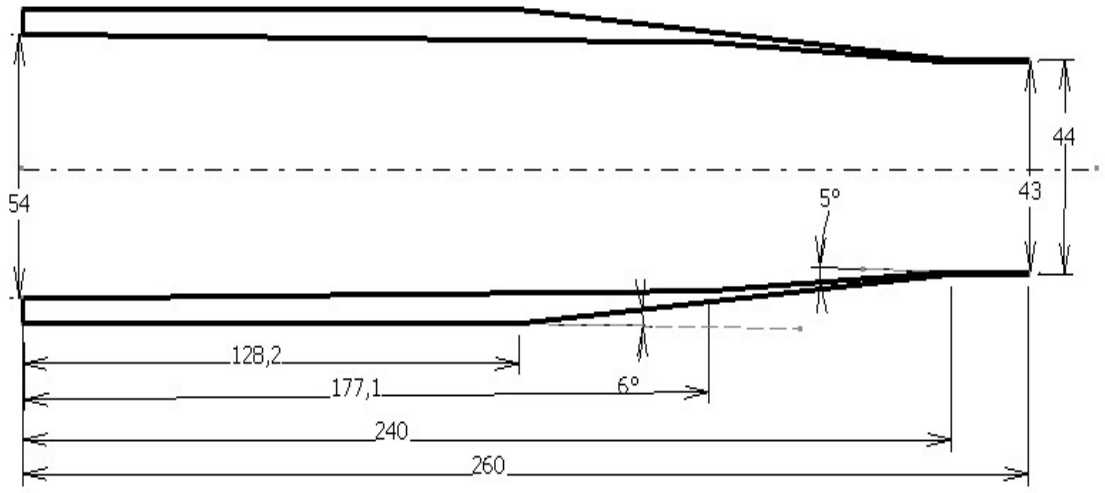

Figure B.2 - Sketch of the 43 mm nozzle used on the coaxial study.

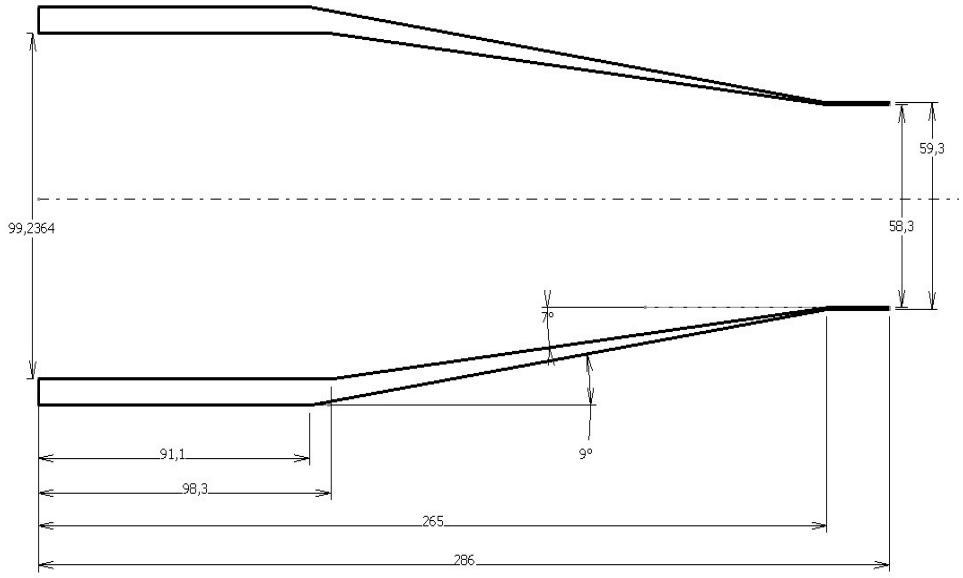

Figure B.3 - Sketch of the 58 mm nozzle used on the coaxial study.

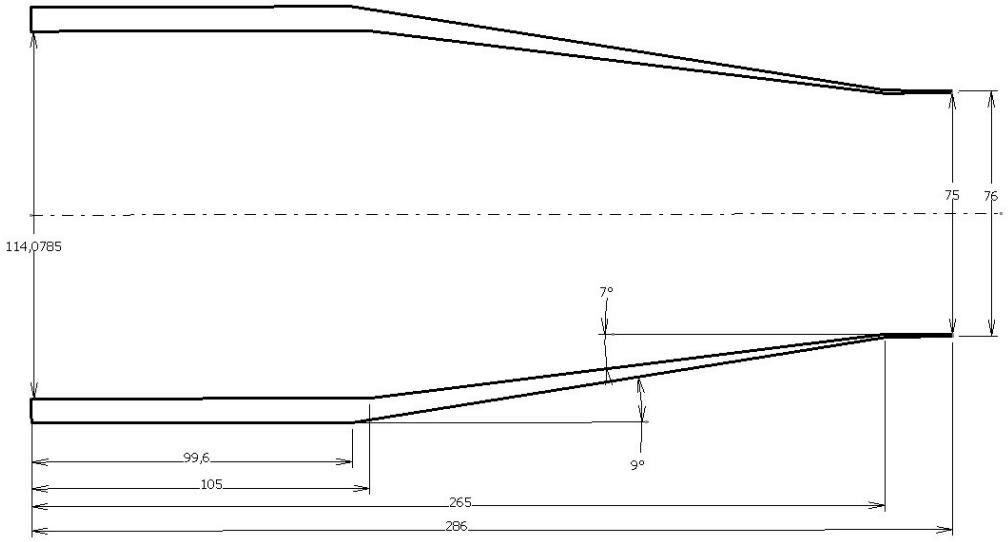

Figure B.4 - Sketch of the 75 mm nozzle used on the coaxial study.

References

[1] Lee, J. J., Lukachko, S. P., Waitz, I, A. and Schafer, A., "Historical and Future Trends in Aircraft Performance, Cost and Emissions", *Annual Review of Energy Environment*, vol. 26, pp. 167-200, 2001.

[2] Boeing Current Market Outlook 2010-2029, available in Boeing website in http://www.boeing.com/commercial/cmo/Boeing_Current_Market_Outlook_2010_to_2009.pdf, accessed on 05/01/2011.

[3] Smith, M., *Aircraft Noise*, Cambridge aerospace series, 3, Cambridge University Press, Cambridge, New York, 1989.

[4] International Civil Aviation Organization (ICAO): *International Standards and recommended practices. Environmental protection. Annex 16 to the convention on international civil aviation*, vol. I, 2nd edition, International Civil Aviation Organization, 1988.

[5] Federal Aviation Administration (FAA): from 1969 onwards, *Federal Aviation Regulations (FAR), Part 36. Noise Standards: Aircraft Type and Airworthiness Certification*, U.S. Department of Transportation (DOT), Washington D.C.

[6] Brentner, K. S., "Aerodynamic Impact on Noise and Emissions", Session IV in "Potential Impacts of Advanced Aerodynamic Technology on Air Transportation System Productivity", *NASA Technical Memorandum 109154*, edited by Bushnell, D. M., September, 1994.

[7] Bjorn, V.S.; Albery, C.B.; Shilling, R.; McKinley, R.L., "U.S. Navy Flight Deck Hearing Protection Use Trends: Survey Results", in New Directions for Improving Audio Effectiveness (pp. 1-1 – 1-20), Meeting Proceedings RTO-MP-HFM-123, Paper 1. Neuilly-sur-Seine, France: RTO, 2005.

[8] Lilley, G. M., "On the noise from jets", *AGARD CP-131*, 1974.

[9] List, E. J., "Turbulent Jets and Plumes", *Annual Review of Fluid Mechanics*, vol. 14, pp. 198-212, 1982.

[10] Goldstein, M. E., "Aeroacoustics", McGraw-Hill Inc., US, 1976.
[11] Van Dyke, M, "An Album of Fluid Motion", The Parabolic Press, Stanford, CA, 1982.

[12] Morley, A. W. “Estimation of aeroplane noise level: some empirical laws with an account of the present experiments on which they are based”, *Aircraft Engineering and Aerospace Technology,* vol. 11 (123), pp.187-189, 1939.

[13] Lighthill, M.J. “On Sound Generated Aerodynamically. I - General Theory”. *Proceedings of the Royal Society of London, Series A, Mathematical and Physical Sciences*, vol. 211, n. 1107, pp. 564-587. Mar. 1952.

[14] Lassiter, L. W. & Hubbard, H. H., “Experimental studies of noise from subsonic jets in still air”, NACA TN-2757, 1952.

[15] Lighthill, M.J. “On Sound Generated Aerodynamically. II - Turbulence as a Source of Sound”. *Proceedings of the Royal Society of London, Series A, Mathematical and Physical Sciences*, vol. 222, n. 1148, pp. 1-32, Feb. 1954.

[16] Lassiter, L. W. & Hubbard, H. H., “The near noise field of static jets and some model studies of devices for noise reduction”, *NACA Report 1261*, 1956.

[17] Bodony, D. J. and Lele, S. K., “On using large-eddy simulation for the prediction of noise from cold and heated turbulent jets”, *Physics and Fluids*, vol. 17, 085103, 2005.

[18] Lilley, G.M., Morris, P.J., and Tester, B.J., “On the Theory of Jet Noise and its Application”, AIAA paper No. 73-987, October 1973.

[19] Goldstein, M. E., “A generalized acoustic analogy”, *Journal of Fluid Mechanics*, vol. 488, pp. 315-333, 2003.

[20] Davies, P. O. A. L., Fisher, M. J. and Barratt, M. J., “The characteristics of the turbulence in the mixing region of a round jet”, *Journal of Fluid Mechanics*, vol. 15, pp. 337-367, 1963.

[21] Bradshaw, P., Ferriss, D. H. and Johnson, R. F., “Turbulence in the noise producing region of a circular jet”, *Journal of Fluid Mechanics*, vol. 19, pp. 591-624, 1964.

[22] Tanna, H. K., “An experimental study of jet noise part I: turbulent mixing noise”, *Journal of Sound and Vibration*, vol. 50, pp. 405-428, 1977.

[23] Tanna, H. K., "An experimental study of jet noise part II: shock associated noise", *Journal of Sound and Vibration*, vol. 50, pp. 429-444, 1977.

[24] Viswanathan, K., "Aeroacoustics of hot jets", *Journal of Fluid Mechanics*, vol. 516, pp. 39-82, 2004.

[25] Hubbard, H. H., "Aeroacoustics of Flight Vehicles: Theory and Practice, Volume 1: Noise Sources", NASA Reference Publication 1258, Vol. 1, *WRDC Technical Report 90-3052*, 1991.

[26] Uzun, A., Lyrintzis, A. S. and Blaisdell, G. A., "Coupling of integral acoustics methods with LES for jet noise prediction", *International Journal of Aeroacoustics*, vol. 3(4), pp. 297-346, 2005.

[27] Hünecke, K., "Jet Engines: Fundamentals of Theory, Design and Operation", Airlife Publishing, 2010.

[28] Ko, N. W. M., and Kwan, A. S. H., "The initial region of subsonic coaxial jets", *Journal of Fluid Mechanics*, vol. 73, no. 2, pp. 305-332, 1976.

[29] Fisher, M. J., Preston, G. A., and Bryce, W. D., "A Modelling of the Noise from Simple Coaxial Jets, Part I: With Unheated Primary Flow", *Journal of Sound and Vibration*, vol. 29, no. 3, pp. 385-403, 1998.

[30] Almeida, O. "Aeroacoustics of Dual-Stream Jets with Application of Turbofan Engines",348f., Thesis of Doctor of Science, Aeronautics Institute of Technology, Sao Jose dos Campos, 2009.

[31] Callender, B., Gutmark, R., and Martens, S., "A Far-Field Investigation into Chevron Nozzle Mechanisms and Trends," 41st AIAA Aerospace Sciences Meeting and Exhibit, AIAA Paper 2003-1058, 2003.

[32] Callender, B., Gutmark, R., and Martens, S., "A Near-Field Investigation into Chevron Nozzle Mechanisms", 41st AIAA Aerospace Sciences Meeting and Exhibit, AIAA Paper 2003-3210, 2003.

[33] Callender, B., Gutmark, R., and Martens, S., "A PIV Flow Field Investigation of Chevron Nozzle Mechanisms", 42nd AIAA Aerospace Sciences Meeting and Exhibit, AIAA Paper 2004-191, 2004.

[34] Bridges, J. and Brown, C. A., "Parametric Testing of Chevrons on Single-flow Hot Jets", 10th AIAA/CEAS Aeroacoustics Conference, AIAA Paper 2004-2824, 2004.

[35] Koch, L. D., Bridges, J., and Khavaran, A., "Mean Flow and Noise Prediction for a Separate Flow Jet with Chevron Mixers", 42nd AIAA Aerospace Sciences Meeting and Exhibit, AIAA Paper 2004-189, 2004.

[36] Papamoschou, D., "Directional Suppression of Noise from a High-Speed Jet," *AIAA Journal*, Vol. 39, No.3, 2001, pp. 380-387.

[37] Papamoschou, D. and Debiasi, M., "Conceptual Development of Quiet Turbofan Engines for Supersonic Aircraft," *AIAA Journal of Propulsion and Power*, Vol. 39, No.3, 2001, pp. 380-387.

[38] Papamoschou, D., "New Method for Jet Noise Suppression in Turbofan Engines," *AIAA Journal*, Vol. 42, No.11, 2004, pp. 2245-2253.

[39] Papamoschou, D., "Fan Flow Deflection in Simulated Turbofan Exhaust," *AIAA Journal*, Vol. 44, No.12, 2006, pp. 3088-3097.

[40] Zaman, K. B .M. Q., and Papamoschou, D. "Noise- and Flow-Field of Jets from an Eccentric Coannular Nozzle," 42nd AIAA Aerospace Sciences Meeting and Exhibit, AIAA Paper 2004-0005, 2004.

[41] Shupe, R. S., "Noise Reduction and Flow Characteristics in Asymmetric Dual-Stream Jets", 232p, Thesis of Master of Science, University of California, Irvine, 2007.

[42] Viswanathan, K., "An Elegant Concept for Reduction of Jet Noise from Turbofan Engines", 10th AIAA/CEAS Aeroacoustics Conference, AIAA Paper 2004-2975, 2004.

[43] Paliath, U. and Morris, P. J., "Prediction of jet noise from rectangular nozzles", 44th AIAA Aerospace Sciences Meeting and Exhibit, paper AIAA 2006-618, 2006.

[44] Birch, S. F., Lyubimov, D. A., Maslov, V. P. and Secundov, A. N., "Noise Prediction for Chevron Nozzle Flows", 12th AIAA/CEAS Aeroacoustics Conference, AIAA Paper 2006-2600, 2006.

[45] Engblom, W. A., Khavaran, A., and Bridges, J., "Numerical Prediction of Chevron Nozzle Noise Reduction Using WIND-MGBK Methodology," 10th AIAA/CEAS Aeroacoustics Conference, AIAA Paper 2004-2979, 2004.

[46] Stone, J. R., Berton, J. J., Krejsa, E. A and Clark, B. J., "Initial Development and Calibration of a Design Guide for Jet Noise Reduction", 40th AIAA/ASME/SAE/ASEE Joint Propulsion Conference and Exhibit, AIAA paper 2004-3315, 2004.

[47] Stone, J. R., Krejsa, E. A. and Clark, B. J., "Jet Noise Modeling for Coannular Nozzles Including the Effects of Chevrons", *NASA CR-2003-212522*, 2003.

[48] Stone, J. R., Khavaran, A., Hunter, C. A., "Assessment of Current Jet Noise Prediction Capabilities", 14th AIAA/CEAS Aeroacoustics Conference, AIAA paper 2008-2933, 2008;

[49] Viswanathan, K., Shur, M., Strelets, M. and Spalart, P. R., "Numerical Prediction of Noise from Round and Beveled Nozzles", Euromech Colloquium 467: Turbulent Flow and Noise Generation, Marseille, 2005.

[50] Mead, C. J., and Copplestone, R. A., "Further investigation of concepts for reducing the exhaust noise of HBPR aeroengines", Restricted-Commercial document from DERA as part of the CARAD programme, 1998.

[51] Papamoschou, D., and Debiasi, M., "Directional Suppression of Noise from a High-Speed Jet," *AIAA Journal*, vol. 39, No. 3, pp. 390-387, March 2001.

[52] Zaman, K. B. M. Q., Bridges, J. E., and Papamoschou, D., "Offset stream technology – comparison of results from UCI and GRC Experiments", 45th AIAA Aerospace Sciences Meeting and Exhibit, AIAA paper 2007-438, 2007.

[53] Brown, C. A., Bridges, J. E., and Henderson, B., "Offset Stream Technology Test – Summary of Results", *NASA/TM – 2007-214992*, 2007.

[54] Dippold, V., Foster, L. and Wiese, M., "Computational Analyses of Offset Stream Nozzles for Noise Reduction", 13th AIAA/CEAS Aeroacoustics Conference, AIAA paper 2007-3589, 2007.

[55] Harris, A. E., "Test Techniques for Engine/Airframe Integration, AGARD 69th Fluid Dynamics Panel Meeting and Symposium on Aerodynamic Engine/Airframe for High Performance Aircraft and Missiles".

[56] Nicholson, L. F., "Engine-airframe integration", *Royal Aeronautical Society Journal*, vol. 61, November, 1957.

[57] Engineering Science Data Unit (ESDU), "An introduction to aircraft noise", London: ESDU, 2002. (ESDU Data Item 02020)

[58] Elkoby, R., "Full-scale Propulsion Airframe Aeroacoustics Investigation", 11th AIAA/CEAS Aeroacoustics Conference, AIAA paper 2005-2807, 2005.

[59] Thomas, R. H. and Kinzie, K. W., "Jet-Pylon Interaction of High Bypass Ratio Separate Flow Nozzle Configurations", 10th AIAA/CEAS Aeroacoustics Conference, AIAA paper 2004-2827, 2004.

[60] Birch, S. F., Lyubimov, D. A. , Buchshtab, P. A., Secundov, A. N. and Yakubovsky, K. Ya., "Jet-Pylon Interaction Effects", 11th AIAA/CEAS Aeroacoustics Conference , AIAA paper 2005-3082, 2005.

[61] Tam, C. K. W., "Recent advances in computational aeroacoustics", *Fluid Dynamics Research*, vol. 38(9), pp. 591-615, 2006.

[62] Colonius, T., "Computational Aeroacoustics: Overview and Numerical Methods", Lecture Series 2006-5 Computational Aeroacoustics, von Karman Institute for Fluid Dynamics, April, 2006.

[63] Wang, M., Freund, J. B., and Lele, S. K., "Computational prediction of flow-generated sound", *Annual Review of Fluids Mechanics*, vol. 38, pp. 438-512, 2006.

[64] Colonius, T. And Lele, S. K., "Computational aerpacoustics: Progress in nonlinear problems of sound generation", *Progress in Aerospace Sciences*, vol. 40 (6), pp. 345-416, 2006.

[65] Farassat F., Myers M. K., "Extension of Kirchhoff's formula to radiation from moving surfaces", *Journal of Sound and Vibration*, vol. 123(3), pp. 451–61, 1988.

[66] Freund J. B., Lele S. K., Moin P., "Calculation of the radiated sound field using an open Kirchhoff surface", *AIAA Journal*, vol. 34(5), pp. 909–916, 1996.

[67] Lyrintzis A. S., “Integral acoustic methods: From the (CFD) near-field to the (acoustic) far-field”, *International Journal of Aeroacoustics*, vol. 2(2), pp. 95–128, 2003.

[68] Ffowcs Williams, J. E. and Hawkings, D. L., “Sound generation by turbulence and surfaces in arbitrary motion”, *Proceedings of the Royal Society of London A*, vol. 264, pp. 321-342, 1969.

[69] Freund J. B., Lele S.K., Moin P., “Direct numerical simulation of a Mach 1.92 turbulent jet and its sound field”, *AIAA Journal*, vol. 38(11), pp. 2023–2031, 2000.

[70] Mitchell, B. E., Lele, S. K., Moin, P., “Direct computation of the sound from a compressible co-rotating vortex pair”, *AIAA Paper* 92-0374, 1992.

[71] Mitchell, B. E., Lele, S. K., Moin P., “Direct computation of the sound from a compressible co-rotating vortex pair”, *Journal of Fluid Mechanics*, vol. 285, pp.181–202, 1995.

[72] Freund, J. B., “Noise sources in a low-Reynolds-number turbulent jet at Mach 0.9”, *Journal of Fluid Mechanics*, vol. 439, pp. 277-305, 2001.

[73] Manning, T. A., Lele, S. K., “A numerical investigation of sound generation in supersonic jet screech”, 6th AIAA/CEAS Aeroacoutics Conferece, paper 2000-2081, 2000.

[74] Suzuki T. and Lele, S. K., “Shock leakage through an unsteady vortex-laden mixing layer: application to jet screech”, *Journal of Fluid Mechanics*, vol. 490, pp.139–167, 2003.

[75] Estivalezes, J. L., and Gamet, L., “From jet flow computations to far-field noise prediction”, FED-Vol. 238, *1996 Fluids Engineering Division Conference*, Volume 3, 1996.

[76] Gamet, L., and Estivalezes, J. L., “Application of large-eddy simulations and Kirchhoff method to jet noise prediction”, *AIAA Journal*, vol. 36(12), pp. 2170-2178, 1998.

[77] http://www.grc.nasa.gov/WWW/Acoustics/analysis/software/jetnoise.htm, accessed on 05/03/2011.

[78] Bechara, W., Bailly, C., and Lafon, P., “Stochastic approach to noise modeling for free turbulent flows”, *AIAA Journal*, vol.32(3), pp. 455–463, 1994.

[79] Bailly, C., and Juvé, D., "A stochastic approach to compute subsonic noise using linearized euler's equations", *AIAA Paper* 99-1872, 1999.

[80] Bilsson, M., "Computational Techniques for Jet Noise Predictions", Ph.D Thesis, 126f., Department of Thermo and Fluid Dynamics, Chalmers University of Technology, Göteborg, Sweden, 2002.

[81] Putnam, T. W., "Review of Aircraft Noise Propagation", *NASA TM X-56033*, September, 1975.

[82] Morse, P. M. and Ingard, K. U., "Theoretical Acoustics", Princeton University Press, New Jersey, 1986.

[83] Powles, C. J. and Tester, B. J., "Asymptotic and numerical solutions for shielding of noise sources by parallel coaxial jet flows", AIAA-2008-2975, 2008.

[84] Powles, C. J. and Tester, B. J., "Installation effects study: ISVR study on jet shielding effect", *TURNEX – project report: 516079*, November, 2007.

[85] Tester, B. J. and Morfey, C. L, "Developments in jet noise modeling theoretical predictions and comparisons with measured data", *Journal of Sound and Vibration*, vol. 46, pp. 79-103, 1976.

[86] Wundrow, D. W., and Khavaran, A. "On the applicability of high-frequency approximations to Lilley's equation". *Journal of Sound and Vibration*, vol. 272, pp. 793–830, 2004.

[87] Gerhold, C. H., "Analytical model of jet shielding", *AIAA paper*, vol. 21, pp. 694–698, 1982.

[88] Morfey, C. L., and Joseph, P. F., "Shear-layer refraction corrections for off-axis sources in a jet flow", *Journal of Sound and Vibration*, vol. 239, pp. 819–848, 2001.

[89] Suzuki, T., and Lele, S. K., "Refracted arrival waves in a zone of silence from a finite thickness mixing layer", *Journal of the Acoustical Society of America*, vol. 111, pp. 716-728, 2002.

[90] Freund, J.B., and Fleischman, T.G., "Ray traces through unsteady jet turbulence". *International Journal of Aeroacoustics*, vol. 1 (1), pp. 83–96, 2002.

[91] Spalart, P. R., Shur, M. L., and Strelets, M.Kh, "Identification of sound sources in large-eddy simulations of jets". 13th AIAA/CEAS Aeroacoustics Conference, AIAA-2007-3616, 2007.

[92] Pierce, A. D., Acoustics: An Introduction to Its Physical Principles and Applications, Acoustic Society of America, 1989.

[93] Blokhintzev, D., "The propagation of sound in an inhomogeneous and moving medium I". *The Journal of the Acoustical Society of America*, vol. 18(2), pp. 322–328, 1945.

[94] Tan, S. Y., and Tan, H. S., "Modeling and measurements of channel impulse response for indoor wireless communication system design", IEE, Proceedings on Microwave, Antennas, and Propagation, vol. 142(6), pp. 405–410, 1995.

[95] Patwari, N., Durgin G., and Rappaport, T.S., "An advanced 3d ray launching method for wireless propagation prediction", IEEE 47th Vehicular Technology Conference. Technology in Motion, vol. 2, pp. 785–789, 1997.

[96] McLaugling, P., "A Contribution to the Jet Noise Installation Problem", 179f. Thesis (PhD) – University of Southampton, Southampton – UK, 2011.

[97] Larsson, J., "Computational Aero Acoustics for Vehicle Applications", Thesis for the Degree of Licentiate in Engineering, Department of Thermo and Fluid Dynamics, Chalmers University of Technology, 2002.

[98] Tam, C. K. W. "Jet noise: Since 1952", *Theoretical and Computation Fluid Dynamics*, vol. 10(6), pp. 393-405, 1998.

[99] Ffowcs-Williams, J.E., "The Noise from Turbulence Convected at High Speed", *Phil. Trans. Roy. Soc. (Lond.)*, vol. A255, pp. 469-503, 1963.

[100] Ribner, H. S., "Aerodynamic Sound from Fluid Dilatations", *U.T.I.A. Report No. 86*, 1962.

[101] Curle, N., "The influence of solid boundaries upon aerodynamic sound", Proc. Roy. Soc., vol. A 231, p. 505-514, 1955.

[102] Howe, M. S., "Acoustics of Fluid-Structure Interactions". Cambridge Monographs on Mechanics. Cambridge University Press, Cambridge, 1998.

[103] Möhring, W. "On vortex sound at low mach number". *Journal of Fluid Mechanics*, vol. 85, p. 685-691, 1978.

[104] Powell, A. "Theory of vortex sound". *Journal of the Acoustical Society of America*, vol. 36(1), p. 177-195, 1964.

[105] Phillips, O.M., "On the generation of Sound by Supersonic Turbulent Shear Layers", *Journal of Fluid Mechanics*, vol. 9, pp. 1-28, 1960.

[106] Lilley, G.M., Morris, P.J., and Tester, B.J., "On the Theory of Jet Noise and its Application", *AIAA paper* No. 73-987, October 1973.

[107] Mani, R., Balsa, T.F., and Gliebe, P.R., "High-velocity jet noise source location and reduction". *Task 2, Federal Aviation Administrations Report, FAA-RD-76-II*, 1978.

[108] Azarpeyvand, M., "Some Aspects of RANS Based Jet Noise Prediction", 190f. Thesis (PhD) – University of Southampton, Southampton – UK, 2008.

[109] Khavaran, A., and Bridges, J., "Modelling of fine-scale turbulence mixing noise", *Journal of Sound and Vibration*, vol. 279, pp. 1131-1154, 2005.

[110] Khavaran, A., Bridges, J., and Freund, J.B., "A parametric study of fine-scale turbulence mixing noise", 8th AIAA/CEAS Aeroacoustics Conference, AIAA 2002-2419, 2002.

[111] Khavaran, A., and Krejsa, E.A., "On the role of anisotropy in turbulent mixing noise", 4th AIAA/CEAS Aeroacoustics Conference, AIAA-1998-2289, 1998.

[112] Frendi, A., Dorland, W.D., and Wang, T. S., "A jet engine noise measurement and prediction tool", *Journal of Acoustical Society of America*, vol. 122(1), pp. 2036-2042, 2002.

[113] Frendi, A., Nesman, T., and Wang, T. S., "On the effect of time scalling on the noise radiated by an engine plume", *Journal of Sound and Vibration*, vol. 256, pp. 969-979, 2002.

[114] Ribner, H. S., "Quadrupole correlation governing the pattern of jet noise", *Journal of Fluid Mechanics*, vol. 38, pp. 1-24, 1969.

[115] Jordan, P. and Gervais, Y., "Modeling self- and shear-noise mechanisms in inhomogeneous, anisotropic turbulence", *Journal of Sound and Vibration*, vol. 279, pp. 529-555, 2005.

[116] Uberoi, M.S., "Quadrupole velocity correlations and pressure fluctuations in isotropic turbulence", *Journal of Aeronautical Science*, vol. 20, pp. 197-204, 1953.

[117] Ribner, H.S., "Theory of two-point correlations of jet noise", NASA *TN D-8330*, 1976.

[118] Batchelor, G.K., "The Theory of Homogeneous Turbulence", Cambridge U.P., Cambridge, England, 1960.

[119] Harper-Bourne, M., "Jet near field noise prediction", 8th AIAA/CEAS Aeroacoustics Conference, AIAA-2002-2554, 2002.

[120] Self, R.H., "Jet noise prediction using the Lighthill acoustic analogy", *Journal of Sound and Vibration*, vol. 275, pp. 757-768, 2004.

[121] Morris, P.J., and Boluriaan, S., "The prediction of jet noise from CFD data", 10th AIAA/CEAS Aeroacoustics Conference, AIAA-2004-2977, 2004.

[122] Jordan, P., Gervais, Y., Valiere, J. C., Foulon, H., "Final results from single point measurements". *Project deliverable D3.4, JEAN—EU 5th Framework Programme*, G4RD-CT2000-00313, Laboratoire d' Etude Aerodynamiques, Poitiers, 2002.

[123] Goldberg, U., Batten, P., Palaniswamy, S., Chakravarthy S., Peroomiam, O., "Hypersonic flow predictions using linear and nonlinear turbulence closures", *Journal of Aircraft*, 37(4), pp. 671-675, 2000.

[124] Ilario, C.R.I, Almeida, O., Batten, P., "Investigation of an Axi-symmetric Subsonic Turbulent Jet using Computational Aeroacoustics tools", 13th AIAA/CEAS Aeroacoustics Conference, AIAA-2007-3656, Rome, 2007.

[125] Ilario, C.R.I, Almeida, O., Meneghini, J.R., "Numerical and Empirical Approaches for Jet Noise Reduction: Investigation of Co-flow Effects", 15th AIAA/CEAS Aeroacoustics Conference, AIAA-2009-3405, Miami, 2009.

[126] Batten, P., Ribaldone, E. Casella, M., Chakravarthy, S., "Towards a Generalized Non-Linear Acoustics Solver", 10th AIAA/CEAS Aeroacoustics Conference, AIAA-2004-3001, City-DC, 2004.

[127] Jordan, P., "Results from Acoustic Field Measurements", project deliverable D3.6, JEAN-EU. *In.: FRAMEWORK PROGRAM, 5,* G4RD-CT-2000-00313. Poitiers: Laboratorie d'Etude Aerodynamiques. 2002.

[128] Pope, S. B., "Explanation of the Turbulent Round-Jet/Plane-Jet Anomaly", *AIAA Journal*, vol. 16(3), pp. 279-281, 1978.

[129] Nallasamy, M., "Survey of Turbulence Models for the Computational of Jet Flow and Noise", *NASA/CR-1999-206592*, 1999.

[130] Balsa, T.F., Gliebe, P.R., Kantola, R.A, Wang, J.C.F, Mani, R., "High Velocity Jet Noise Source Location and Reduction: Task 2 – Theoretical Developments and Basic Experiments", Washington-DC: *Federal Aviation Administration Report*, FAA-RD-76-79-II, 1978.

[131] Morfey, C.L., Szewczyk, V., "Jet Noise Modelling by Geometric Acoustics. part I: Theory and Prediction Outside the Cone of Silence", *ISVR Technical Report N.77-91*, University of Southampton, 1991.

[132] Tanna, H. K. and Morris, P. J., "In-Flight Simulation Experiments on Turbulent Jet Mixing Noise," *Journal of Sound and Vibration*, vol. 53, pp. 389–405, 1977.

[133] Cocking, B. J., "A Prediction Method for the Effects of Flight on Subsonic Jet Noise," *Journal of Sound and Vibration*, vol. 53, pp.435–453, 1977.

[134] Michalke, A. and Michel, U., "Prediction of Jet Noise in Flight from Static Tests," *Journal of Sound and Vibration*, vol. 67, pp. 341–367, 1979.

[135] Tam, C.K.W. and Auriault, L., "Jet Mixing Noise From Fine-Scale Turbulence", *AIAA Journal*, vol. 37(2), pp. 145-153, 1999.

[136] Fluent Incorporation. Fluent 6.3: user's guide. Documentation, 2006.

[137] Shih, T. H., Lumley, J. L., Zhu, J., "A Realizable Reynolds Stress Albebraic Equation Mode", NASA TM-105993, 1993.

[138] Lien, F. S., Leschziner, M. A., "Low-Reynolds number eddy-viscosity modelling based on non-linear stressstrain/vorticity relations". In: Rodi, W. and Bergeles, G. (eds), Engineering Turbulence Modelling and Experiments 3, Elsevier, Amsterdam, pp. 91-100, 1966.

[139] Metacomp Technologies, Inc., User's Manual, 2009.